BioMed Research International

Osteogenic Biomaterials in Contemporary Dentistry

Guest Editors: Seong-Hun Kim, Jae-Pyung Ahn, Homayoun H. Zadeh, and Eric J. W. Liou

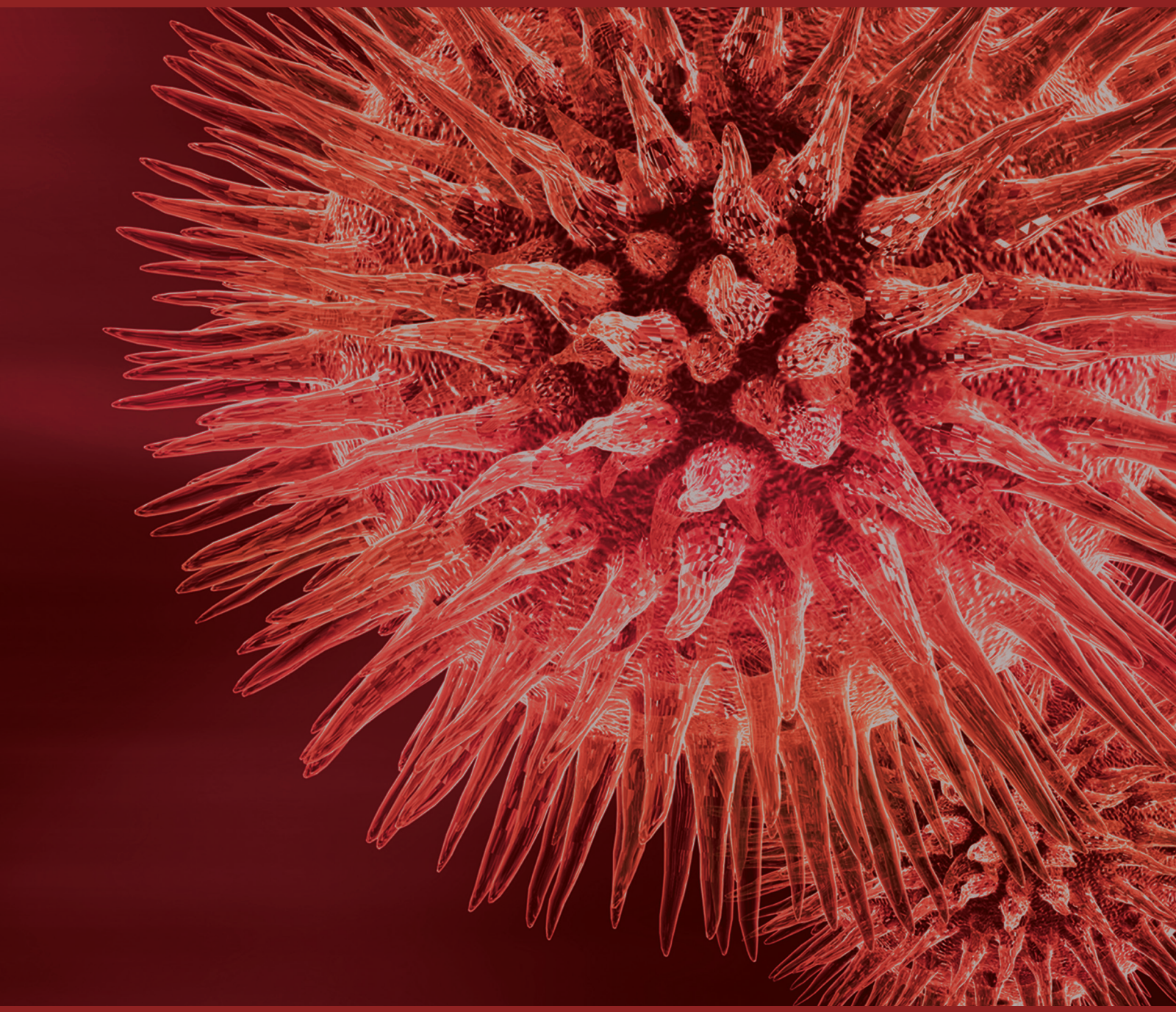

Osteogenic Biomaterials in Contemporary Dentistry

BioMed Research International

Osteogenic Biomaterials in Contemporary Dentistry

Guest Editors: Seong-Hun Kim, Jae-Pyung Ahn, Homayoun H. Zadeh, and Eric J. W. Liou

Contents

Hindawi Publishing Corporation
BioMed Research International
Volume 2015, Article ID 945320, 2 pages
http://dx.doi.org/10.1155/2015/945320

Editorial

Osteogenic Biomaterials in Contemporary Dentistry

Seong-Hun Kim,[1] Jae-Pyung Ahn,[2] Homayoun H. Zadeh,[3] and Eric J. W. Liou[4]

[1]*Department of Orthodontics, School of Dentistry, Kyung Hee University, No. 1 Hoegi-dong, Dongdaemun-gu, Seoul 130-701, Republic of Korea*
[2]*Advanced Analysis Center, Korea Institute of Science and Technology, 5 Hwarang-ro 14-gil, Seongbuk-gu, Seoul 136-791, Republic of Korea*
[3]*Laboratory of Immune Regulation and Tissue Engineering (LITE), Division of Periodontology, Diagnostic Sciences & Dental Hygiene, Ostrow School of Dentistry, University of Southern California, 925 34th Street, Room 4278, Los Angeles, CA 90089-0641, USA*
[4]*Department of Orthodontic and Craniofacial Dentistry, The Chang Gung University, Taipei, Taiwan*

Correspondence should be addressed to Seong-Hun Kim; bravortho@khu.ac.kr

Received 3 March 2015; Accepted 3 March 2015

There have been developments and applications of osteogenic biomaterial substitutes in dentistry to replace missing dentition or to reinforce existing dentitions. The dentistry in practice has evolved into new treatment modality with the development and application of novel biocompatible materials. The examples are dental implants, bone graft materials, surgical plates, and any modification to increase biocompatibility and stability in dentition. These materials cover everything from replacing the missing teeth and/or degenerated supporting structures to the induction of new bone formation. Also, the osseointegrated materials further allowed orthopedic force application on these materials as skeletal anchorage to control tooth movements. Currently, modifications of the surface treatment or combination of osseoinductive materials to improve potential osseointegration are continuously endeavored.

This special issue delivers original research on different aspects, studies on the application of the novel biomaterials to fill bone defect rapidly with new bone, improvement of osseointegration through variety of surface treatment, and the possibility of alumina toughened zirconia for the new implant material, and also covers clinical research on a modified dental implant as a gateway to the human body: implant mediated drug delivery system.

First, we discuss the studies of novel biomaterial application for new bone formation in bony defect. Rapid bone defect filling with normal bone is a challenge in orthopaedics and dentistry. A study by S. Ansari et al. developed a strategy for bone tissue engineering that entails application of immobilized anti-BMP-2 monoclonal antibodies (mAbs) to capture endogenous BMPs in vivo and promote antibody-mediated osseous regeneration (AMOR). These data have potential implications for the mechanism of action of AMOR, suggesting that anti-BMP-2 may capture endogenous osteogenic BMPs, which may in turn mediate de novo bone formation. Strontium ranelate (SrRan) has been shown to in vitro decrease bone resorption and increase bone formation and represents a potential agent with the capacity to accelerate bone defect filling.

G. Zacchetti et al.'s study demonstrates that Sr is integrated both in cortical and in trabecular bone healing of the defect in SrRan-treated rats and improves the bone material level properties of the healing bone mainly after 4 weeks of treatment. These results open up new perspectives for the use of SrRan in clinical studies as a pharmacologic agent with a potential beneficial effect on bone defect repair.

A. Monje et al.'s comprehensive systematic review aimed at assessing the feasibility of allogeneic block grafts by means of survival rate, histologic analysis, and causes of failure, for augmentation of the atrophic maxilla, provides a current state of the art about this treatment modality. Therefore, this study can be of a very meaningful importance for clinicians in

the decision making of selecting the ideal source for bone block grafting.

This special issue illuminates the clinical evaluation of the bone graft materials that have been used conventionally and introduces the histological identification of changes in tissue adjacent to the biomaterials through three original research articles. Particularly, clinical experiment on the management of the thin alveolus which has been considered as tooth movement limitation in orthodontics and the scientific analysis of the methods have been discussed in depth.

Alveolar augmented corticotomy is effective in accelerating orthodontic tooth movement, but the effect only lasts for a relatively short time. A study by D.-Y. Lee et al. demonstrated the stable results in a long-term (12 weeks) experiment using xenograft materials in beagle experiment. Absorbable collagen membrane could control the texture of bone surface.

K.-B. Lee et al. researched the different types of bone graft materials on the treatment effect of augmented corticotomy. The remarkable thing is that not only allograft or xenograft but also synthetic graft material showed comparable new bone formation. Augmented corticotomy showed stable results regardless of the graft material types, and in particular synthetic bone material showed dramatic new bone formation.

The study of H.-J. Choi et al. was to investigate the underlying biology of the immediate periodontal response to orthodontic tooth movement after the augmented corticotomy with alloplastic bone grafts. The results demonstrated that measurable tooth movement began as early as 3 days after the intervention in beagle dogs. Based on the results and histological findings, augmented corticotomy-facilitated orthodontic tooth movement might enhance the condition of the periodontal tissue and the stability of the outcomes of orthodontic treatment.

There has been increased interest in search of the new biomaterial for dental implant. We would like to examine the possibility of alumina toughened zirconia for the new implant material through several articles.

S. Y. Kim et al.'s study classified the influence of different topographies and hydrophilicities of Ti surfaces on the expression of various functional factors in PDLSCs involved in osteogenesis in the absence of osteogenic supplements and evaluated biomarkers of cellular activity, including the expression of transcription factors and signaling molecules of PDLSCs on the Ti surfaces.

The relevance of J. Markhoff et al.'s research was to develop a glass solder matrix for coating zirconia ceramics to improve osseointegration of ceramic dental implants with adequate mechanical properties at once. Thereby, the existing advantages in esthetic appearance and hypersensitivity of ceramic dental implants in contrast to metallic implants may become effective in clinical application in the near future.

The results of R. Olivares-Navarrete et al.'s study indicate that effects of the complex SLA topography are greater than the effect of acid etching or grit blasted on regulation of osteogenesis, osteoclastogenesis, and angiogenesis on multipotent BMCs and committed osteoblasts. 1α,25(OH)2D3 had a major role in enhancing these effects that was sex depended.

Alumina-zirconia composites have attracted significant interest in the past few years for orthopedic and dental use. Although yttria stabilized zirconia is the only ceramic currently employed for dental implant fabrication, several reasons suggest that alumina-zirconia composites may conveniently substitute this monolithic material. Here, F. Mussano et al. report the results of the experiments performed in vitro and in vivo to assess the behavior of alumina toughened zirconia (ATZ) dental implants. It is important to underline that ATZ is different from zirconia-toughened alumina (ZTA) due to the relative percentage of the two materials and the consequent mechanical and possibly biological properties.

Another topic enlightened in this special issue is dental implant. It is about neither improving osseointegration potential nor improving functional occlusion of implant, but it is a preliminary study on the prospect of dental implant as a drug delivery system. In an article by Y.-S. Park et al., they developed and proposed a new implant mediated drug delivery system (IMDDS) through a modified titanium implant. In the nearest future, the IMDDS may provide a novel approach to treat patients with chronic diseases.

In conclusion, we debated about the current status of osteogenic biomaterials in contemporary dentistry, the osteogenic biomaterial types, the application of the material, and the future study. We would like to suggest a right direction of osteogenic biomaterial in this special issue because comprehension of recent advances in biomaterial of dentistry would lead to appropriate applications of these biomaterials and successful strategies to improve treatment outcomes to better serve patients.

Seong-Hun Kim
Jae-Pyung Ahn
Homayoun H. Zadeh
Eric J. W. Liou

Hindawi Publishing Corporation
BioMed Research International
Volume 2015, Article ID 157360, 9 pages
http://dx.doi.org/10.1155/2015/157360

Research Article

An Alumina Toughened Zirconia Composite for Dental Implant Application: *In Vivo* Animal Results

Gianmario Schierano,[1] Federico Mussano,[1] Maria Giulia Faga,[2,3] Giulio Menicucci,[1] Carlo Manzella,[1] Cristian Sabione,[1] Tullio Genova,[1] Mitzy Mauthe von Degerfeld,[4] Bruno Peirone,[4] Adele Cassenti,[5] Paola Cassoni,[5] and Stefano Carossa[1]

[1]*Department of Surgical Sciences, CIR Dental School, University of Turin, Via Nizza 230, 10126 Turin, Italy*
[2]*CNR-IMAMOTER, Strada delle Cacce 73, 10135 Turin, Italy*
[3]*CNR-IMAMOTER (Headquarters), Via Canal Bianco 28, 44124 Ferrara, Italy*
[4]*Department of Veterinary Sciences, University of Turin, Largo Paolo Braccini 2, 10095 Grugliasco, Torino, Italy*
[5]*Department of Medicine, University of Turin, Via Santena 7, 10126 Turin, Italy*

Correspondence should be addressed to Federico Mussano; federico.mussano@unito.it

Received 25 July 2014; Revised 29 September 2014; Accepted 15 October 2014

Academic Editor: Seong-Hun Kim

Ceramic materials are widely used for biomedical applications because of their remarkable biological and mechanical properties. Composites made of alumina and zirconia are particularly interesting owing to their higher toughness with respect to the monolithic materials. On this basis, the present study is focused on the *in vivo* behavior of alumina toughened zirconia (ATZ) dental implants treated with a hydrothermal process. A minipig model was implemented to assess the bone healing through histology and mRNA expression at different time points (8, 14, 28, and 56 days). The novel ATZ implant was compared to a titanium clinical standard. The implants were analyzed in terms of microstructure and surface roughness before *in vivo* tests. The most interesting result deals with a statistically significant higher digital histology index for ATZ implants with respect to titanium standard at 56 days, which is an unprecedented finding, to the authors' knowledge. Even if further investigations are needed before proposing the clinical use in humans, the tested material proved to be a promising candidate among the possible ceramic dental implants.

1. Introduction

Titanium implants have the longest traceable record of predictable clinical performance with very high success rate [1]; however they are not without possible drawbacks [2]. In fact, titanium might be an allergen [3–5] and may diffuse not only within the adjacent tissues, as it is proven by the elevated concentrations found in the vicinity of oral implants [6] and in regional lymph nodes [7], but also systemically [8]. As a possible alternative to titanium, ceramic materials have been already investigated and clinically used for years.

Alumina and yttria stabilized zirconia (Y-TZP) ceramics are suitable for biomedical applications, due to their good mechanical and tribological properties and proved biocompatibility [9–14]. Pure alumina has been widely used as femoral heads because of its high wear resistance, but no application requiring osseointegration has been implemented to date due to its high inertness. As far as TZP is concerned, it was initially employed to replace alumina in femoral heads owing to its higher fracture toughness, but the high number of failures led to reconsider its suitability in this field. Indeed, depending on temperature, zirconia exists in three phases: monocline, cubic, and tetragonal. Monocline phase is the most stable at room temperature, even if its mechanical properties are inferior to those of tetragonal phase, so that the latter is preferred. However, tetragonal phase should be stabilized to prevent tetragonal phase transformation [15]. Once the transformation occurs, the process continuously proceeds from the surface to the bulk, resulting in a volumetric expansion followed by failure [15]. Even if zirconia materials transform most rapidly at temperature ranging between 200°C and 300°C, at low temperatures the process is enhanced by the presence of water, available *in vivo* [15–22]. Zirconia stabilized materials are employed in orthopedics

and dentistry, although in very low percentage with respect to commercially pure titanium and titanium alloys (Ti6Al4V), probably because of the unlucky history as femoral heads [23] and the survival rate inferior to that of titanium implants [24].

To overcome the limits of both monolithic materials, researchers have focused on the preparation of composites made of alumina and zirconia [25–27], already successfully applied as femoral heads [28, 29]. The advantages of these oxidic composites owed mainly to the limited transition from the tetragonal phase to the monocline one, which enhances the mechanical performance [23], and to an increase of the material toughness [30, 31]. The combination of alumina and zirconia allows compensating the moderate toughness of alumina and the ageing effect of zirconia. It has been shown that, when the percentage of ZrO_2 is kept under the 22% wt [32], ageing phenomena do not occur independently from the grain size.

The mechanical stability is not the only requirement a good implant material should possess, since bioactivity is necessary to ensure proper osseointegration. When dealing with bone bonding materials, bioactivity can be described as the ability to grow bonelike apatite on the material surfaces [33]. Apatite formation in simulated body fluid (SBF) is preferentially induced whenever particular hydroxyl sites are on the surface, which can be achieved through acidic and/or alkali treatments [34]. Consistently, Faga et al. [35] described the formation of acicular hydroxyapatite crystals onto the surface of alumina toughened zirconia (ATZ) samples treated hydrothermally. Furthermore, alumina zirconia ceramics may elicit slightly better biological responses than the commercially pure titanium usually employed for dental implants [36]. Ceramic materials are also very suitable for aesthetic oral rehabilitations, which may be required when dental implants are located in the anterior part of the mouth, as it would preclude the dark shimmer of titanium implants [37–39].

The aforementioned promising properties of ATZ treated with phosphoric acids, in terms of mechanical and bioactivity features, prompted the authors to study the *in vivo* behaviour of such material. For this purpose, implants made of ATZ were placed within the bone of recipient animals, using a titanium clinical standard for comparison since no papers on this topic are present in literature. For sake of completeness, fatigue tests were performed according to UNI EN ISO 14801:2008 standards and surface properties were studied. Indeed, as load bearing medical devices, dental implants are not suitable to clinical use if they present defects possibly affecting their mechanical strength, which may lead to early failure under the chewing load; such might be the case of large porosities within ceramic bulk materials.

2. Material and Methods

2.1. Implants. Powders with high purity were used to produce the oxidic implants (Tosoh ZrO_2-20wt %Al_2O_3, (TZ-3Y20AB), as "ready to press" powders, so that no additional mixing was required before pressing. Green samples were obtained by linear pressuring at 80 MPa followed by Cold Isostatic Pressing under 200 MPa. The optimized conditions for sintering process were: heating 50°C/h up to 700°C, dwelling for 2 h at 700°C, and heating of 100°C/h up to temperature sintering of 1500°C and dwelling for 2 h at this temperature. Hardness, toughness, and strength of the full dense material was measured on proper specimens, as reported elsewhere by Faga et al. [35]. The materials were then subjected to Computer Aided Manufacturing obtaining one-piece dental implants of 11.5 × 4.25 mm. The surface treatment was obtained by hydrothermal cycles (patent number: TO2012A000029 and PCT/IB2013/050425). Implants were then treated with phosphoric acid under hydrothermal conditions with the purpose of inducing bioactivity [35]. As a control, dental implants with TiUnite surface were purchased from Nobel Biocare (Nobel Biocare Italia, Agrate Brianza, Italy).

2.2. Microscopy. Microstructure was studied by means of a Scanning Electron Microscope Zeiss EVO 50 with Energy Dispersion Spectroscopy analyzer for elemental composition detection.

2.3. Roughness. The surface roughness was measured by using a noncontact profilometer, Talysurf CCI 3000A on the screw. The tests were performed within an air-conditioned laboratory, where temperature is kept at 20°C, on a representative surface of 90 mm^2.

2.4. Mechanical Tests. Mechanical tests were run in triplicate according to UNI EN ISO 14801:2008 by using a monoaxial machine for both the dynamic and static tests (Italsigma, Italy) equipped with a loading cell (max. load: 3 kN). In static conditions, the speed was 0.2 mm/minute, the preload: 2N. Based on the ISO standards mentioned above, the static tests aim to define the load to be applied when performing the dynamic tests. Therefore, a value inferior to the 80% of F_{mean}, which is the mean value of the static test strength (F_{Max}) of the three samples, was applied to the samples for 5×10^6 cycles in a sinusoidal way. The minimal strength F_{min} corresponded to the 10% of the maximal strength F_{max} ($R = 0{,}1$).

2.5. In Vivo Experiments

2.5.1. Experimental Design. The *in vivo* experiment was conducted on 16 minipigs. Eight experimental implants per animal were inserted in the right tibia: 4 hydrothermally treated ATZ and 4 Nobel Ti-Unite (Nobel Biocare Italia, Agrate Brianza, Italy). Four animals were sacrificed at 8, 14, 28, and 56 days after the implant placement. The tibias were block-sectioned and subjected to histomorphometric (4 samples per animal) and biomolecular analysis (4 samples per animal). Outcomes were analyzed in terms of new bone apposition by a digital histology index (DHI) and RNA profiling.

2.5.2. Animal. Sixteen adult minipigs (mean weight 65.94 kg SD = 2.84) were used in the experiment (CISRA, Turin, Italy). The minipigs were fed standard pelleted cereal food and were given water *ad libitum*. The animals underwent an acclimation period of 1 week prior to surgery. Abiding

with Italian law, all animal experiments were approved by an academic ethics committee.

2.5.3. Surgical Procedure. After preanesthetic sedation with 2% xylazine (Rompun 2%, Bayer, Milan, Italy; 2.3 mg/kg) and tiletamine/zolazepam (Zoletil 100-Virbac 20%, Laboratoires Virbac, Carros, France; 6.3 mg/kg), surgery was performed under intubation anesthesia with isoflurane/halothane and O_2. The right hind leg was prepared in a standard sterile fashion. After exposing the tibia, the implants were inserted with a 40 Ncm torque. Then, the flap was closed and the surgical access sutured so as to completely cover the implants, whose head reached the bone level. Each tibia received 8 implants: 4 ceramic ones and 4 titanium implants. Tibial bone specimens were collected at this stage to determine baseline (time 0) values for the RNA analysis. At the established time points, animals were euthanized by preanesthesia with 2% xylazine (Rompun 2%, Bayer) (2.2 mg/kg) and tiletamine/zolazepam (6.6 mg/kg) and an intracardiac injection of embutramide, mebezonium iodide, and tetracaine hydrochloride (70 mg/kg). Finally, the tibias were exposed and dissectedinto slices.

2.5.4. Expression of Osteogenic Markers. To protect the RNA, all specimens (8, 14, 28, and 56 days) were placed in RNA Later (Qiagen, Milan, Italy) and stored at −80°C until testing. Before the RNA purification (RNeasy Mini Kit Quiagen, Valencia, CA, USA), the samples were disrupted using a TissueRuptor. Total RNA was subjected to reverse transcription (High Capacity cDNA RT Kit; Cat#: 4368814 Applied Biosystems, USA). The cDNA obtained underwent real-time polymerase chain reaction (RT-PCR) using commercially available primer/probe cocktails for *Sus scrofa* (TaqMan Gene Expression Assays collagen, type I, alpha 1 assay ID: Ss03373340_m1; secreted protein, acidic, cysteine-rich (osteonectin) assay ID: Ss03392006_m1; bone gamma-carboxyglutamate (gla) protein assay ID: Ss03373655_s1; bone morphogenetic protein 2 assay ID: Ss03373798_g1 Applied Biosystems, USA), following the manufacturer's protocol. Glyceraldehyde 3-dehydrogenase (TaqMan Gene Expression Assays, glyceraldehyde-3-phosphate dehydrogenase assay ID: Ss03374854_g1Applied Biosystems, USA) was used as internal control.

2.5.5. Histological Analysis of the Peri-Implant Bone. To evaluate the bone healing and remodeling, histologic analysis was performed at 8, 14, 28, and 56 days after implant. After block section of the implants along with the adjacent bone, the specimens were fixed in 4% formalin for 24 hours and decalcified for 3 to 4 weeks in a mixture of 50% formic acid and 10% sodium citrate tribasic. While the implants were removed, the peri-implant bone samples were embedded with paraffin wax and cut into 3 μm thick sections, along the longitudinal implant axis, using a motorized microtome. Polylysine coated slides were used to enhance the adhesion of the tissue section during staining procedures. The histological structure of the peri-implant bone was assessed by traditional haematoxylin and eosin staining and for optical microscopy. The digital histology index (DHI) was manually determined using an imaging computer software (Olympus Dot Slide BX51) on the virtual histology slide. Briefly, on each virtual slide, the newly formed bone was measured by tracing a line at the interface between bone and implant within a given length (a standard length of 4 cm was adopted). The ratio of newly formed bone to the total bone-implant interface taken into consideration was expressed as a percentage. The DHI was measured on both sides of each slide. Two specimens per time points per material were obtained and at least 10 slides were made from each block sectioned histological sample. In addition, morphometric parameters such as (1) presence of necrotic or fibrous tissue and (2) amount of organized grouped osteoclasts and osteoblasts, together with (3) blood vessels and (4) *de novo* formed bone, were assessed by two independent histologists.

2.5.6. Histomorphometrical Reconstruction. Forty serial sections, 3 μm thick, were cut from the 56-day-paraffin-embedded blocks and stained as described above. Afterwards, the slides were acquired by an automated microscope to generate virtual colored slides, which were converted into grey scale images so as to allow further image processing. The three-dimensional reconstruction of the samples was performed using *Amira 4.0*, an advanced volume modeling software (TGS Template Graphics Software, http://www.tgs.com). Three different volumes were delimitated from the cortex to the medullar space and a percentage of bone density was calculated based on a densitometric analysis of the white voxels, the cortical bone being taken as a reference (100%).

2.5.7. Statistical Analysis. Data from RT-PCR and DHI were analysed by GraphPad Prism 5 (GraphPad Software Inc, La Jolla, CA, USA). RT-PCR was independently repeated at least three times ($n = 3$), on the samples derived from peri-implant bone ($n = 2$ per material per time point). As for the DHI, each specimen ($n = 2$ per material per time point) generated at least 10 virtual histological slides. Statistical analysis was performed by using the one-way analysis of variance (ANOVA) with *post hoc* Dunnett's test or the Student's t-test, as appropriate. A P value of <0.001 was considered significant.

3. Results

3.1. Morphology and Surface Analysis. The implant morphology is reported in Figure 1 for titanium and ceramic implants, respectively. As for the titanium implant (Figure 1(a)), only the fixture was considered for the analysis. Its geometry is represented by a set of threads, identical in each part of the screw and placed at the same distance from each other. Regarding the ceramic implant (Figure 1(b)), as it is a one piece, fixture and abutment could not be separated. The intrabony screw shows a series of threads, similar to that observed for titanium implant, in the upper part (the one closer to the abutment), while some threads having a "cup profile" are present in the apical part. Such a geometry was realized with the purpose to favor the osseointegration. Indeed, during the implant placement, the geometry of

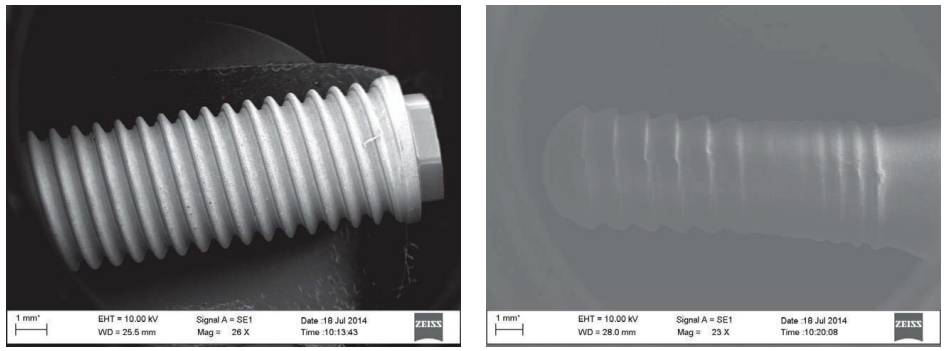

(a) (b)

Figure 1: Implant geometry. Note: SEM images were acquired at low magnification to depict the shape of the titanium implant (a) and the alumina toughened zirconia implant (b).

Table 1: Static mechanical tests.

	F_{Max} (N)
A-01	675.6
A-02	912.03
A-03	737.3

Table 2: Dynamic mechanical tests.

	A-04	A-05	A-06
Flexural moment (Nmm)			
M_{mean}	586.7	566.2	567.1
M_{dyn}	480.0	463.3	464.0
M_{max}	1066.8	1029.5	1031.0
M_{min}	106.7	102.9	103.1
Compression force (N)			
F_{mean}	95.4	95.7	95.5
F_{dyn}	78.0	78.3	79.0
F_{max}	173.4	174.1	175.5
F_{min}	17.3	17.4	17.5

the threads does not allow a complete flowing of the removed bone. It is supposed that the residual bone could act as nucleation center for the following bone growth, so that the osseointegration may be promoted.

A detail of the implant surfaces is reported in Figure 2. The titanium exhibits some pores along the whole surface, while the ceramic appears fully dense. The topography of the implant surface is shown in Figure 3 (Titanium, (a); ATZ, (b)). Sa values are 3.4 μm and 5.4 μm for titanium and ATZ implants, respectively.

3.2. Mechanical Tests. As reported in the experimental section, the static test has the aim to set the conditions for dynamic tests. The results (Table 1) indicate a quite high variability of the load to failure, typical for brittle materials like ceramics. Indeed, ceramic materials generally fail because of the presence of some defects, like pores, inclusions, microcracks, and combinations. This kind of fracture mechanism leads to a large distribution of the strength, considerably higher than that of ductile materials, as metals and their alloys. An index of the variability of the strengths is represented by the Weibull Modulus: the lower the modulus, the higher the distribution. As for oxidic materials such as alumina and zirconia, Weibull modulus is about 10, while for ductile materials it is one order of magnitude higher [40]. The results of dynamic tests are reported in Table 2. All the three samples survived after five million cycles of fatigue solicitations.Therefore ATZ implants were suited to undergo further *in vivo* experiments as they met the UNI EN ISO 14801:2008 standards that are mandatory for allowing the human use.

3.3. Bone Markers. No significant difference could be detected between ATZ and titanium at the time points taken into consideration (8, 14, 28, and 56 days) for the bone markers observed (collagen type I, osteonectin, osteocalcin, and BMP-2) in peri-implant bone tissue (Figure 4).

3.4. Histological Analysis. Presence of osteoid at the bone-implant interface was noted at the earliest (8 days) time point whereas little or no interfacial unmineralized matrix was seen at all other time points for both ATZ and titanium hosting bones. A minimal amount of necrotic osteocytes were noted only at 8 days in proximity to the implant surface in both groups (Figure 5(a)), at the cortical bone level, probably due to the transitory overheating during the implant site preparation. The cellular remodeling of the bone fragments was similar between the ATZ and titanium groups and activity peaked at 8 days after implantation.

Both treatment and control groups showed a steady increase in the overall digital histology index up to 56 days (Figure 6). The DHI values differed in a statistically significant way between the ATZ and the titanium samples at day 56 (ATZ = 53.3% ± 6.5, Ti = 35.3% ± 1.9). At the earlier time points, no significant difference could be found (at 28 days: ATZ = 45.4% ± 4.5, Ti = 32.1% ± 6.4) (Figure 7).

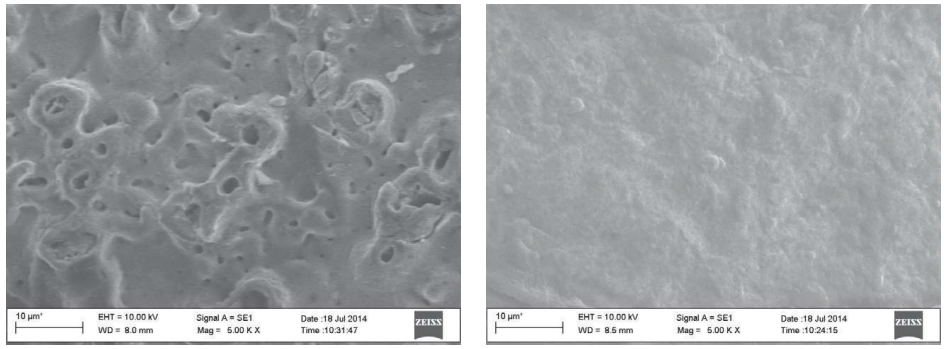

(a) (b)

Figure 2: Implant surface morphology. Note: SEM images were acquired at high magnification to depict the surface morphology of the titanium implant (a) and the alumina toughened zirconia implant (b).

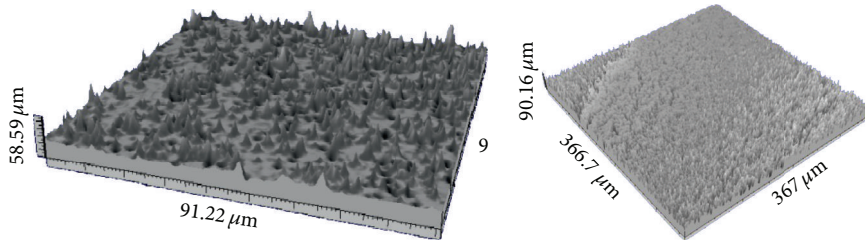

(a) (b)

Figure 3: Implant topography. Note: Surface roughness of titanium (a) and alumina toughened zirconia (b) implants was determined and graphically portrayed.

3.5. Histomorphometrical Reconstruction. The densitometric analysis of the white voxels of the medial and the apical areas of the samples concerning the 56th day is reported in Table 3. A statistical significant difference between the medial area values of ATZ and Ti was found (Student's t-test $P < 0.001$).

Table 3: Histomorphometrical reconstruction: percentage of medullar bone density showed as mean ± standard deviation.

Voxel density	Medial area	Apical area
Alumina toughened zirconia	52.4 ± 2.6%	24 ± 4.2%
Titanium	44.2 ± 3.1%	19 ± 4.5%

4. Discussion

There is still a huge concern about the long-term durability of the Y-TZP (yttria-stabilized tetragonal zirconia polycrystal), due to the low temperature degradation (LTD) of zirconia [15–19], despite its excellent biological properties [30, 31]. In the present study, alumina-zirconia composites were chosen for manufacturing dental implants, based on their reported mechanical performances superior to those of the monolithic oxides [29, 41]. Unsurprisingly, the ATZ implants tested following the ISO standards that regulate dental implants under static and dynamic load (UNI EN ISO 14801:2008) showed satisfactory mechanical behavior. Thus, alumina toughened zirconia appears as a viable alternative to yttria stabilized zirconia, as its higher resistance to crack growth is durable and may withstand the so called ageing process taking place in aqueous environment. ATZ was selected for the *in vivo* experiment portrayed in the present paper on the basis of previous data dealing with the bioactivity assessed as per Faga et al. [35]. Indeed, only with a particular hydrothermal treatment was it possible to achieve hydroxyapatite precipitation on the ATZ samples, which did not occur, for instance, on the ZTA specimens [35].

At the end of the manufacturing process, the ATZ implants were analysed by scanning electron microscopy and submitted to profilometry for roughness evaluation, before the placement into the recipient animals, adopting a swine model previously described [42]. As a control, an anodized titanium oxide layer (TiUnite) containing anatase and rutile and endowed with a moderately rough porous surface topography was selected [43]. The ATZ implants showed an average roughness (Sa = 5.4 μm) higher than that of the titanium implants (Sa = 3.4 μm). Topography and surface roughness are known to positively affect the healing process [44–46]. Indeed, increasing the level of roughness ameliorates osseointegration [47], as it was acknowledged in a 2009 consensus statement [48].

Biomolecular, histological and histomorphometrical analyses were used to examine the differences in the healing and remodeling processes between the two different

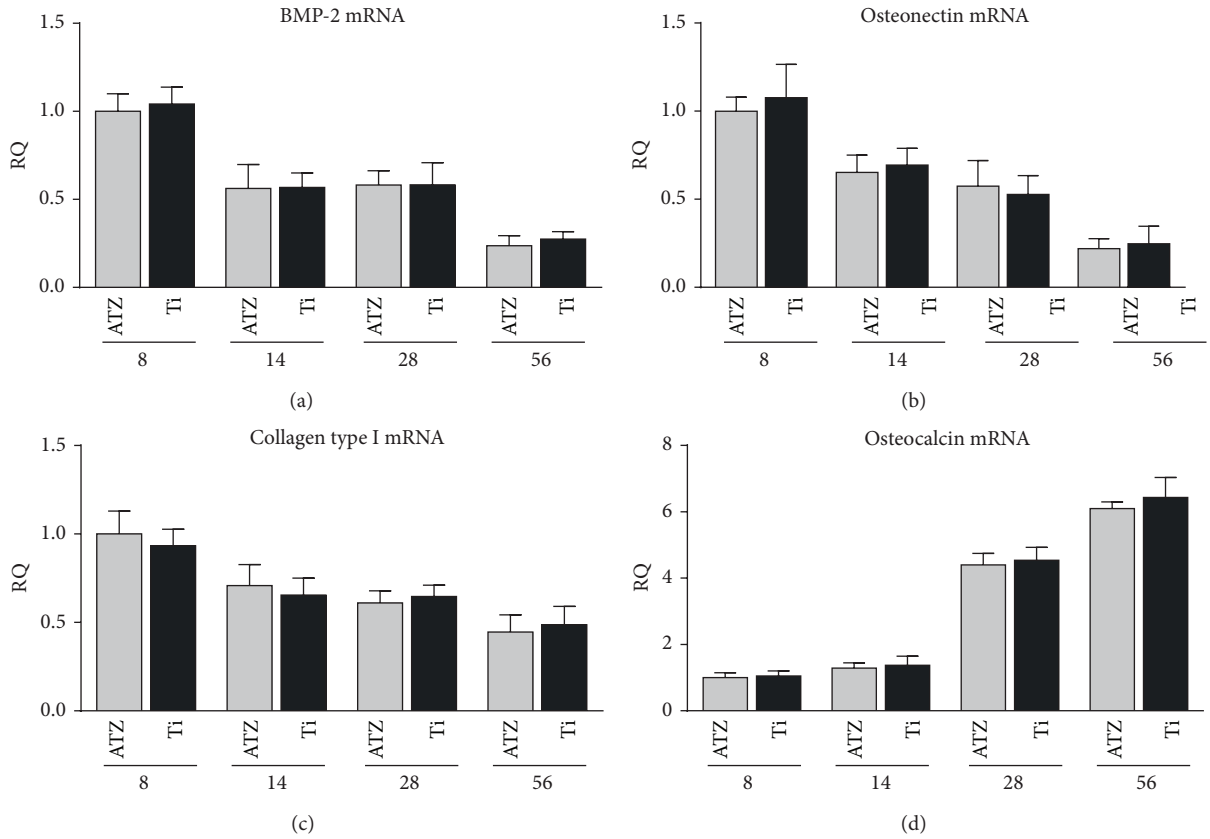

Figure 4: Expression of the osteogenic differentiation markers. Quantitative real-time polymerase chain reaction (RT-PCR) analysis of BMP-2 (a), osteonectin (b), collagen type I (c), and osteocalcin (d) transcript level ($n = 3$ for each condition for each time point). One-way analysis of variance (ANOVA) with *post hoc* Dunnett's test was used to assess statistical significance.

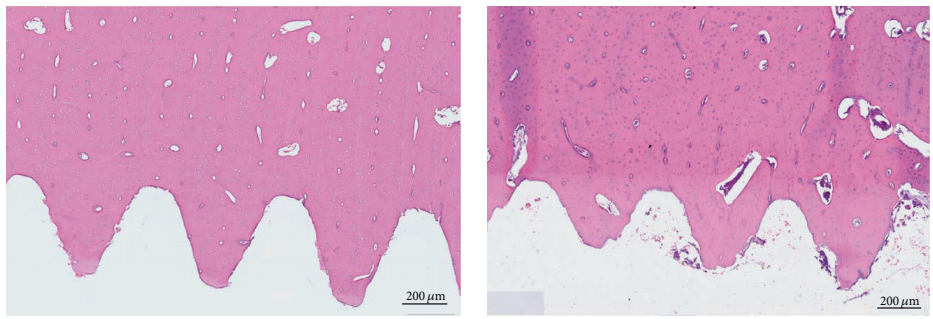

Figure 5: Representative histological images of cortical bone at 8 days. Note: E&E stain showing sporadic necrotic lacunae within cortical bone in proximity to the implant surface at 8 days (a) and healthy bone (b). This phenomenon occurred only at the earliest time point in a few cases for both alumina toughened zirconia and titanium implants and may be due the preparation of the implant site by drilling.

implant materials. Four different time points were evaluated. Representative of the early phase of healing were 8 and 14 days, while intermediate and mature bone healing were reasonably foreseen at 28 and 56 days, respectively, based on earlier experiments [49]. Interestingly, hydrothermally treated ATZ implants showed a statistically significant higher digital histology index than the titanium implants at 56 days, which is an unprecedented finding, to the authors' knowledge. Consistently, the 3D image analysis used to quantify the peri-implant bone at 56 days indicated the presence of a bone matrix denser along the ATZ than the titanium implants, particularly in the medial area.

Although ATZ is able to elicit a satisfying biological response *in vitro*, even in absence of modifications and when roughness is excluded by mirror polishing [50], no significant difference between the anodized titanium surface and the hydrothermally treated ATZ surface was detected at the mRNA level. These data could appear contradictory.

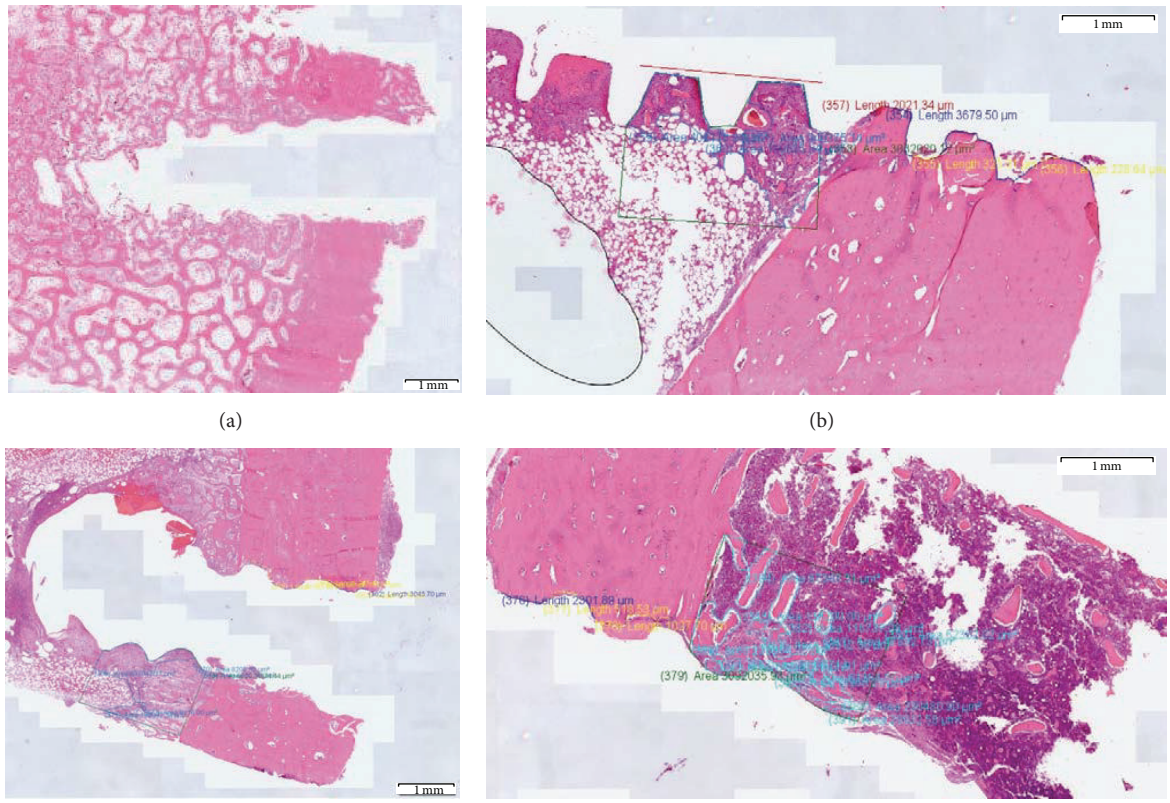

FIGURE 6: Representative histological images of DHI calculation. Representative samples of the virtual histological slides used to calculate DHI at day 56 are reported for titanium (a, b) and alumina toughened zirconia (c, d) implants, respectively, at lower (a, c) and higher (b, d) magnification.

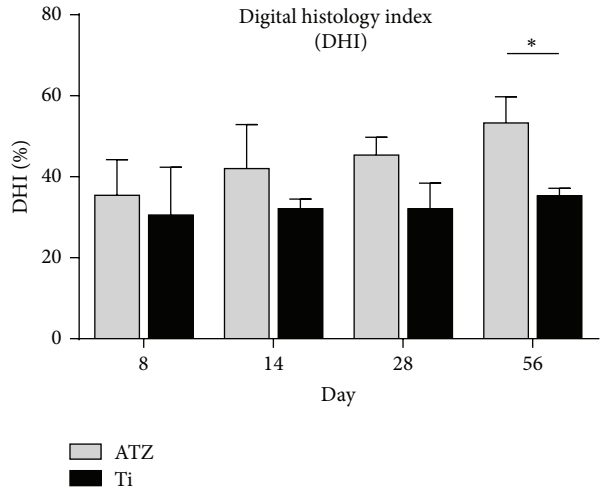

FIGURE 7: Digital Histology Index (DHI). Note: The DHI values differed in a statistically significant way (Student's t-test $P < 0.001$) between the alumina toughened zirconia (ATZ) and the titanium samples at day 56 (ATZ = 53.3% ± 6.5, Ti = 35.3% ± 1.9). At 28 days no significant difference could be found (ATZ = 45.4% ± 4.5, Ti = 32.1% ± 6.4).

However, the expression level of the investigated osteogenic markers has been normalized between the two different conditions, not taking into account the differences in the total number of cells that are effectively recruited by the two materials. Indeed, the amount of cells in the peri-implant area may differ greatly between ATZ and titanium, even if the osteogenic gene expression profile was similar in the bone forming cells growing along either ATZ or titanium. Hence, DHI was not merely dependent on the gene expression, but it could rather be affected by other surface characteristics

more active on cell recruitment and proliferation than on osteoinductive features.

Based on this study, further investigations are needed before recommending the clinical use in humans, although the tested material proved to be a promising candidate among the possible ceramic dental implants.

Conflict of Interests

The authors declare that there is no conflict of interests regarding the publication of this paper.

Authors' Contribution

G. Schierano, F. Mussano, and M. G. Faga equally contributed to the paper.

Acknowledgments

The authors wish to thank Dr. Giorgio Fantini and Dr. Stefano Capello for their kind help during the 3D image processing. This research was funded by the Piedmont Region with the NANOPRO Project grant (*"NANO structured Bioceramics for PRO sthetic Orthopaedic and Dental Application: Processing, Surface Functionalization and Biological Evalutation" Bando Regionale per la Ricerca Industriale e lo Sviluppo Precompetitivo* for the year 2006). No involvement is to be reported at any stage of the study or while preparing the paper.

References

[1] P. Papaspyridakos, C. J. Chen, S. K. Chuang, and H. P. Weber, "Implant loading protocols for edentulous patients with fixed prostheses: a systematic review and meta-analysis," *International Journal of Oral & Maxillofacial Implants*, vol. 29, pp. 256–270, 2014.

[2] M. Andreiotelli, H. J. Wenz, and R.-J. Kohal, "Are ceramic implants a viable alternative to titanium implants? A systematic literature review," *Clinical Oral Implants Research*, vol. 20, no. 4, pp. 32–47, 2009.

[3] L. Evrard, D. Waroquier, and D. Parent, "Allergies to dental metals. Titanium: a new allergen," *Revue Médicale de Bruxelles*, vol. 31, no. 1, pp. 44–49, 2010.

[4] P. D. Pigatto, G. Guzzi, L. Brambilla, and C. Sforza, "Titanium allergy associated with dental implant failure: letters to the Editor," *Clinical Oral Implants Research*, vol. 20, no. 8, p. 857, 2009.

[5] A. Sicilia, S. Cuesta, G. Coma et al., "Titanium allergy in dental implant patients: a clinical study on 1500 consecutive patients," *Clinical Oral Implants Research*, vol. 19, no. 8, pp. 823–835, 2008.

[6] S. O. Koutayas, T. Vagkopoulou, S. Pelekanos, P. Koidis, and J. R. Strub, "Zirconia in dentistry. Part 2. Evidence-based clinical breakthrough," *The European Journal of Esthetic Dentistry*, vol. 4, no. 4, pp. 348–380, 2009.

[7] K. Onodera, K. Ooya, and H. Kawamura, "Titanium lymph node pigmentation in the reconstruction plate system of a mandibular bone defect," *Oral Surgery, Oral Medicine, Oral Pathology*, vol. 75, no. 4, pp. 495–497, 1993.

[8] J. J. Jacobs, A. K. Skipor, L. M. Patterson et al., "Metal release in patients who have had a primary total hip arthroplasty: a prospective, controlled, longitudinal study," *Journal of Bone and Joint Surgery A*, vol. 80, no. 10, pp. 1447–1458, 1998.

[9] R.-J. Kohal, S. B. M. Patzelt, F. Butz, and H. Sahlin, "One-piece zirconia oral implants: one-year results from a prospective case series. 2. Three-unit fixed dental prosthesis (FDP) reconstruction," *Journal of Clinical Periodontology*, vol. 40, no. 5, pp. 553–562, 2013.

[10] C. Larsson and P. Vult von Steyern, "Five-year follow-up of implant-supported Y-TZP and ZTA fixed dental prostheses. A randomized, prospective clinical trial comparing two different material systems," *The International Journal of Prosthodontics*, vol. 23, no. 6, pp. 555–561, 2010.

[11] H. Schliephake, T. Hefti, F. Schlottig, P. Gédet, and H. Staedt, "Mechanical anchorage and peri-implant bone formation of surface-modified zirconia in minipigs," *Journal of Clinical Periodontology*, vol. 37, no. 9, pp. 818–828, 2010.

[12] S. Zinelis, A. Thomas, K. Syres, N. Silikas, and G. Eliades, "Surface characterization of zirconia dental implants," *Dental Materials*, vol. 26, no. 4, pp. 295–305, 2010.

[13] H. J. Wenz, J. Bartsch, S. Wolfart, and M. Kern, "Osseointegration and clinical success of zirconia dental implants: a systematic review," *International Journal of Prosthodontics*, vol. 21, no. 1, pp. 27–36, 2008.

[14] J. Zhou, J. Mah, P. Shrotriya, C. Mercer, and W. O. Soboyejo, "Contact damage in an yttria stabilized zirconia: implications," *Journal of Materials Science: Materials in Medicine*, vol. 18, no. 1, pp. 71–78, 2007.

[15] S. Deville, G. Guénin, and J. Chevalier, "Martensitic transformation in zirconia part II. Martensite growth," *Acta Materialia*, vol. 52, no. 19, pp. 5709–5721, 2004.

[16] S. Deville and J. Chevalier, "Martensitic relief observation by atomic force microscopy in yttria-stabilized zirconia," *Journal of the American Ceramic Society*, vol. 86, no. 12, pp. 2225–2227, 2003.

[17] J. Chevalier, B. Cales, and J. M. Drouin, "Low-temperature aging of Y-TZP ceramics," *Journal of the American Ceramic Society*, vol. 82, no. 8, pp. 2150–2154, 1999.

[18] J. Chevalier, L. Gremillard, and S. Deville, "Low-temperature degradation of zirconia and implications for biomedical implants," *Annual Review of Materials Research*, vol. 37, pp. 1–32, 2007.

[19] S. Lawson, "Environmental degradation of zirconia ceramics," *Journal of the European Ceramic Society*, vol. 15, no. 6, pp. 485–502, 1995.

[20] X. Guo, "On the degradation of zirconia ceramics during low-temperature annealing in water or water vapor," *Journal of Physics and Chemistry of Solids*, vol. 60, no. 4, pp. 539–546, 1999.

[21] C. Piconi and G. Maccauro, "Zirconia as a ceramic biomaterial," *Biomaterials*, vol. 20, no. 1, pp. 1–25, 1999.

[22] Y. Kawai, M. Uo, Y. Wang, S. Kono, S. Ohnuki, and F. Watari, "Phase transformation of zirconia ceramics by hydrothermal degradation," *Dental Materials Journal*, vol. 30, no. 3, pp. 286–292, 2011.

[23] J. Chevalier, "What future for zirconia as a biomaterial?" *Biomaterials*, vol. 27, no. 4, pp. 535–543, 2006.

[24] R. B. Osman, M. V. Swain, M. Atieh, S. Ma, and W. Duncan, "Ceramic implants (Y-TZP): are they a viable alternative to titanium implants for the support of overdentures? A randomized clinical trial," *Clinical Oral Implants Research*, 2013.

[25] G. Maccauro, G. Bianchino, S. Sangiorgi et al., "Development of a new zirconia-toughened alumina: promising mechanical

properties and absence of in vitro carcinogenicity," *International Journal of Immunopathology and Pharmacology*, vol. 22, no. 3, pp. 773–779, 2009.

[26] S. F. Yang, L. Q. Yang, Z. H. Jin, T. W. Guo, L. Wang, and H. C. Liu, "New nano-sized Al_2O_3-BN coating 3Y-TZP ceramic composites for CAD/CAM-produced all-ceramic dental restorations. Part I. Fabrication of powders," *Nanomedicine: Nanotechnology, Biology and Medicine*, vol. 5, no. 2, pp. 232–239, 2009.

[27] D. J. Kim, M. H. Lee, D. Y. Lee, and J. S. Han, "Mechanical properties, phase stability, and biocompatibility of (Y,Nb)-TZP/Al_2O_3 composite abutments for dental implant," *Journal of Biomedical Materials Research*, vol. 53, no. 4, pp. 438–443, 2000.

[28] S. Affatato, M. Testoni, G. L. Cacciari, and A. Toni, "Mixed-oxides prosthetic ceramic ball heads. Part II: effect of the ZrO2 fraction on the wear of ceramic on ceramic joints," *Biomaterials*, vol. 20, no. 20, pp. 1925–1929, 1999.

[29] A. H. de Aza, J. Chevalier, G. Fantozzi, M. Schehl, and R. Torrecillas, "Crack growth resistance of alumina, zirconia and zirconia toughened alumina ceramics for joint prostheses," *Biomaterials*, vol. 23, no. 3, pp. 937–945, 2002.

[30] J. R. Kelly and I. Denry, "Stabilized zirconia as a structural ceramic: an overview," *Dental Materials*, vol. 24, no. 3, pp. 289–298, 2008.

[31] I. Denry and J. R. Kelly, "State of the art of zirconia for dental applications," *Dental Materials*, vol. 24, no. 3, pp. 299–307, 2008.

[32] S. Deville, J. Chevalier, G. Fantozzi et al., "Low-temperature ageing of zirconia-toughened alumina ceramics and its implication in biomedical implants," *Journal of the European Ceramic Society*, vol. 23, no. 15, pp. 2975–2982, 2003.

[33] T. Kokubo and H. Takadama, "How useful is SBF in predicting in vivo bone bioactivity?" *Biomaterials*, vol. 27, no. 15, pp. 2907–2915, 2006.

[34] D. K. Pattanayak, T. Kawai, T. Matsushita, H. Takadama, T. Nakamura, and T. Kokubo, "Effect of HCl concentrations on apatite-forming ability of NaOH-HCl- and heat-treated titanium metal," *Journal of Materials Science: Materials in Medicine*, vol. 20, no. 12, pp. 2401–2411, 2009.

[35] M. G. Faga, A. Vallée, A. Bellosi et al., "Chemical treatment on alumina-zirconia composites inducing apatite formation with maintained mechanical properties," *Journal of the European Ceramic Society*, vol. 32, no. 10, pp. 2113–2120, 2012.

[36] H.-C. Ko, J.-S. Han, M. Bächle, J.-H. Jang, S.-W. Shin, and D.-J. Kim, "Initial osteoblast-like cell response to pure titanium and zirconia/alumina ceramics," *Dental Materials*, vol. 23, no. 11, pp. 1349–1355, 2007.

[37] U. Covani, C. Bortolaia, A. Barone, and L. Sbordone, "Buccolingual crestal bone changes after immediate and delayed implant placement," *Journal of Periodontology*, vol. 75, no. 12, pp. 1605–1612, 2004.

[38] J. Cosyn, N. Hooghe, and H. de Bruyn, "A systematic review on the frequency of advanced recession following single immediate implant treatment," *Journal of Clinical Periodontology*, vol. 39, no. 6, pp. 582–589, 2012.

[39] L. Den Hartog, J. J. R. H. Slater, A. Vissink, H. J. A. Meijer, and G. M. Raghoebar, "Treatment outcome of immediate, early and conventional single-tooth implants in the aesthetic zone: a systematic review to survival, bone level, soft-tissue, aesthetics and patient satisfaction," *Journal of Clinical Periodontology*, vol. 35, no. 12, pp. 1073–1086, 2008.

[40] J. B. Quinn and G. D. Quinn, "A practical and systematic review of Weibull statistics for reporting strengths of dental materials," *Dental Materials*, vol. 26, no. 2, pp. 135–147, 2010.

[41] A. H. de Aza, J. Chevalier, G. Fantozzi, M. Schehl, and R. Torrecillas, "Slow-crack-growth behavior of zirconia-toughened alumina ceramicsprocessed by different methods," *Journal of the American Ceramic Society*, vol. 86, no. 1, pp. 115–120, 2003.

[42] G. Schierano, R. A. Canuto, R. Navone et al., "Biological factors involved in the osseointegration of oral titanium implants with different surfaces: a pilot study in minipigs," *Journal of Periodontology*, vol. 76, no. 10, pp. 1710–1720, 2005.

[43] P. Schüpbach, R. Glauser, A. Rocci et al., "The human bone-oxidized titanium implant interface: a light microscopic, scanning electron microscopic, back-scatter scanning electron microscopic, and energy-dispersive X-ray study of clinically retrieved dental implants," *Clinical Implant Dentistry and Related Research*, vol. 7, no. 1, pp. S36–S43, 2005.

[44] G. E. Romanos and C. B. Johansson, "Immediate loading with complete implant-supported restorations in an edentulous heavy smoker: histologic and histomorphometric analyses," *The International Journal of Oral & Maxillofacial Implants*, vol. 20, no. 2, pp. 282–290, 2005.

[45] R. Crespi, P. Capparé, E. Gherlone, and G. E. Romanos, "Immediate versus delayed loading of dental implants placed in fresh extraction sockets in the maxillary esthetic zone: a clinical comparative study," *International Journal of Oral and Maxillofacial Implants*, vol. 23, no. 4, pp. 753–758, 2008.

[46] V. Borsari, G. Giavaresi, M. Fini et al., "Physical characterization of different-roughness titanium surfaces, with and without hydroxyapatite coating, and their effect on human osteoblast-like cells," *Journal of Biomedical Materials Research B: Applied Biomaterials*, vol. 75, no. 2, pp. 359–368, 2005.

[47] D. M. D. Ehrenfest, P. G. Coelho, B.-S. Kang, Y.-T. Sul, and T. Albrektsson, "Classification of osseointegrated implant surfaces: materials, chemistry and topography," *Trends in Biotechnology*, vol. 28, no. 4, pp. 198–206, 2010.

[48] N. P. Lang and S. Jepsen, "Implant surfaces and design (Working Group 4)," *Clinical Oral Implants Research*, vol. 20, no. 4, pp. 228–231, 2009.

[49] G. Preti, G. Martinasso, B. Peirone et al., "Cytokines and growth factors involved in the osseointegration of oral titanium implants positioned using piezoelectric bone surgery versus a drill technique: a pilot study in minipigs," *Journal of Periodontology*, vol. 78, no. 4, pp. 716–722, 2007.

[50] A. Vallée, M. G. Faga, F. Mussano et al., "Alumina-zirconia composites functionalized with laminin-1 and laminin-5 for dentistry: effect of protein adsorption on cellular response," *Colloids and Surfaces B: Biointerfaces*, vol. 114, pp. 284–293, 2014.

Hindawi Publishing Corporation
BioMed Research International
Volume 2015, Article ID 365014, 9 pages
http://dx.doi.org/10.1155/2015/365014

Research Article

Regulation of Osteoblast Differentiation by Acid-Etched and/or Grit-Blasted Titanium Substrate Topography Is Enhanced by 1,25$(OH)_2D_3$ in a Sex-Dependent Manner

Rene Olivares-Navarrete,[1] Sharon L. Hyzy,[1] Barbara D. Boyan,[1,2] and Zvi Schwartz[1,3]

[1]*Department of Biomedical Engineering, School of Engineering, Virginia Commonwealth University, 601 W. Main Street, Richmond, VA 23284, USA*
[2]*Department of Biomedical Engineering, Georgia Institute of Technology, 313 Ferst Drive NW, Atlanta, GA 30332, USA*
[3]*Department of Periodontics, University of Texas Health Science Center at San Antonio, 7703 Floyd Curl Drive, San Antonio, TX 78229, USA*

Correspondence should be addressed to Barbara D. Boyan; bboyan@vcu.edu

Received 25 July 2014; Accepted 14 September 2014

Academic Editor: Seong-Hun Kim

This study assessed contributions of micron-scale topography on clinically relevant titanium (Ti) to differentiation of osteoprogenitor cells and osteoblasts; the interaction of this effect with 1α,25-dihydroxyvitamin D_3 (1α,25$(OH)_2D_3$); and if the effects are sex-dependent. Male and female rat bone marrow cells (BMCs) were cultured on acid-etched (A, R_a = 0.87 μm), grit-blasted (GB, R_a = 3.90 μm), or grit-blasted/acid-etched (SLA, R_a = 3.22 μm) Ti. BMCs were sensitive to surface topography and underwent osteoblast differentiation. This was greatest on SLA; acid etching and grit blasting contributed additively. Primary osteoblasts were also sensitive to SLA, with less effect from individual structural components, demonstrated by enhanced local factor production. Sex-dependent responses of BMCs to topography varied with parameter whereas male and female osteoblasts responded similarly to surface treatment. 1α,25$(OH)_2D_3$ enhanced cell responses on all surfaces similarly. Effects were sex-dependent and male cells grown on a complex microstructured surface were much more sensitive than female cells. These results indicate that effects of the complex SLA topography are greater than acid etching or grit blasting alone on multipotent BMCs and committed osteoblasts and that individual parameters are sex-specific. The effect of 1α,25$(OH)_2D_3$ was sex dependent. The results also suggest that levels of 1α,25$(OH)_2D_3$ in the patient may be important in osseointegration.

1. Introduction

Current dental practice employs implants with a variety of surface modifications, yielding improved bone-to-implant contact and patient outcomes. Alterations in surface microtopography change the adsorption of proteins to the implant surface, which also affects cell attachment and differentiation [1–3]. Many studies, including those from our group, have shown that surface microroughness influences osteoblast response [4–6]. A series of studies assessing the role of specific surface properties using electro-micromachined, acid-etched, or grit-blasted/acid-etched titanium (Ti) substrates showed that the greatest osteoblast differentiation was present on the more topographically complex surfaces, with both micron- and submicron-scale features [7–9].

For an implant to become osseointegrated, cells that migrate to the area must attach to the surface and then differentiate into mature osteoblasts. Recently, we demonstrated that commercially available human mesenchymal stem cells are also sensitive to Ti surface microtopography and exhibit osteoblast differentiation even in the absence of media supplements typically used to promote mineralized bone nodule formation [6]. Wnt5a mediated the effects of the surface through the noncanonical Wnt signaling pathway [10]. Stangl et al. [11] showed that a human fetal osteoblast cell line responded preferentially to changes in microtopography

of commercially pure Ti surfaces, indicating that progenitor cells in the osteoblast lineage are affected as well.

Grit blasting and acid etching are widely used in combination to modify titanium implants. Grit blasting imparts macron- and micron-scale topographic structures on implant surfaces, while acid etching creates micron-, submicron-, and nanoscale topographies. The application of these two techniques in combination creates implant surfaces with a complex topography that has been well studied in osseointegration *in vivo* [12, 13] and osteoblasts *in vitro* [14]. These studies demonstrate that the topographical features of Ti surfaces affect differentiation of osteoprogenitor cells and maturation of osteoblast lineage cells. However, less is known about the individual contributions of these substrate features to directing osteoblastic differentiation of progenitor cells or maturation of committed osteoblasts.

Several reports have shown surface-dependent differences of osteoblasts in response to osteotropic hormones such as 1α,25-dihydroxyvitamin D_3 (1α,25$(OH)_2D_3$) [15–18]. Interestingly, not only are responses to 1α,25$(OH)_2D_3$ on complex microstructured surfaces greater than on smooth surfaces, but there are sex-specific differences in hormone responses as well. Our group has demonstrated that calvarial osteoblasts from male donors exhibit a more robust response to 1α,25$(OH)_2D_3$ than cells from female donors, increasing important osteogenic markers as well as soluble factors that increase the angiogenic and osteogenic microenvironment [15]. Similarly, sex-specific responses to a variety of stimuli have been observed in myotubes [19], angiogenesis [20], spleen, and thymus [21, 22]. These observations suggest that osteoblast cells may also respond to surface roughness modifications in a sex-dependent manner.

The aim of the present study was to evaluate the role of topographic surface features in osteogenic differentiation of rat bone marrow stromal cells (BMCs) and in the maturation of rat calvarial osteoblasts and to assess whether the effects of specific surface treatments, either alone or in combination, are sex-dependent. In addition, we examine how treatment with 1α,25$(OH)_2D_3$ modifies the responses of male and female primary cells to these surface topographies.

2. Materials and Methods

2.1. Preparation and Characterization of Ti Disks. Titanium (Ti) disks were prepared from 1 mm thick sheets of grade 2 unalloyed Ti (ASTM F67 "Unalloyed Titanium for Surgical Implant Applications") with a 15 mm diameter to fit in a 24-well culture plate as previously described [16, 23, 24]. Briefly, disks were washed in acetone and processed through a 2% ammonium fluoride, 2% hydrofluoric acid, and 10% nitric acid solution at 55°C for 30 s to pretreat Ti disks. Submicron-scale rough (A) surfaces were produced by treating pretreated disks with heated, concentrated acid, resulting in R_a of 870 nm. GB surfaces were produced by coarse grit blasting with 0.25–0.50 mm corundum grit at 5 bars until the surface reached a uniform gray tone pretreatment disks (R_a = 3.90 μm). To produce disks with a mixed topography (SLA), grit-blasted disks were acid-etched (R_a = 3.22 μm). Scanning electron microscopic images and surface characterization have been described previously [8, 14].

2.2. Bone Marrow Cell Isolation and Response. Bone marrow cells (BMCs) were isolated from the tibias and femurs of 100–125 gram male and female Sprague-Dawley rats under Georgia Institute of Technology Institutional Animal Care and Use Committee Protocols and following appropriate guidelines. For each sex, marrow was isolated and pooled from the tibias and femurs of four animals. Marrow was flushed from the intramedullary canal of each bone into a sterile conical tube using a 5 mL syringe and 18-gauge needle. Marrow was briefly incubated with Collagenase IA (Sigma Aldrich, St. Louis, MO) to release the cells from the matrix. The cells were pelleted and plated in a flask for expansion. Cells were cultured in Mesenchymal Stem Cell Growth Media (Lonza Biosciences, Walkersville, MD). At first passage, cells were plated on tissue culture polystyrene (TCPS) or Ti surfaces (A, GB, SLA) at 5,000 cells/cm^2 (based on a 15 mm diameter smooth surface) and grown to confluence on TCPS, typically after 7 days. At confluence, media were changed and cells incubated for an additional 24 hours.

2.3. Rat Osteoblast Cultures. Osteoblasts were isolated from frontal and parietal (calvaria) bones of 100–125 gram male and female Sprague-Dawley rats using enzymatic isolation as described previously [25]. Briefly, rat bones cleaned of periosteum and soft tissues were cut into 1-2 mm^2 pieces. The bone chips were washed three times in Hank's balanced salt solution (HBSS, Invitrogen, Carlsbad, CA) containing 3% penicillin-streptomycin (Invitrogen). After washing, bone chips were digested with an enzymatic cocktail of collagenase IA and dispase (Invitrogen) in HBSS for 1 hour at 37°C. The supernatants of the first two digestions were discarded to avoid contamination by fibroblasts. The bone chips were digested three more times using the same method; at each step, the digestion media were collected and quenched with Dulbecco's modification of Eagle's medium (DMEM, cellgro, Manassas, VA) supplemented with 10% fetal bovine serum (Thermo Fisher HyClone, Waltham, MA) and 1% penicillin-streptomycin (Invitrogen). Calvaria from eight rats per sex were pooled for each experiment.

To confirm osteoblastic phenotype of isolated rat calvarial cells, we also examined cell responses to 24-hour treatment with the osteotropic hormone 1α,25$(OH)_2D_3$ (Enzo Life Sciences, Plymouth Meeting, PA) after confluence on TCPS. Both male and female rat cells exhibited dose-dependent decreases in cell number and increased alkaline phosphatase specific activity and osteocalcin levels in response to treatment with 10^{-10} M, 10^{-9} M, and 10^{-8} M 1α,25$(OH)_2D_3$ (data not shown).

Validated rat osteoblasts were plated on TCPS or Ti surfaces at a density of 10,000 cells per cm^2. Media were exchanged at 24 hours and then every 48 hours until the cells reached confluence on TCPS. At confluence, the cells were treated with vehicle (0.001% ethanol) or 10^{-8} M 1α,25$(OH)_2D_3$ for 24 hours and harvested as described below.

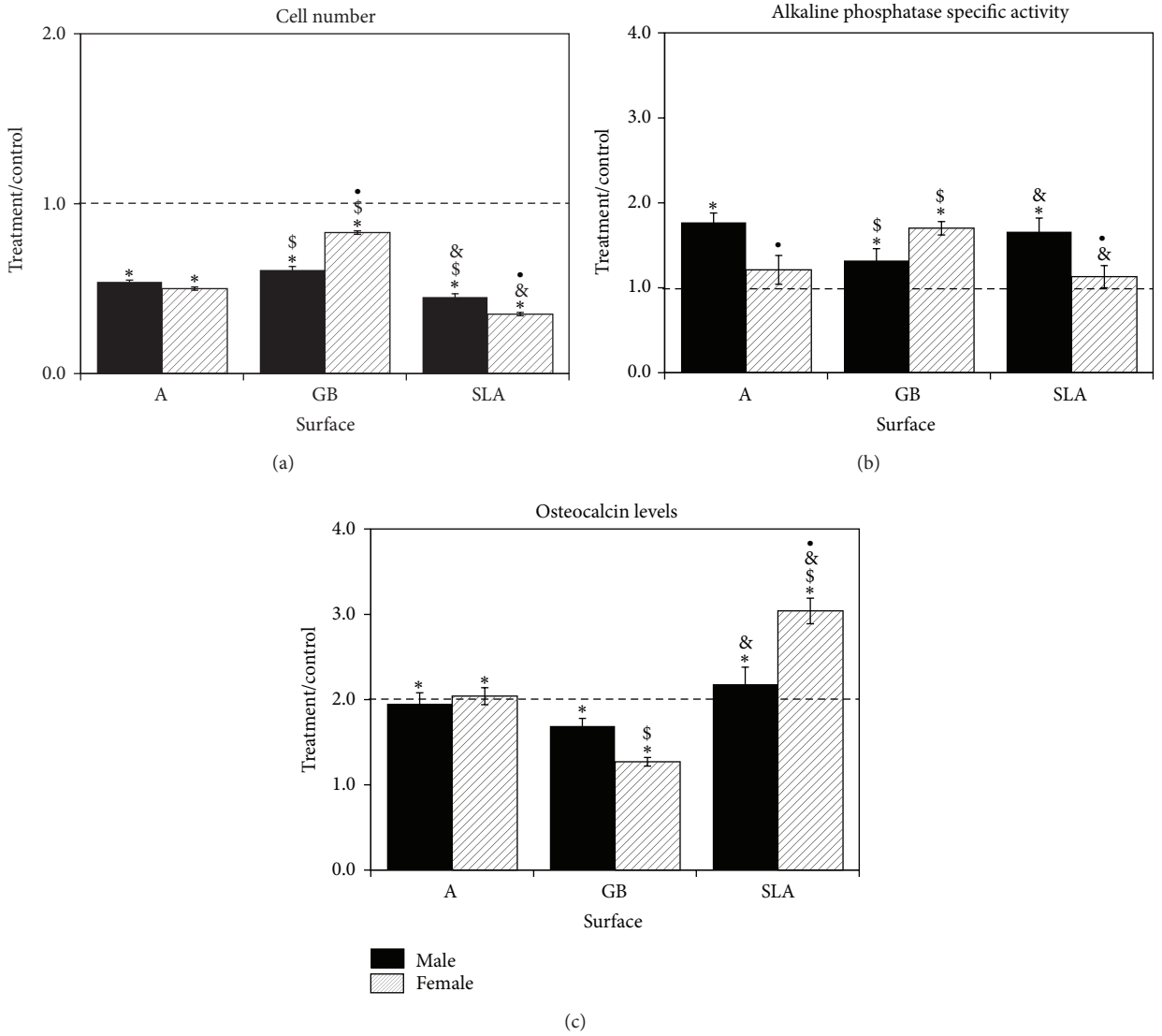

Figure 1: Response of rat BMCs to microstructured titanium surfaces. Male and female BMCs were cultured on TCPS, A, GB, or SLA surfaces and grown to confluence. Cell number (a), alkaline phosphatase specific activity (b), and osteocalcin levels (c) were measured. Data are displayed as treatment/control of cells on Ti surfaces to cells on TCPS. $^{*}P < 0.05$ versus TCPS; $^{\$}P < 0.05$ versus A surface; $^{\&}P < 0.05$ versus GB; $^{\bullet}P < 0.05$, female versus male.

2.4. Biochemical and Immunoassays. Cell number was determined in all cultures 24 hours after cells on TCPS reached confluence. Cells were released from the surfaces using two sequential 10 m incubations in 0.25% trypsin at 37°C, to ensure that any remaining cells were removed from rough Ti surfaces, and counted using an automatic cell counter (Z1 Particle Counter, Beckman Coulter, Fullerton, CA). Osteoblast differentiation and maturation were evaluated using alkaline phosphatase specific activity as an early marker and osteocalcin secretion as a later marker [26]. Cellular alkaline phosphatase specific activity (orthophosphoric monoester phosphohydrolase, alkaline; E.C. 3.1.3.1) of the cell lysates was assayed by measuring the release of *p*-nitrophenol from *p*-nitrophenylphosphate at pH 10.2 and results were normalized to total protein content of the cell lysates (Pierce BCA Protein Assay, Thermo Fisher, Rockford, IL). Levels of osteocalcin in the conditioned media were measured by immunoassay (Osteocalcin EIA, Biomedical Technologies, Stoughton, MA).

The conditioned media were also assayed for growth factors and cytokines. Active TGF-β1 was measured prior to acidification of the conditioned media, using an enzyme-linked immunosorbent assay (R&D Systems, Minneapolis, MN). Total TGF-β1 was measured after acidifying the media and latent TGF-β1 was defined as total TGF-β1 minus active TGF-β1. Osteoprotegerin (OPG) was measured using an ELISA kit (DuoSet, R&D Systems, Minneapolis, MN). Vascular endothelial growth factor (VEGF) was measured in the conditioned media of BMCs using an ELISA kit (R&D Systems). Immunoassays were normalized to total cell number.

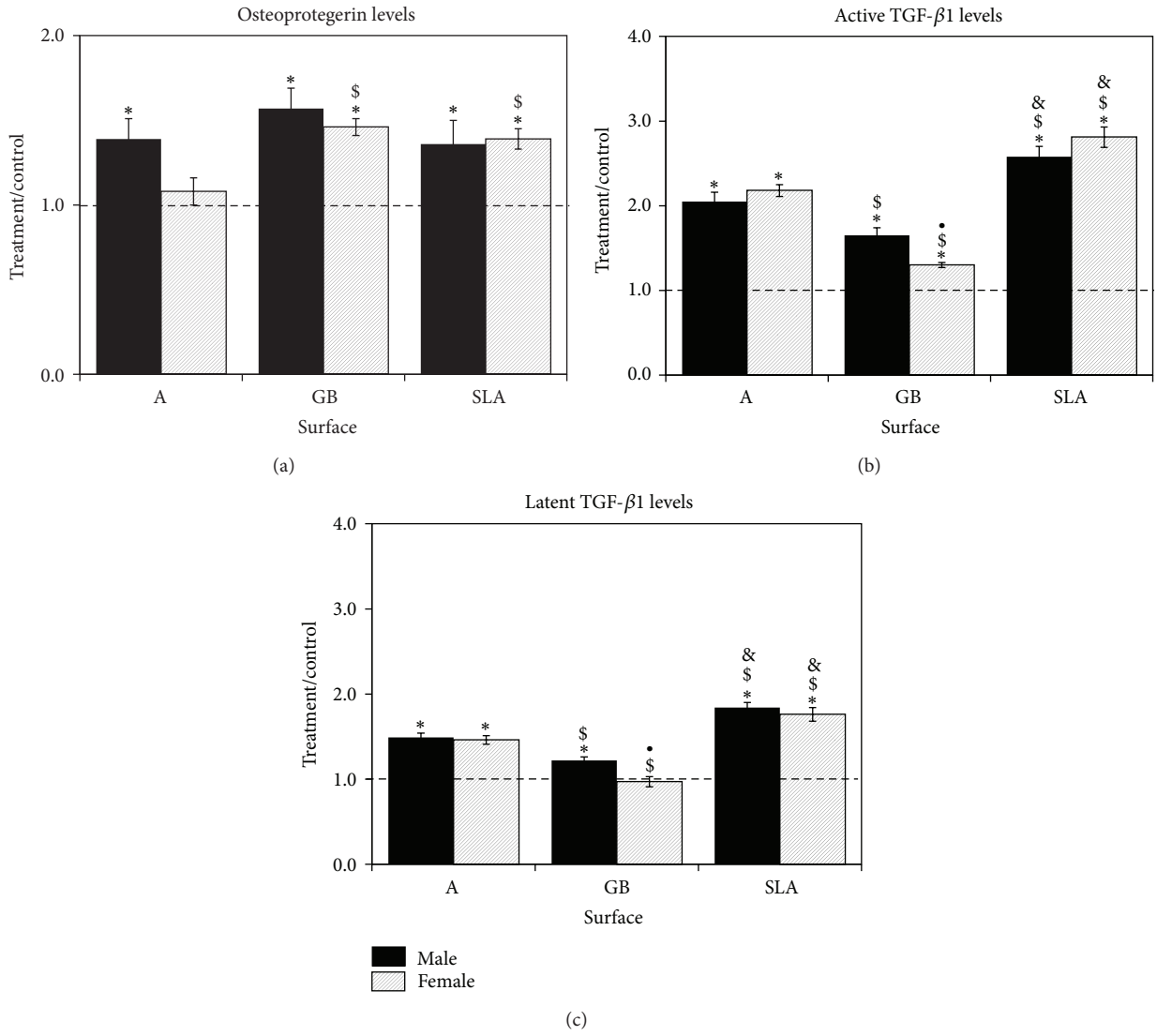

Figure 2: Response of rat BMCs to microstructured titanium surfaces. Male and female BMCs were cultured on TCPS or Ti disks and grown to confluence. OPG (a), active TGF-β1 (b), and latent TGF-β1 (c) were measured in the conditioned media. Data are displayed as treatment/control of cells on Ti surfaces to cells on TCPS. $^{*}P < 0.05$ versus TCPS; $^{\$}P < 0.05$ versus A surface; $^{\&}P < 0.05$ versus GB; $^{\bullet}P < 0.05$, female versus male.

2.5. Statistical Analysis. Data presented are treatment/control ratios from one of two experiments, both with comparable results. Responses on TCPS serve as controls. For each experiment, each variable was tested in six independent cultures. Data were first analyzed by ANOVA; when statistical differences were detected, a post hoc analysis of Bonferroni's modification of Student's t-test was used. P values <0.05 were considered to be significant.

3. Results

BMCs had lower cell number when cultured on Ti substrates in comparison to TCPS (Figure 1(a)). This effect was significantly lower on SLA compared to GB and A and significantly lower on A than GB. Female cells had higher cell number on GB and lower cell number on SLA than male cells. Alkaline phosphatase specific activity was sensitive to surface topography in a sex-specific manner (Figure 1(b)). Activity was increased in male cells on A and SLA in comparison to TCPS. However, in female BMC cultures, activity was increased only on in cells on GB. Both male and female BMCs exhibited increased osteocalcin in their conditioned media on all surfaces (SLA > A > GB) (Figure 1(c)). This effect was comparable in male and female cultures on GB surfaces, but cells isolated from female rats produced more osteocalcin on SLA than males.

OPG was increased in male cells by 30–50% on all surfaces (Figure 2(a)). Female BMCs showed a comparable increase in OPG on GB and SLA surfaces over levels on TCPS when compared to males. However, female cells cultured on A surfaces did not exhibit increased OPG in comparison to TCPS. Male BMCs produced more active (Figure 2(b)) and

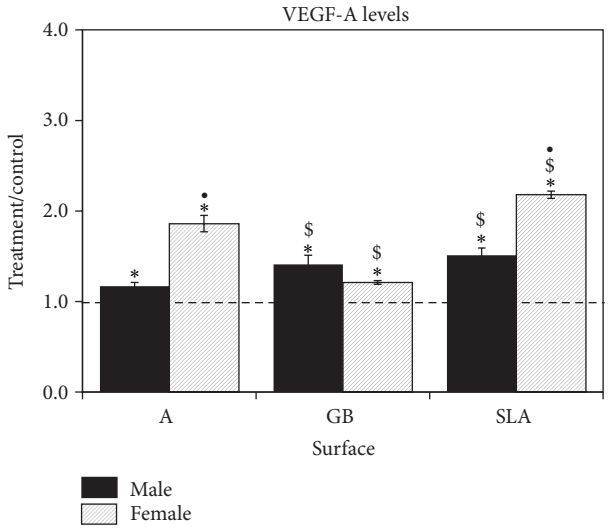

Figure 3: Response of rat BMCs to microstructured titanium surfaces. Male and female BMCs were cultured on TCPS or Ti disks and grown to confluence. VEGF was measured in the conditioned media. Data are displayed as treatment/control of cells on Ti surfaces to cells on TCPS. $^{*}P < 0.05$ versus TCPS; $^{\$}P < 0.05$ versus A surface; $^{\&}P < 0.05$ versus GB; $^{\bullet}P < 0.05$, female versus male.

latent (Figure 2(c)) TGF-β1 on all Ti substrates (SLA > A > GB) in comparison to TCPS. Female cells produced similar levels of active TGF-β1 on A and SLA in comparison to male cells; however, they secreted less active and latent TGF-β1 on GB than male cells.

VEGF was also produced in a surface-dependent, sex-specific manner by BMC cells (Figure 3). Male cells produced more VEGF on GB and SLA than on TCPS. In contrast, female cells produced more VEGF on A and SLA than on GB. Female cells produced more VEGF-A on acid-etched A and SLA surfaces than male cells.

Osteoblasts had reduced cell numbers when cultured on Ti surfaces when compared to TCPS (Figure 4(a)). This was less pronounced in cultures grown on GB surfaces compared to A and SLA surfaces and was most pronounced on SLA. 1α,25$(OH)_2D_3$ enhanced the decreased cell number of cells grown on SLA surface. In male cells on all surfaces decreased cell number but only affected female cells on SLA. Alkaline phosphatase specific activity was greater in osteoblast cultures grown on Ti substrates in comparison to TCPS (Figure 4(b)). 1α,25$(OH)_2D_3$ increased activity on all surfaces examined. Alkaline phosphatase specific activity was significantly stimulated in osteoblasts from male rats in comparison to female cells. Levels of osteocalcin in the conditioned media were higher in osteoblast cultures on all Ti surfaces compared to TCPS (Figure 4(c)). 1α,25$(OH)_2D_3$ increased osteocalcin in male and female osteoblast cultures, but the stimulatory effect was significant and more than three times greater in the male cells compared to female cells. Moreover, the stimulatory effects of 1α,25$(OH)_2D_3$ were less robust on GB than on A or SLA in the male cells.

OPG was also increased in osteoblast cultures on Ti surfaces in comparison to TCPS (SLA > A > GB) (Figure 5(a)). This was even more evident in female osteoblast cultures. 1α,25$(OH)_2D_3$ increased OPG by more than 100% in osteoblasts on all surfaces (A, SLA > GB) with no difference between male and female. The response of female osteoblasts was less robust on A and SLA but was comparable to the male cells on GB. Active TGF-β1 was increased in male and female osteoblasts on all surfaces in comparison to control (SLA < A < GB) (Figure 5(b)). Treatment with 1α,25$(OH)_2D_3$ caused significant increases in TGF-β1 in male and female cells on all surfaces (GB < A < SLA). In the untreated osteoblasts, there was no difference between male and female cells in TGF-β1 levels. However, treatment with 1α,25$(OH)_2D_3$ caused a statistically greater increase in male cells than in female cells on A and GB surfaces; however, there was no difference on SLA substrates. Latent TGF-β1 was increased in male osteoblasts on all surfaces in comparison to control and in female osteoblasts grown on A and SLA surfaces; female osteoblasts on GB surfaces were not significantly different from control (Figure 5(c)). Treatment with 1α,25$(OH)_2D_3$ increased latent TGF-β1 in male and female cells on all surfaces following a similar pattern (GB < A < SLA). Male cells had significantly higher levels of latent TGF-β1 than females on all surfaces after treatment with 1α,25$(OH)_2D_3$; untreated female osteoblasts had lower levels of TGF-β1 on GB surfaces than male cells.

4. Discussion

This study examined the effects of different clinically relevant surfaces on osteoprogenitor differentiation and osteoblast maturation. BMCs grown on Ti surfaces that were acid-etched, grit-blasted, or grit-blasted and acid-etched exhibited a similar reduction in cell number and enhancement of alkaline phosphatase activity and OPG levels. However, the SLA surface, which is the combination of acid etching and grit blasting, significantly enhanced in an additive manner the production of osteocalcin, active and latent TGF-β1, and VEGF in comparison to the other surfaces. These results using primary rat BMCs were similar to the effects of SLA on human mesenchymal stem cells obtained from Lonza that were described previously [6]. The results also demonstrated that the effect of the surface was sex-dependent for some but not all parameters. The clinical importance of this observation in females needs to be examined.

Osteoblast cultures grown on the same Ti surfaces showed similar results with respect to proliferation and maturation as BMCs: reduced proliferation and enhanced production of osteocalcin, OPG, and active and latent TGF-β1. The effects of surface topography were enhanced on SLA, as has been noted previously for the human osteoblast-like MG63 cell line [5, 16, 27]. Both male and female osteoblasts respond similarly to the different surfaces, with the exception of increased levels of OPG in cultures of female cells grown on SLA. These results may indicate that both sexes can osseointegrate well with the appropriate surface and that SLA has a better ability to enhance osteoblastic differentiation and maturation in comparison to either processing method alone.

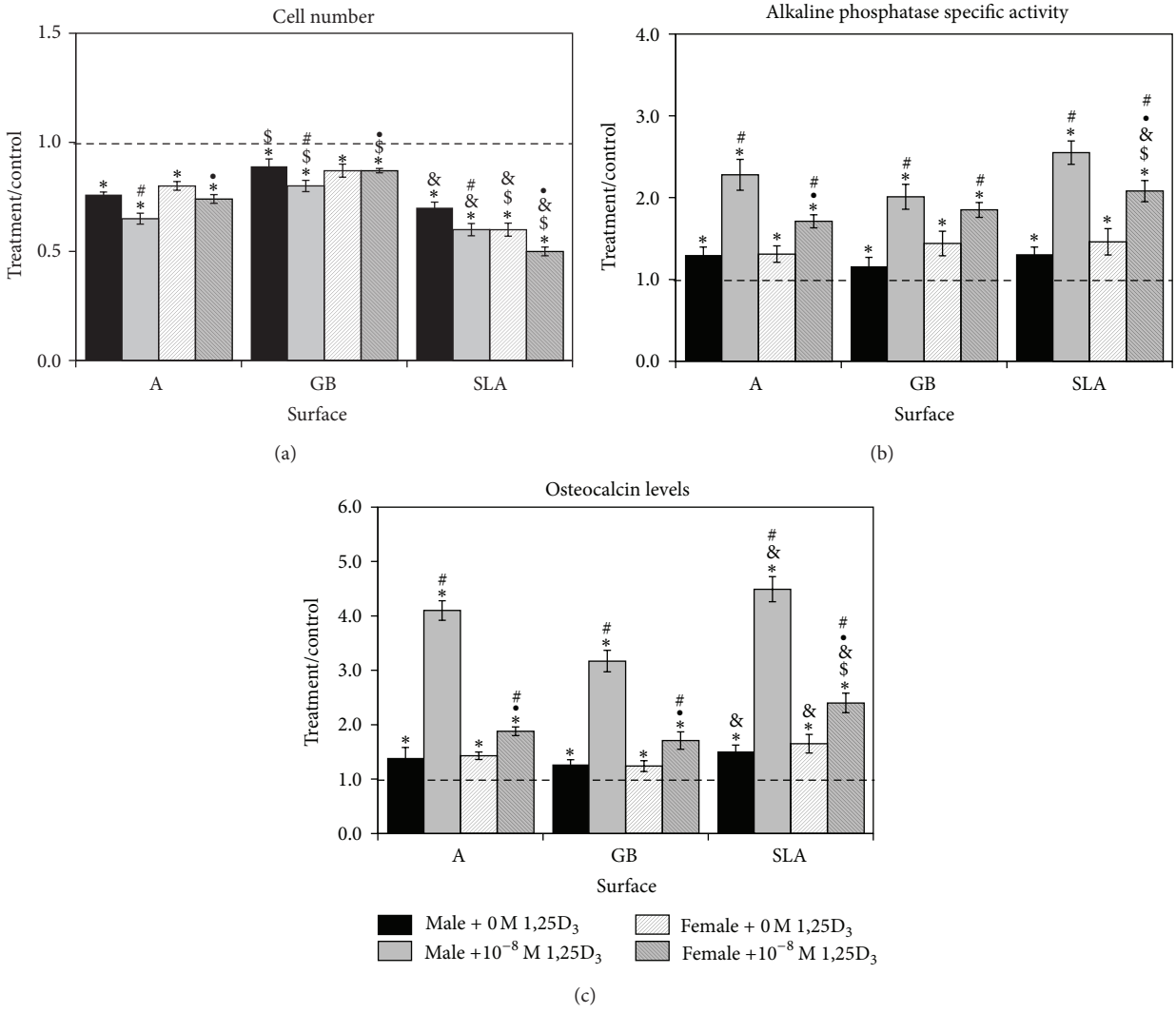

FIGURE 4: Effect of Ti surface topography with or without $1\alpha,25(OH)_2D_3$ on osteoblast differentiation of rat calvarial osteoblasts. Male and female calvarial osteoblasts were cultured on TCPS or Ti disks. At confluence, cells were treated for 24 hours with 10^{-8} M $1\alpha,25(OH)_2D_3$. Cell number (a), alkaline phosphatase specific activity (b), and osteocalcin levels (c) were measured. Data are displayed as treatment/control of cells on Ti surfaces to cells on TCPS. $^{*}P < 0.05$ versus TCPS; $^{\$}P < 0.05$ versus A surface; $^{\&}P < 0.05$ versus GB; $^{\bullet}P < 0.05$, female versus male; $^{\#}P < 0.05$ versus 0 M $1\alpha,25(OH)_2D_3$.

Establishment of a healthy vasculature is critical for implant osseointegration [28]. Both male and female cells increased levels of VEGF in response to Ti surfaces, indicating the cells have begun to signal for new vasculature in response to the surface. However, while male BMCs showed a greater increase in VEGF on GB and SLA surfaces, female BMCs increased VEGF production in response to the submicron-scale topographic features induced by acid etching. Similar studies using human alveolar osteoblasts have shown that VEGF production is increased in cells grown on A and SLA surfaces [29], and previous studies from our group showed that VEGF levels also increased in human mesenchymal stem cells and MG63 cells in response to surface topography [6, 30]. Additionally, in vitro studies have shown that androgen induced a sex-dependent effect on angiogenesis in a Matrigel assay [20].

Previously we demonstrated that fetal rat calvarial osteoblasts are more sensitive to treatment with $1\alpha,25(OH)_2D_3$ when cultured on Ti substrates [31]. In the present study, we sought to decouple the topographic features that enhanced osteoblast response to $1\alpha,25(OH)_2D_3$ using adult rat osteoblasts. The rat osteoblasts cultured on Ti respond to $1\alpha,25(OH)_2D_3$ with decreased cell number and increased alkaline phosphatase specific activity and osteocalcin production in comparison to cells cultured on TCPS. In contrast, this differential response to the vitamin D metabolite may be due to an increased maturation state of the cells grown on Ti substrates at the time of treatment, as has been demonstrated in other studies [31–33].

The effects of $1\alpha,25(OH)_2D_3$ on the rat osteoblasts were sex-dependent. Treatment with $1\alpha,25(OH)_2D_3$ increased OPG protein levels in both male and female osteoblasts,

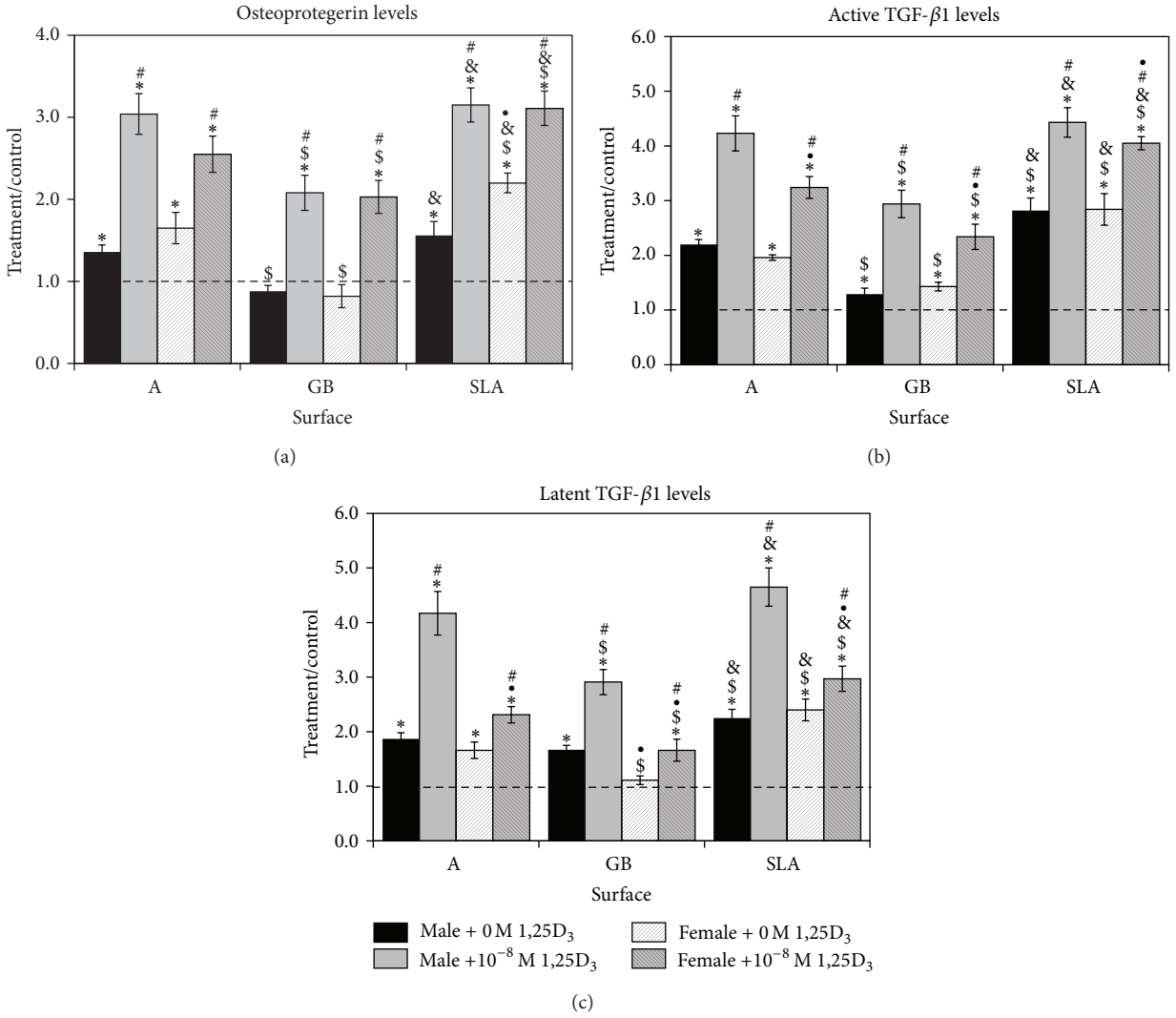

Figure 5: Effect of Ti surface topography with or without $1\alpha,25(OH)_2D_3$ on osteoblast differentiation of rat calvarial osteoblasts. Male and female calvarial osteoblasts were cultured on TCPS or Ti disks. At confluence, cells were treated for 24 hours with 10^{-8} M $1\alpha,25(OH)_2D_3$. OPG (a), active TGF-β1 (b), and latent TGF-β1 (c) were measured in the conditioned media. Data are displayed as treatment/control of cells on Ti surfaces to cells on TCPS. $^{*}P < 0.05$ versus TCPS; $^{\$}P < 0.05$ versus A surface; $^{\&}P < 0.05$ versus GB; $^{\bullet}P < 0.05$, female versus male; $^{\#}P < 0.05$ versus 0 M $1\alpha,25(OH)_2D_3$.

although this effect was greater in males. This confirms previous results in our laboratory demonstrating upregulation of OPG mRNA expression and protein levels after treatment with $1\alpha,25(OH)_2D_3$ in human osteoblast and MG63 cells cultured on SLA surfaces [15, 34]. Interestingly, treatment of male osteoblasts with $1\alpha,25(OH)_2D_3$ increased latent TGF-β1 more than active TGF-β1; in female osteoblasts, the greatest response was in active TGF-β1. Previous studies indicate that active TGF-β1 increases in response to $1\alpha,25(OH)_2D_3$ treatment, possibly due to activation of latent TGF-β1 [35, 36]. However, the dimorphism in the response suggests that in female osteoblasts $1\alpha,25(OH)_2D_3$ shifts TGF-β1 levels towards the active form to inhibit bone remodeling [37], while in male cells there is more latent TGF-β1 to allow cells to progress towards terminal osteoblast differentiation [32].

$1\alpha,25(OH)_2D_3$ enhanced osteoblast maturation and inhibited osteoblast proliferation on all surfaces. When calculated as fold increase, this effect was similar on all surfaces examined. These results indicate that each of these surfaces affects the osteoblast phenotype and makes cells more sensitive to the hormone effect.

The effect of $1\alpha,25(OH)_2D_3$ on osteoblast cells grown on rough surfaces was sex-dependent since the enhancement of all the parameters examined was significantly higher in male cells in comparison to female cells. These results are in agreement with other studies that have found that femoral neck osteoblasts from males have larger increases in osteocalcin secretion in response to $1\alpha,25(OH)_2D_3$ than female cells [38]. Clinically, vitamin D deficiency has been correlated with decreased bone mineral density in male, but not female, patients [39]. These results may indicate that

males are more sensitive to vitamin D levels and suggest that if we would like to achieve maximum osseointegration clinically, especially in compromised cases, we could examine the patient's vitamin D levels and supplement as needed if levels are outside the normal range.

The results of the present study indicate that BMCs, the first cells to recognize the surface *in vivo*, are sensitive to surface topography and can undergo osteogenic differentiation in response to surface cues. The effect was mainly in response to the complex SLA topography and the surface treatments (acid etching and grit blasting) contribute additively to this effect. BMC response to the topographies in this study exhibited sex dependence in some parameters, indicating that they are differentially regulated by both substrate structural elements and cell sex. Primary osteoblasts were also sensitive mainly to the complex SLA topography, with less effect of the individual structural components. Osteoblast response to topography was not sex-dependent to the extent seen in the BMCs. Treatment with $1\alpha,25(OH)_2D_3$ enhanced osteoblast response to the surfaces examined, with a similar fold increase on all surfaces. The response of osteoblasts to $1\alpha,25(OH)_2D_3$ is sex-dependent and male cells grown on a complex microstructure surface are much more sensitive $1\alpha,25(OH)_2D_3$ treatment.

5. Conclusions

These results demonstrate that both surface roughness and systemic hormones can affect bone formation at the implant site. While males and females have similar responses to surface roughness, they differ in production of local factors regulating bone resorption and in the magnitude of the response $1\alpha,25(OH)_2D_3$. These factors are important as future modifications are made to tailor implants to sex-specific differences to improve osseointegration and long-term implant life.

Disclosure

The funding sources had no role in study design, data collection, data analysis/interpretation, or paper publication.

Disclaimer

The content of this paper is solely the responsibility of the authors and does not necessarily represent the official views of the National Institutes of Health (NIH).

Conflict of Interests

The authors declare that there is no conflict of interests regarding the publication of this paper.

Acknowledgments

This study was supported by a grant from the ITI Foundation. The National Institute of Arthritis and Musculoskeletal and Skin Diseases of the National Institutes of Health supported research reported in this paper under award no. AR052102. Institut Straumann AG (Basel, Switzerland) provided Ti disks as a gift.

References

[1] K. Cai, J. Bossert, and K. D. Jandt, "Does the nanometre scale topography of titanium influence protein adsorption and cell proliferation?" *Colloids and Surfaces B: Biointerfaces*, vol. 49, no. 2, pp. 136–144, 2006.

[2] J. Protivínský, M. Appleford, J. Strnad, A. Helebrant, and J. L. Ong, "Effect of chemically modified titanium surfaces on protein adsorption and osteoblast precursor cell behavior," *International Journal of Oral and Maxillofacial Implants*, vol. 22, no. 4, pp. 542–550, 2007.

[3] L. Hao and J. Lawrence, "Wettability modification and the subsequent manipulation of protein adsorption on a Ti6Al4V alloy by means of CO_2 laser surface treatment," *Journal of Materials Science: Materials in Medicine*, vol. 18, no. 5, pp. 807–817, 2007.

[4] D. M. Brunette, J. Ratkay, and B. Chehroudi, *Behaviour of Osteoblasts on Micromachined Surfaces*, University of Toronto Press, Toronto, Canada, 1991.

[5] J. Y. Martin, Z. Schwartz, T. W. Hummert et al., "Effect of titanium surface roughness on proliferation, differentiation, and protein synthesis of human osteoblast-like cells (MG63)," *Journal of Biomedical Materials Research*, vol. 29, no. 3, pp. 389–401, 1995.

[6] R. Olivares-Navarrete, S. L. Hyzy, D. L. Hutton et al., "Direct and indirect effects of microstructured titanium substrates on the induction of mesenchymal stem cell differentiation towards the osteoblast lineage," *Biomaterials*, vol. 31, no. 10, pp. 2728–2735, 2010.

[7] B. D. Boyan, S. Lossdörfer, L. Wang et al., "Osteoblasts generate an osteogenic microenvironment when grown on surfaces with rough microtopographies," *European Cells and Materials*, vol. 6, pp. 22–27, 2003.

[8] G. Zhao, O. Zinger, Z. Schwartz, M. Wieland, D. Landolt, and B. D. Boyan, "Osteoblast-like cells are sensitive to submicron-scale surface structure," *Clinical Oral Implants Research*, vol. 17, no. 3, pp. 258–264, 2006.

[9] O. Zinger, G. Zhao, Z. Schwartz et al., "Differential regulation of osteoblasts by substrate microstructural features," *Biomaterials*, vol. 26, no. 14, pp. 1837–1847, 2005.

[10] R. Olivares-Navarrete, S. L. Hyzy, D. L. Hutton et al., "Role of non-canonical Wnt signaling in osteoblast maturation on microstructured titanium surfaces," *Acta Biomaterialia*, vol. 7, no. 6, pp. 2740–2750, 2011.

[11] R. Stangl, B. Rinne, S. Kastl et al., "The influence of pore geometry in CP Ti-implants—a cell culture investigation," *European Cells and Materials*, vol. 2, pp. 1–9, 2001.

[12] D. L. Cochran, P. V. Nummikoski, F. L. Higginbottom, J. S. Hermann, S. R. Makins, and D. Buser, "Evaluation of an endosseous titanium implant with a sandblasted and acid-etched surface in the canine mandible: radiographic results," *Clinical Oral Implants Research*, vol. 7, no. 3, pp. 240–252, 1996.

[13] M. M. Bornstein, H. Harnisch, A. Lussi, and D. Buser, "Clinical performance of wide-body implants with a sandblasted and acid-etched (SLA) surface: results of a 3-year follow-up study in a referral clinic," *International Journal of Oral and Maxillofacial Implants*, vol. 22, no. 4, pp. 631–638, 2007.

[14] G. Zhao, A. L. Raines, M. Wieland, Z. Schwartz, and B. D. Boyan, "Requirement for both micron- and submicron scale structure for synergistic responses of osteoblasts to substrate surface energy and topography," *Biomaterials*, vol. 28, no. 18, pp. 2821–2829, 2007.

[15] R. Olivares-Navarrete, S. L. Hyzy, R. A. Chaudhri, G. Zhao, B. D. Boyan, and Z. Schwartz, "Sex dependent regulation of osteoblast response to implant surface properties by systemic hormones," *Biology of Sex Differences*, vol. 1, no. 1, article 4, 2010.

[16] B. D. Boyan, R. Batzer, K. Kieswetter et al., "Titanium surface roughness alters responsiveness of MG63 osteoblast-like cells to 1α,25-$(OH)_2D_3$," *Journal of Biomedical Materials Research*, vol. 39, no. 1, pp. 77–85, 1998.

[17] C. H. Lohmann, E. M. Tandy, V. L. Sylvia et al., "Response of normal female human osteoblasts (NHOst) to 17β-estradiol is modulated by implant surface morphology," *Journal of Biomedical Materials Research*, vol. 62, no. 2, pp. 204–213, 2002.

[18] Z. Schwartz, B. F. Bell, L. Wang, G. Zhao, R. Olivares-Navarrete, and B. D. Boyan, "Beta-1 integrins mediate substrate dependent effects of 1α,25$(OH)_2D_3$ on osteoblasts," *The Journal of Steroid Biochemistry and Molecular Biology*, vol. 103, no. 3–5, pp. 606–609, 2007.

[19] F. Salehzadeh, A. Rune, M. Osler, and L. Al-Khalili, "Testosterone or 17beta-estradiol exposure reveals sex-specific effects on glucose and lipid metabolism in human myotubes," *Journal of Endocrinology*, vol. 210, no. 2, pp. 219–229, 2011.

[20] D. P. Sieveking, P. Lim, R. W. Y. Chow et al., "A sex-specific role for androgens in angiogenesis," *Journal of Experimental Medicine*, vol. 207, no. 2, pp. 345–352, 2010.

[21] C. Thangavel, R. N. Dhir, D. V. Volgin, and B. H. Shapiro, "Sex-dependent expression of CYP2C11 in spleen, thymus and bone marrow regulated by growth hormone," *Biochemical Pharmacology*, vol. 74, no. 10, pp. 1476–1484, 2007.

[22] Y. Almaden, A. J. Felsenfeld, M. Rodriguez et al., "Proliferation in hyperplastic human and normal rat parathyroid glands: role of phosphate, calcitriol, and gender," *Kidney International*, vol. 64, no. 6, pp. 2311–2317, 2003.

[23] G. Zhao, Z. Schwartz, M. Wieland et al., "High surface energy enhances cell response to titanium substrate microstructure," *Journal of Biomedical Materials Research—Part A*, vol. 74, no. 1, pp. 49–58, 2005.

[24] F. Rupp, L. Scheideler, N. Olshanska, M. de Wild, M. Wieland, and J. Geis-Gerstorfer, "Enhancing surface free energy and hydrophilicity through chemical modification of microstructured titanium implant surfaces," *Journal of Biomedical Materials Research A*, vol. 76, pp. 323–334, 2006.

[25] C. G. Bellows, J. E. Aubin, H. N. M. Heersche, and M. E. Antosz, "Mineralized bone nodules formed in vitro from enzymatically released rat calvaria cell populations," *Calcified Tissue International*, vol. 38, no. 3, pp. 143–154, 1986.

[26] J. B. Lian, G. S. Stein, J. L. Stein, and A. J. van Wijnen, "Transcriptional control of osteoblast differentiation," *Biochemical Society Transactions*, vol. 26, no. 1, pp. 14–21, 1998.

[27] K. Kieswetter, Z. Schwartz, T. W. Hummert et al., "Surface roughness modulates the local production of growth factors and cytokines by osteoblast-like MG-63 cells," *Journal of Biomedical Materials Research*, vol. 32, no. 1, pp. 55–63, 1996.

[28] B. Frerich, N. Lindemann, J. Kurtz-Hoffmann, and K. Oertel, "In vitro model of a vascular stroma for the engineering of vascularized tissues," *International Journal of Oral and Maxillofacial Surgery*, vol. 30, no. 5, pp. 414–420, 2001.

[29] X. Rausch-Fan, Z. Qu, M. Wieland, M. Matejka, and A. Schedle, "Differentiation and cytokine synthesis of human alveolar osteoblasts compared to osteoblast-like cells (MG63) in response to titanium surfaces," *Dental Materials*, vol. 24, no. 1, pp. 102–110, 2008.

[30] A. L. Raines, R. Olivares-Navarrete, M. Wieland, D. L. Cochran, Z. Schwartz, and B. D. Boyan, "Regulation of angiogenesis during osseointegration by titanium surface microstructure and energy," *Biomaterials*, vol. 31, no. 18, pp. 4909–4917, 2010.

[31] C. H. Lohmann, L. F. Bonewald, M. A. Sisk et al., "Maturation state determines the response of osteogenic cells to surface roughness and 1,25-dihydroxyvitamin D3," *Journal of Bone and Mineral Research*, vol. 15, no. 6, pp. 1169–1180, 2000.

[32] L. F. Bonewald, M. B. Kester, Z. Schwartz et al., "Effects of combining transforming growth factor β and 1,25-dihydroxyvitamin D_3 on differentiation of a human osteosarcoma (MG-63)," *The Journal of Biological Chemistry*, vol. 267, no. 13, pp. 8943–8948, 1992.

[33] R. Majeska and G. A. Rodan, "The effect of 1,25(OH)2D3 on alkaline phosphatase in osteoblastic osteosarcoma cells," *The Journal of Biological Chemistry*, vol. 257, no. 7, pp. 3362–3365, 1982.

[34] S. Lossdörfer, Z. Schwartz, L. Wang et al., "Microrough implant surface topographies increase osteogenesis by reducing osteoclast formation and activity," *Journal of Biomedical Materials Research Part A*, vol. 70, no. 3, pp. 361–369, 2004.

[35] Z. Schwartz, R. Olivares-Navarrete, M. Wieland, D. L. Cochran, and B. D. Boyan, "Mechanisms regulating increased production of osteoprotegerin by osteoblasts cultured on microstructured titanium surfaces," *Biomaterials*, vol. 30, no. 20, pp. 3390–3396, 2009.

[36] A. Gurlek, M. R. Pittelkow, and R. Kumar, "Modulation of growth factor/cytokine synthesis and signaling by 1α,25-dihydroxyvitamin D_3: implications in cell growth and differentiation," *Endocrine Reviews*, vol. 23, no. 6, pp. 763–786, 2002.

[37] G. R. Mundy, "The effects of TGF-beta on bone," *Ciba Foundation Symposium*, vol. 157, pp. 137–143, 1991.

[38] M. Naves, D. Álvarez-Hernández, J. L. Fernández-Martín et al., "Effect of VDR gene polymorphisms on osteocalcin secretion in calcitriol-stimulated human osteoblasts," *Kidney International, Supplement*, vol. 63, no. 85, pp. S23–S27, 2003.

[39] J. S. Lim, K. M. Kim, Y. Rhee, and S.-K. Lim, "Gender-dependent skeletal effects of vitamin D deficiency in a younger generation," *Journal of Clinical Endocrinology and Metabolism*, vol. 97, no. 6, pp. 1995–2004, 2012.

Hindawi Publishing Corporation
BioMed Research International
Volume 2014, Article ID 742180, 7 pages
http://dx.doi.org/10.1155/2014/742180

Research Article

Surface Modifications of Dental Ceramic Implants with Different Glass Solder Matrices: *In Vitro* Analyses with Human Primary Osteoblasts and Epithelial Cells

Jana Markhoff,[1] Enrico Mick,[1] Aurica Mitrovic,[2] Juliane Pasold,[1] Katharina Wegner,[1] and Rainer Bader[1]

[1] *Department of Orthopaedics, Research Lab for Biomechanics and Implant Technology, University Medicine Rostock, Doberaner Straße 142, 18057 Rostock, Germany*
[2] *ZM Praezisionsdentaltechnik GmbH, Breite Straße 16, 18055 Rostock, Germany*

Correspondence should be addressed to Jana Markhoff; jana.markhoff@med.uni-rostock.de

Received 22 July 2014; Accepted 25 August 2014; Published 14 September 2014

Academic Editor: Seong-Hun Kim

Ceramic materials show excellent esthetic behavior, along with an absence of hypersensitivity, making them a possible alternative implant material in dental surgery. However, their surface properties enable only limited osseointegration compared to titanium implants. Within this study, a novel surface coating technique for enhanced osseointegration was investigated biologically and mechanically. Specimens of tetragonal zirconia polycrystal (TZP) and aluminum toughened zirconia (ATZ) were modified with glass solder matrices in two configurations which mainly consisted of SiO_2, Al_2O_3, K_2O, and Na_2O. The influence on human osteoblastic and epithelial cell viability was examined by means of a WST-1 assay as well as live/dead staining. A C1CP-ELISA was carried out to verify procollagen type I production. Uncoated/sandblasted ceramic specimens and sandblasted titanium surfaces were investigated as a reference. Furthermore, mechanical investigations of bilaterally coated pellets were conducted with respect to surface roughness and adhesive strength of the different coatings. These tests could demonstrate a mechanically stable implant coating with glass solder matrices. The coated ceramic specimens show enhanced osteoblastic and partly epithelial viability and matrix production compared to the titanium control. Hence, the new glass solder matrix coating could improve bone cell growth as a prerequisite for enhanced osseointegration of ceramic implants.

1. Introduction

Titanium and titanium alloys are widely used materials in dental and orthopedic replacement surgery. However, mechanical benefits, excellent biocompatibility, early osseointegration, and high corrosion resistance due to the titanium passivation oxide layer [1–4] are accompanied by the dark grey color, the gingiva eventually becoming translucent, and tissue discoloration, as well as allergic reactions and sensitivities [5–7]. Over the years, ceramics were also proven to be an adequate alternative implant material. In particular, oxide ceramics such as alumina (Al_2O_3) and zirconia (ZrO_2) enable promising osseointegration with concurrent mechanical and chemical stability, and wear and corrosion resistance are representative [8–10]. Furthermore, reduced bacterial adhesion and less plaque enrichment [9, 11], as well as a low allergic potential and esthetic appearance, indicate superiority in the field of dentistry [5, 7]. Cell adherence and thereby growth, migration, and differentiation are crucial and are influenced by implant material and surface topography [4, 12–14]. To date, *in vitro* experiments have shown controversial results with respect to increased cell behavior on either smooth or roughened titanium or ceramic implant surfaces [7, 15–17]. For improved osseointegration and secondary stability, bioglass coatings [18–20] and various implant surface modification techniques like sandblasting, acid etching, and titanium plasma spray were used [1, 4, 21].

In a preliminary study, the surface modification of ceramics with glass solder matrices was investigated with respect to the mechanical properties surface roughness and adhesive

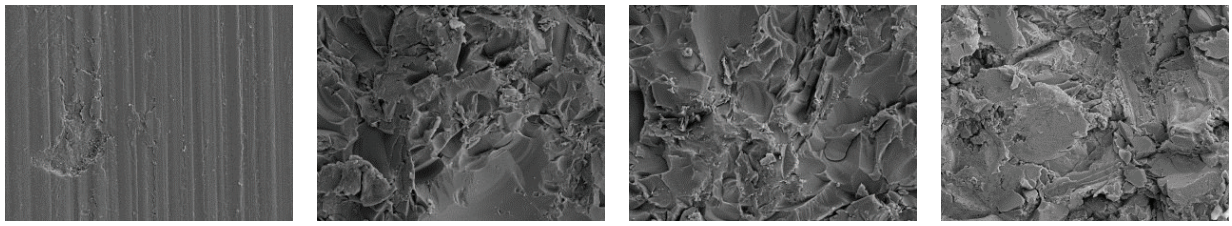

(a) (b) (c) (d)

Figure 1: Field emission scanning electron microscopy images of different specimen surfaces. (a) Native TZP-A; (b) TZP-A with glass matrix S1; (c) TZP-A with glass matrix S2; (d) rough titanium. Magnification = 1000x.

strength [22]. The present study aimed to investigate the cell biological response of human osteoblasts and gingival epithelial cells to ceramic implants coated with two different glass solder matrices. Furthermore, surface roughness, adhesive strength, and bending strength of the different glass solder matrices should be evaluated.

2. Materials and Methods

2.1. Specimens. Ceramic specimens manufactured by Metoxit AG (Thayngen, Switzerland), according to DIN EN 60267, were used for the present investigations. On the one hand, tetragonal zirconia polycrystal with alumina (TZP-A), consisting of ZrO_2, Y_2O_3, and Al_2O_3 at levels of approximately 95%, 5%, and 0.25%, was utilized, while, on the other hand, alumina-toughened zirconia (ATZ) with approximately 76% ZrO_2, 20% Al_2O_3, and 4% Y_2O_3 was tested. Two different kinds of samples were fabricated: Ø10 × 5 mm pellets were fabricated for roughness and adhesive strength testing as well as for all cell biological investigations; bending tests were performed on ceramic rods with dimensions of Ø4.3 × 60 mm.

2.2. Surface Modification. The surfaces of the ceramic specimens were modified with glasses of silica-based materials taken from the DCM hotbond series [23], which can be applied for the conditioning of mixed ceramics or pure zirconia. They mainly contain SiO_2 (60–70%), Al_2O_3 (4–10%), K_2O (6–10%), and Na_2O (6–10%). Two different configurations of the glass matrix were applied to the ceramics: S1 and S2 (equal to HT1 in [22]) with grit sizes of 9.2 μm and 12.6 μm, respectively, and curing temperatures of 1000°C and 1035°C, respectively. The application procedure is described in detail in [22]. Subsequent to that, the glass surfaces were sandblasted with corundum (Al_2O_3) at a jet pressure of 1 bar and cleaned via an ultrasonic bath (distilled water) afterwards. The pellets were coated on their cylindrical end faces and the rods were modified circumferentially.

2.3. Mechanical Investigations

2.3.1. Surface Roughness. The surface topography of bilaterally coated TZP-A pellets was determined using a profilometer (Hommel-Etamic T1000, Jenoptik AG, Jena, Germany). Surface roughness parameters (R_a and R_z) were recorded performing threefold (0°, 60°, and 120°) line scans on each coated surface. The corresponding results were referenced to untreated TZP-A, sandblasted TZP-A, and sandblasted titanium.

Furthermore, field emission scanning electron microscopy (FESEM) was conducted using the MERLIN VP Compact microscope (Carl Zeiss, Jena, Germany) to evaluate modification of the surface structure of the TZP-A pellets by two different configurations of glass matrix in comparison to untreated TZP-A and sandblasted titanium specimens.

2.3.2. Adhesive Strength. Determination of the adhesive strength of the glass solder matrices was performed consistent with Mick et al. [22]. Bilaterally coated TZP-A pellets were bonded to sandblasted titanium (grade V) cylinders using HTK Ultra Bond 100 (HTK Hamburg GmbH, Hamburg, Germany). A universal testing machine (Z050, Zwick GmbH & Co. KG, Ulm, Germany) was used for performing pull-off tests at a crosshead speed of 5 mm/min. The maximum force was measured and converted into the adhesive strength of the particular surface modification.

2.3.3. Bending Strength. In order to determine the influence of the coating procedure on the bending strength of the ceramic base bodies, 4-point-bending tests were performed on ceramic rods in the style of EN 843-1. The abovementioned universal testing machine Z050 was equipped with custom-made bearings with a support span of 40 mm and a loading span of 20 mm (see Figure 1), ensuring a constant bending moment between the load bearings. The crosshead speed was set to 0.7 mm/min, enabling failure of the rod within 60 seconds. The bending strength of each sample was derived from the maximum force and geometry of the test setup. TZP-A and ATZ rods were tested in native, sandblasted, and coated conditions. Furthermore, some samples were also tested after burning without any glass matrix on the surface to investigate the influence of mere tempering on the bending strength of TZP-A.

2.4. Cell Biological Investigations

2.4.1. Isolation and Cultivation. Isolation of human primary osteoblasts followed a previously described procedure [24]. The samples for the *in vitro* experiments were collected after patient agreement had been obtained. The

study was approved by the Local Ethical Committee (registration number: A2010-10). Human primary osteoblasts were isolated from the spongiosa of the femoral heads of patients undergoing primary total hip replacement. Cells were cultivated in osteogenic cell culture medium (Modified Eagle's Medium Dulbecco (Biochrom AG, Berlin, Germany)) containing 10% FCS, 1% penicillin/streptomycin, 1% amphotericin B, and 1% HEPES buffer (all: Gibco-Invitrogen, Darmstadt, Germany), as well as the osteogenic additives dexamethasone (100 mM), L-ascorbic acid (50 μg/mL), and β-glycerophosphate (10 mM) (all: Sigma-Aldrich, Munich, Germany) until they reached confluence. The osteogenic character of the isolated cells was verified by conducting alkaline phosphatase staining using a fuchsin + substrate chromogen (DAKO, Hamburg, Germany).

The gingival epithelial cell line Ca9-22 was ordered from the Leibniz Institute DSMZ—German Collection of Microorganisms and Cell Cultures (Brunswick, Germany). Cell cultivation was performed using Dulbecco's Modified Eagle's Medium (DMEM) supplemented with 10% FCS until cells reached confluence.

Human osteoblasts in the second passage and gingival epithelial cells (20,000 cells/500 μL each) were transferred to native ceramic specimens (TZP-A, ATZ) and ceramic specimens coated with glass solder matrices S1 and S2, as well as titanium specimens (R_z = 20 μm) as a control.

2.4.2. Analyses of Cell Viability and Matrix Production. After 96 hours of cultivation, metabolic activity of osteoblasts and epithelial cells, respectively, was determined via mitochondrial dehydrogenase activity (WST-1) (Roche, Grenzach-Wyhlen, Germany). Thereby, the tetrazolium salt WST is transformed to formazan by mitochondrial succinate dehydrogenase from the metabolically active cells. The adsorption was measured at 450 nm in a microplate reader (Opsys MRTM, Dynex Technologies GmbH, Denkendorf, Germany) and was found to be directly proportional to the metabolic cell activity. Qualitative cell viability was analyzed by means of live/dead staining with the two fluorescence dyes calcein AM for vital cells and ethidium homodimer-1 for dead ones (Live/Dead cell viability assay, Invitrogen, Darmstadt, Germany). An enzyme-linked immunosorbent assay (Metra C1CP EIA Kit, Quidel, Buende, Germany) was used to verify the synthesis of procollagen type 1 in the osteoblasts.

2.4.3. Statistical Analysis. The statistical significance of all data was evaluated by ANOVA post hoc LSD using IBM SPSS Statistics Version 20 (IBM Corp., New York, USA). Significance level was set to $P < 0.05$.

3. Results

3.1. Mechanical Investigations. The average surface roughness R_z of TZP-A samples modified with glass solder matrix S1 (20.56 ± 2.31 μm) was significantly higher than that of the references native TZP-A (1.57 ± 0.16 μm; $P < 0.001$) and sandblasted TZP-A (4.28 ± 0.61 μm; $P < 0.001$) but lower than sandblasted titanium (22.82 ± 0.61 μm; $P = 0.006$). S2 showed significantly higher average surface roughness (20.44 ± 1.23 μm [22]) compared to native and sandblasted TZP-A (each $P < 0.001$), which was lower than sandblasted titanium ($P = 0.008$). The glass solder matrices S1 and S2 did not differ significantly in average surface roughness ($P > 0.05$). The mean roughness index, R_a, showed the same tendencies and differences when comparing S1 (3.49 ± 0.20 μm) and S2 (3.61 ± 0.23 μm) to each other ($P > 0.05$) and to the reference surfaces of native TZP-A (0.20 ± 0.03 μm) and sandblasted TZP-A (0.65 ± 0.08 μm) ($P < 0.001$). However, there were no significant differences in mean roughness index when comparing S1 and S2 to sandblasted titanium (3.63 ± 0.08 μm; $P > 0.05$). Exemplary field emission scanning electron microscopy images of native and modified TZP-A specimens as well as titanium surfaces are shown in Figure 1.

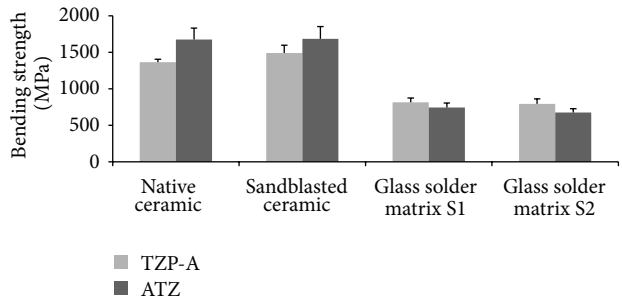

Figure 2: Bending strength of native ceramics, sandblasted ceramics, and ceramics after surface modifications (S1 and S2); $n = 5$ for TZP-A and $n = 10$ for ATZ.

Adhesive strength of the surface modification S1 was determined as 73.2 ± 7.2 MPa showing no significant difference in comparison to S2 (72.4 ± 11.8 MPa [22]; $P > 0.05$). Bending strength of native TZP-A rods (1365 ± 40 MPa) was raised significantly to 1491 ± 106 MPa due to sandblasting ($P = 0.027$). Coating with S1 led to a significant decrease (815 ± 58 MPa; $P < 0.001$). S2 showed significantly lower bending strength (793 ± 71 MPa) compared to native TZP-A ($P < 0.001$). Sandblasted ATZ specimens (1684 ± 169 MPa) did not have a significantly different bending strength than those under native conditions (1674 ± 157 MPa; $P > 0.05$). Surface modification with S1 (743 ± 62 MPa) and S2 (674.6 ± 53 MPa) resulted in significantly lower bending strength compared to native ATZ (each $P < 0.001$). For both ceramics, S1 and S2 did not differ significantly in bending strength (each $P > 0.05$). Figure 2 shows the corresponding results.

Furthermore, the comparison of native and heated sandblasted TZP-A revealed a significant decrease in bending strength to 1075 ± 82 MPa after heating ($P < 0.001$).

3.2. Cell Activity and Viability. Influence of oxide ceramics (TZP-A, ATZ) with two different glass solder matrix coatings on human osteoblasts and gingival epithelial cell lines was determined. Analysis of metabolic activity after 96 hours revealed a nonsignificant increased activity of human osteoblasts cultured on both TZP-A and ATZ ceramics with the S1 glass solder matrix compared to the titanium control and the native ceramic (Figure 3). Moreover, the glass solder

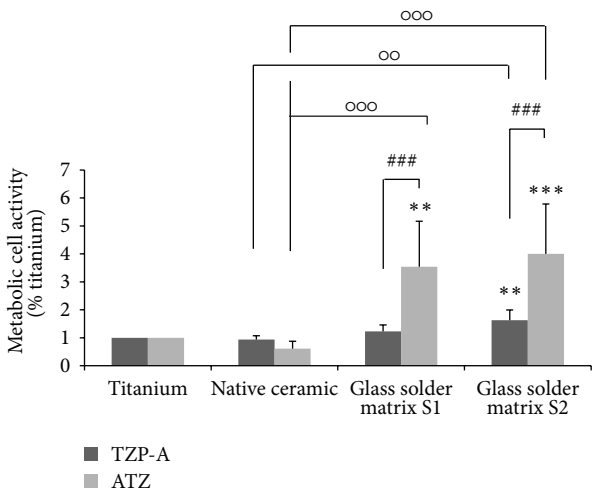

Figure 3: Metabolic activity of human osteoblasts cultured for 96 hours on specimens with different surface properties. Values are means ± SD (TZP-A $n = 15$; ATZ $n = 8$). Statistical significance levels ($^{**}P \leq 0.01$; $^{***}P \leq 0.001$) compared to titanium (∗), between the native and modified ceramics (∘) and the relative ceramic types (#).

matrix S2 with a higher grit size (12.6 μm) and burned with a higher curing temperature (1035°C) resulted in a significant increase of metabolic cell activity in contrast to the titanium control (TZP-A: $P = 0.006$; ATZ: $P \leq 0.001$) and the native ceramics (TZP-A: $P = 0.002$; ATZ: $P \leq 0.001$). Metabolic activity was significantly increased on ATZ with the glass solder matrix S1 compared to titanium ($P = 0.002$) and the native ceramic ($P = 0.001$). Furthermore, cell activity was significantly higher on ATZ over TZP-A (both: $P \leq 0.001$). At least, data indicate a slightly decreased cell viability of osteoblasts cultured on the native ceramic specimens compared to titanium.

Live/dead staining was conducted after 96 hours of cultivation to obtain a qualitative overview of bone cell viability. Thereby, living bone cells on each surface were displayed in large areas (Figure 4). Cells on the native ceramics also exhibit unsettled areas. Osteoblasts on the glass solder matrix S2 showed the highest metabolic activity in the WST-1 test.

Additionally, the gingival compatibility of the coated ceramic materials was proven with a gingival epithelial cell line (Ca9-22). Thereby, cell viability was decreased on the native and S1 coated ceramic specimens compared to titanium. Cell viability on ATZ with the glass solder matrix S2 was significantly increased compared to all other ceramic specimens (Figure 5). Live/dead staining showed large areas of cells on all specimens which were especially dense on titanium and ATZ with the glass solder matrix S2.

3.3. Collagen Synthesis. The measurement of procollagen type 1 synthesis revealed an increased matrix production for all ceramic surfaces compared to titanium (Figure 6). Thereby, synthesis on the glass solder matrix S1 on ATZ was significantly higher than on titanium ($P = 0.008$) and the native ceramic specimens ($P = 0.049$).

4. Discussion

The application of ceramic implants in the field of dentistry as an alternative to the widely used titanium has gained importance. Thereby, cellular response is dictated by the implant material and surface topography [8]. To examine the influence of material and surface topographies, osteoblasts and epithelial cells were cultivated on alumina (ATZ) and zirconia (TZP-A) ceramics in three modifications with rough titanium serving as a control. Since Mick et al. [22] found that acid etching does not improve the mechanical properties of glass ceramic coatings and Bächle et al. [11] asserted no additional effect on cellular behavior, this procedure was omitted in the present study. The native ceramic specimens with a smooth surface resulted in the lowest cell metabolic activity. This might have been caused by a lower cell attachment proven by large unsettled areas in the live/dead staining. Reduced cell adhesion on smooth surfaces was previously described [15]. In general, pointing to our material control, osteoblast adhesion and proliferation on rough titanium is ensured, pointing to the metabolic activity and live/dead staining, and has been proven in several works [1, 16, 17]. Our data exhibit the clearly increased metabolic activity of human osteoblasts on the roughened ceramic specimens coated with glass solder matrices. The advantages of ceramics, both alumina and zirconia, over titanium for osteoblasts' behavior *in vitro* were proven several times [5, 6, 8, 11, 25]. The synthesis of procollagen type 1 in human osteoblasts was increased on all ceramic specimens, mainly on modified ones, as mentioned by Depprich et al., so far [3]. Moreover, silicate-based bioglass seems to have stimulatory effects on osteoblast growth and differentiation [18]. Overall, rougher surfaces appear to be beneficial for enhanced osteoblast proliferation and adhesion [4, 8, 16, 26]. In our study, the gingival epithelial cells responded to the examined surfaces partially opposite to the osteoblasts and exhibited a slightly decreased viability and less dense cell layers on the native and S1 coated ceramic specimens, which is supported by several works [27, 28]. Nevertheless, cell viability was significantly increased on the S2 coated ceramic specimens. At the same time, the negative effects of titanium roughness on epithelial cells [21] and the preference for smooth titanium were described [28]. Continuative tests with human epithelial cells should be performed to verify the influence of materials and surface topographies. In further studies, the behavior of fibroblasts as stromal cells could also be determined. On the one hand, their adhesion and proliferation has been proven to be enhanced by rough surfaces [29, 30]. On the other hand, smoother surfaces are preferred [15], but not clearly specified for titanium or ceramic [5].

In subsequent studies, further data regarding cellular activity as alkaline phosphatase activity or expression of osteogenic marker proteins as osteocalcin should be gathered to confirm the present results. Furthermore, iterative tests with epithelial cells and also fibroblasts should be done determining collagen synthesis and GAG production. In addition, FESEM images of cell seeded ceramic specimens could be performed to analyse cell behavior or cell orientation on the different surfaces.

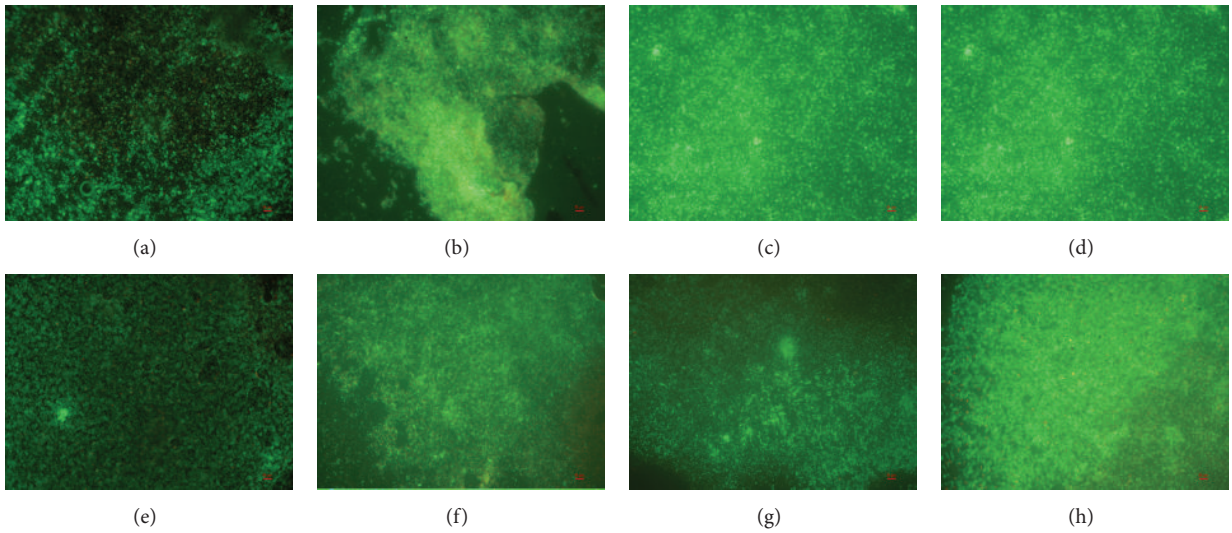

Figure 4: Live/dead staining of human osteoblasts cultured for 96 hours on specimens with different surface properties. (a)/(e) Titanium; (b) native TZP-A ceramic; (c) TZP-A with glass solder matrix S1; (d) TZP-A with S2; (f) native ATZ ceramic; (g) ATZ with S1; (h) ATZ with S2. Living cells are displayed in green and dead ones in red. Scale bar: 50 μm.

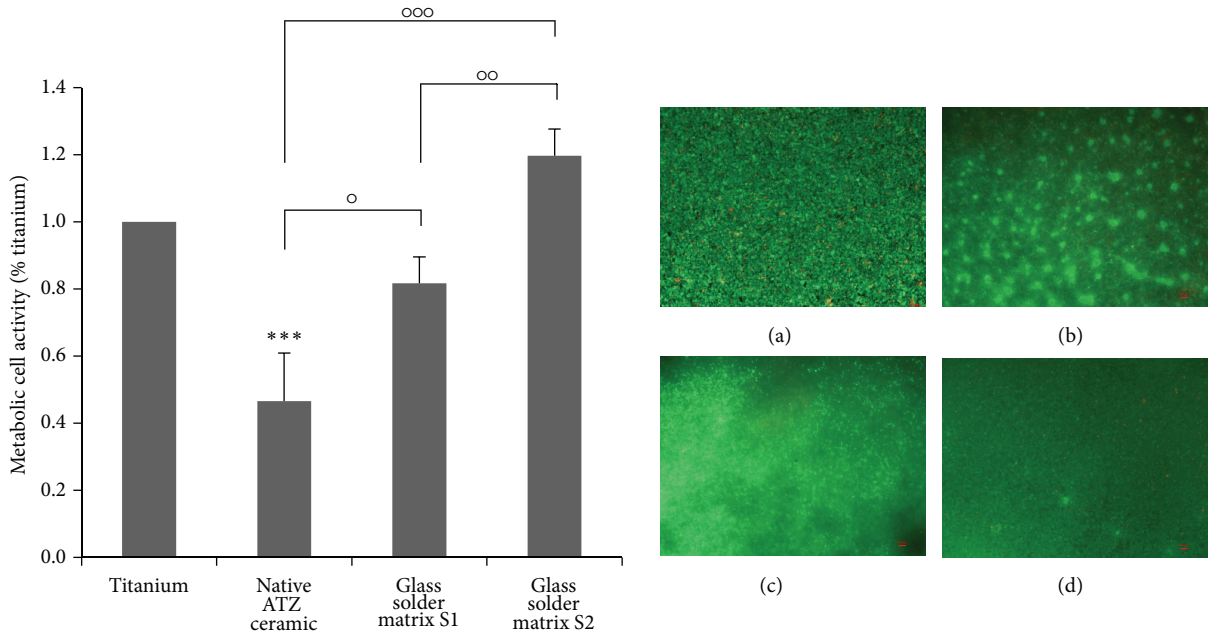

Figure 5: Left: metabolic activity of the gingival epithelial cell line Ca9-22 cultured for 96 hours on specimens with different surface properties. Values are means ± SD ($n = 4$). Statistical significance levels ($^{\circ}P \leq 0.05$; $^{\circ\circ}P \leq 0.01$; $^{***}P < 0.001$) compared to titanium ($*$) and between the native and the modified ceramics ($\circ$). Right: Live/dead staining of Ca9-22 cells cultured on (a) native titanium, (b) native ATZ ceramic, (c) ATZ with glass solder matrix S1, and (d) ATZ with glass solder matrix S2. Living cells are displayed in green and dead ones in red. Scale bar: 50 μm.

Apart from the cell biological results we found that ceramic specimens coated with glass solder matrices showed higher surface roughness values than those of the native references and sandblasted ceramics, which are comparable to sandblasted titanium, constituting a promising precondition for cellular response [31]. These findings are supported by field emission scanning electron microscopy images, which show the relatively plain surface of the native ceramic in its machined condition and in contrast the modified ceramic and titanium surfaces with comparable rough topographies.

The adhesive strength of both coating configurations is clearly below the tensile strength of the utilized bonding agent (approximately 100 MPa). However, the minimum adhesive strength of coatings as demanded by ASTM standard F-1147 is exceeded, which indicates a high stability of the glass solder matrix coatings. Furthermore, the necessary

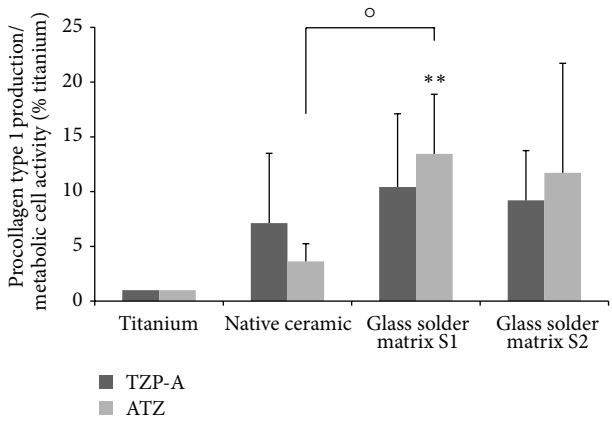

Figure 6: Synthesis of procollagen type 1 of human osteoblasts cultured for 96 hours on specimens with different surface properties. Values are means ± SD (TZP-A $n \geq 4$; ATZ $n \geq 5$). Statistical significance levels ($^{\circ}P \leq 0.05$; $^{**}P \leq 0.01$) compared to titanium ($*$) and between the native and modified ceramics ($\circ$).

preconditioning of ceramic surfaces via sandblasting prior to coating with glass was proven not to have a negative influence on the bending strength of the samples. However, the coating process itself led to a significant decrease. Application of the pure heating process to TZP-A samples showed that this huge decrease is partly generated by the influence of temperature, which is consistent with the findings of Guazzato et al. [32]. The decline in bending strength may be indicated by the structural effects of glass solder particles diffusing into the ceramic base material. This should be investigated separately. Nevertheless, the remaining bending strength of about 700 MPa to 800 MPa is still within the range of commercially available zirconia [33].

5. Conclusion

The ceramic material with glass solder matrix coating was shown to be suitable for replacing titanium as a standard implant material in dental surgery regarding mechanical properties and enhanced osteoblastic metabolic activity and collagen synthesis. Studies with human epithelial cells have revealed similar results but should be performed with other human cells like fibroblasts.

Conflict of Interests

The authors J. Markhoff, E. Mick, J. Pasold, K. Wegner, and R. Bader declare that there is no conflict of interests. A. Mitrovic is a Managing Partner of ZM Praezisionsdentaltechnik GmbH.

Acknowledgments

The content of the proposed paper was developed within the framework of a project funded by the German Ministry for Economy (BMWi) via Zentrales Innovationsprogramm Mittelstand (ZIM). Furthermore, the authors kindly thank DOT GmbH (Rostock, Germany) for conditioning the titanium cylinders for adhesive testing. The authors also thank Dental Creativ Management GmbH (Rostock, Germany) for supplying the glass solders, Metoxit AG (Thayngen, Switzerland) for supplying the ceramic specimens, and the EMZ, University Medicine Rostock, for enabling FESEM analysis.

References

[1] L. le Guehennec, M.-A. Lopez-Heredia, B. Enkel, P. Weiss, Y. Amouriq, and P. Layrolle, "Osteoblastic cell behaviour on different titanium implant surfaces," *Acta Biomaterialia*, vol. 4, no. 3, pp. 535–543, 2008.

[2] J. Marchi, V. Ussui, C. S. Delfino, A. H. A. Bressiani, and M. M. Marques, "Analysis in vitro of the cytotoxicity of potential implant materials. I: zirconia-titania sintered ceramics," *Journal of Biomedical Materials Research B: Applied Biomaterials*, vol. 94, no. 2, pp. 305–311, 2010.

[3] R. Depprich, M. Ommerborn, H. Zipprich et al., "Behavior of osteoblastic cells cultured on titanium and structured zirconia surfaces," *Head and Face Medicine*, vol. 4, no. 1, article 29, 2008.

[4] M. Bächle and R. J. Kohal, "A systematic review of the influence of different titanium surfaces on proliferation, differentiation and protein synthesis of osteoblast-like MG63 cells," *Clinical Oral Implants Research*, vol. 15, no. 6, pp. 683–692, 2004.

[5] A. Pae, H. Lee, H.-S. Kim, Y.-D. Kwon, and Y.-H. Woo, "Attachment and growth behaviour of human gingival fibroblasts on titanium and zirconia ceramic surfaces," *Biomedical Materials*, vol. 4, no. 2, Article ID 025005, 2009.

[6] R. J. Kohal, M. Baechle, J. S. Han, D. Hueren, U. Huebner, and F. Butz, "In vitro reaction of human osteoblasts on alumina-toughened zirconia," *Clinical Oral Implants Research*, vol. 20, no. 11, pp. 1265–1271, 2009.

[7] A. Noro, M. Kaneko, I. Murata, and M. Yoshinari, "Influence of surface topography and surface physicochemistry on wettability of zirconia (tetragonal zirconia polycrystal)," *Journal of Biomedical Materials Research B: Applied Biomaterials*, vol. 101, no. 2, pp. 355–363, 2013.

[8] U. Hempel, T. Hefti, M. Kalbacova, C. Wolf-Brandstetter, P. Dieter, and F. Schlottig, "Response of osteoblast-like SAOS-2 cells to zirconia ceramics with different surface topographies," *Clinical Oral Implants Research*, vol. 21, no. 2, pp. 174–181, 2010.

[9] M. Hisbergues, S. Vendeville, and P. Vendeville, "Review zirconia: established facts and perspectives for a biomaterial in dental implantology," *Journal of Biomedical Materials Research B: Applied Biomaterials*, vol. 88, no. 2, pp. 519–529, 2009.

[10] I. Rocchietta, F. Fontana, A. Addis, P. Schupbach, and M. Simion, "Surface-modified zirconia implants: tissue response in rabbits," *Clinical Oral Implants Research*, vol. 20, no. 8, pp. 844–850, 2009.

[11] M. Bächle, F. Butz, U. Hübner, E. Bakalinis, and R. J. Kohal, "Behavior of CAL72 osteoblast-like cells cultured on zirconia ceramics with different surface topographies," *Clinical Oral Implants Research*, vol. 18, no. 1, pp. 53–59, 2007.

[12] K. Anselme, M. Bigerelle, B. Noel et al., "Qualitative and quantitative study of human osteoblast adhesion on materials with various surface roughnesses," *Journal of Biomedical Materials Research*, vol. 49, no. 2, pp. 155–166, 2000.

[13] M. Gahlert, S. Röhling, M. Wieland, S. Eichhorn, H. Küchenhoff, and H. Kniha, "A comparison study of the osseointegration of zirconia and titanium dental implants:

a biomechanical evaluation in the maxilla of pigs," *Clinical Implant Dentistry and Related Research*, vol. 12, no. 4, pp. 297–305, 2010.

[14] B. Setzer, M. Bächle, M. C. Metzger, and R. J. Kohal, "The gene-expression and phenotypic response of hFOB 1.19 osteoblasts to surface-modified titanium and zirconia," *Biomaterials*, vol. 30, no. 6, pp. 979–990, 2009.

[15] K. Mustafa, A. Odén, A. Wennerberg, K. Hultenby, and K. Arvidson, "The influence of surface topography of ceramic abutments on the attachment and proliferation of human oral fibroblasts," *Biomaterials*, vol. 26, no. 4, pp. 373–381, 2005.

[16] S. K. Nishimoto, M. Nishimoto, S.-W. Park et al., "The effect of titanium surface roughening on protein absorption, cell attachment, and cell spreading," *International Journal of Oral and Maxillofacial Implants*, vol. 23, no. 4, pp. 675–680, 2008.

[17] D. Kubies, L. Himmlová, T. Riedel et al., "The interaction of osteoblasts with bone-implant materials: 1. The effect of physicochemical surface properties of implant materials," *Physiological Research*, vol. 60, no. 1, pp. 95–111, 2011.

[18] A. Oliva, A. Salerno, B. Locardi et al., "Behaviour of human osteoblasts cultured on bioactive glass coatings," *Biomaterials*, vol. 19, no. 11-12, pp. 1019–1025, 1998.

[19] P. Torricelli, E. Verné, C. V. Brovarone et al., "Biological glass coating on ceramic materials: *in vitro* evaluation using primary osteoblast cultures from healthy and osteopenic rat bone," *Biomaterials*, vol. 22, no. 18, pp. 2535–2543, 2001.

[20] N. N. Aldini, M. Fini, G. Giavaresi et al., "Improvement in zirconia osseointegration by means of a biological glass coating: an in vitro and in vivo investigation," *Journal of Biomedical Materials Research*, vol. 61, no. 2, pp. 282–289, 2002.

[21] B. Baharloo, M. Textor, and D. M. Brunette, "Substratum roughness alters the growth, area, and focal adhesions of epithelial cells, and their proximity to titanium surfaces," *Journal of Biomedical Materials Research A*, vol. 74, no. 1, pp. 12–22, 2005.

[22] E. Mick, J. Markhoff, A. Mitrovic, A. Jonitz, and R. Bader, "New coating technique of ceramic implants with different glass solder matrices for improved osseointegration-mechanical investigations," *Materials*, vol. 6, no. 9, pp. 4001–4010, 2013.

[23] M. Hopp and A. Zothner, "Verfahren zur Konditionierung der Oberflächen von Dentalkomponenten und Verwendung des Verfahrens," Tech. Rep. DE102009051655B3, 2010.

[24] K. Lochner, A. Fritsche, A. Jonitz et al., "The potential role of human osteoblasts for periprosthetic osteolysis following exposure to wear particles," *International Journal of Molecular Medicine*, vol. 28, no. 6, pp. 1055–1063, 2011.

[25] S. H. Gong, H. Lee, A. Pae et al., "Gene expression of MC3T3-E1 osteoblastic cells on titanium and zirconia surface," *Journal of Advanced Prosthodontics*, vol. 5, no. 4, pp. 416–422, 2013.

[26] R. L. Sammons, N. Lumbikanonda, M. Gross, and P. Cantzler, "Comparison of osteoblast spreading on microstructured dental implant surfaces and cell behaviour in an explant model of osseointegration: a scanning electron microscopic study," *Clinical Oral Implants Research*, vol. 16, no. 6, pp. 657–666, 2005.

[27] E. Rompen, O. Domken, M. Degidi, A. E. P. Pontes, and A. Piattelli, "The effect of material characteristics, of surface topography and of implant components and connections on soft tissue integration: a literature review," *Clinical Oral Implants Research*, vol. 17, supplement 2, pp. 55–67, 2006.

[28] L. Raisanen, M. Kononen, J. Juhanoja et al., "Expression of cell adhesion complexes in epithelial cells seeded on biomaterial surfaces," *Journal of Biomedical Materials Research*, vol. 49, no. 1, pp. 79–87, 2000.

[29] J. Marchi, C. S. Delfino, J. C. Bressiani, A. H. A. Bressiani, and M. M. Marques, "Cell proliferation of human fibroblasts on alumina and hydroxyapatite-based ceramics with different surface treatments," *International Journal of Applied Ceramic Technology*, vol. 7, no. 2, pp. 139–147, 2010.

[30] L. Raffaelli, P. R. Iommetti, E. Piccioni et al., "Growth, viability, adhesion potential, and fibronectin expression in fibroblasts cultured on zirconia or feldspatic ceramics *in vitro*," *Journal of Biomedical Materials Research Part A*, vol. 86, no. 4, pp. 959–968, 2008.

[31] M. Herrero-Climent, P. Lázaro, J. Vicente Rios et al., "Influence of acid-etching after grit-blasted on osseointegration of titanium dental implants: *in vitro* and *in vivo* studies," *Journal of Materials Science: Materials in Medicine*, vol. 24, no. 8, pp. 2047–2055, 2013.

[32] M. Guazzato, L. Quach, M. Albakry, and M. V. Swain, "Influence of surface and heat treatments on the flexural strength of Y-TZP dental ceramic," *Journal of Dentistry*, vol. 33, no. 1, pp. 9–18, 2005.

[33] M. Marrelli, C. Maletta, F. Inchingolo, M. Alfano, and M. Tatullo, "Three-point bending tests of zirconia core/veneer ceramics for dental restorations," *International Journal of Dentistry*, vol. 2013, Article ID 831976, 5 pages, 2013.

Hindawi Publishing Corporation
BioMed Research International
Volume 2014, Article ID 814578, 12 pages
http://dx.doi.org/10.1155/2014/814578

Review Article

On the Feasibility of Utilizing Allogeneic Bone Blocks for Atrophic Maxillary Augmentation

Alberto Monje,[1] Michael A. Pikos,[2] Hsun-Liang Chan,[1] Fernando Suarez,[1] Jordi Gargallo-Albiol,[3] Federico Hernández-Alfaro,[3] Pablo Galindo-Moreno,[4] and Hom-Lay Wang[1]

[1] *Department of Periodontics and Oral Medicine, School of Dentistry, University of Michigan, Ann Arbor, MI, USA*
[2] *Private practice, Palm Beach, FL, USA*
[3] *Department of Oral Surgery and Implant Dentistry, International University of Catalonia, Barcelona, Spain*
[4] *Department of Oral Surgery and Implant Dentistry, University of Granada, Granada, Spain*

Correspondence should be addressed to Alberto Monje; amonjec@umich.edu

Received 15 April 2014; Accepted 2 July 2014; Published 11 September 2014

Academic Editor: Seong-Hun Kim

Purpose. This systematic review was aimed at assessing the feasibility by means of survival rate, histologic analysis, and causes of failure of allogeneic block grafts for augmenting the atrophic maxilla. *Material and Methods*. A literature search was conducted by one reviewer in several databases. Articles were included in this systematic review if they were human clinical trials in which outcomes of allogeneic bone block grafts were studied by means of survival rate. In addition other factors were extracted in order to assess their influence upon graft failure. *Results*. Fifteen articles fulfilled the inclusion criteria and subsequently were analyzed in this systematic review. A total of 361 block grafts could be followed 4 to 9 months after the surgery, of which 9 (2.4%) failed within 1 month to 2 months after the surgery. Additionally, a weighed mean 4.79 mm (95% CI: 4.51–5.08) horizontal bone gain was computed from 119 grafted sites in 5 studies. Regarding implant cumulative survival rate, the weighed mean was 96.9% (95% CI: 92.8–98.7%), computed from 228 implants over a mean follow-up period of 23.9 months. Histologic analysis showed that allogeneic block grafts behave differently in the early stages of healing when compared to autogenous block grafts. *Conclusion*. Atrophied maxillary reconstruction with allogeneic bone block grafts represents a reliable option as shown by low block graft failure rate, minimal resorption, and high implant survival rate.

1. Introduction

An unavoidable series of events results in bone resorption after tooth extraction [1–4]. Consequently, grafting procedures are common treatments in the dental setting to correct these deficiencies and to allow for proper three-dimensional implant placement. Numerous alternatives such as distraction osteogenesis or guided bone regeneration (GBR) have been proposed [5]. Recently, advances in implant macrodesign [6–8] as well as technical advancement [9–11] have limited the need for grafting procedures. Nonetheless, for extensive/severely atrophic maxillary ridges, block grafting remains a predictable approach [12, 13].

For block grafting procedures, the use of autogenous bone has been claimed to be the "gold standard" due to its osteogenic, osteoinductive, and osteoconductive properties [14]. While intraoral bone block grafts such as mandibular ramus and symphysis grafts can be harvested with minimal morbidity the amount of available bone remains its big disadvantage. On the other hand, extraoral bone block grafts, such as calvaria or iliac crest, provide the greater quantity of bone but increased cost and are often associated with high morbidity in the donor site. Due to these limitations and drawbacks, clinicians have opted to use either allogeneic or xenogeneic bone blocks for the reconstruction of severe atrophy defects of the maxilla [15–31]. When these

alternatives are employed, they not only reduce the possibility of morbidity, but also shorten the treatment length, hence increasing patients' acceptance and satisfaction.

Nevertheless, integration of allogeneic or xenogeneic block bone to the native bone might be arduous due to the scarcity of cells within the graft. The mechanism of forming new mineralized tissue is mediated by the mesenchymal cells that can differentiate into osteoblasts which are coordinated by glycoproteins [32]. Following an inflammatory process, new bone is formed after gradual substitution [33] which leads to obtain implant primary stability and subsequent osseointegration.

Promising results have been reported with regards to the use these alternative block grafts plus different biomaterials for bone regeneration [35, 36]. Depending on their sources, they can be obtained either from human cadaver (allogeneic grafts) or from animal origin (xenogeneic grafts). However, the fate of xenografts remains unclear due to their nonosteoinductive capacity. On the other hand, the use of allogeneic block graft harvested from the same species represents a better alternative to the use of autogenous block bone. The first bone allografts were performed in late 19th century by a group of surgeons whom reconstructed an infected humerus with a graft harvested from the tibia of the same patient [37]. In 1990 the US Navy Tissue Bank was established which made the use of bone allografts popular [38]. In 1999, the first case of allogeneic block bone graft for regeneration in oral surgery was reported. In that case, dental implants for oral rehabilitation were successfully placed 3 months after the grafting procedure [36]. Since then, many studies have been carried out intending to show the reliability of allografts to assist in bone regeneration. Nonetheless, as far as we know, there is limited information that has been pooled and analyzed in an attempt to answer the fate of allogeneic block grafts for the rehabilitation of atrophic maxillae [15–21, 24–31]. Therefore, this systematic review aimed at assessing the feasibility of allogeneic block grafts by means of survival rate, histologic analysis, and causes of failure, for augmentation of the atrophic maxilla.

2. Material and Methods

2.1. Information Sources and Development of Focused Question. An electronic literature search was conducted by one reviewer (AM) in several databases, including MEDLINE, EMBASE, Cochrane Central Register of Controlled Trials, and Cochrane Oral Health Group Trials Register databases for articles written in English from January, 2000, up to December, 2013. The PICO question was as follows. Do edentulous patients restored by allograft bone blocks in the atrophic maxillae have acceptable clinical outcomes when compared to other types of block grafts by means of survival rate and histologic examination? The reporting of these meta-analyses adhered to the PRISMA (Preferred Reporting Items for Systematic Review and Meta-Analyses) statement [39].

2.2. Screening Process. Combinations of controlled terms (MeSH and EMTREE) and keywords were used whenever possible. The search terms used, where "[mh]" represented the MeSH terms and "[tiab]" represented title and/or abstract, for the PubMed search were "bone graft" [mh] OR "bone grafting" [ti] OR "dental implantation, endosseous" [mh] OR "dental implants" [mh] AND "bone graft" [tiab] OR "grafting" [mh] AND block [tiab] AND allogeneic [tiab] English [la] NOT letter [pt] OR comment [pt] OR editorial [pt] NOT "animals" [mh] NOT "humans" [mh]. Additionally, a manual search of implant-related journals, including *Clinical Implant Dentistry and Related Research, Journal of Oral and Maxillofacial Implants, Clinical Oral Implants Research, Implant Dentistry, Journal of Dental Research, Journal of Clinical Periodontology, Journal of Periodontology, and The International Journal of Periodontics & Restorative Dentistry,* from January, 2012, up to December, 2013, was also performed to ensure a thorough screening process.

2.3. Eligibility Criteria. Articles were included in this systematic review if they met the following inclusion criteria: prospective human clinical trials in which outcomes of allograft bone blocks were studied by means of survival rate. Accordingly, several factors such as study design, number of patients included at the last follow-up assessment, number of sites grafted, type of bone augmentation (vertical/horizontal/both), type of bone block studied, placement of membrane, whether any other grafting material was further used, and healing period were extracted from the selected studies and analyzed. Furthermore, in order to address the aim of this study, other parameters related to block graft survival, block graft behavior (resorption pattern), and histologic findings were further extracted (Table 1). On the contrary, case report or case series with less than 10 subjects included, systematic reviews, animal studies, retrospective cohort, and those studies in which information was not clear enough were excluded from this meta-analysis. References in the excluded articles were also checked seeking for studies that fulfilled our inclusion criteria. The Newcastle-Ottawa scale (NOS) was used to assess the quality of such studies for a proper understanding of nonrandomized studies [40].

2.4. Data Analysis. Demographic data, graft features, and surgical techniques were extracted from individual study. For meta-analyses of the horizontal bone gain and implant survival rate, the numbers of blocks and implants and the mean horizontal bone gain with standard deviation as well as the mean implant survival rate were retrieved from the included studies, if available. The weighted mean (WM) and the 95% confidence interval (CI) of the two variables were estimated using a computer program (Comprehensive Meta-analysis Software, Biostat, NJ, USA). The random effect model was applied to account for methodological differences among studies. Forest plots were computed to graphically represent the weighed means and 95% CI of the outcomes using "block graft site" and "implant" as the analysis unit for the horizontal bone gain and implant survival, respectively. For block survival rate, the Kaplan-Meier estimator was used to plot the survival curve. The number of grafts, mean followup time, the number of failed grafts, and time when the grafts failed were extracted from the studies. Data were input

Table 1: Description of the studies included in the present systematic review aiming to assess the feasibility of allogeneic bone block grafts.

(a)

Author (year)	Study design	Groups	Number of patients	Number of sites grafted	Location of grafted sites	Bone agumentation (V/H)	Type of bone block graft	Membrane (Y/N)	Additional grafting material/growth factor	Bone augmentation achieved at baseline	Healing period (months)	Resorption (%)
Acocella et al., (2012) [15]	Prospective case series	NCG	16	18	Anterior/posterior	H	Monocortical fresh-frozen	N	N	4.62 ± 0.8 mm	9	11.45 ± 8.37
Barone et al., (2009) [16]	Prospective case series	NCG	13	24	Anterior (13)/posterior (9)	H (19)/V (5)	Corticocancellous deep-frozen	N	Cancellous allograft particles	NM	5	NM
Chaushu et al., (2010) [17]	Prospective case series	NCG	101	90	Anterior (58)/Posterior (32)	NC	Cancellous fresh-frozen	Y	N	NM	6	NM
Contar et al., (2009) [19]	Prospective case series	NCG	15	34	Anterior/posterior	H	Cancellous/cortical fresh-frozen	N	N	NM	NC	NM
Contar et al., (2011) [18]	Prospective case series	NCG	18	39	Anterior/posterior	NC	Cancellous/cortical fresh-frozen Cortical fresh-frozen	N	N	NM	9	NM
Wallace and Gellin (2010) [31]	Prospective case series	NCG	12	16	Anterior/posterior	H	Cancellous fresh-frozen	Y	MCA + rhPDGF-BB	4.6 ± 5.2 mm	5	NM
Spin-Neto et al. (2013) [29]	Prospective case series	AL AT	13 13	17 17	Anterior (14)/posterior (3)	H	Corticocancellous deep-frozen Mandibular ramus	Y	N	NC	6	NC
Novell et al., (2012) [27]	Prospective case series	NCG	12	20	Anterior/posterior	H/H + V	Cortical/cancellous fresh-frozen	Y	Freeze-dried allograft particles	NC	NM	NM
Deluiz et al., (2013) [20]	Prospective case series	NCG	24	24	Anterior/posterior	H	Corticocancellous fresh-frozen	N	Freeze-dried allograft particles	NC	8	13.02 ± 3.86
Nissan et al., (2011) [26]	Prospective case series	NCG	20	28	Anterior	H (27)/V (12)	Cancellous fresh-frozen	Y	Particulate BBM	NM	6	NM
Nissan et al. (2011) [24]	Prospective case series	NCG	31	46	Anterior	H (42)/V (27)	Cancellous fresh-frozen	Y	Particulate BBM	NM	6	10 ± 1
Nissan et al., (2008) [25]	Prospective case series	NCG	11	11	Anterior	H/V	Cancellous fresh-frozen	Y	Particulate BBM	NM	6	NM
Lumetti et al., (2014) [21]	RCT	AL AT	12 12	12 12	Anterior/posterior	H	Corticocancellous fresh-frozen Mandibular ramus	Y	Particulate fresh-frozen	1.5 ± 0.91 cm^3 0.44 ± 1.04 cm^3	6	52 ± 25.87 25 ± 12.73
Spin-Neto et al. (2013) [30]	Prospective case series	AL AT	6 6	17 12	Anterior/posterior	H	Cortical fresh-frozen Mandibular ramus	Y	N	NM NM	7	NM NM
Peleg et al., (2010) [28]	Prospective case series	NCG	34	38	Anterior (31)/posterior (7)	H/H + V	Corticocancellous fresh-frozen	Y	N	NM	4	NM

(b)

Author (year)	Final bone gain (mm)	Number of implant placed	Implant loading protocol	Followup of implants (months)	Implant survival	Failed blocks (%)	Failed blocks (%)		Histological findings		
							Timing (months)	Cause	Timepoint (months)	Newly formed bone (%)	Characteristics
Acocella et al., (2012) [15]	4.09 ± 0.8	34	4	30	100	0	—	—	9	61.96 ± 11.77	A high number of empty osteocyte lacunae were still present and, fibrous tissue was more present than in the samples taken previously. Newly-formed bone was surrounded by non-vital bone with empty osteocyte lacunae in way of resorption

(b) Continued.

Author (year)	Final bone gain (mm)	Number of implant placed	Implant loading protocol	Followup of implants (months)	Implant survival	Failed blocks (%)			Histological findings		
						Failed blocks (%)	Timing (months)	Cause	Timepoint (months)	Newly formed bone (%)	Characteristics
Barone et al., (2009) [16]	NM	38	NM	6	94.73	8.33	1	Early exposure and infection of vertical onlay grafts	NM	NM	NM
Chaushu et al., (2010) [17]	NM	NM	NM	NM	NM	6.66	NC	Membrane exposure, incision line opening, soft tissue perforations, recipient site infection	NM	NM	NM
Contar et al., (2009) [19]	NM	51	NC	35	100	0	—	—	NC	NM	Mature and compact osseous tissue surrounded by marrow spaces
Contar et al., (2011) [18]	NM	58	NM	NM	NM	0	—	—	9	NM	Lamellar arrangement around Haversian canals interspersed with osteocytes in lacunae. No evidence of inflammatory infiltrate. The central portions revealed osteocytes with higher number of empty lacunae
Wallace & Gellin (2010) [31]	8.39 ± 1.95	NM	NM	NM	NM	0	—	—	NM	NM	NM
Spin-Neto et al. (2013) [29]	NC	NM	NM	NM	NM	11.76	2	Fixation screws loosened causing inflammation	NM	NM	NM
		NM	NM	NM	NM	0	—	—			
Novell et al., (2012) [27]	NM	NC	NC	60	100	5	1	Failure occurred in the posterior area	NM	NM	NM
Deluiz et al., (2013) [20]	NC	75	NM	NM	98.67	0	—	—	4, 6, 8	NM	Newly formed bone with osteocytes observed in all the timepoints. Osteocyte presence was higher at 4 months. Vessels were also detected abundantly in the samples
Nissan et al., (2011) [24]	H (5 ± 0.5)/V (2 ± 0.5)	31	0 (12)/6 (19)	42	96	7.2	1	Because of soft tissue breakdown, infection and loss of fixation	NM	NM	NM
Nissan et al. (2011) [24]	H (5 ± 0.5)/V (2 ± 0.5)	63	6	34	100	4.4	1	Because of soft tissue breakdown, infection and loss of fixation	NM	NM	NM
Nissan et al., (2008) [25]	H (5 ± 0.5)/V (NM)	11	0	18	100	0	—	—	NM	NM	NM

(b) Continued.

Author (year)	Final bone gain (mm)	Number of implant placed	Implant loading protocol	Followup of implants (months)	Implant survival	Failed blocks (%)			Histological findings		
						Failed blocks (%)	Timing (months)	Cause	Timepoint (months)	Newly formed bone (%)	Characteristics
Lumetti et al., (2014) [21]	NC	NM	NM	NM	NM	0	—	—	6	NC	Osteocyte lacunae mostly empty. Newly formed bone contained viable osteocytes. Bone forming osteoblasts and fluorescent labeling detected. Dense connective tissue with the presence of inflammatory cells (WM score = 1.67) and eroded areas
						0	—	—		NC	Osteocyte lacunae mostly empty. Newly formed bone contained viable osteocytes. Bone forming osteoblasts and fluorescent labeling detected. WM inflammatory score = 1
Spin-Neto et al. (2013) [29]	NM	40	NM	NM	NM	0	—	—	7	NM	Large segments of necrotic bone with empty osteocytes lacunae and little osteoclastic activity. Blood vessels were invading the Haversian canals of the material. No direct contact was found between remodeled and grafted bone.
											Some osteoclastic activity surrounded by connective tissue with no presence of inflammatory cells by newly formed bone failed to invade the graft.
	NM					0	—	—		NM	Small areas of necrotic bone with abundant presence of osteocytes. Inexistent difference between the grafted and the host bone
Peleg et al., (2010) [28]	NM	NC	NC	NC	NC	0	—	—	NM	NM	NM

RCT: randomized controlled trial; AL: allogenous graft; AT: autogenous graft; H: horizontal; V: vertical; Y: yes; N: no; MCA: mineralized cortical allograft; BBM: bobine bone mineral; NC: no clear; NM: not metioned; NCG: no control group.

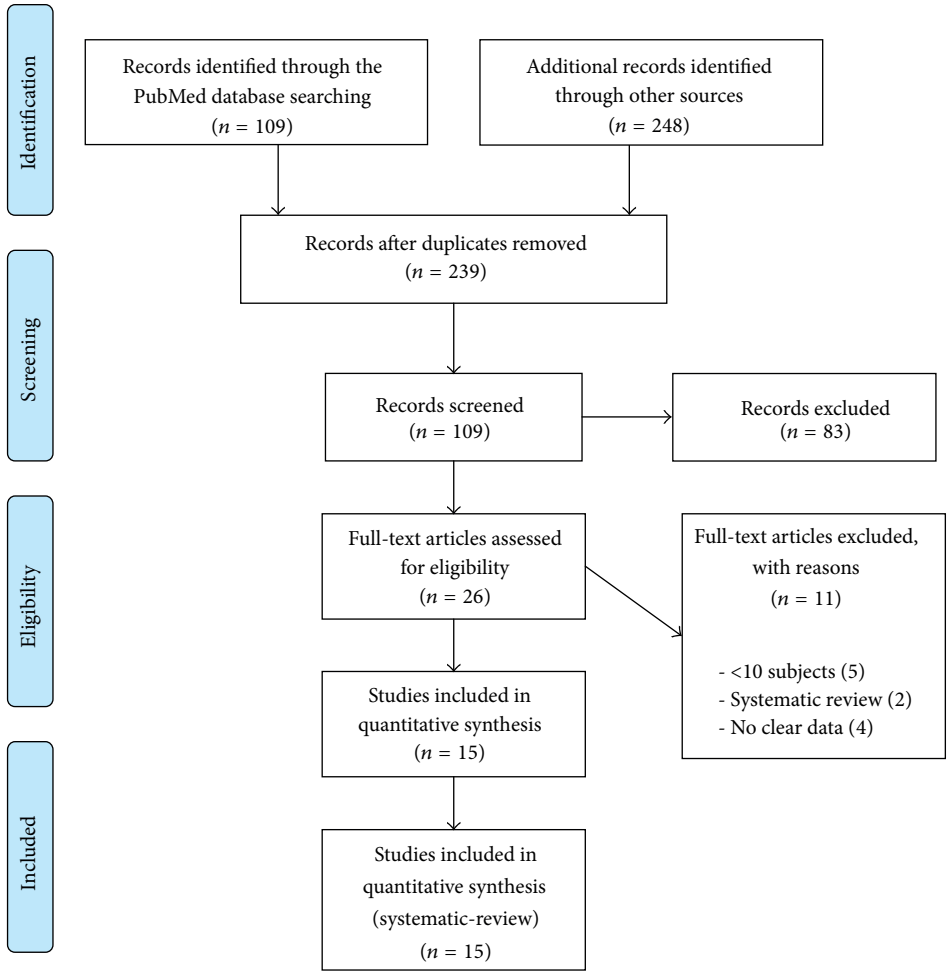

Figure 1: Identification, screening, and eligibility criteria for the studies included in this systematic review.

into a spreadsheet and computed by commercially available software (SPSS v 22.0, IBM, Chicago, IL, USA). All analyses were performed by one blinded investigator (H-LC).

3. Results

3.1. Study Selection. An initial screening yielded a total of 239 articles, of which 109 potentially relevant articles were selected after evaluation of their abstract. Next, 26 papers of full text of these articles were then obtained and reviewed. Of these, only 15 articles fulfilled the inclusion criteria and subsequently were analyzed in this systematic review (Figure 1). Details of all included studies were summarized in Table 1. Reasons for exclusion were case reports or <10 subjects included (5) [22, 41–44], and systematic/narrative reviews (2) [35, 36]. In addition, four more studies were excluded due to not clearly displaying appropriate data or to providing lack of the required data for this systematic review [23, 34, 45, 46]. On the other hand, all the included studies detected were prospective case series (14) and randomized controlled trials (1) [15–21, 24–31]. In some instances, when there was possibility to clearly identify blocks survival/failure by location, mandible block grafts were excluded inasmuch as the aim of the study was only to report their feasibility in the maxillae.

3.2. Study Quality. All the articles included in the present systematic review were prospective human clinical trials evaluating survival of allogeneic block grafts placed in the atrophic maxilla. The Newcastle-Ottawa scale (NOS) was used to assess the quality of such studies for a proper understanding of nonrandomized studies [40]. The fact that some studies came from the same group might leads to risk of bias due to repeated data; however, it was thoroughly assessed to make sure this was not the case. Thereupon, according to the NOS, a mean score of 6.06 ± 1.04 was obtained, indicating the adequate (medium-high) level of evidence of the included studies.

3.3. Failure Rate of Allogeneic Bone Blocks. A total of 361 block grafts were followed until 4 to 9 months after the surgery, of which 9 failed within 1 to 2 months after the surgery. The cumulative survival rate of the block grafts was 98% (Figure 2). Of the 9 reported failed cases, 5 were corticocancellous and the other 4 were cancellous grafts; 7 were combined with the use of membrane and the other 2 were not. Due

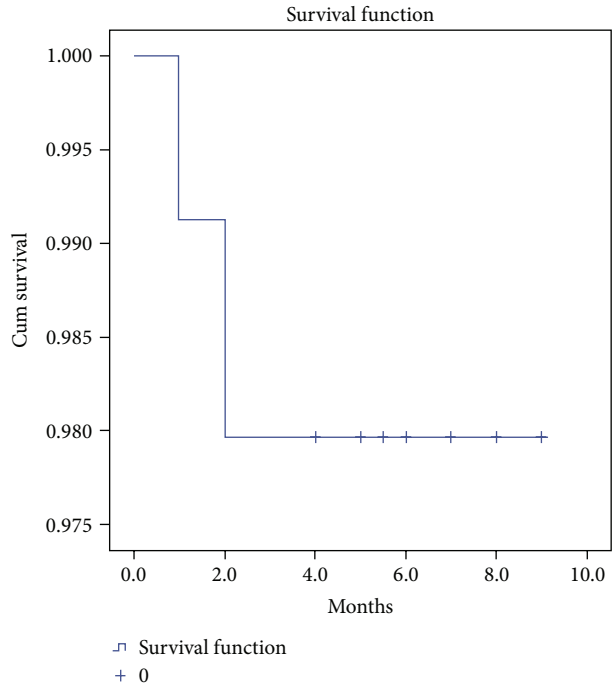

Figure 2: Cumulative survival rate of allogeneic bone block grafts placed in the maxillae.

to the limited number of failed cases, the effect of the graft type and membrane use on graft failure was not analyzed.

3.4. Timing and Causes of Failure of Allogeneic Bone Blocks. It was shown that block grafts failed generally in early stages of graft healing (≤2 months) [16, 20, 27, 30]. This suggested that the odds of grafts success increase from the third month on. Early membrane exposure was found to be the main reason for block graft failure [16, 20, 27, 30]. Moreover, it was reported that fixation screw loosening was the second leading cause for block graft failure [29].

3.5. Resorptive Pattern and Final Bone Gain of Allogeneic Bone Blocks. A weighed mean of 4.79 mm (95% CI: 4.51–5.08) horizontal bone gain was computed from 119 grafted sites in 5 studies [15, 24–26, 31]. Allogeneic block graft resorption ranged from 10 ± 10% [24] to 52 ± 25.97% [21] at 6 months after grafting (Figure 3). However, it is important to note that the mean value was found to be relatively low (21.70 ± 30.55%) [15, 20, 21, 24]. In addition, high heterogeneity was also found among these studies. Interestingly, even though the sample size is small it was noticed the longer the healing, the less bone gain was obtained. On the other hand, allogeneic block grafts resulted in 2 ± 0.5 mm vertical bone augmentation [24, 26].

3.6. Implant Cumulative Survival Rate. The weighed mean implant survival rate was 96.9% (95% CI: 92.8–98.7%), computed from 228 implants over a mean follow-up period of 23.9 months (Figure 4) [15, 16, 19, 20, 24–27].

3.7. Histomorphometric and Histologic Characteristics of Allogeneic Bone Blocks. Six studies reported the histologic characteristics at reentry for implant placement [15, 18–21, 30]. Of these, only two compared the outcome with a control group, which in these cases were autogenous block grafts harvested from the mandibular ramus (Table 1) [21, 30]. Acocella et al. [15] showed that after a healing period of 9 months, a high number of empty osteocyte lacunae were still present. Additionally, newly formed bone (61.96 ± 11.77%) was surrounded by nonvital bone with empty osteocyte lacunae. Contar et al. [18] reported lamellar arrangement around Haversian canals interspersed with osteocytes in lacunae. In addition, in the center of the block grafts osteocytes with higher number of empty lacunae were noticed. On the other hand, when histologic results are compared among groups, behavioral dissimilarities are displayed. Lumetti et al. [21] demonstrated that after 6 months of healing osteocyte lacunae were mostly empty for the allogeneic block graft group. Furthermore, it was reported that newly formed bone contained viable osteocytes at that point. In these samples, bone forming osteoblasts and fluorescent labeling were detected. Dense connective tissue with the presence of inflammatory cells and eroded areas were also observed in such group. Minimal differences were shown for the autogenous block grafts group in which no connective tissue was found and where the presence of inflammatory cells was meaningfully lower. Contrarily, Spin-Neto et al. [30] found major dissimilarities between the groups. For the allogeneic bone block large segments of necrotic bone with empty osteocytes lacunae and little osteoclastic activity, along with blood vessels invading the Haversian

Ref.	Sample size	Mean (mm)	SE	Lower limit	Upper limit	Weight (%)	Mean and 95% CI
Acocella et al. [15]	18	4.09	0.19	3.72	4.46	19.32	
Wallace & Gellin [31]	16	4.56	0.49	3.61	5.52	6.84	
Nissan et al. [26]	28	5.00	0.10	4.82	5.19	25.44	
Nissan et al. [26]	4 6	5.00	0.07	4.86	5.14	26.54	
Nissan et al. [25]	11	5.00	0.15	4.70	5.30	21.85	
All	119	4.79	0.15	4.51	5.08	100.00	

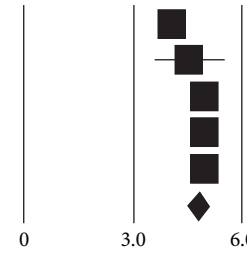

Figure 3: A weighed mean 4.79 mm (95% CI: 4.51–5.08) horizontal bone gain was computed from 119 grafted sites in 5 studies.

Ref.	Implant no	Survival rate (%)	Lower limit	Upper limit	Weight	Mean and 95% CI
Acocella et al. [15]	34	98.60	80.90	99.90	14.91	
Barone et al. [16]	38	94.70	81.20	98.70	16.67	
Contar et al. [19]	51	98.60	80.90	99.90	22.37	
Nissan et al. [26]	31	96.00	79.90	99.30	13.60	
Nissan et al. [26]	63	99.20	88.70	100.00	27.63	
Nissan et al. [25]	11	95.80	57.50	99.70	4.82	
All	228	96.90	92.80	98.70	100.00	

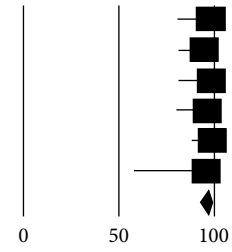

Figure 4: The weighed mean implant survival rate was 96.9% (95% CI: 92.8–98.7%), computed from 228 implants over a mean follow-up period of 23.9 months.

canals of the material were found. In addition, no direct contact between remodeled and grafted bone was found. For the autogenous block grafts small areas of necrotic bone with abundant presence of osteocytes were detected. Finally, no difference between the graft and the host bone was noticed.

4. Discussion

The use of autogenous grafts for bone augmentation of the atrophic maxilla was first documented by Branemark and is still considered the "gold standard" material due to their osteogenic potential for tissue regeneration [47]. Indeed, this property provides autogenous grafts more predictability by means of host-graft tissue integration. Nevertheless, it also presents some limitations. For instance, Nkenke et al. reported that patients might notice disturbances of the inferior alveolar nerve even 12 months after harvesting bone from the symphysis [48]. In addition, Clavero and Lundgren [49] found that half of the patients enrolled that underwent harvesting surgery from the mandibular ramus or chin experienced permanent altered sensation of the lower lip-chin. Other drawbacks are the additional cost and the possible need of general anesthesia and/or hospitalization. Also, excessive graft resorption of the autogenous bone block can be another concern. Nyström et al. observed a reduction in width of iliac crest onlay block grafts from 12.2 mm to 8.7 mm at 12 months [50]. Widmark et al. discovered that bone resorption of block grafts harvested from the mandible and used for horizontal augmentation of the anterior maxilla was 60% [51]. Similar findings were reported by Ozaki and Buchman in an animal study (56% of resorption of intramembranous blocks) [52]. Hence, all these facts have encouraged clinicians in seeking alternatives to autogenous bone for vertical and horizontal bone augmentation.

On the other hand, allogeneic grafts have proven to be successful in terms of integration with the host bone due to their osteoinductive potential [53, 54]. In addition, these grafts offer several benefits in comparison to autogenous grafts by means of reducing morbidity, discomfort, and operation time. Within limitations this systematic review showed that, regardless of subtype, allogeneic bone block grafts represent a feasible alternative to autogenous block grafts in augmenting the atrophic maxilla. Additionally, our results also confirm that allogeneic block grafts remain stable over the studies period when compared to previous findings [50–52]. Data from studies showed allogeneic block grafts resorbed ranged from 10 ± 10% [24] to 52 ± 25.97% [21] at 6 months after grafting. Nonetheless, it is important to note that the mean value was found to be relatively low (21.70 ± 30.55%) [15, 20, 21, 24], which is significantly lower than what Lumetti et al. [21], reported when fresh-frozen allogeneic block grafts were used.

Results from this review showed a mean gain of 4.79 mm horizontal and 2 mm vertical bone was obtained [15, 24–26, 31]. This is comparable to autogenous bone grafts but

without the associated donor site morbidity and higher resorptive rate; hence, we can imply that allogeneic block grafts can be a good alternative graft material for augmenting atrophic maxilla. Even though our purpose was to assess the reliability of allogeneic block grafts to augment the atrophic maxilla vertically and horizontally, no clear conclusion can be drawn with regard to vertical bone augmentation due to the limited data. Rocchietta et al. point out that vertical bone augmentation represents a technical challenge and there is paucity of evidence to claim any treatment approach as the most predictable [55]. On the contrary, Nissan et al. [24, 26] showed that it is possible not only to succeed by means of stability but also to achieve nonnegligible bone gain of 2 ± 0.5 mm. Therefore, precautions must be exercised when interpreting the results obtained in this systematic review especially in the arena of vertical bone augmentation.

In order to accomplish the principle of GBR as described by Melcher [56], a membrane must be placed to cover the graft to exclude unwanted cells into the wound. Nonetheless, Kusiak et al. found that barrier membrane has a limited effect on the onlay block [57]. Interestingly, other authors claim that the use of membranes might lead to a higher prevalence of complications, such as membrane exposure and subsequent infection [51, 58]. Notwithstanding, by using newly developed bioabsorbable membranes, clinicians have achieved better results overcoming the drawbacks presented by the non-bioabsorbable membranes [59, 60]. In the present study, meta-analysis of the data becomes impossible due to number of failed cases. Nevertheless, only two out of the nine failed blocks membranes were not placed.

It is important to evaluate the survival rate of implants placed following ridge augmentation. Data from this systematic review showed a mean implant survival rate of 96.9% (95% CI: 92.8–98.7%), computed from 228 implants over a mean follow-up period of 23.9 months. Hence, it can be concluded that allogeneic block grafts for augmentation of resorbed maxillae behave similar to native bone in supporting implant osseointegration. This is in agreement with Clementini et al. who demonstrated a high survival rate as long as implants are placed following a delayed placement protocol after onlay bone grafting [61]. Nonetheless, the ideal time to place implants after allogeneic block grafting remains to be determined.

Another factor of importance is the histological behavior of allogeneic block grafts and their incorporation to host bone. Graft revascularization is critical to the success of bone grafting in general and to block bone grafting in particular. Allogeneic grafts, in contrast to xenogeneic grafts, still maintain vital cells despite the preservation process that they undergo [62]. Simpson et al. [62] in an *in vitro* study showed the osteopromotive capacity of fresh frozen allografts. This systematic review demonstrated that allogeneic block grafts in the early stages of healing behave differently than do autogenous block grafts. However it remains unclear about the fate of this biomaterial in the late stage of bone remodeling. Furthermore, it is worth noting that a high heterogeneity among studies existed when examining the histologic characteristics. While Lumetti et al. [21] reported minimal differences for allogeneic blocks when compared to autogenous blocks, Spin-Neto et al. [30] found major dissimilarities between them For the allogeneic bone block, large segments of necrotic bone with empty osteocytes lacunae and little osteoclastic activity, and minimal number of blood vessels invading Haversian canals were found. In addition, there is no direct contact between remodeled and grafted bone was found. For autogenous block grafts small areas of necrotic bone with abundant presence of osteocytes were detected. No difference between the graft and host bone was noticed [30].

Future research must be conducted to clarify numerous unknowns. From the clinical perspective, a large randomized clinical trial should be designed to compare the long-term fate of allogeneic blocks when compared to intramembranous and endochondral autogenous block grafts. In addition, it remains unclear which type of allogeneic block graft represents the most reliable one by means of bone gain and interaction with host bone. Generally speaking, bone resorption potentially relies upon numerous parameters that were shown to play a role; for instance, buccal bone thickness is known to determine the percentage of bone loss. Nevertheless, it is yet to be determined the influence of thickness upon final volume gain. Finally, it will be interesting to find out if additional of biologic agents (e.g., bone morphogenetic proteins) can be used to speed up or improve allogeneic block graft maturation.

5. Conclusion

Within the limitations of this systematic review, it can be concluded that the use of allogeneic bone block grafts represent a reliable alternative to autogenous block grafts for augmenting the atrophic maxilla. Furthermore, implants placed in allogeneic block augmented bone can achieve similar implant survival rates. However, due to the heterogeneity among the selected studies and limitation of sample size, results from this study should be interpreted with caution. Future studies to include larger sample size, longer followup, and better controlled are encouraged.

Conflict of Interests

The authors declare that there is no conflict of interests regarding the publication of this paper.

Acknowledgment

The present study was partially funded by the University of Michigan Department of Periodontics and Oral Medicine.

References

[1] G. E. Carlsson, B. Bergman, and B. Hedegård, "Changes in contour of the maxillary alveolar process under immediate dentures. A longitudinal clinical and x-ray cephalometric study covering 5 years.," *Acta Odontologica Scandinavica*, vol. 25, no. 1, pp. 45–75, 1967.

[2] D. A. Atwood and W. A. Coy, "Clinical, cephalometric, and densitometric study of reduction of residual ridges," *The Journal of Prosthetic Dentistry*, vol. 26, no. 3, pp. 280–295, 1971.

[3] J. Pietrokovski and M. Massler, "Alveolar ridge resorption following tooth extraction," *The Journal of Prosthetic Dentistry*, vol. 17, no. 1, pp. 21–27, 1967.

[4] L. Schropp, A. Wenzel, L. Kostopoulos, and T. Karring, "Bone healing and soft tissue contour changes following single-tooth extraction: a clinical and radiographic 12-month prospective study," *International Journal of Periodontics and Restorative Dentistry*, vol. 23, no. 4, pp. 313–323, 2003.

[5] C. H. F. Hämmerle, R. E. Jung, and A. Feloutzis, "A systematic review of the survival of implants in bone sites augmented with barrier membranes (guided bone regeneration) in partially edentulous patients," *Journal of Clinical Periodontology*, vol. 29, supplement 3, pp. 226–231, 2002.

[6] A. Monje, H. Chan, J. Fu, F. Suarez, P. Galindo-Moreno, and H. Wang, "Are short dental implants (< 10 mm) effective? A meta-analysis on prospective clinical trials," *Journal of Periodontology*, vol. 84, no. 7, pp. 895–904, 2013.

[7] I. Ortega-Oller, F. Suárez, P. Galindo-Moreno et al., "The influence of implant diameter on its survival: a meta-analysis based on prospective clinical trials," *Journal of Periodontology*, vol. 85, no. 4, pp. 569–580, 2013.

[8] B. Pommer, S. Frantal, J. Willer, M. Posch, G. Watzek, and G. Tepper, "Impact of dental implant length on early failure rates: a meta-analysis of observational studies," *Journal of Clinical Periodontology*, vol. 38, no. 9, pp. 856–863, 2011.

[9] A. Monje, H. Chan, F. Suarez, P. Galindo-Moreno, and H. Wang, "Marginal bone loss around tilted implants in comparison to straight implants: a meta-analysis.," *The International journal of oral & maxillofacial implants*, vol. 27, no. 6, pp. 1576–1583, 2012.

[10] R. Crespi, R. Vinci, P. Capparé, G. E. Romanos, and E. Gherlone, "A clinical study of edentulous patients rehabilitated according to the "all on four" immediate function protocol.," *The International Journal of Oral & Maxillofacial Implants*, vol. 27, no. 2, pp. 428–434, 2012.

[11] R. Davó, "Zygomatic implants placed with a two-stage procedure: a 5-year retrospective study," *European Journal of Oral Implantology*, vol. 2, no. 2, pp. 115–124, 2009.

[12] P. Tessier, H. Kawamoto, D. Matthews et al., "Autogenous bone grafts and bone substitutes–tools and techniques: I. A 20,000-case experience in maxillofacial and craniofacial surgery," *Plastic and Reconstructive Surgery*, vol. 116, supplement 5, pp. 6S–24S, 2005, discussion 92S-94S.

[13] A. Monje, F. Monje, P. Galindo-Moreno, J. Montanero-Fernandez, F. Suarez, and H. Wang, "Microstructural and densiometric analysis of extra oral bone block grafts for maxillary horizontal bone augmentation: a comparison between calvarial bone and iliac crest," *Clinical Oral Implants Research*, vol. 25, no. 6, pp. 659–664, 2014.

[14] T. Albrektsson and C. Johansson, "Osteoinduction, osteoconduction and osseointegration," *European Spine Journal*, vol. 10, supplement 2, pp. S96–S101, 2001.

[15] A. Acocella, R. Bertolai, E. Ellis III, J. Nissan, and R. Sacco, "Maxillary alveolar ridge reconstruction with monocortical fresh-frozen bone blocks: A clinical, histological and histomorphometric study," *Journal of Cranio-Maxillofacial Surgery*, vol. 40, no. 6, pp. 525–533, 2012.

[16] A. Barone, P. Varanini, B. Orlando, P. Tonelli, and U. Covani, "Deep-frozen allogeneic onlay bone grafts for reconstruction of atrophic maxillary alveolar ridges: a preliminary study," *Journal of Oral and Maxillofacial Surgery*, vol. 67, no. 6, pp. 1300–1306, 2009.

[17] G. Chaushu, O. Mardinger, M. Peleg, O. Ghelfan, and J. Nissan, "Analysis of complications following augmentation with cancellous block allografts," *Journal of Periodontology*, vol. 81, no. 12, pp. 1759–1764, 2010.

[18] C. M. M. Contar, J. R. Sarot, M. B. da Costa et al., "Fresh-frozen bone allografts in maxillary ridge augmentation: histologic analysis," *The Journal of Oral Implantology*, vol. 37, no. 2, pp. 223–231, 2011.

[19] C. M. M. Contar, J. R. Sarot, J. Bordini Jr., G. H. Galvão, G. V. Nicolau, and M. A. N. Machado, "Maxillary ridge augmentation with fresh-frozen bone allografts," *Journal of Oral and Maxillofacial Surgery*, vol. 67, no. 6, pp. 1280–1285, 2009.

[20] D. Deluiz, L. S. Oliveira, F. R. Pires, and E. M. B. Tinoco, "Time-dependent changes in fresh-frozen bone block grafts: tomographic, histologic, and histomorphometric findings," *Clinical Implant Dentistry and Related Research*, 2013.

[21] S. Lumetti, U. Consolo, C. Galli et al., "Fresh-frozen bone blocks for horizontal ridge augmentation in the upper maxilla: 6-month outcomes of a randomized controlled trial," *Clinical Implant Dentistry and Related Research*, vol. 16, no. 1, pp. 116–123, 2014.

[22] R. H. Lyford, M. P. Mills, C. I. Knapp, E. T. Scheyer, and J. T. Mellonig, "Clinical evaluation of freeze-dried block allografts for alveolar ridge augmentation: a case series," *International Journal of Periodontics and Restorative Dentistry*, vol. 23, no. 5, pp. 417–425, 2003.

[23] L. G. S. MacEdo, L. A. Mazzucchelli-Cosmo, N. L. MacEdo, A. S. F. Monteiro, and W. R. Sendyk, "Fresh-frozen human bone allograft in vertical ridge augmentation: clinical and tomographic evaluation of bone formation and resorption," *Cell and Tissue Banking*, vol. 13, no. 4, pp. 577–586, 2012.

[24] J. Nissan, O. Mardinger, S. Calderon, G. E. Romanos, and G. Chaushu, "Cancellous bone block allografts for the augmentation of the anterior atrophic maxilla," *Clinical Implant Dentistry and Related Research*, vol. 13, no. 2, pp. 104–111, 2011.

[25] J. Nissan, G. E. Romanos, O. Mardinger, and G. Chaushu, "Immediate nonfunctional loading of single-tooth implants in the anterior maxilla following augmentation with freeze-dried cancellous block allograft: a case series," *International Journal of Oral and Maxillofacial Implants*, vol. 23, no. 4, pp. 709–716, 2008.

[26] J. Nissan, O. Gross, O. Mardinger, O. Ghelfan, R. Sacco, and G. Chaushu, "Post-traumatic implant-supported restoration of the anterior maxillary teeth using cancellous bone block allografts," *Journal of Oral and Maxillofacial Surgery*, vol. 69, no. 12, pp. e513–e518, 2011.

[27] J. Novell, F. Novell-Costa, C. Ivorra, O. Fariñas, A. Munilla, and C. Martinez, "Five-year results of implants inserted into freeze-dried block allografts," *Implant Dentistry*, vol. 21, no. 2, pp. 129–135, 2012.

[28] M. Peleg, Y. Sawatari, R. N. Marx et al., "Use of corticocancellous allogeneic bone blocks for augmentation of alveolar bone defects.," *The International journal of oral & maxillofacial implants*, vol. 25, no. 1, pp. 153–162, 2010.

[29] R. Spin-Neto, A. Stavropoulos, L. A. V. D. Pereira, E. Marcantonio, and A. Wenzel, "Fate of autologous and fresh-frozen allogeneic block bone grafts used for ridge augmentation. A CBCT-based analysis," *Clinical Oral Implants Research*, vol. 24, no. 2, pp. 167–173, 2013.

[30] R. Spin-Neto, R. A. L. Del Barrio, L. A. V. D. Pereira, R. A. C. Marcantonio, E. Marcantonio, and E. Marcantonio Jr., "Clinical similarities and histological diversity comparing fresh frozen

onlay bone blocks allografts and autografts in human maxillary reconstruction," *Clinical Implant Dentistry and Related Research*, vol. 15, no. 4, pp. 490–497, 2013.

[31] S. Wallace and R. Gellin, "Clinical evaluation of freeze-dried cancellous block allografts for ridge augmentation and implant placement in the Maxilla," *Implant Dentistry*, vol. 19, no. 4, pp. 272–279, 2010.

[32] J. Glowacki, L. B. Kaban, J. E. Murray, J. Folkman, and J. B. Mulliken, "Application of the biological principle of induced osteogenesis for craniofacial defects," *The Lancet*, vol. 1, no. 8227, pp. 959–962, 1981.

[33] P. Å. Köndell, T. Mattsson, and P. Åstrand, "Immunological responses to maxillary on-lay allogeneic bone grafts," *Clinical Oral Implants Research*, vol. 7, no. 4, pp. 373–377, 1996.

[34] J. Nissan, O. Mardinger, M. Strauss, M. Peleg, R. Sacco, and G. Chaushu, "Implant-supported restoration of congenitally missing teeth using cancellous bone block-allografts," *Oral Surgery, Oral Medicine, Oral Pathology, Oral Radiology and Endodontology*, vol. 111, no. 3, pp. 286–291, 2011.

[35] P. P. T. Araújo, K. P. Oliveira, S. C. L. Montenegro, A. F. P. Carreiro, J. S. P. Silva, and A. R. Germano, "Block allograft for reconstruction of alveolar bone ridge in implantology: a systematic review," *Implant Dentistry*, vol. 22, no. 3, pp. 304–308, 2013.

[36] J. Waasdorp and M. A. Reynolds, "Allogeneic bone onlay grafts for alveolar ridge augmentation: a systematic review.," *The International Journal of Oral & Maxillofacial Implants*, vol. 25, no. 3, pp. 525–531, 2010.

[37] H. H. De Boer, "The history of bone grafts," *Clinical Orthopaedics and Related Research*, no. 226, pp. 292–298, 1988.

[38] H. W. Leslie and S. Bottenfield, "Donation, banking, and transplantation of allograft tissues," *Nursing Clinics of North America*, vol. 24, no. 4, pp. 891–905, 1989.

[39] A. Liberati, D. G. Altman, J. Tetzlaff et al., "The PRISMA statement for reporting systematic reviews and meta-analyses of studies that evaluate health care interventions: explanation and elaboration," *PLoS Medicine*, vol. 6, no. 7, Article ID e1000100, 2009.

[40] A. Stang, "Critical evaluation of the Newcastle-Ottawa scale for the assessment of the quality of nonrandomized studies in meta-analyses," *European Journal of Epidemiology*, vol. 25, no. 9, pp. 603–605, 2010.

[41] K. U. Gomes, J. L. Carlini, C. Biron, A. Rapoport, and R. A. Dedivitis, "Use of allogeneic bone graft in maxillary reconstruction for installation of dental implants," *Journal of Oral and Maxillofacial Surgery*, vol. 66, no. 11, pp. 2335–2338, 2008.

[42] S. Kim, J. Park, and S. Lim, "Placement of implant after bone graft using J block allograft," *Implant Dentistry*, vol. 19, no. 1, pp. 21–28, 2010.

[43] J. A. Leonetti and R. Koup, "Localized maxillary ridge augmentation with a block allograft for dental implant placement: case reports," *Implant Dentistry*, vol. 12, no. 3, pp. 217–226, 2003.

[44] W. T. Pendarvis and J. B. Sandifer, "Localized ridge augmentation using a block allograft with subsequent implant placement: a case series," *International Journal of Periodontics and Restorative Dentistry*, vol. 28, no. 5, pp. 509–515, 2008.

[45] F. Carinci, R. Guidi, M. Franco et al., "Implants inserted in fresh-frozen bone: a retrospective analysis of 88 implants loaded 4 months after insertion," *Quintessence International*, vol. 40, no. 5, pp. 413–419, 2009.

[46] M. Chiapasco, G. Di Martino, T. Anello, M. Zaniboni, and E. Romeo, "Fresh frozen versus autogenous iliac bone for the rehabilitation of the extremely atrophic maxilla with onlay grafts and endosseous implants: preliminary results of a prospective comparative study," *Clinical Implant Dentistry and Related Research*, 2013.

[47] P. I. Branemark, J. Lindström, O. Hallén, U. Breine, P. H. Jeppson, and A. Ohman, "Reconstruction of the defective mandible," *Scandinavian Journal of Plastic and Reconstructive Surgery*, vol. 9, no. 2, pp. 116–128, 1975.

[48] E. Nkenke, S. Schultze-Mosgau, M. Radespiel-Tiöger, F. Kloss, and F. W. Neukam, "Morbidity of harvesting of chin grafts: a prospective study," *Clinical Oral Implants Research*, vol. 12, no. 5, pp. 495–502, 2001.

[49] J. Clavero and S. Lundgren, "Ramus or chin grafts for maxillary sinus inlay and local onlay augmentation: comparison of donor site morbidity and complications," *Clinical Implant Dentistry and Related Research*, vol. 5, no. 3, pp. 154–160, 2003.

[50] E. Nyström, H. Nilson, J. Gunne, and S. Lundgren, "A 9-14 year follow-up of onlay bone grafting in the atrophic maxilla," *International Journal of Oral and Maxillofacial Surgery*, vol. 38, no. 2, pp. 111–116, 2009.

[51] G. Widmark, B. Andersson, and C.-J. Ivanoff, "Mandibular bone graft in the anterior maxilla for single-tooth implants: presentation of a surgical method," *International Journal of Oral and Maxillofacial Surgery*, vol. 26, no. 2, pp. 106–109, 1997.

[52] S. R. Buchman and W. Ozaki, "The ultrastructure and resorptive pattern of cancellous onlay bone grafts in the craniofacial skeleton," *Annals of Plastic Surgery*, vol. 43, no. 1, pp. 49–56, 1999.

[53] D. Dallari, M. Fini, C. Stagni et al., "In vivo study on the healing of bone defects treated with bone marrow stromal cells, platelet-rich plasma, and freeze-dried bone allografts, alone and in combination," *Journal of Orthopaedic Research*, vol. 24, no. 5, pp. 877–888, 2006.

[54] M. S. Myerson, S. K. Neufeld, and J. Uribe, "Fresh-frozen structural allografts in the foot and ankle," *Journal of Bone and Joint Surgery A*, vol. 87, no. 1, pp. 113–120, 2005.

[55] I. Rocchietta, F. Fontana, and M. Simion, "Clinical outcomes of vertical bone augmentation to enable dental implant placement: a systematic review," *Journal of Clinical Periodontology*, vol. 35, no. 8, pp. 203–215, 2008.

[56] A. H. Melcher, "On the repair potential of periodontal tissues," *Journal of Periodontology*, vol. 47, no. 5, pp. 256–260, 1976.

[57] J. F. Kusiak, J. E. Zins, and L. A. Whitaker, "The early revascularization of membranous bone," *Plastic and Reconstructive Surgery*, vol. 76, no. 4, pp. 510–516, 1985.

[58] E. Picfte, P. Alberius, N. Samman, and A. Linde, "Experience with e-PTFE membrane application to bone grafting of cleft maxilla," *International Journal of Oral and Maxillofacial Surgery*, vol. 24, no. 5, pp. 327–332, 1995.

[59] C. H. F. Hämmerle and N. P. Lang, "Single stage surgery combining transmucosal implant placement with guided bone regeneration and bioresorbable materials," *Clinical Oral Implants Research*, vol. 12, no. 1, pp. 9–18, 2001.

[60] G. Tawil, G. El-Ghoule, and M. Mawla, "Clinical evaluation of a bilayered collagen membrane (Bio-Gide) supported by autografts in the treatment of bone defects around implants," *International Journal of Oral and Maxillofacial Implants*, vol. 16, no. 6, pp. 857–863, 2001.

[61] M. Clementini, A. Morlupi, C. Agrestini, and A. Barlattani, "Immediate versus delayed positioning of dental implants in

guided bone regeneration or onlay graft regenerated areas: a systematic review," *International Journal of Oral and Maxillofacial Surgery*, vol. 42, no. 5, pp. 643–650, 2013.

[62] D. Simpson, G. Kakarala, K. Hampson, N. Steele, and B. Ashton, "Viable cells survive in fresh frozen human bone allografts," *Acta Orthopaedica*, vol. 78, no. 1, pp. 26–30, 2007.

Hindawi Publishing Corporation
BioMed Research International
Volume 2014, Article ID 873918, 8 pages
http://dx.doi.org/10.1155/2014/873918

Research Article

Periodontal Responses to Augmented Corticotomy with Collagen Membrane Application during Orthodontic Buccal Tipping in Dogs

Dong-Yeol Lee,[1,2] Hyo-Won Ahn,[3] Yeek Herr,[1] Young-Hyuk Kwon,[1] Seong-Hun Kim,[3] and Eun-Cheol Kim[2]

[1] *Department of Periodontology, School of Dentistry, Kyung Hee University, No. 1, Hoegi-dong, Dongdaemun-gu, Seoul 130-701, Republic of Korea*
[2] *Department of Oral and Maxillofacial Pathology and Research Center for Tooth and Periodontal Regeneration (MRC), School of Dentistry, Kyung Hee University, Seoul 130-701, Republic of Korea*
[3] *Department of Orthodontics, School of Dentistry, Kyung Hee University, No. 1, Hoegi-dong, Dongdaemun-gu, Seoul 130-701, Republic of Korea*

Correspondence should be addressed to Seong-Hun Kim; bravortho@khu.ac.kr and Eun-Cheol Kim; eckim@khu.ac.kr

Received 7 April 2014; Revised 27 May 2014; Accepted 10 June 2014; Published 9 September 2014

Academic Editor: Homayoun H. Zadeh

This prospective randomized split-mouth study was performed to examine the effects of absorbable collagen membrane (ACM) application in augmented corticotomy using deproteinized bovine bone mineral (DBBM), during orthodontic buccal tipping movement in the dog. After buccal circumscribing corticotomy and DBBM grafting into the decorticated area, flaps were repositioned and sutured on control sides. ACM was overlaid and secured with membrane tacks, on test sides only, and the flaps were repositioned and sutured. Closed coil springs were used to apply 200 g orthodontic force in the buccolingual direction on the second and third premolars, immediately after primary flap closure. The buccal tipping angles were $31.19 \pm 14.60^{\circ}$ and $28.12 \pm 11.48^{\circ}$ on the control and test sides, respectively. A mean of $79.5 \pm 16.0\%$ of the buccal bone wall was replaced by new bone on the control side, and on the test side $78.9 \pm 19.5\%$ was replaced. ACM application promoted an even bone surface. In conclusion, ACM application in augmented corticotomy using DBBM might stimulate periodontal tissue reestablishment, which is useful for rapid orthodontic treatment or guided bone regeneration. In particular, ACM could control the formation of mesenchymal matrix, facilitating an even bone surface.

1. Introduction

Augmented corticotomy, combining corticotomy and alveolar bone augmentation, is associated with favorable clinical outcomes in orthodontics. In particular, in Class III malocclusion, it promotes retention of the periodontal ligament and prevents bony dehiscence during mandibular anterior decompensation [1, 2]. The bone graft between the periosteum and the cortical surface functions as a scaffold for bone formation. In particular, alveolar bone thickness in the apical areas of the mandibular incisors increases significantly after bone grafting [2]. However, reports including histological observations of the periodontal reactions to augmented corticotomy using absorbable collagen membrane (ACM) are rare.

ACM is commonly used in dentistry, due to its biocompatibility and ability to promote wound healing [3]. Absorbable collagen barrier membranes inhibit migration of epithelial cells, promote attachment of new connective tissue, are not strongly antigenic, prevent blood loss by promoting platelet aggregation leading to early clot formation and wound stabilization, and do not require surgical removal [4, 5]. Collagen membranes may also facilitate primary wound closure via fibroblast chemotactic properties [5], even after membrane exposure [6]. Compared to nonabsorbable e-PTFE membranes, resorbable barriers allow for fewer

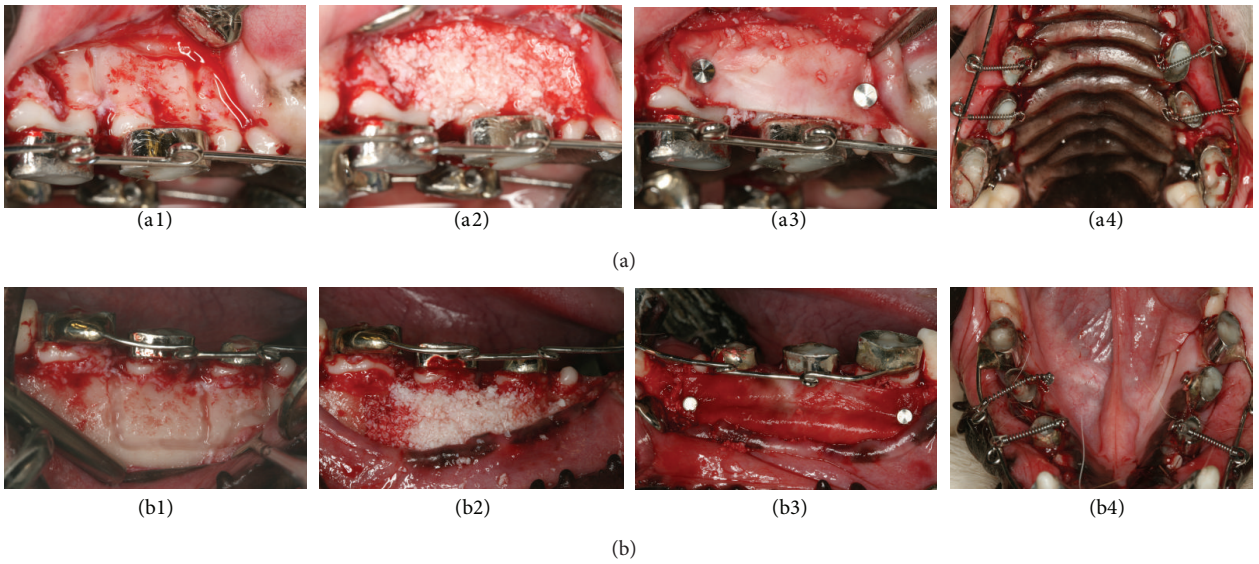

Figure 1: Surgical procedure in the (a) maxilla and (b) mandible. (1) Full-thickness flap reflection and buccal circumscribing corticotomy. (2) DBBM grafting on both the control and the test side. (3) ACM application with membrane tacks, on the test side only. (4) Primary flap closure and activation of the closed coil spring (200 g orthodontic force) for buccal tipping movement of the second and third premolars.

exposures and therefore reduce the effects of infection on newly formed bone [4]. Use of collagen membranes in particular, with bone mineral as a support and space maintainer, has achieved predictable treatment outcomes [7–10].

ACM has properties comparable to those of nonabsorbable membrane, when used in guided tissue regeneration (GTR) [11, 12] and guided bone regeneration (GBR) [13, 14]. The use of a bone graft material in combination with collagen membrane improves clinical outcomes of intrabony defects [15, 16]. Therefore, application of a barrier membrane in augmented corticotomy could stabilize the graft material during healing and prevent bony dehiscence that can cause gingival recessions in soft tissue, ultimately improving bone regeneration potential.

In this study, we examined the effects of ACM application in augmented corticotomy with deproteinized bovine bone mineral (DBBM), during orthodontic buccal tipping movement in the dog.

2. Materials and Methods

2.1. Animals. The experimental protocols used in this study were approved by the Kyung Hee Medical Center Institutional Animal Care and Use Committee (KHMC-IACUC 11-021). We used a prospective, randomized, split-mouth study design in 2 male beagles, aged over 1 year and weighing 10–13 kg. The animals were caged individually with regulated light and temperature. They were fed a normal soft diet and had access to water *ad libitum*.

For the clinical and surgical procedures, the dogs were anesthetized with a mixture of tiletamine-zolazepam (5–10 mg/kg intramuscularly; Zoletil 100, Virbac, Carros, France) and xylazine (5 mg/kg intravenously using a catheter in an ear vessel; Rompun, Bayer Korea, Seoul, Republic of Korea). They were sacrificed under general anesthesia with an overdose of thiopental, 12 weeks after the surgery.

2.2. Clinical Examination. The experimental teeth were the second and third premolars of both maxillae and mandibles. Probing depth (PD) and the width of keratinized tissue (WKT) on the buccal sides of the second and third premolars were measured with a periodontal probe (Hu-Friedy, Chicago, IL, USA) at 3 sites (mesial, middle, and distal) on the buccal aspect before the surgery (baseline). Alginate impressions were made to fabricate study models. The canine and fourth premolar were banded for use as anchors, and thick wire (ø 0.9 mm) was welded to the buccal surface of the bands, which was subsequently used to locate the canine and fourth premolar. Lingual buttons were welded to the lingual surface of the band located on the second and third premolars (Figure 1).

2.3. Surgical Procedure. After the animals were anesthetized to fix the orthodontic appliances to the teeth, local anesthesia with 2% lidocaine solution (1 : 100,000 epinephrine; Lidocaine HCL, Huons, Seoul, Republic of Korea) was induced at the surgical sites. Control and test sides were randomly assigned in the mandible and maxilla. A total of 16 teeth were included in the study, 8 teeth each in the control and test sides. Intrasulcular incisions were made from the canines to the first molars, and full-thickness flaps were reflected. Circumscribing corticotomy was performed with a round bur (ø 1.5 mm) under sterile saline irrigation, and DBBM (Bio-Oss, Geistlich Biomaterials, Wolhusen, Switzerland) was grafted into the decorticated area. On control sides, flaps were repositioned and sutured. On test sides, ACM (Bio-Gide, Geistlich Biomaterials) was overlaid on the grafts and secured with membrane tacks (Membrane Pin, Dentium Co., Seoul,

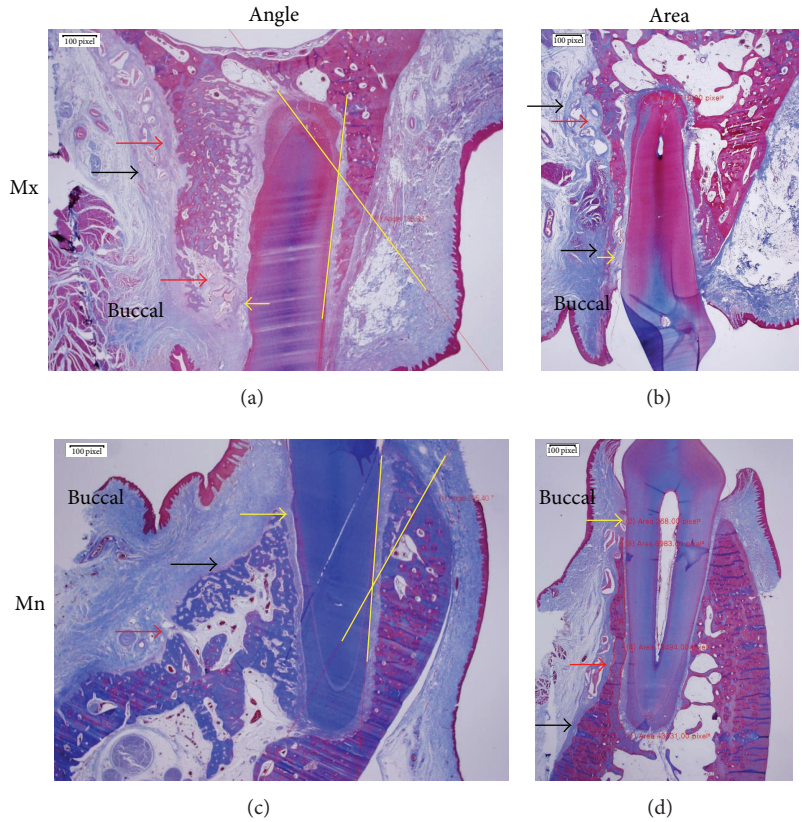

FIGURE 2: Representative micrographs for measuring the buccal tipping angle ((a), (c)) and bone area ((b), (d)) in the maxilla ((a), (b)) and mandible ((c), (d)). Red, yellow, and black arrows indicate the bone-derived, PDL-derived, and buccal mesenchymal matrices, respectively. Intersection of the yellow lines represents buccal tipping angle ((a), (c)). New bone area (%) was calculated by subtracting old bone area from total bone area. Masson's trichrome stain was used, and the original magnification was ×12.5.

Republic of Korea), and then flaps were sutured. After primary flap closure, closed coil springs were activated to apply 200 g orthodontic force in the buccolingual direction and initiate immediate buccal tipping movement of the second and third premolars (Figure 1), in the control and test sides. The antibiotic gentamycin and the anti-inflammatory analgesic ketoprofen were intramuscularly administered twice daily for 6 days. Mechanical plaque control was performed once a week. PD and WKT were measured again when the animals were sacrificed.

2.4. Histological Examination. The experimental sites were dissected, and retrieved block specimens were immersed in 10% neutral-buffered formalin for 14 days. Decalcification was performed by using 5% nitric acid for 6 days. Due to the large size of the block retrieved from the canine to the fourth premolar, 5% nitric acid was utilized for rapid decalcification, as it is a strong acid [17]. Notably, in a similar study designed for immunohistology, the use of EDTA or 10% aqueous or formic acid would be suitable [18]. However, as the aim of this study was not immunohistological analysis, due to time considerations, nitric acid was used to decalcify the retrieved block mass [19]. The specimens were then dehydrated through an ethanol series and embedded in paraffin. One slide was processed per experimental tooth. Buccolingual sections (5 μm) were stained with Masson's trichrome. Histological examinations were performed under a light microscope (Olympus BX 51, Olympus, Tokyo, Japan) equipped with a DP21 camera. Each slide was photographed, and the resulting images were saved. Three examiners used imaging software (cellSens version 1.6, Olympus) to measure the buccal tipping angle (°) and bone area (%). The buccal tipping angle was measured from the reversal line of the lingual/palatal bone wall to the lingual/palatal root surface (Figures 2(a) and 2(c), yellow lines). New bone area was calculated by subtracting old bone area from total bone area (%) on the buccal side from crest to apex level. Grafted particles embedded in and bridged with new bone were included in the calculation, but floating particles in connective tissue were excluded (Figure 2).

2.5. Statistical Analysis. One slide was obtained per tooth. As the experimental areas were P2 and P3, a total of 16 slides were obtained. The control and test groups each included 8 slides. All data were analyzed using commercially available software (SPSS version 18.0, SPSS, Inc., Chicago, IL, USA). The Wilcoxon test was used to compare the baseline and postsurgical values. The Mann-Whitney U test was used to

Table 1: Probing depth, width of keratinized tissue, buccal tipping angle, and new bone area.

		PD (mm)	WKT (mm)	Angle (°)	NB (%)
Control	Baseline	1.636 ± 0.492	3.955 ± 0.461$^{\#}$	31.19 ± 14.60	79.5 ± 16.0
	12 weeks	1.773 ± 0.685†	3.500 ± 0.802$^{\#}$		
Test	Baseline	1.682 ± 0.451*	4.000 ± 0.787	28.12 ± 11.48	78.9 ± 19.5
	12 weeks	2.386 ± 0.755*,†	3.750 ± 0.935		

$^{*\dagger\#}P < 0.05$.

compare the test and control sides. The α error was set at 0.05. Interexaminer differences were evaluated with the intraclass correlation coefficient (ICC).

3. Results

3.1. Clinical and Histomorphometric Findings. All the experimental sites showed uneventful healing and minimal, if any, inflammatory signs. PD increased after the surgery on both the test (by 0.704 mm; $P = 0.001$) and the control (by 0.136 mm; $P = 0.011$) sides. The increase in PD was more prominent on test sides than control sides. On the control sides, the WKT reduced significantly by 0.455 mm ($P = 0.028$). However, on test sides, the WKT reduction of 0.250 mm was not significant ($P = 0.410$) (Table 1). The ICCs for the buccal tipping angle and bone area measurements were 0.997 and 0.956, respectively ($P < 0.001$ in both cases). The buccal tipping angles were 31.19° ± 14.60° and 28.12° ± 11.48° on the control and test sides, respectively, and this difference was not statistically significant ($P = 0.406$). The new bone area was 79.5 ± 16.0% on the control side, and on the test side it was 78.9 ± 19.5%, not a statistically significant difference ($P = 0.949$) (Table 1). Approximately 79% of buccal bone wall was reformed. There were no statistically significant differences in new bone formation at the buccal wall, or in tipping movement, between the groups.

3.2. Histological Observations. Connective tissue within the buccal bone was designated bone-derived mesenchymal matrix (Figure 2, red arrow) and that in the periodontal ligament (PDL) was designated PDL-derived mesenchymal matrix (Figure 2, yellow arrow). Thick, dense connective tissue covering the buccal bone surface was designated buccal mesenchymal matrix (Figure 2, black arrow).

Bone formation was substantial in the bone-derived mesenchymal matrix (Figure 3). Some areas did not show DBBM particles. However, most of the particles were embedded in or bridged with new bone and/or encapsulated by the bone-derived and/or buccal mesenchymal matrix. Two features were prominent. One was the considerable amount of bone formation from the bone-derived mesenchymal matrix (Figure 3, white arrowheads), and the other was reformation of the buccal bone crest from bone-derived and/or PDL-derived mesenchymal matrix in the coronal direction along the root surfaces (Figure 3, red arrowheads, Figures 4(a) and 4(b)). In this study, original buccal bone at the crest was not seen, and encapsulated graft particles were embedded in bone-/PDL-derived mesenchymal matrices (Figures 4(a) and 4(b)). Bone modeling was not localized; it was apparent throughout the buccolingual alveolar and basal bone. The buccal mesenchymal matrix covered the buccal bone surface and seemed to play a role in periosteum. Enlarged bone marrow filled with fat tissue was also a distinguishing phenomenon. The maxillary buccal bone surface in the middle/apical area was flatter on the test side than on the control side (Figure 3(b), white arrowheads, Figure 5). Gingival recession was absent, but root surface resorption was sometimes observed.

4. Discussion

It has been assumed that, in alveolar remodeling during orthodontic tooth movement, the amounts of bone resorption and formation are equal. However, recent computed tomography (CT) studies have shown that alveolar bone thickness decreases in the direction of tooth movement [20–22]. The remodeling capacity of alveolar bone cannot compensate for bone loss in every case. Once the cortical plate is fenestrated, the buccal root surface becomes devoid of cortical bone [20–22], and subsequent osteogenesis is insufficient to cover the root surface completely. CT scans have not shown newly formed cortical plate in patients who develop fenestration [23, 24]. In addition, histological studies have not demonstrated regeneration of the cortical plate [25, 26]. Therefore, orthodontic tooth movement beyond the alveolar housing can cause periodontal problems such as fenestration, dehiscence of the buccal cortical plate in hard tissue, and gingival recession in soft tissue. Our results, however, show that augmented corticotomy using DBBM combined with ACM application enables reformation of buccal bone crest on the pressure side, such that buccal soft tissue height could be maintained despite excessive buccal tipping movement. In our study, PD was increased slightly but statistically significantly. WKT was slightly reduced; however, we consider the amount of that reduction negligible from a clinical point of view. Clinical attachment level (CAL) was not measured, but the extent of the change in CAL was thought to be insignificant clinically.

The ability of bone to adapt to mechanical loads is brought about by continuous bone resorption and formation. If these processes occur at different locations, bone morphology can be altered. Frost [27] termed this phenomenon "bone modeling." If bone resorption and formation are balanced, old bone is continuously replaced by new bone, the mechanical integrity of the bone is maintained, and no morphological changes occur. Frost [28, 29] termed this lack of morphological changes "bone remodeling." As shown in

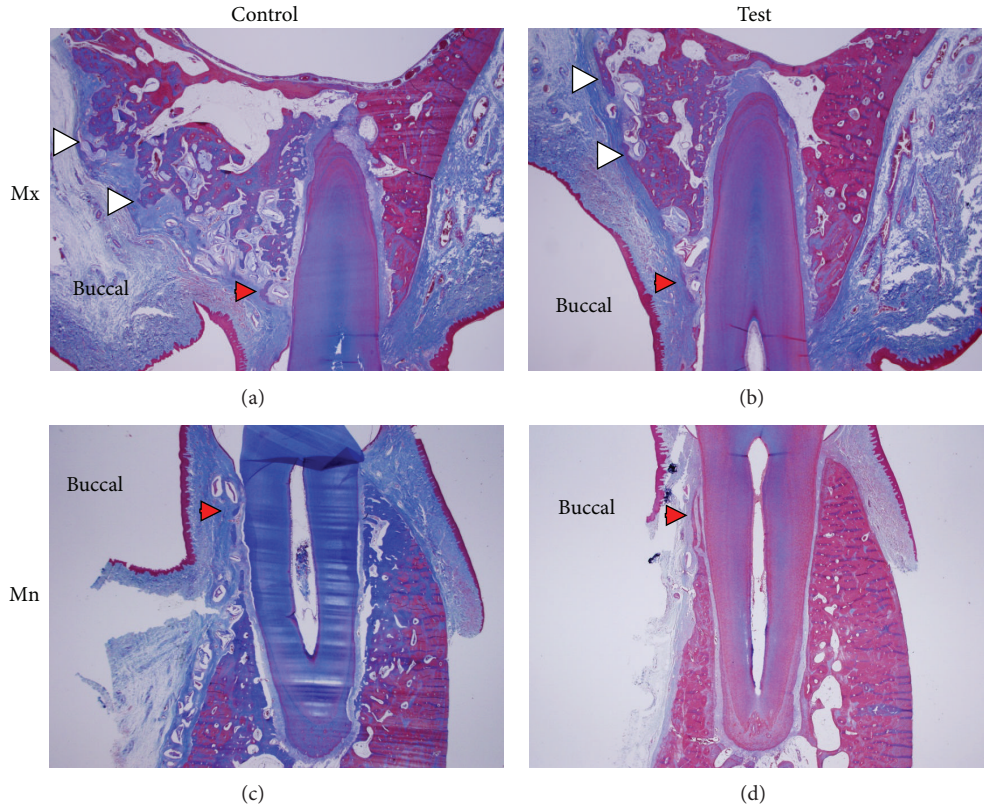

Figure 3: Micrographs of buccolingual sections from the control ((a), (c)) and test sides ((b), (d)) in the maxilla ((a), (b)) and mandible ((c), (d)). Red arrowheads indicate bone formation over DBBM particles in the crest area. White arrowheads in (a) (control) indicate exophytic new bone formation from the buccal bone wall by bone-derived mesenchymal matrix that formed irregular bone surfaces. White arrowheads in (b) (test) indicate new bone formation from the buccal bone wall by bone-derived mesenchymal matrix that formed even bone surfaces. Masson's trichrome stain was used, and the original magnification was ×12.5.

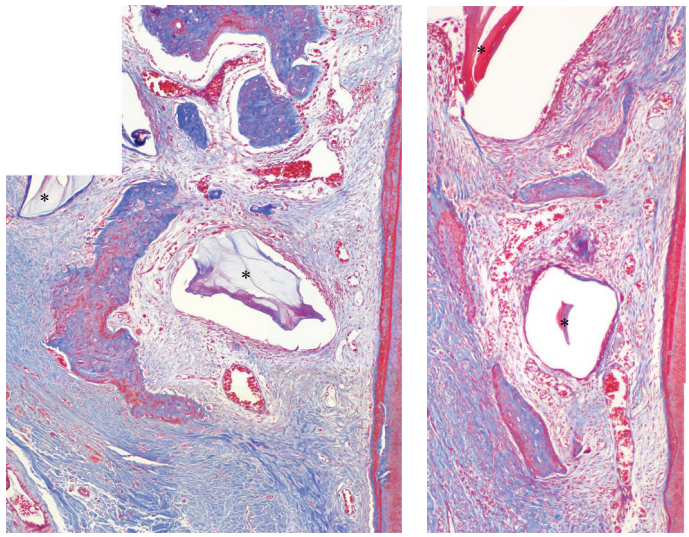

Figure 4: New bone formation in the crest area. (a) Magnification of red arrow head in Figure 3(a) (control). (b) Magnification of red arrowhead in Figure 3(b) (test). Newly formed bone islands covered the grafted DBBM particle (∗) along the root surfaces in PDL-derived mesenchymal matrix. R: root. Masson's trichrome stain was used, and the original magnification was ×100.

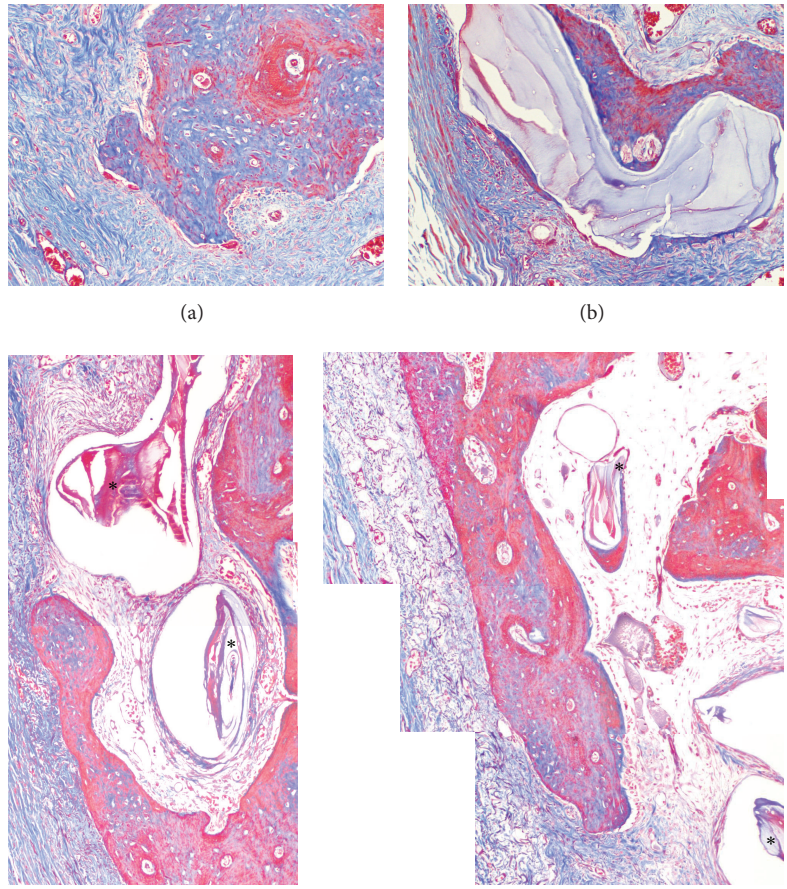

Figure 5: New bone formation in the apical area. (a), (b) Magnification of white arrowheads in Figure 3(a) (control). Exophytic bone formation from the bone surface by bone-derived mesenchymal matrix formed irregular bone surfaces. (c), (d) Magnification of white arrowheads in Figure 3(b) (test). ACM restricted the flow or extension of bone-derived mesenchymal matrix and resulted in an even surface. The grafted DBBM particles (∗) which were encapsulated by matrix or connected to newly formed bone are indicated. Masson's trichrome stain was used, and the original magnification was ×100.

Figures 3 and 4, bone formation from the PDL-/bone-derived mesenchymal matrix recovered the buccal bone crest, and newly formed bone islands covered graft particles (Figure 4) and old bone (Figure 3(d), red arrowhead). The original buccal bone plate and most of the DBBM graft particles were resorbed. The expansion of mesenchymal matrices enabled reformation of bone crest and formed new bone on the buccal side. These phenomena are thought to represent "bone modeling," which maintains soft tissue height at the buccal bone crest. In this bone modeling, periodontal tissue reestablishment was demonstrated. The effect of membrane application was prominent in the middle/apical area of buccal bone (Figures 3 and 5). This suggests that ACM can control the shape of the bone surface, as well as performing its primary function.

Yaffe et al. [30] investigated regional acceleratory phenomenon (RAP) by using radiological methods. They reported enlarged bone marrow and striking resorption of the cortical bone, both on the surface and in the alveolar bone proper, on the buccal aspect. Our study yielded the same histological finding. In addition, the expansion of bone marrow and buccal bone by the bone-derived mesenchymal matrix is thought to contribute to bone modeling and remodeling.

Some bone formation or modeling at the buccal crest might function as a compensatory mechanism [31]. Orthodontic tooth movement is a stimulating factor for bone apposition [32, 33]. However, whether the stimulating factor for compensatory bone formation was corticotomy or orthodontic force was not clear in this study. Further research is required to elucidate the stimulating factors in this context.

This study demonstrated an optimal response to applied forces, because the response was mediated by the PDL, spongiosa [34], and periosteum. More active and extensive bone modeling and remodeling suggest that accelerated tooth movement associated with augmented corticotomy is due to increased bone turnover and RAP [35], as shown by our results. Further, Nowzari et al. [36] reported that the alveolar

ridge maintains its original thickness and configuration despite buccal tipping movement. Our study also demonstrated that the alveolar ridge width does not decrease, and the buccal bone crest is maintained despite excessive buccal tipping movement. Moreover, Machado et al. [37] reported a reduction of 1.1 mm in apical root resorption of the maxillary central incisors, in comparison with traditional orthodontics. However, in the current study, only root surface resorption was found at some buccal and apical pressure areas.

Wilcko et al. [38] suggested that when the relatively thin alveolar housing over the root surface undergoes demineralization, the remaining collagenous soft tissue matrix of the bone could be readily transported with the root surface, in the direction of movement, a phenomenon termed "bone matrix transportation." When retained in the desired position, the matrix is remineralized. Our study demonstrated new bone in almost 79% of the buccal bone wall at 12 weeks after augmented corticotomy with DBBM, irrespective of the application of ACM. Nevertheless, whether bone matrix transportation occurred is not clear, and its mechanism should be investigated. This phenomenon could be part of bone modeling/remodeling and activation. In the grafted areas, new bone emerged from the existing bone surface and bridged the DBBM particles in the bone- or PDL-derived mesenchymal matrix. Bone modeling and remodeling might have occurred simultaneously and resulted in graft entrapment and resorption over the 12 weeks. The phenomena associated with augmented corticotomy with DBBM may be multifactorial responses and may not be caused by bone matrix transportation.

5. Conclusions

Buccal tipping angle and new bone formation in the buccal wall are not directly affected by the use of ACM in augmented corticotomy. However, the use of ACM in augmented corticotomy can promote an even buccal bone surface morphology. Augmented corticotomy using DBBM combined with ACM application may stimulate periodontal tissue reestablishment, and intact PDL and periosteum are prerequisites for optimal therapeutic outcomes. It may be particularly suitable for rapid orthodontic treatment or GBR.

Conflict of Interests

The authors declare that there is no conflict of interests regarding the publication of this paper.

Authors' Contribution

Drs. Seong-Hun Kim and Eun-Cheol Kim contributed equally to this work.

Acknowledgments

All the authors of this paper certify that this research is original, not under consideration for publication elsewhere, and free of conflict of interests. This work was supported by the National Research Foundation of Korea (NRF), funded by the Korean Government (MEST) (no. 2012R1A5A2051388).

References

[1] S.-H. Kim, I. Kim, D. Jeong, K. Chung, and H. Zadeh, "Corticotomy-assisted decompensation for augmentation of the mandibular anterior ridge," *The American Journal of Orthodontics and Dentofacial Orthopedics*, vol. 140, no. 5, pp. 720–731, 2011.

[2] H.-W. Ahn, D.-Y. Lee, Y.-G. Park, S.-H. Kim, K.-R. Chung, and G. Nelson, "Accelerated decompensation of mandibular incisors in surgical skeletal Class III patients by using augmented corticotomy: a preliminary study," *American Journal of Orthodontics and Dentofacial Orthopedics*, vol. 142, no. 2, pp. 199–206, 2012.

[3] D. Quteish, S. Singrao, and A. E. Dolby, "Light and electron microscopic evaluation of biocompatibility, resorption and penetration characteristics of human collagen graft material," *Journal of Clinical Periodontology*, vol. 18, no. 5, pp. 305–311, 1991.

[4] N. Miller, J. Penaud, B. Foliguet, H. Membre, P. Ambrosini, and M. Plombas, "Resorption rates of 2 commercially available bioresorbable membranes. A histomorphometric study in a rabbit model," *Journal of Clinical Periodontology*, vol. 23, no. 12, pp. 1051–1059, 1996.

[5] G. Juodzbalys, A. M. Raustia, and R. Kubilius, "A 5-year follow-up study on one-stage implants inserted concomitantly with localized alveolar ridge augmentation," *Journal of Oral Rehabilitation*, vol. 34, no. 10, pp. 781–789, 2007.

[6] P. Bunyaratavej and H. Wang, "Collagen membranes: a review," *Journal of Periodontology*, vol. 72, no. 2, pp. 215–229, 2001.

[7] H. Wang and L. Boyapati, ""pASS" principles for predictable bone regeneration," *Implant Dentistry*, vol. 15, no. 1, pp. 8–17, 2006.

[8] M. Simion, A. Scarano, L. Gionso, and A. Piattelli, "Guided bone regeneration using resorbable and nonresorbable membranes: a comparative histologic study in humans," *International Journal of Oral and Maxillofacial Implants*, vol. 11, no. 6, pp. 735–742, 1996.

[9] M. Simion, U. Misitano, L. Gionso, and A. Salvato, "Treatment of dehiscences and fenestrations around dental implants using resorbable and nonresorbable membranes associated with bone autografts: a comparative clinical study," *The International Journal of Oral and Maxillofacial Implants*, vol. 12, no. 2, pp. 159–167, 1997.

[10] C. H. F. Hämmerle and N. P. Lang, "Single stage surgery combining transmucosal implant placement with guided bone regeneration and bioresorbable materials," *Clinical Oral Implants Research*, vol. 12, no. 1, pp. 9–18, 2001.

[11] S. Garrett, "Periodontal regeneration around natural teeth," *Annals of Periodontology*, vol. 1, no. 1, pp. 621–666, 1996.

[12] P. Locci, M. Calvitti, S. Belcastro et al., "Phenotype expression of gingival fibroblasts cultured on membranes used in guided tissue regeneration," *Journal of Periodontology*, vol. 68, no. 9, pp. 857–863, 1997.

[13] D. Buser, C. Dahlin, and R. K. Schenk, *Guided Bone Regeneration in Implant Dentistry*, Quintessence Publishing, Chicago, Ill, USA, 1st edition, 1994.

[14] M. E. Fritz, "Implant therapy II," *Annals of Periodontology*, vol. 1, no. 1, pp. 796–815, 1996.

[15] N. Blumenthal and J. Steinberg, "The use of collagen membrane barriers in conjunction with combined demineralized bone-collagen gel implants in human infrabony defects," *Journal of Periodontology*, vol. 61, no. 6, pp. 319–327, 1990.

[16] C. C. Chen, H.-L. Wang, F. Smith, G. N. Glickman, Y. Shyr, and R. B. O'Neal, "Evaluation of a collagen membrane with and without bone grafts in treating periodontal intrabony defects," *Journal of Periodontology*, vol. 66, no. 10, pp. 838–847, 1995.

[17] W. H. B. Mawhinney, E. Richardson, and A. J. Malcolm, "Technical methods. Control of rapid nitric acid decalcification," *Journal of Clinical Pathology*, vol. 37, no. 12, pp. 1409–1415, 1984.

[18] H. H. W. Verdenius and L. Alma, "A quantitative study of decalcification methods in histology," *Journal of Clinical Pathology*, vol. 11, no. 3, pp. 229–236, 1958.

[19] J. B. Matthews and G. I. Mason, "Influence of decalcifying agents on immunoreactivity of formalin-fixed paraffin-embedded tissue," *Histochemical Journal*, vol. 16, no. 7, pp. 771–787, 1984.

[20] W. M. Wainwright, "Faciolingual tooth movement: its influence on the root and cortical plate," *American Journal of Orthodontics*, vol. 64, no. 3, pp. 278–302, 1973.

[21] H. Wehrbein, R. A. W. Fuhrmann, and P. R. Diedrich, "Human histologic tissue response after long-term orthodontic tooth movement," *American Journal of Orthodontics and Dentofacial Orthopedics*, vol. 107, no. 4, pp. 360–371, 1995.

[22] K. Nam, J. Kang, S. Moon et al., "Alveolar bone loss around incisors in class I bidentoalveolar protrusion patients: a retrospective 3D CBCT study," *Dentomaxillofacial Radiology*, vol. 41, no. 6, pp. 481–488, 2012.

[23] S. Sarikaya, B. Haydar, S. Ciğer, and M. Ariyürek, "Changes in alveolar bone thickness due to retraction of anterior teeth," *American Journal of Orthodontics and Dentofacial Orthopedics*, vol. 122, no. 1, pp. 15–26, 2002.

[24] A. Vardimon, A. Spiegler, and S. Pitaru, "Rapid palatal expansion. Part 2: dentoskeletal changes in cats with patent versus synostosed midpalatal suture," *American Journal of Orthodontics and Dentofacial Orthopedics*, vol. 113, no. 5, pp. 488–497, 1998.

[25] T. Karring, S. Nyman, B. Thilander, and I. Magnusson, "Bone regeneration in orthodontically produced alveolar bone dehiscences," *Journal of Periodontal Research*, vol. 17, no. 3, pp. 309–315, 1982.

[26] C. E. Wingard and G. M. Bowers, "The effects of facial bone from facial tipping of incisors in monkeys," *Journal of Periodontology*, vol. 47, no. 8, pp. 450–454, 1976.

[27] H. M. Frost, "The regional acceleratory phenomenon: a review," *Henry Ford Hospital Medical Journal*, vol. 31, no. 1, pp. 3–9, 1983.

[28] H. M. Frost, "The biology of fracture healing. An overview for clinicians. Part I," *Clinical Orthopaedics and Related Research*, no. 248, pp. 283–293, 1989.

[29] H. M. Frost, "The biology of fracture healing. An overview for clinicians. Part II," *Clinical Orthopaedics and Related Research*, no. 248, pp. 294–309, 1989.

[30] A. Yaffe, N. Fine, and I. Binderman, "Regional accelerated phenomenon in the mandible following mucoperiosteal flap surgery," *Journal of Periodontology*, vol. 65, no. 1, pp. 79–83, 1994.

[31] S. Shimpo, Y. Horiguchi, Y. Nakamura et al., "Compensatory bone formation in young and old rats during tooth movement," *European Journal of Orthodontics*, vol. 25, no. 1, pp. 1–7, 2003.

[32] A. D. Vardimon, C. E. Nemcovsky, and E. Dre, "Orthodontic tooth movement enhances bone healing of surgical bony defects in rats," *Journal of Periodontology*, vol. 72, no. 7, pp. 858–864, 2001.

[33] S. Kim, S. Moon, S. Kang, and Y. Park, "Effects of low-level laser therapy after Corticision on tooth movement and paradental remodeling," *Lasers Surgery Medicine*, vol. 47, no. 7, pp. 524–533, 2009.

[34] M. T. Wilcko, W. M. Wilcko, J. J. Pulver, N. F. Bissada, and J. E. Bouquot, "Accelerated osteogenic orthodontics technique: a 1-stage surgically facilitated rapid orthodontic technique with alveolar augmentation," *Journal of Oral and Maxillofacial Surgery*, vol. 67, no. 10, pp. 2149–2159, 2009.

[35] Y. A. Mostafa, M. M. S. Fayed, S. Mehanni, N. N. ElBokle, and A. M. Heider, "Comparison of corticotomy-facilitated vs standard tooth-movement techniques in dogs with miniscrews as anchor units," *American Journal of Orthodontics and Dentofacial Orthopedics*, vol. 136, no. 4, pp. 570–577, 2009.

[36] H. Nowzari, F. K. Yorita, and H. C. Chang, "Periodontally accelerated osteogenic orthodontics combined with autogenous bone grafting," *The Compendium of Continuing Education in Dentistry*, vol. 29, no. 4, pp. 2–8, 2008.

[37] I. Machado, D. J. Ferguson, M. T. Wilcko, and W. M. Wilcko, "Root resorption after orthodontic treatment with or without alveolar corticotomy," *Revista Venezolana de Ortodoncia*, vol. 19, pp. 647–653, 2002.

[38] M. T. Wilcko, W. M. Wilcko, and N. F. Bissada, "An evidence-based analysis of periodontally accelerated orthodontic and osteogenic techniques: a synthesis of scientific perspectives," *Seminars in Orthodontics*, vol. 14, no. 4, pp. 305–316, 2008.

Hindawi Publishing Corporation
BioMed Research International
Volume 2014, Article ID 417541, 13 pages
http://dx.doi.org/10.1155/2014/417541

Research Article

Dynamics of Alloplastic Bone Grafts on an Early Stage of Corticotomy-Facilitated Orthodontic Tooth Movement in Beagle Dogs

Hyung-Joo Choi,[1,2] Dong-Yeol Lee,[3] and Tae-Woo Kim[1]

[1] *Seoul National University School of Dentistry & Dental Research Institute, Seoul 110-768, Republic of Korea*
[2] *Seoul Barun Dental Clinic, Anyang, Gyeonggi-do 431-050, Republic of Korea*
[3] *Department of Oral and Maxillofacial Pathology and Research Center for Tooth & Periodontal Regeneration (MRC), School of Dentistry, Kyung Hee University, Seoul 130-701, Republic of Korea*

Correspondence should be addressed to Tae-Woo Kim; taewoo@snu.ac.kr

Received 22 July 2014; Accepted 5 August 2014; Published 3 September 2014

Academic Editor: Seong-Hun Kim

Alveolar augmented corticotomy is effective in accelerating orthodontic tooth movement, but the effect only lasts for a relatively short time. Therefore, the purpose of this study was to investigate the underlying biology of the immediate periodontal response to orthodontic tooth movement after a corticotomy with alloplastic bone grafts. The results demonstrated that measurable tooth movement began as early as 3 days after the intervention in beagle dogs. Based on the results and histological findings, augmented corticotomy-facilitated orthodontic tooth movement might enhance the condition of the periodontal tissue and the stability of the outcomes of orthodontic treatment.

1. Introduction

New appliances, materials, and mechanics of orthodontic treatment are being developed every day, but much of the biology of orthodontic tooth movement still needs to be clarified. Many adjunctive modalities are available to accelerate orthodontic tooth movement in humans, such as corticotomy [1–9], distraction osteogenesis [10], mechanical vibration [11], medication with local prostaglandins, and low-level laser treatment [12, 13]. Among these interventions, corticotomy is known to be the most effective means to accelerate orthodontic tooth movement [7, 14]. In experiments that used a split-mouth design, with corticotomy performed on one side and the other side serving as the control, the velocity of the tooth movement was accelerated on the corticotomy side [1, 15–17], and the amount of movement doubled over the duration of the experiments [15–18].

The initial microscopic changes and early application of orthodontic force have been emphasized in corticotomy-facilitated orthodontic tooth movement [14], and it has been hypothesized that a corticotomy or an osteotomy can lead to intensified osteoclastic activity resulting in local osteopenia and increased bone remodeling [2, 15, 19, 20]. To date, however, the immediate periodontal response has not been fully elucidated. Most researchers have either studied the small animals such as rats, cats, or rabbits [2, 6, 18–20], for relatively long periods of 6–12 weeks [4, 5], or carried out gross observational studies with no histologic measurements [1, 2, 9, 17, 21].

The purpose of this study was to investigate the immediate periodontal response to a corticotomy with alloplastic bone grafts in beagle dogs.

2. Materials and Methods

2.1. Animal Subjects. Five adult male beagle dogs, weighing 10–13 kg, were used in the experiment, and their selection, care, and preparation, together with the surgical protocol, were carried out according to the guidelines for animal experiments (IRB no. KHMC-IACUC2012-024). They were caged separately under regulated conditions and fed a normal diet

and water *ad libitum* to secure the experimental orthodontic appliances.

For the preparation processes and surgical procedures, the animals were anesthetized with a mixture of tiletamine-zolazepam and xylazine, via intramuscular and intravenous injections using a catheter in the vessel of the ear.

2.2. Study Preparation. Alginate impressions of each beagle were taken to make study models, and orthodontic appliances were custom-made for each model. The canine and fourth premolar teeth were banded to form anchor teeth, and a Ø 0.9 mm stainless steel wire was welded onto the buccal surface of the bands. The second and third premolars were banded with a lingual button. After 2 weeks, the animals were anesthetized to fit the orthodontic appliances to the teeth (Figure 1).

2.3. Surgical Procedures for the Corticotomy and Alloplastic Bone Graft. Under general anesthesia, 2% lidocaine with 1 : 100,000 epinephrine was also infiltrated to the surgical sites. An intrasulcus incision was performed with a no. 12 blade from the canine tooth to the first molar, and a full-thickness flap was lifted. The circumscribing corticotomy (Figure 2(a)) was performed with a round bur (Ø 1.5 mm) under sterile saline irrigation. Alloplastic bone material (MBCP+, Biomatlante, Vigneux de Bretagne, France), composed of 20% hydroxyl apatite and 80% β-tri-calcium phosphate, was used for the graft. The graft bone was soaked with blood, and 1 g of the MBCP+ was grafted onto the surgical surface (Figure 2(b)). The mucoperiosteal flaps were repositioned and sutured with 5–0 nylon and primary closure was obtained (Figure 2(c)). A closed coil spring made of nickel-titanium shape memory wire of 200 g force was applied to the second and third premolars in a buccolingual direction (Figure 2(d)).

All of the surgical procedures were performed under sterile conditions to prevent infection. After surgery, antibiotics and anti-inflammatory analgesics were administered by intramuscular injection twice a day for 6 days. A 1% chlorhexidine-gluconate solution dressing was applied simultaneously for infection control. A soft diet was supplied for 1 or 2 weeks and then a normal diet. Mechanical plaque control was performed once a week. The animals were euthanized with an overdose of thiopental sodium after 1 day, 3 days, 1 week, 2 weeks, and 4 weeks following the surgery (Figure 3).

2.4. Histological Processing and Analysis. Following a predetermined time schedule, after the animals were killed, their maxillae and mandibles were dissected, and the sections containing the canine to the fourth premolar teeth were retrieved. The block specimens were rinsed in sterile saline and immediately immersed in 10% neutral-buffered formalin fixatives for 14 days. The block specimens were large, and rapid decalcification was performed for 6 days using 5% nitric acid because it is sufficiently strong [22]. Had this study been designed for immunohistology, the use of ethylene-diamine-tetra-acetic acid or 10% aqueous or formic acid would have been suitable [23], but this was not the case [5, 24]. The specimens were then dehydrated through a series of ethanol solutions of increasing concentrations and embedded in paraffin. Buccolingual sections were sliced with a microtome set at 5 μm and stained with the Masson's trichrome solution. One slide was processed per experimental tooth.

Histological examinations were conducted using a light microscope (Olympus BX 51, Olympus, Tokyo, Japan) equipped with a DP controller 3.2.276.2 and DP manager 3.1.1.208 (Olympus, Tokyo, Japan). After microscopic examination, a photograph of each slide was taken with a digital camera (Olympus DP 71, Olympus, Tokyo, Japan). With imaging software (cellSens version 1.6, Olympus), we measured the buccal tipping angle (°) and distance (μm). The buccal tipping angle was measured from the reversal line of the lingual/palatal bone wall to the lingual/palatal root surface. The buccal tipping distance was measured from the lingual/palatal alveolar crest to the shortest lingual/palatal root surface. A total of 40 slides were fabricated and examined. After taking photographs, the amount of tooth movement was measured three times in each slide for angular changes and linear displacement.

2.5. Statistical Data Analysis. Statistical data analysis was performed using the R programming language [25]. The data on tooth movement did not fulfill the parametric conditions of normality and equality of variance after the D'Agostino normality test was performed. We therefore conducted the Kruskal-Wallis rank sum test to determine whether there existed a significant between-group difference in general and the Wilcoxon test to find a significant pair between two groups. The Bonferroni correction and the Type I error were applied to counteract the problem of multiple comparisons. The data were analyzed with a confidence level of 95%.

3. Results

3.1. Clinical Findings. Figure 4 shows the amount of tooth movement for each beagle dog. Due to the minimal tooth movement, the buccal tipping angle at 1 day could not be measured. No significant difference was observed between the teeth in the maxilla and those in the mandible or in the right or left part of the dentition. When the tipping movement was measured from the angular changes, no statistically significant difference was found among the experimental groups (Figure 4(a)). However, the linear measurements demonstrated statistically significant differences between 1 day and 3 days and between 2 weeks and 4 weeks after the start of the experiment (Figure 4(b)).

3.2. Histological Observations. After 1 day of orthodontic movement, a microphotograph of the buccopalatal/lingual section (Figure 5) showed compression of the periodontal ligament (PDL) (Figure 5(b)), extravasations of red blood cells (RBC) (Figure 5(c)), and reduced capillaries (Figure 5(e)) on the pressure side. No significant finding was observed on the tension side.

At 3 days, the PDL was more severely compressed and fewer cells were found in the PDL space (Figure 6(c)) on the

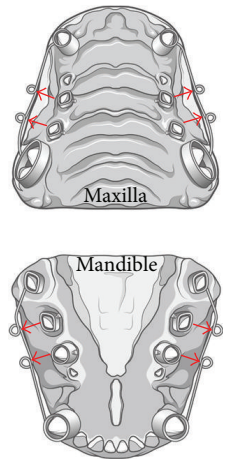

Figure 1: Orthodontic appliances were custom-made for each study model. The canine and fourth premolar teeth were banded to form an anchor tooth, and a Ø 0.9 mm stainless steel wire was welded on the buccal surface of the bands. The second and third premolars were banded with a lingual button. After 4 weeks, the animals were anesthetized to fit the orthodontic appliances to the teeth. The arrows indicate the direction of force.

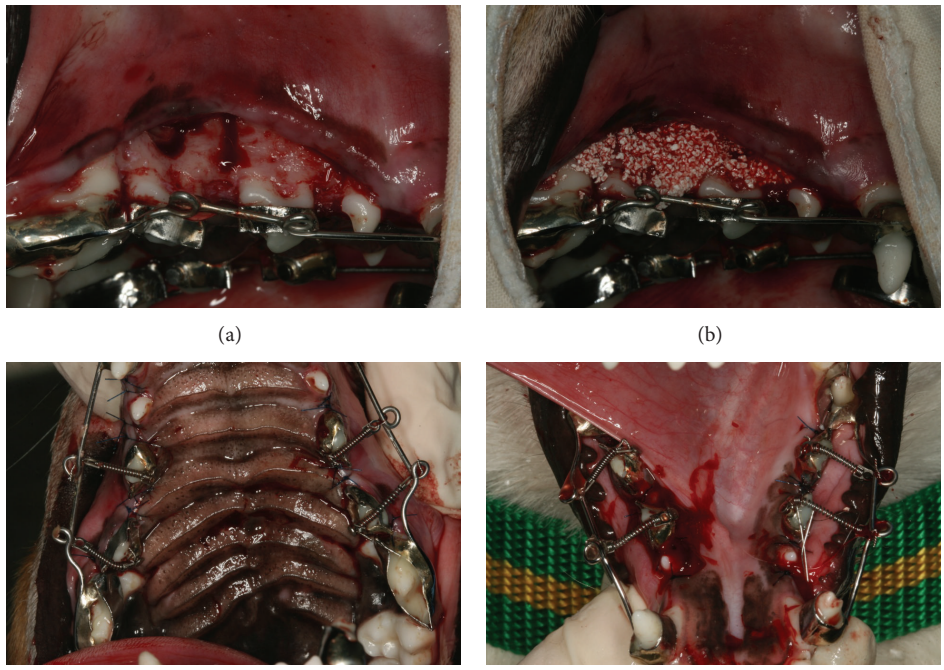

Figure 2: Surgical procedure. (a) Corticotomy: the circumscribing corticotomy was performed with a round bur (Ø 1.5 mm) under sterile saline irrigation. (b) MBCP$^+$ (Biomatlante, Vigneux de Bretagne, France), composed of 20% hydroxyl apatite and 80% β-tri-calcium phosphate, was used as the alloplastic bone graft material. The graft bone was applied soaked in blood; 1 g of the MBCP$^+$ was grafted on the surgical surface. (c) A closed coil spring made of nickel-titanium shaped memory wire of 200 g force was applied to the second and third premolars in a buccolingual direction in the maxilla and (d) in the mandible.

buccal pressure side. The tension side at the lingual alveolar bone crest contained more cells than the pressure side and active osteoblasts forming a new bone (Figure 6(h)).

At 1 week after the start of the experiment, most of grafted MBCP+ particles were well maintained (Figure 7). On the pressure side, the PDL space was slightly widened compared with that at 3 days (Figure 7(b)), and the tension side contained abundant PDL fibroblasts and active osteoblasts (Figures 7(d), 7(e), and 7(f)).

At 2 weeks, undermining resorption and a resorption bay were observed on the buccal pressure side (Figures 8(b), 8(c), 8(q), and 8(l)). In contrast, on the buccal tension

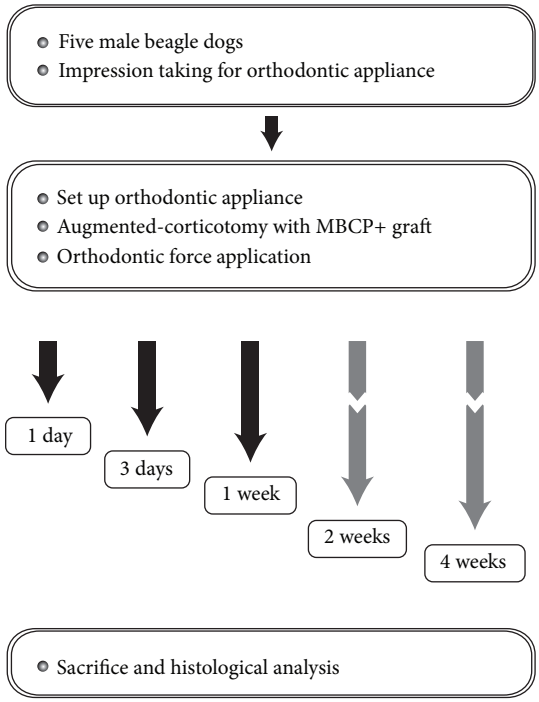

Figure 3: Schematic diagram describing the experiment design.

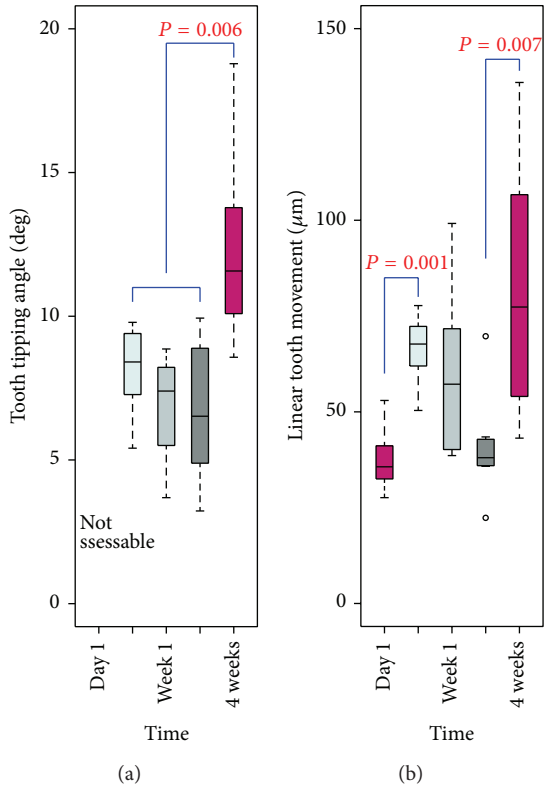

Figure 4: Box plots for the tooth movement measurements. (a) No statistically significant difference in the angular tooth movement was observed over time. (b) However, the linear measurements demonstrated statistically significant differences between 1 day and 3 days and between 2 weeks and 4 weeks after the start of the experiment.

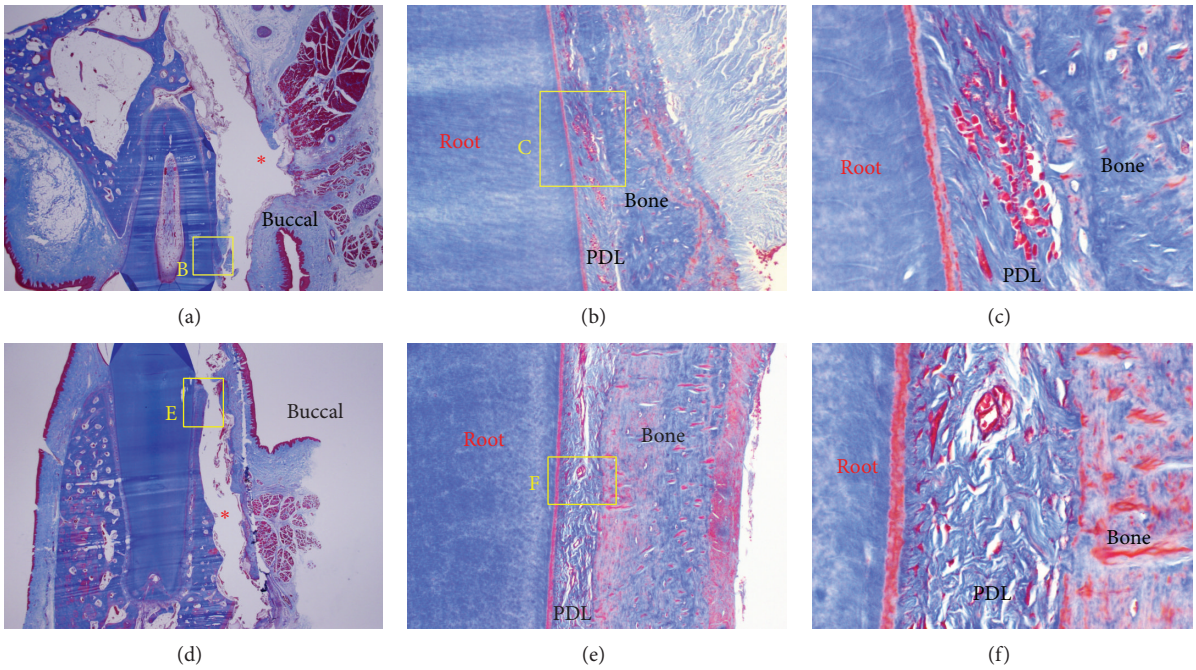

Figure 5: Microphotograph of a buccopalatal/lingual section of the 1-day experiment. (a) Maxilla. (b) Higher magnification of (a). On the pressure side, the PDL was compressed. (c) Higher magnification of (b). Extravasation of RBC was observed. (d) Mandible. (e) Higher magnification of (d). Compression of the PDL was shown, and reduced capillaries were identified. (f) Higher magnification of (e). The number of cells was reduced, and grafted MBCP+ particles were lost in the process of making the histological section; the red ∗ in (a) and (d) indicates empty spaces that were occupied by MBCP+ graft particles. Masson's trichrome stain. Original magnification was ×12.5 for (a) and (d), ×100 for (b) and (e), and ×400 for (c) and (f).

side, new bone formation surrounding and bridging the MBCP+ particles was seen (Figures 8(d), 8(j), and 8(f)) due to abundant osteoblasts (Figures 8(e) and 8(k)).

At 4 weeks after the start of the experiment, new bone formation along the PDL formed a new buccal bone wall on the pressure side (Figure 9(a)). Also, a new bone island was formed in the center of the bone-derived mesenchymal matrix (Figure 9(d)), and osteoblasts and osteocytes were observed (Figure 9(e)). On the buccal side, grafted MBCP+ particles were bridged with newly formed bone in the bone-derived mesenchymal matrix. Entrapped osteocytes and aggregated osteoblasts were observed (Figure 9(g)). The palatal crestal (Figure 9(j)) and apical (Figure 9(l)) tension sides showed aggregated osteoblasts and active forms of osteoblasts, and a new bone-forming buccal bone wall and crest were observed (Figure 9(o): native bone (red star) and new bone (yellow star)). New bone was formed on the outer and inner surfaces of the native bone (Figures 9(n) and 9(q)), and the outer portion of the bone-derived mesenchymal matrix could be seen (Figure 9(t)).

4. Discussion

The biological mechanism by which the tooth movement is facilitated after a corticotomy has been suggested to be mediated by a regional acceleratory phenomenon [26, 27], which might boost the appearance of the macrophages that eliminate the hyaline as early as 1 week after the application of orthodontic force [15, 19]. For this reason, we designed an experiment to determine immediate periodontal responses, which represents the first study to observe the immediate effect of corticotomy-facilitated orthodontic tooth movement. Two studies previously reported observations made 3 days after a corticotomy in rats [2, 20]. However, the results obtained in small animals may differ from those in larger animals [14]. We believe that the current study is unique because we observed the histological responses of periodontal tissue as early as 1 day, 3 days, 1 week, 2 weeks, and 4 weeks after a corticotomy and force application for orthodontic tooth movement in larger animals.

In most experiments in dogs or rats, corticotomy-facilitated tooth movement was observed at a rate of about 1 mm per month, which was almost double that observed on the control side [15–18]. In this study, we observed significant tooth movement within 3 days (Figure 4). We measured the width of the PDL at the crest of the lingual/palatal sides, which does not represent the direct distance of clinical tooth movement. The significant tooth movement observed 4 weeks after the start of the experiment was to be expected, but this obviously occurred earlier in the experiment. The tooth movement measurements demonstrated a similar pattern in angular changes and linear displacement, as shown in Figure 4. We conjectured that this might imply that the

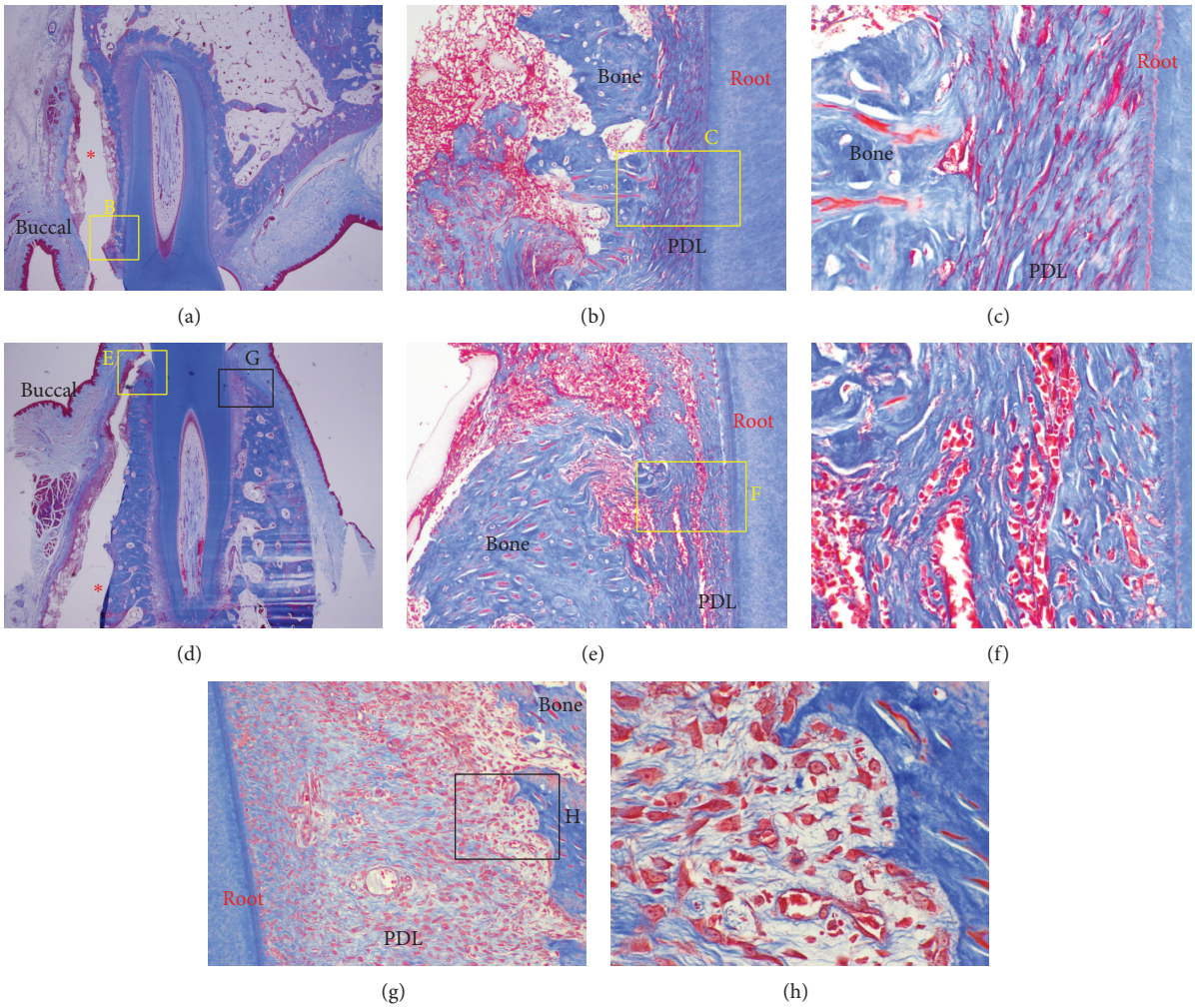

Figure 6: Microphotograph of a buccopalatal/lingual section of the 3-day experiment. (a) Maxilla. (b) Higher magnification of (a). On the pressure side, the PDL was more severely compressed. (c) Higher magnification of (b). Few cells were observed in the PDL space. (d) Mandible. (e) Higher magnification of (d). In common with the maxilla, the PDL was severely more compressed on the pressure side. (f) Higher magnification of (d). Extravasation of RBC was observed in the PDL space. (g) Tension side at the lingual bone crest. The tension side showed abundant cells compared with the pressure side. (h) Higher magnification of (g). Active osteoblasts forming new bone were observed. Grafted MBCP+ particles were lost in the process of making the histological section; the red ∗ in (a) and (d) indicates empty spaces which were occupied by MBCP+ graft particles. Masson's trichrome stain. Original magnification was ×12.5 for (a) and (d), ×100 for (b), (e), and (g), and ×400 for (c), (f), and (h).

pattern of rapid tooth movement was not a bodily translation in general but mostly occurred through tipping of the tooth. Therefore, during clinical orthodontic treatment, methods to control for unwanted tipping should also be considered.

Despite the similar pattern between the angular and linear changes, the linear measurements exhibited a statistically significant difference while the angular changes did not. Linear measurements are assessed between two points while degrees of angles are measured between three points, from which a variation in angular measurements can be produced. This may be the cause of the larger variation in angular measurements than in linear measurements.

A typical cell-free zone on the pressure side and an inflammatory reaction were seen on the 1- and 3-day slides (Figures 5 and 6). A force of 200 g may be strong for tipping movement, but it was difficult to determine the hyalinization layer in the 1- and 3-day slides. The corticotomy was probably responsible for this, but the underlying mechanism was not clear. The progenitor cells regarded as osteoblasts in the 3-day slides showed strong cellular activity.

On the 1-week slide, we observed that the PDL space was widened at the pressure side compared with that of the 3-day slide (Figure 7(b)). This could be explained by undermining resorptions. On the tension side, active osteoblasts forming a new bone were observed. This new bone formation is a common phenomenon in orthodontic tooth movement.

Interestingly, new bone surrounding the graft materials was observed on the compression side on the 2-week slides

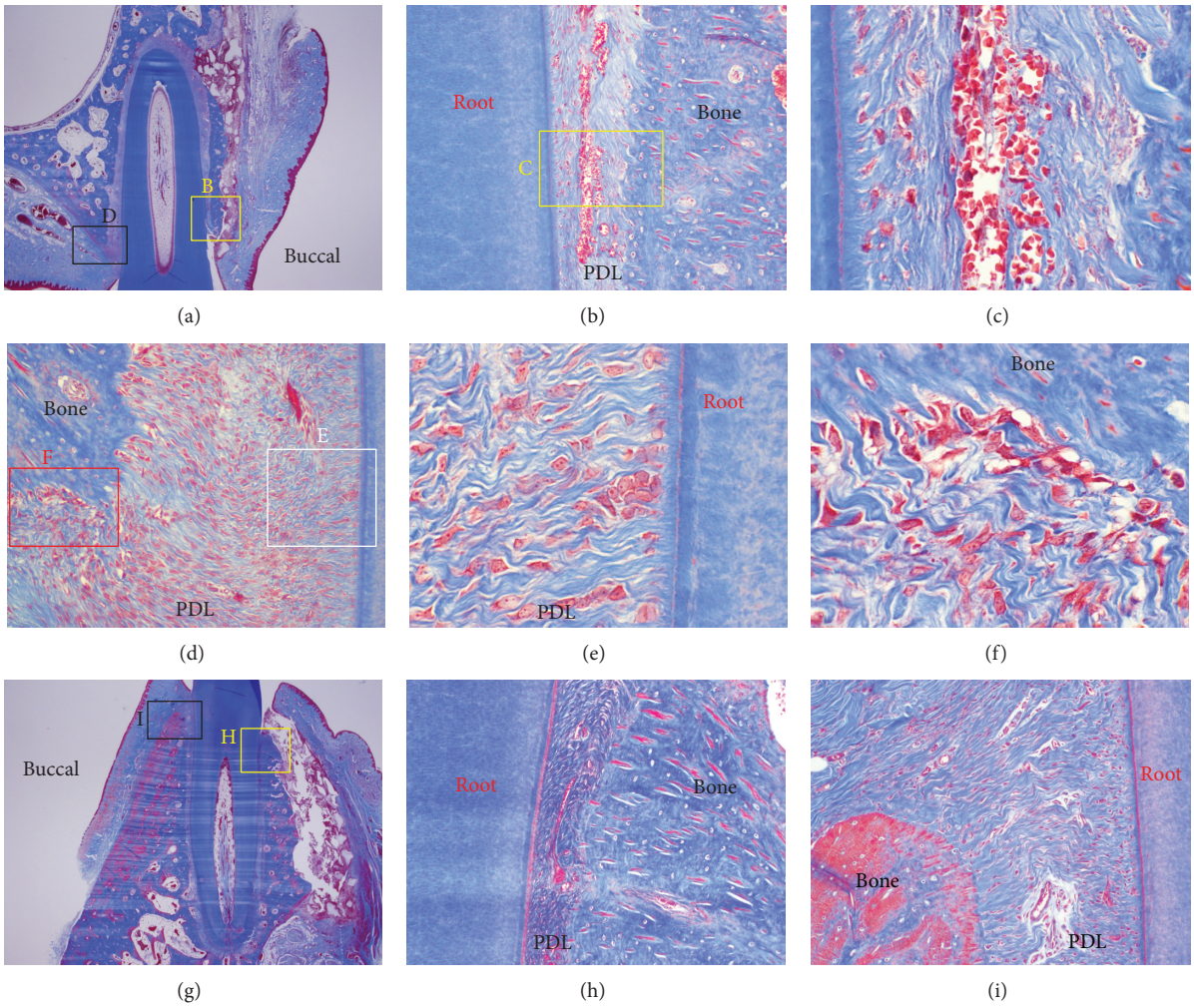

FIGURE 7: Microphotograph of a buccopalatal/lingual section of the 1-week experiment. Most of the grafted MBCP+ particles were well maintained. (a) Maxilla. (b) Higher magnification of (a). On the pressure side, the PDL space was wider than at 3 days. (c) Higher magnification of (b). Extravasation of RBC was observed in the PDL space. (d) Tension side at the palatal bone crest. The tension side showed abundant cells compared with the pressure side and a widened PDL space. (e) Higher magnification of (d). Abundant PDL fibroblasts were seen. (f) Higher magnification of (d). Active osteoblasts forming a new bone were observed. (g) Mandible. Most of the grafted MBCP+ particles were well maintained. (h) Higher magnification of (g). Pressure side. The PDL was compressed. (i) Higher magnification of (g). The tension side showed a widened PDL space. Masson's trichrome stain. Original magnification was ×12.5 for (a) and (g), ×100 for (b), (d), (h), and (i), and ×400 for (c) and (f).

(Figure 8(d)) and at the buccal sides distant from PDL (Figures 8(s), 8(t), and 8(u)). Graft particles were bridged by newly formed bone and osteoclastic and osteoblastic activities were both seen (Figure 8(u)).

From the findings of the 4-week sections, the new bone formation in the center of the MBCP+ graft material on the buccal side was very distinctive (Figures 9(h) and 9(i)), and many entrapped osteocytes and aggregated osteoblasts were observed (Figure 9(g)). However, the cause of this new bone formation on the buccal sides around the graft materials was not certain. Further studies could provide the answer.

The slides taken at 2 and 4 weeks did not show a distinctive loss of periodontal attachment, and the small areas of root resorption that were seen were not significant.

Orthodontic patients have complained about the length of their treatment, and it has become necessary to develop adjunctive methods to tackle this problem [1, 3, 7–13]. Alveolar corticotomy is effective in accelerating orthodontic tooth movement [2, 7, 14]. However, according to pertinent studies [1, 14, 17], the regional acceleratory phenomenon only persists for about 4 months, after which the tooth movement rate returns to normal. To make use of this "window" period in an effective, efficient, and efficacious way, it is imperative to understand the underlying biology of early periodontal responses to tooth movement after augmented corticotomy and to develop appropriate clinical procedures. Also, from the clinical point of view, it is important to determine how to reduce the length of total treatment time. When should

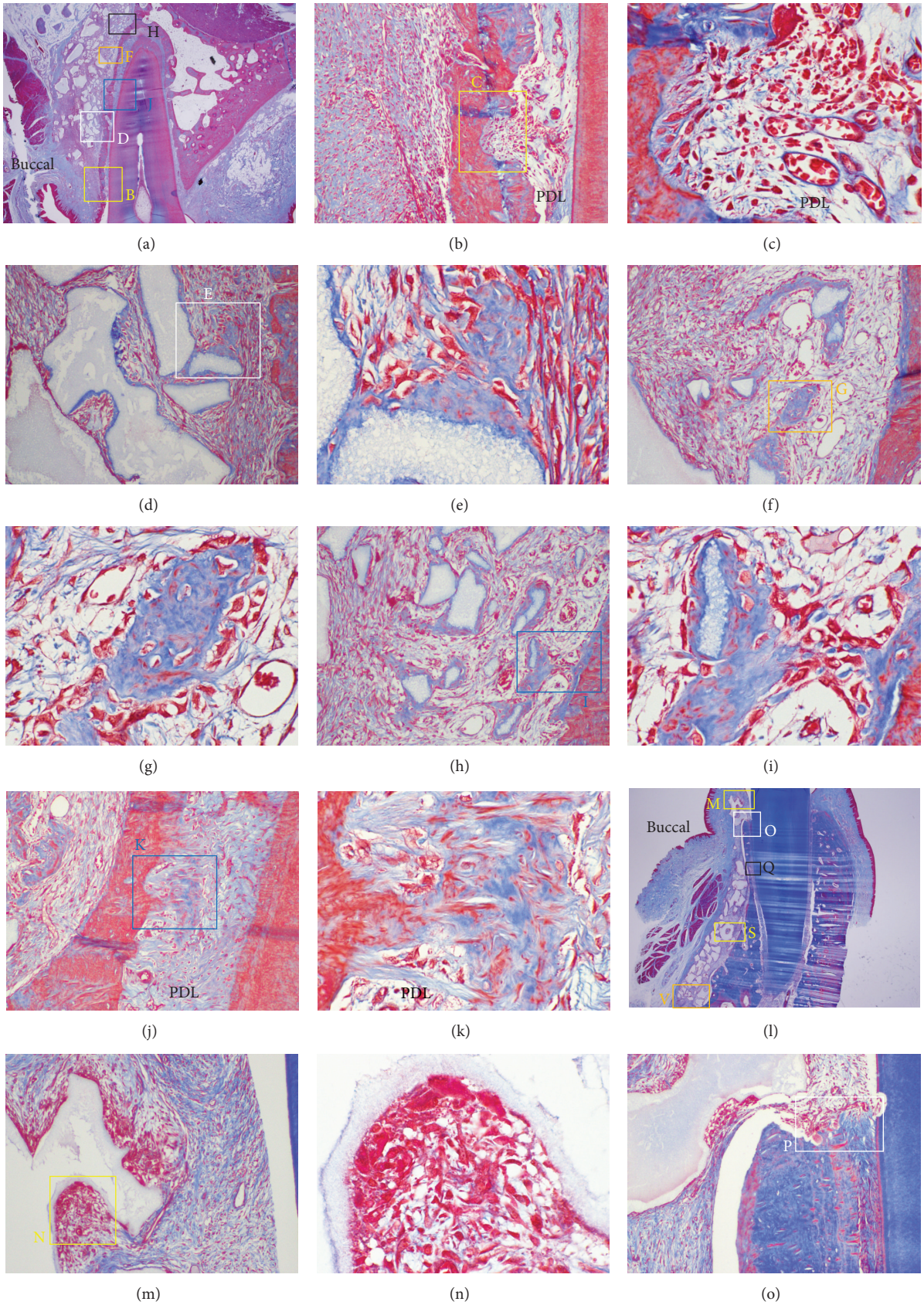

Figure 8: Continued.

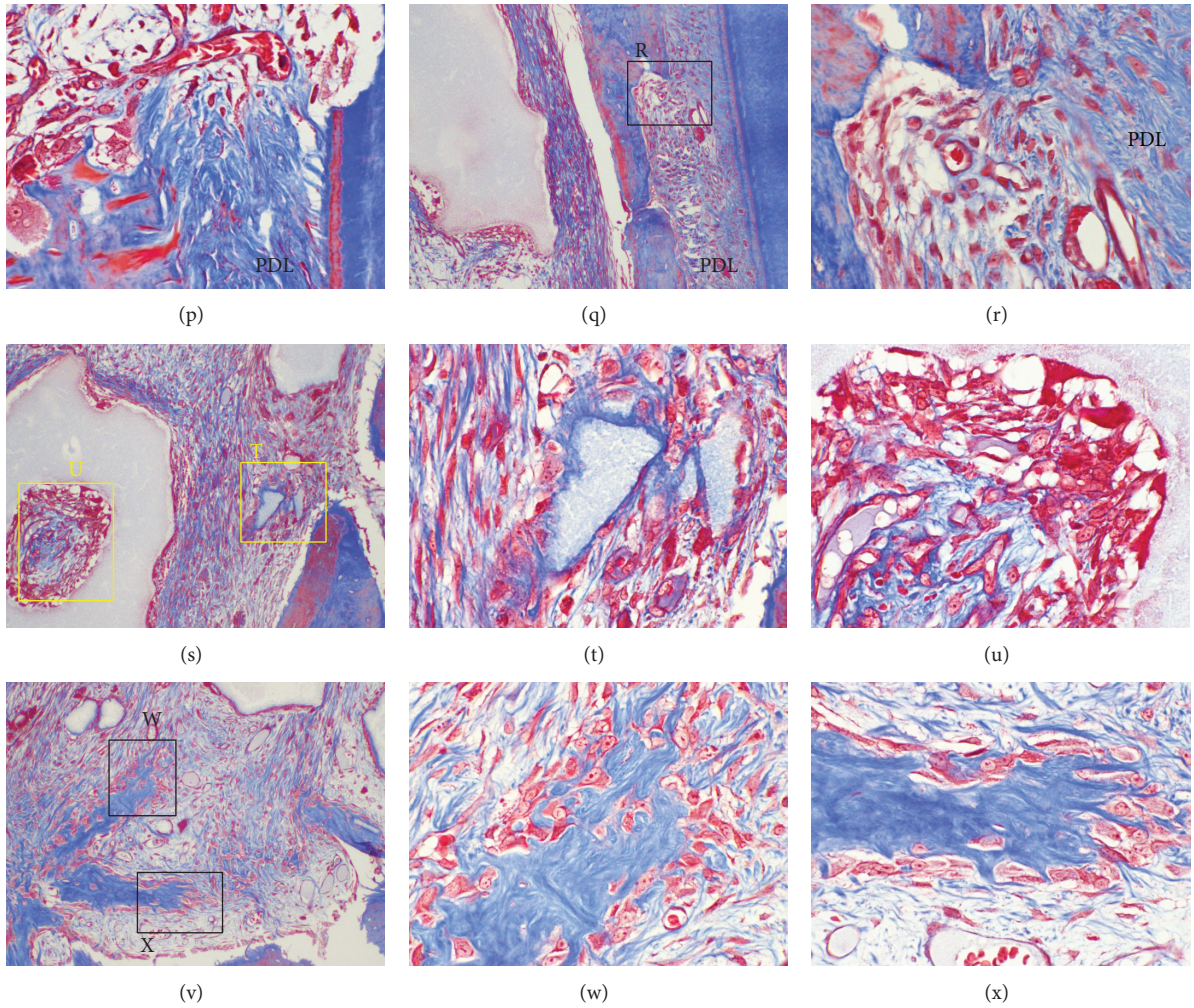

FIGURE 8: Microphotograph of a buccopalatal/lingual section of the 2-week experiment. (a) Maxilla. Most of the grafted MBCP+ particles were well maintained. (b) Higher magnification of (a) at the crest area. Undermining resorption on the pressure side was observed. (c) Higher magnification of (b). Extravasation of RBC was observed in the PDL space. Resorption bays, which indicate undermining resorption on the pressure side, were also observed. (d) Higher magnification of (a) at the buccal bone surface. New bone formation surrounding the grafted MBCP+ particles was observed. Grafted MBCP+ particles were bridged by newly formed bone. (e) Higher magnification of (d). Abundant osteoblasts were forming new bone. (f) Higher magnification of (a). Osteoblasts were forming a new bone island. (h) Higher magnification of (a). Grafted particles encircled by new bone were bridged with the buccal bone surface. (j) Higher magnification of (a). New bone was formed in the PDL space at the buccal tension area. New bone was formed from the bone. (l) Mandible. Most of the grafted MBCP+ particles were well maintained. (m) Higher magnification of (l) at the crest area. Grafted particles were resorbed by osteoclasts. (n) Higher magnification of (m). (o) Higher magnification of (l). (p) Higher magnification of (l). Bone and root surface resorption by osteoclasts were observed. (q) Higher magnification of (l). Undermining resorption at the buccal bone in the PDL area was observed. (r) Higher magnification of (q). Many osteoblasts filled the resorption bay. (s) Higher magnification of (l). Active new bone formation was found at the buccal bone surface in the apical area. (t) Higher magnification of (s). Many osteoblasts were forming a new bone encircling the grafted MBCP+ particles. (u) Higher magnification of (s). Osteoclastic and osteoblastic activities were both observed. (v) Higher magnification of (l). New bone islands were formed. (w) Higher magnification of (v). (x) Higher magnification of (v). Abundant osteoblasts were actively forming new bone islands. Masson's trichrome stain. Original magnification was ×12.5 for (a) and (l); ×100 for (b), (d), (f), (h), (j), (m), (o), (q), (s), and (v), and ×400 for (c), (e), (g), (i), (k), (n), (p), (r), (t), (u), (w), and (x).

the corticotomy be performed? How often should orthodontic force be applied? What magnitude of force would be optimal? These are still widely open questions that are worthy of further investigation.

Although there is no doubt that this procedure could align teeth within a shorter period of time [1, 3, 8, 14, 28–31], at the present time, we cannot expect augmented corticotomy-facilitated orthodontic tooth movement to reduce the entire length of orthodontic treatment noticeably in adult patients. In addition, there is a paucity of information in the available research to assert that grafting enhances the stability of orthodontic treatment [14]. To prove this, well-designed randomized controlled clinical trials should be performed.

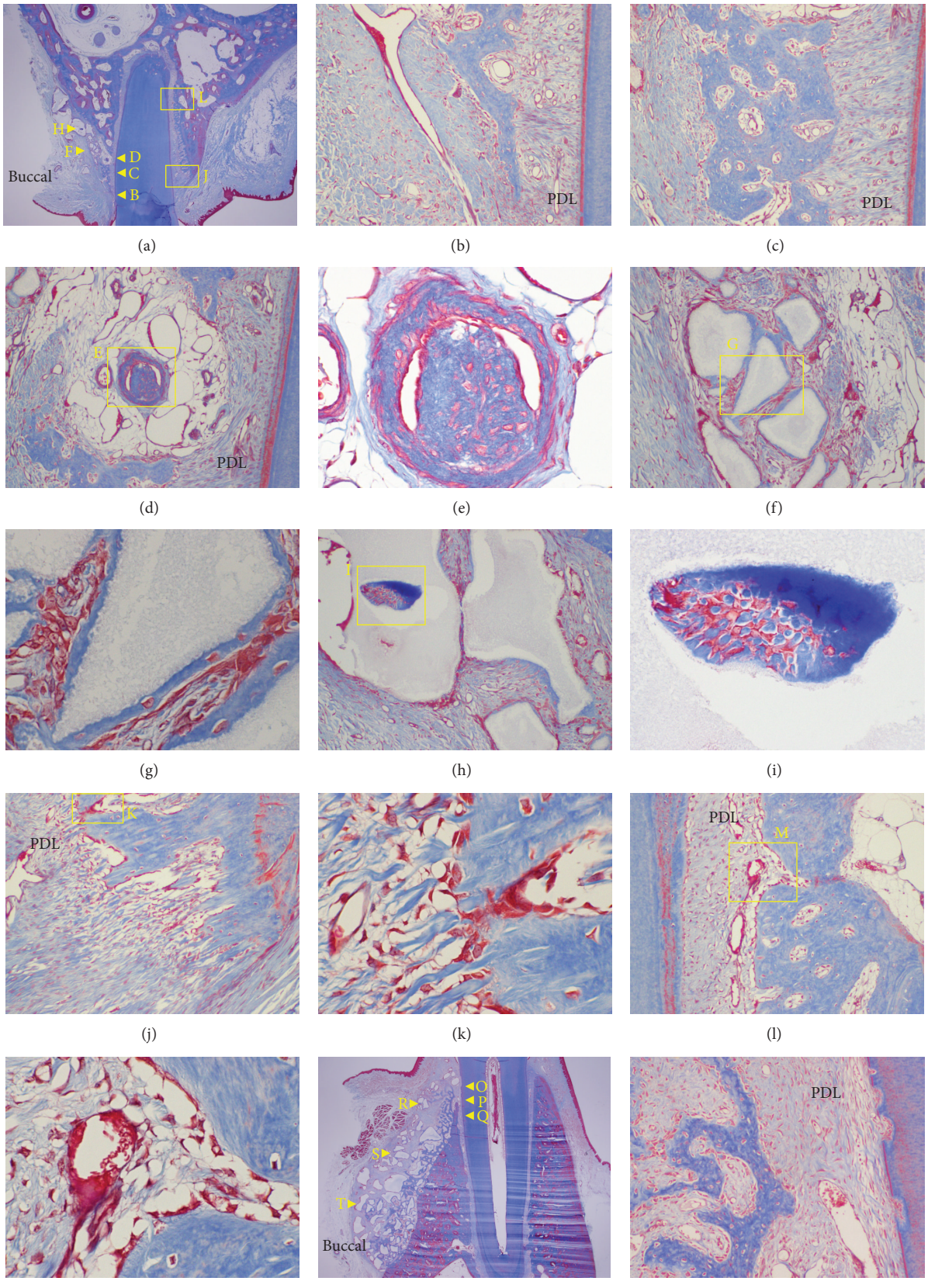

(m)

Figure 9: Continued.

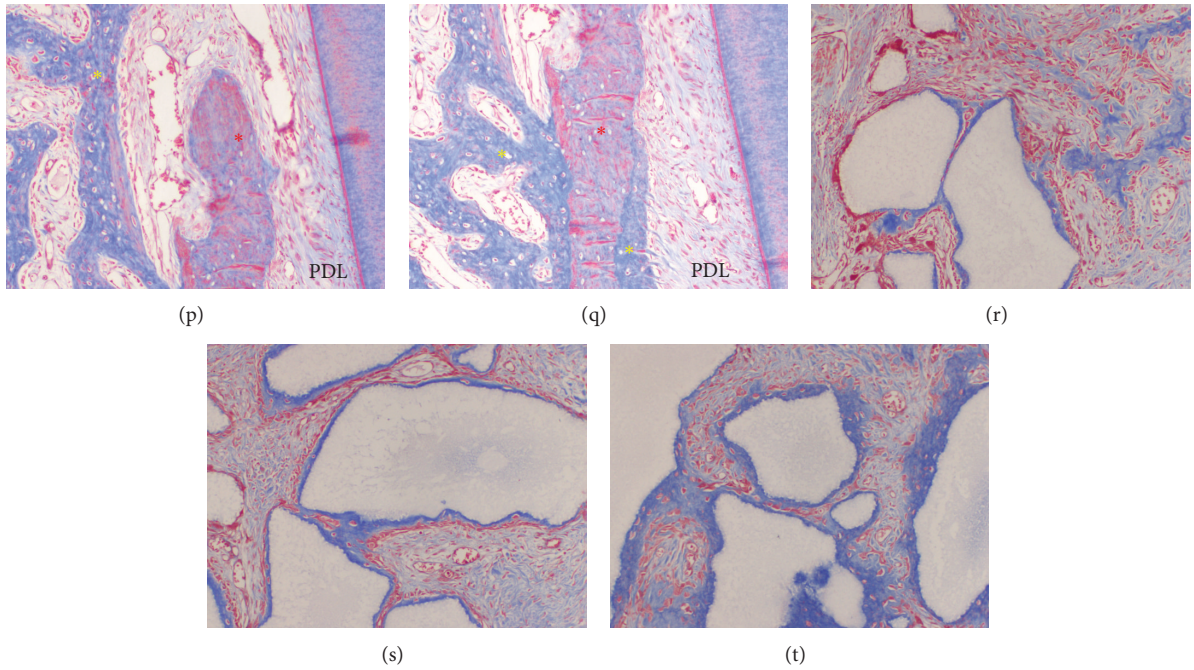

Figure 9: Microphotograph of a buccopalatal/lingual section of the 4-week experiment. (a) Maxilla. Most of the grafted MBCP+ particles were well maintained. New bone formation along the PDL formed a new buccal bone wall. ((b) and (c)) Higher magnification of (a) at the crest area. (d) Higher magnification of (a). The bone-derived mesenchymal matrix bordered the PDL-derived mesenchymal matrix. A new bone island was formed in the center of the bone-derived mesenchymal matrix. (e) Higher magnification of (d). Osteoblasts and osteocytes were observed. (f) Higher magnification of (a). The grafted MBCP+ particles were bridged with newly formed bone in the bone-derived mesenchymal matrix on the buccal side. (g) Higher magnification of (f). Entrapped osteocytes and aggregated osteoblasts were observed. (h) Higher magnification of (a). (i) Higher magnification of (h). New bone was formed in the center of the grafted MBCP+ particles at the buccal side. ((j) and (l)) Higher magnification of (a). The palatal tension side at the crestal (j) and apical (l) areas. ((k) and (m)) Higher magnification of (j) and (l), respectively. Aggregated osteoblasts and active form of osteoblasts were seen. (n) Mandible. (o) Higher magnification of (n) at the crestal area. New bone forming a buccal bone wall and crest was observed. (p) Higher magnification of (n). Native bone (red star) and new bone (yellow star). (q) Higher magnification of (n). New bone (yellow star) was formed on the outer and inner surface of the native bone (red star). ((r), (s), and (t)) Higher magnification of (n). The outer portion of the bone-derived mesenchymal matrix. Grafted MBCP+ particles were bridged by the newly formed bone. Masson's trichrome stain. Original magnification was ×12.5 for (a) and (n), ×100 for (b), (c), (d), (f), (h), (j), (l), (o), (p), (q), (r), (s), and (t), and ×400 for (e), (g), (i), (k), and (m).

The combination of corticotomy with an alveolar graft was introduced by Wilcko et al. and is referred to as accelerated osteogenic orthodontics or periodontally accelerated osteogenic orthodontics [8, 9, 32]. They asserted that bone grafting of the labial and lingual cortical bones would increase the stability of orthodontic treatment, enhance the range of possible tooth movements, increase alveolar bone volume, and provide a more structurally stable periodontium. However, no convincing scientific or histological evidence was available other than clinical reports. In some case reports, increased volume of bone around the alveolus was observed after bone grafting [3, 5, 9]. The present study supported the hypothesis that tooth movement with an augmented corticotomy might enhance orthodontic tooth movement, because we found new bone formation at the buccal surface. However, it focused on initial responses, and further investigation is needed to clarify its findings.

Tooth movement that was thought to be difficult or impossible to produce in the past has become possible due to the development of orthodontic mechanics and new appliances and materials. Therefore, orthodontic treatment is mainly limited by the scope of the alveolar bone, and orthognathic surgery is required when this limit is exceeded. If an augmented corticotomy could increase the alveolar bone volume, this would help patients who have a limited amount of supporting alveolar bone.

Augmented corticotomy surgery is not free from some morbidity. It also requires a skilled clinician, and there may be some discomfort to patients and additional costs.

5. Conclusions

The findings from this study suggest that measurable tooth movement starts as early as 3 days after augmented corticotomy-facilitated orthodontic treatment and that this procedure might enhance the condition of periodontal tissue and the stability of orthodontic treatment outcomes.

Conflict of Interests

The authors declare that they have no conflict of interests. The authors also certify that no financial support was received

from commercial sponsors to conduct this study or the preparation of this paper.

Authors' Contribution

Hyung-Joo Choi and Dong-Yeol Lee contributed equally to this study.

Acknowledgment

This work was supported by the National Research Foundation of Korea, funded by the Korean government (Grant no. 2012R1A5A2051388).

References

[1] S. M. B. E. Aboul-Ela, A. R. El-Beialy, K. M. F. El-Sayed, E. M. N. Selim, N. H. El-Mangoury, and Y. A. Mostafa, "Miniscrew implant-supported maxillary canine retraction with and without corticotomy-facilitated orthodontics," *The American Journal of Orthodontics and Dentofacial Orthopedics*, vol. 139, no. 2, pp. 252–259, 2011.

[2] S. S. Baloul, L. C. Gerstenfeld, E. F. Morgan, R. S. Carvalho, T. E. van Dyke, and A. Kantarci, "Mechanism of action and morphologic changes in the alveolar bone in response to selective alveolar decortication-facilitated tooth movement," *The American Journal of Orthodontics and Dentofacial Orthopedics*, vol. 139, no. 4, supplement, pp. S83–S101, 2011.

[3] S. Kim, I. Kim, D. Jeong, K. Chung, and H. Zadeh, "Corticotomy-assisted decompensation for augmentation of the mandibular anterior ridge," *The American Journal of Orthodontics and Dentofacial Orthopedics*, vol. 140, no. 5, pp. 720–731, 2011.

[4] D. Y. Lee, H. W. Ahn, Y. Herr et al., "Periodontal responses to augmented corticotomy with collagen membrane application during orthodontic buccal tipping," *BioMed Research International*. In press.

[5] K. B. Lee, D. Y. Lee, S. H. Ahn et al., "Tooth movement out of the bony wall using augmented corticotomy with non-autogenous graft materials for bone regeneration," *BioMed Research International*. In press.

[6] W. Lee, G. Karapetyan, R. Moats et al., "Corticotomy-/osteotomy-assisted tooth movement microCTs differ," *Journal of Dental Research*, vol. 87, no. 9, pp. 861–867, 2008.

[7] H. Long, U. Pyakurel, Y. Wang, L. Liao, Y. Zhou, and W. Lai, "Interventions for accelerating orthodontic tooth movement: a systematic review," *Angle Orthodontist*, vol. 83, no. 1, pp. 164–171, 2013.

[8] K. G. Murphy, M. T. Wilcko, W. M. Wilcko, and D. J. Ferguson, "Periodontal accelerated osteogenic orthodontics: a description of the surgical technique," *Journal of Oral and Maxillofacial Surgery*, vol. 67, no. 10, pp. 2160–2166, 2009.

[9] M. T. Wilcko, W. M. Wilcko, J. J. Pulver, N. F. Bissada, and J. E. Bouquot, "Accelerated osteogenic orthodontics technique: a 1-stage surgically facilitated rapid orthodontic technique with alveolar augmentation," *Journal of Oral and Maxillofacial Surgery*, vol. 67, no. 10, pp. 2149–2159, 2009.

[10] S. Sayin, A. O. Bengi, A. U. Gürton, and K. Ortakoğlu, "Rapid canine distalization using distraction of the periodontal ligament: a preliminary clinical validation of the original technique," *Angle Orthodontist*, vol. 74, no. 3, pp. 304–315, 2004.

[11] M. Nishimura, M. Chiba, T. Ohashi et al., "Periodontal tissue activation by vibration: intermittent stimulation by resonance vibration accelerates experimental tooth movement in rats," *The American Journal of Orthodontics and Dentofacial Orthopedics*, vol. 133, no. 4, pp. 572–583, 2008.

[12] D. R. Cruz, E. K. Kohara, M. S. Ribeiro, and N. U. Wetter, "Effects of low-intensity laser therapy on the orthodontic movement velocity of human teeth: a preliminary study," *Lasers in Surgery and Medicine*, vol. 35, no. 2, pp. 117–120, 2004.

[13] M. Yamaguchi, M. Hayashi, S. Fujita et al., "Low-energy laser irradiation facilitates the velocity of tooth movement and the expressions of matrix metalloproteinase-9, cathepsin K, and alpha(v) beta(3) integrin in rats," *European Journal of Orthodontics*, vol. 32, no. 2, pp. 131–139, 2010.

[14] D. P. Mathews and V. G. Kokich, "Accelerating tooth movement: the case against corticotomy-induced orthodontics," *The American Journal of Orthodontics and Dentofacial Orthopedics*, vol. 144, no. 1, pp. 5–13, 2013.

[15] S. Iino, S. Sakoda, G. Ito, T. Nishimori, T. Ikeda, and S. Miyawaki, "Acceleration of orthodontic tooth movement by alveolar corticotomy in the dog," *The American Journal of Orthodontics and Dentofacial Orthopedics*, vol. 131, no. 4, pp. 448–e1, 2007.

[16] Y. A. Mostafa, M. M. S. Fayed, S. Mehanni, N. N. ElBokle, and A. M. Heider, "Comparison of corticotomy-facilitated vs standard tooth-movement techniques in dogs with miniscrews as anchor units," *American Journal of Orthodontics and Dentofacial Orthopedics*, vol. 136, no. 4, pp. 570–577, 2009.

[17] P. A. Sanjideh, P. E. Rossouw, P. M. Campbell, L. A. Opperman, and P. H. Buschang, "Tooth movements in foxhounds after one or two alveolar corticotomies," *European Journal of Orthodontics*, vol. 32, no. 1, pp. 106–113, 2010.

[18] J. Sebaoun, A. Kantarci, J. W. Turner, R. S. Carvalho, T. E. Van Dyke, and D. J. Ferguson, "Modeling of trabecular bone and lamina dura following selective alveolar decortication in rats," *Journal of Periodontology*, vol. 79, no. 9, pp. 1679–1688, 2008.

[19] S. Kim, Y. Park, and S. Kang, "Effects of corticision on paradental remodeling in orthodontic tooth movement," *Angle Orthodontist*, vol. 79, no. 2, pp. 284–291, 2009.

[20] L. Wang, W. Lee, D. Lei, Y. Liu, D. Yamashita, and S. L. Yen, "Tisssue responses in corticotomy- and osteotomy-assisted tooth movements in rats: histology and immunostaining," *The American Journal of Orthodontics and Dentofacial Orthopedics*, vol. 136, no. 6, pp. 770.e1–770.e11, 2009.

[21] S. Kim, S. Moon, S. Kang, and Y. Park, "Effects of low-level laser therapy after corticision on tooth movement and paradental remodeling," *Lasers in Surgery and Medicine*, vol. 41, no. 7, pp. 524–533, 2009.

[22] W. H. B. Mawhinney, E. Richardson, and A. J. Malcolm, "Technical methods. Control of rapid nitric acid decalcification," *Journal of Clinical Pathology*, vol. 37, no. 12, pp. 1409–1413, 1984.

[23] H. H. Verdenius and L. Alma, "A quantitative study of decalcification methods in histology," *Journal of Clinical Pathology*, vol. 11, no. 3, pp. 229–236, 1958.

[24] J. B. Matthews and G. I. Mason, "Influence of decalcifying agents on immunoreactivity of formalin-fixed paraffin-embedded tissue," *Histochemical Journal*, vol. 16, no. 7, pp. 771–787, 1984.

[25] R Development Core Team, *R: A Language and Environment for Statistical Computing*, R Foundation for Statistical Computing, Vienna, Austria, 2014.

[26] H. M. Frost, "The biology of fracture healing: an overview for clinicians. Part II," *Clinical Orthopaedics and Related Research*, no. 248, pp. 294–309, 1989.

[27] H. M. Frost, "The biology of fracture healing. An overview for clinicians. Part I," *Clinical Orthopaedics and Related Research*, no. 248, pp. 283–293, 1989.

[28] T. J. Fischer, "Orthodontic treatment acceleration with corticotomy-assisted exposure of palatally impacted canines: a preliminary study," *Angle Orthodontist*, vol. 77, no. 3, pp. 417–420, 2007.

[29] A. H. Hassan, A. A. Al-Fraidi, and S. H. Al-Saeed, "Corticotomy-assisted orthodontic treatment: review," *The Open Dentistry Journal*, vol. 4, pp. 159–164, 2010.

[30] H. Nowzari, F. K. Yorita, and H. Chang, "Periodontally accelerated osteogenic orthodontics combined with autogenous bone grafting," *Compendium of Continuing Education in Dentistry*, vol. 29, no. 4, pp. 200–218, 2008.

[31] W. M. Wilcko, "Rapid orthodontics with alveolar reshaping: Two case reports of decrowding," *International Journal of Periodontics and Restorative Dentistry*, vol. 21, no. 1, pp. 9–19, 2001.

[32] G. Amit, K. Jps, B. Pankaj et al., "Periodontally accelerated osteogenic orthodontics (PAOO)—a review," *Journal of Clinical and Experimental Dentistry*, vol. 4, no. 5, pp. e292–e296, 2012.

Hindawi Publishing Corporation
BioMed Research International
Volume 2014, Article ID 549785, 10 pages
http://dx.doi.org/10.1155/2014/549785

Research Article

Systemic Treatment with Strontium Ranelate Accelerates the Filling of a Bone Defect and Improves the Material Level Properties of the Healing Bone

Giovanna Zacchetti, Romain Dayer, René Rizzoli, and Patrick Ammann

Division of Bone Disease, Department of Internal Medicine Specialties, Geneva University Hospitals and Faculty of Medicine, 1211 Geneva, Switzerland

Correspondence should be addressed to Patrick Ammann; patrick.ammann@hcuge.ch

Received 2 June 2014; Accepted 22 July 2014; Published 28 August 2014

Academic Editor: Seong-Hun Kim

Rapid bone defect filling with normal bone is a challenge in orthopaedics and dentistry. Strontium ranelate (SrRan) has been shown to in vitro decrease bone resorption and increase bone formation, and represents a potential agent with the capacity to accelerate bone defect filling. In this study, bone tibial defects of 2.5 mm in diameter were created in 6-month-old female rats orally fed SrRan (625 mg/kg/d; 5/7 days) or vehicle for 4, 8, or 12 weeks (10 rats per group per time point) from the time of surgery. Tibias were removed. Micro-architecture was determined by micro-computed tomography (μCT) and material level properties by nanoindentation analysis. μCT analysis showed that SrRan administration significantly improved microarchitecture of trabecular bone growing into the defect after 8 and 12 weeks of treatment compared to vehicle. SrRan treatment also accelerated the growth of cortical bone over the defect, but with different kinetics compared to trabecular bone, as the effects were already significant after 4 weeks. Nanoindentation analysis demonstrated that SrRan treatment significantly increased material level properties of both trabecular bone and cortical bone filling the defect compared to vehicle. SrRan accelerates the filling of bone defect by improving cortical and trabecular bone microarchitecture both quantitatively and qualitatively.

1. Introduction

Comminuted fractures, infection, dental extraction, bone metastasis, and orthopaedic surgery are among the main causes leading to a local loss of bone tissue. The age of the individual, hormonal status, nutrition, and presence of concomitant diseases may negatively affect bone tissue healing and the filling of the defect [1–3]. Bone defect healing occurs naturally after a phase of bleeding and inflammation and terminates with the formation of woven bone which is then remodelled by osteoclasts and replaced by lamellar bone by osteoblasts [4]. In cases of extensive bone loss requiring prosthetic fixation, as well as in fragile osteoporotic individuals, a treatment accelerating bone healing contributes to well-being and quality of life. Several approaches, such as the local or systemic administration of growth factors [5, 6] or mesenchymal stem cells [7–9], can represent advantageous alternatives to bone graft and the insertion of scaffolds of osteoinductive biomaterials.

The administration of anabolic or anticatabolic drugs commonly used to cure osteoporosis might promote bone defect healing by increasing bone formation or inhibiting bone resorption. Among these, the effect of the administration of antiresorptive agents to improve bone healing remains controversial. Bisphosphonates (BPs) do not interfere with the initial phase of bone healing, which is largely osteoclast-independent and leads to the filling of bone defect with woven bone. In some cases, BP administration appears to promote the formation of a larger callus [10] and suppression of the osteoclast activity delays the remodelling of woven bone and the formation of lamellar bone [11–13]. Importantly, treatment with BPs does not induce the regeneration of cortical bone after fracture [14]. Among the anabolic treatments, the systemic and local administration of parathyroid hormone (PTH) was shown to be efficacious for fracture and bone defect healing in rats and humans [15–17]. Depending on the anatomic localization of the bone lesion, the full repair of the cortical shell is crucial to restoring the load

bearing capacity of bones. In osteoporotic nonfractured patients, PTH increases both trabecular bone volume and cortical thickness. However, it increases also cortical porosity, which may adversely affect bone strength [18].

By contrast, with bisphosphonates and PTH, strontium ranelate (SrRan) was shown to have a dual mechanism on bone formation activity and bone resorption mostly in vitro [19–23]. The effect of SrRan in vivo depends on the animal model. In rodents, long-term treatment with SrRan increased vertebral bone mass and had a positive effect on microarchitectural parameters, bone material level properties, and bone strength [24–26]. In monkeys, SrRan decreased histological markers of bone resorption, while preserving bone formation [27]. In ovariectomized rats, SrRan prevented bone loss [28] and had a beneficial effect on fracture healing, thus improving callus resistance to biomechanical torsional testing when compared to PTH [29–31].

The aim of this study was to assess whether the systemic administration of SrRan accelerates the healing of a bone defect created in rat proximal tibia compared to vehicle-treated controls.

2. Material and Methods

2.1. Animals and Diet. All experimental designs and procedures were approved by the Animal Ethics Committee of the University of Geneva, Faculty of Medicine. Sixty 6-month-old Sprague-Dawley female rats (Charles River Laboratories, L'Arbresle, France) were housed individually at 25°C with a 12:12-h light-dark cycle and strictly pair-fed a laboratory diet containing 15% casein, 0.8% phosphorus, 1% calcium, 70–80% carbohydrate, and 5% fat. Demineralized water was available *ad libitum*. Rats were then divided into six groups of 10 animals each. For a period of 4, 8, and 12 weeks after surgery, three groups (one for each time point) were treated with SrRan by gavage at a dose of 625 mg/kg/day, 5 days/week. This dose level leads to blood strontium concentration close to the level in human blood after a therapeutic dose of 2 g/day [28]. The three control groups received 0.5% carboxymethylcellulose aqueous solution by gavage 5 days a week for 4, 8, and 12 weeks with volumes corresponding to those administered in the SrRan-treated group.

2.2. Surgery. Animals were anesthetized with ketamine (100 mg/kg) and xylasine (10 mg/kg) administered as an intraperitoneal injection. Skin of both legs was shaved and cleaned with 70% ethanol. Under aseptic conditions, an anterior 10 mm incision was made to gain access to the proximal medial section of the tibia metaphysis. A standardized drill-hole defect (2.5 mm diameter, 2 mm depth, and approximately 10 mm^3 total volume) was created in the proximal tibia secondary spongiosa of both legs using a dental burr under saline irrigation. The proximal limit of bone defect was delimited by a virtual line perpendicular to the long axis of the tibia and crossing the anterior edge of the growth plate centrally, which is curved both anteriorly and inferiorly in this central region. A second anatomical landmark was a virtual line from the inferior border of the tendinous insertion on the proximal anterior tibial crest to a medial tendinous insertion likely corresponding to the *pes anserinus* in humans. The bone defect was performed midway between these two tendinous insertions. Rotatory speed did not exceed 2000 rpm, and drilling was accompanied by profuse saline irrigation to avoid thermal bone necrosis. After creation of the bone defect, the skin was sutured using a 3–0 resorbable polyglactic suture (Vicryr; Ethicon; Spreitenbach, Switzerland). Blood was sampled before surgery and at the moment of sacrifice from the tip of the tail and the aorta, respectively. At the end of the experiments, all rats were sacrificed by an overdose of ketamine hydrochloride.

2.3. Microcomputerized Tomography (μCt). Tibias were carefully excised immediately after death and frozen at −20°C in plastic bags. Bones were thawed slowly at 4°C and maintained at room temperature the night before μCt analysis. Each proximal tibia was scanned using μCt (μCt 40, Scanco Medical AG, Bassersdorf, Switzerland) as previously described [32, 33]. In summary, three-dimensional images of each tibia were acquired with a voxel size of 20 μm in all spatial directions. No sample preparation was needed and tibia bones were secured in a cylindrical sample holder in NaCl solution. The resulting gray-scale images were segmented using a low-pass filter to remove noise and a fixed threshold to extract the mineralized bone phase. For detection of trabecular bone filling the defect, segmentation parameters were set to sigma: 0.8 voxels, support: 1, and threshold: 3.08 cm^{-1}. The resolution was set to (500 projections with 1024 samples each), and a middle value slice thickness and increment to 21 μm.

Trabecular bone was analysed by setting the volume of interest (VOI) as a circular band of 2.5 mm drawn on a slice-based method, starting from the first slice from the external bone surface containing no cortical bone and moving 30 slices dorsally, including avoidance of undrilled bone. Each slice was calculated directly from the binarized VOI. Total volume (TV) is the volume of the whole sample examined. Bone volume (BV) was calculated using tetrahedrons corresponding to the enclosed volume of the triangulated surface. Mean trabecular thickness (Tb.Th) was determined from the local thickness at each voxel representing bone [34]. Trabecular number (Tb.N) was calculated by taking the inverse of the mean distance between the middle axis of the structure and trabecular separation (Tb.Sp) by applying the technique used for the direct thickness calculation to the non-bone parts of the 3D image. Connectivity density based on Euler number (Conn. D) and the structure model index (SMI) were calculated.

BV/TV, Tb.Th, Tb.N, Tb.Sp, and SMI were also analysed within a subregion of trabecular bone bordering the defect enclosed in a circular stripe of 0.45 mm and excluding the central cavity (Figure 1). For this analysis, the same parameters of segmentation as above were applied; the region of interest was selected within the volume of 30 slices previously analysed.

Scans were successively reformatted to the axial cuts to measure the thickness of cortical bone bridging the defect. The contours of cortical bone were semiautomatically

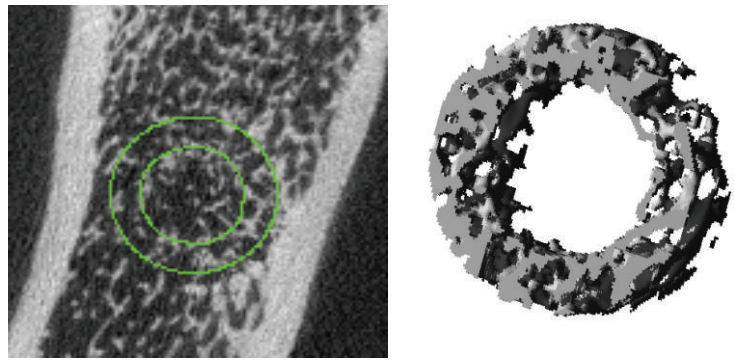

Figure 1: Micro-CT 3D reconstruction of a circular band 0.45 mm wide selected on the peripheral portion of a bone defect in adult female rat tibiae.

drawned within 90 slices along the long axis of the tibia, exclusively including the cortices sealing the gap. For cortical bone, the segmentation parameters were set to sigma: 0.8 voxels, support: 1, and threshold: 3.85 cm^{-1}.

2.4. Nanomechanical Testing. Right tibias were embedded in polymethyl methacrylate (PMMA) (8.00590.2500 Merck, Hohenbrunn, Germany) and blocks were then transversally cut in two pieces at the level of the bone defect using a diamond wire saw (Well Mod 3242-3, Well Diamond Wire Saws SA, Le Locle, Switzerland). The face of the transverse cuts was polished and finished with 0.25 μm diamond solution. After these preparation steps, specimens were frozen at −20°C. The night before the nanomechanical test, specimens were slowly thawed at 4°C, maintained at room temperature, and immersed in saline solution during the whole analysis. Nanoindentation was performed using a nanohardness tester (NHT; CSM Instruments, Peseux, Switzerland). In this test, force-displacement of a pyramidal diamond indenter that was pushed onto the bone was recorded. The nanoindentation tests included five indents within the bone defect and five indents at the junction between old and new formed bone in cortical bone (Figure 2). All the indents were performed at distance of the junction of the PMMA and bone. Indents were made up to 900 nm maximum depth applying an approximate strain rate of 0.066 1/s for both loading and unloading. At maximum load, a 5-s holding period was applied, and the limit of the maximum allowable thermal drift was set to 0.1 nm/s.

2.5. Wavelength X-Ray Dispersive Spectroscopy (WDS). WDS was performed to evaluate the surface distribution of Sr, Ca, and P in the bone of five representative samples from the SrRan-treated and vehicle group (12 weeks of treatment only). Semiquantitative analyses were performed in profiles selected in trabecular bone at the edge with the defect in two representative samples for each treatment group (vehicle and SrRan) using a JEOL 8200 X-ray spectrometer (JEOL 8200 electron microprobe, Ohio, USA). The JEOL 8200 electron microprobe has five wavelength dispersive crystal focusing spectrometers. The crystals used here were pentaerythritol (PET), thallium acid phthalate (TAP), and synthetic 45 Å multilayer

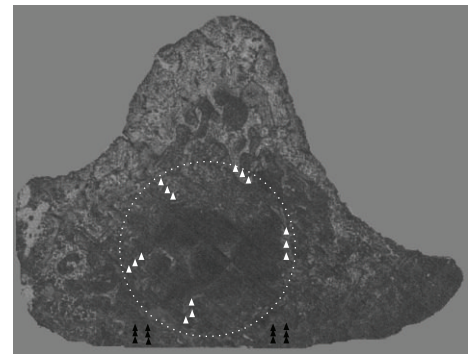

Figure 2: Schematic localization of indents on a representative section of proximal tibia metaphysis cut through the defect. The indents in the trabecular and cortical bone are represented by white and black triangles respectively.

W/Si (LDE1). The primary electron beam energy was operated at 15 KeV, the electron beam current was 10 nA, and the beam spot size was ~10 × 8 μm^2. The bone samples utilized were embedded in PMMA and cut transversally in the middle, across the defect. The surface was polished, finishing with 0.25 μm diamond solution, and coated with carbon to render them conductors and to avoid surface charging.

2.6. Biochemical Assay. Plasma insulin-like growth factor I (IGF-I) was measured by an ELISA kit (Immunodiagnostic Systems, Thebarton, Australia), according to the manufacturer's instructions.

2.7. Statistical Analysis. All results were expressed as means ± SEM. For normally distributed data, significant differences were identified by analysis of variance (ANOVA) and Fisher's *post hoc* test. Alternatively, a Mann-Whitney U test was performed, and the level of significance was set to $P < 0.05$.

3. Results

3.1. Effect of SrRan on the Geometry of Cortical Bone Bordering the Defect. After 4 weeks of SrRan treatment, cortical bone

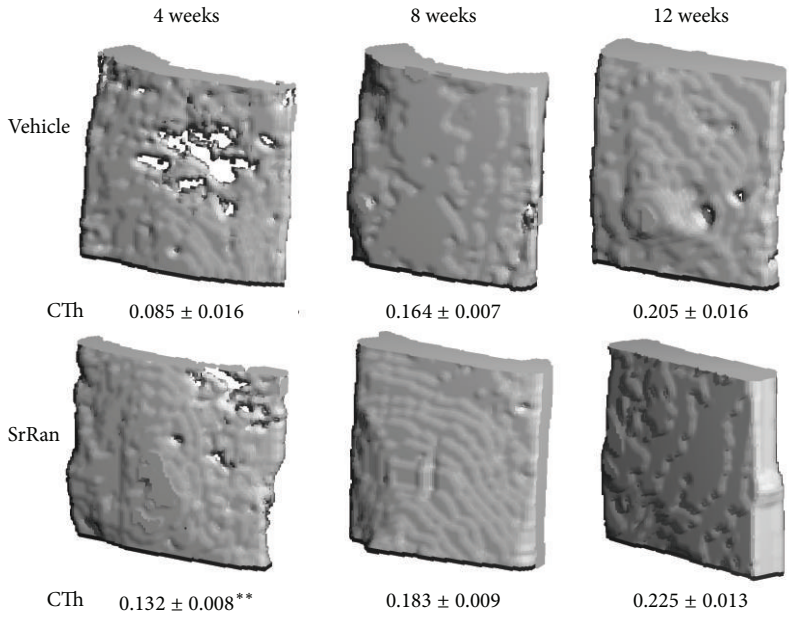

Figure 3: Micro-CT 3D reconstruction of cortical bone healing of a bone defect in proximal tibia metaphysis of adult female rats following 4, 8 or 12 weeks of vehicle or SrRan administration; values represent the cortical thickness (mm). Averages ± SEM, Anova $^{**}P < 0.001$ versus time matched vehicle.

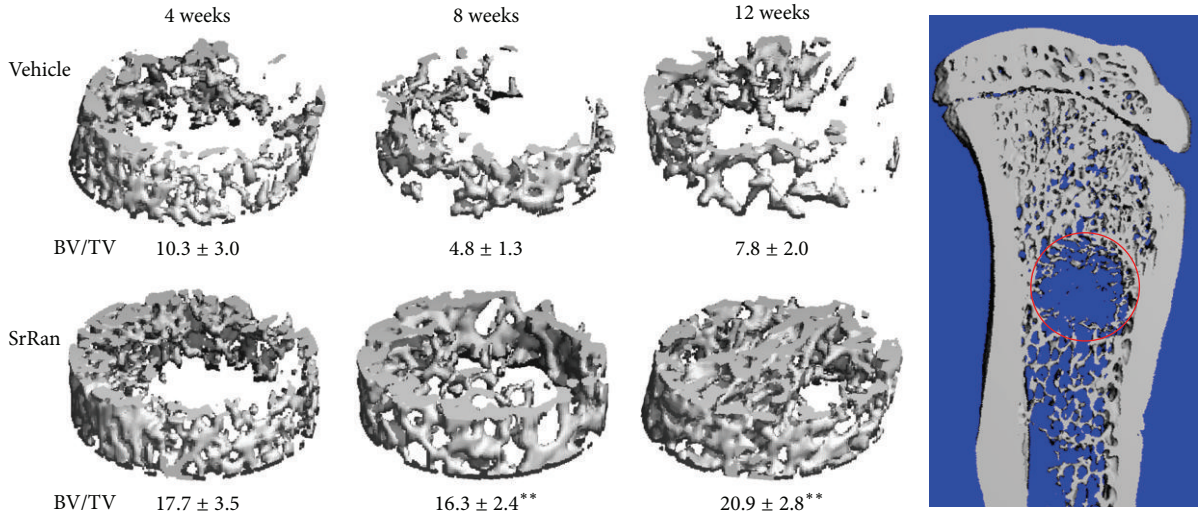

Figure 4: Micro-CT 3D reconstruction of trabecular bone healing of a bone defect in proximal tibia metaphysis of adult female rats following 4, 8 or 12 weeks of SrRan or vehicle administration; values represent the bone volume on total volume (%). Averages ± SEM, Anova $^{**}P < 0.01$ versus time matched vehicle.

thickness (+55%; $P < 0.01$) was higher than vehicle time-matched controls (Figure 3). μCT analysis showed that the cortical bone healing area over the defect was almost completely restored in SrRan-treated rats at 4 weeks; at 8 and 12 weeks, the +12% and +10% higher cortical thicknesses were not significant. After 12 weeks, the cortical bone bridging the defect was fully repaired in both SrRan- and vehicle-treated rats.

3.2. Effect of SrRan on the Microarchitecture of Trabecular Bone Healing the Defect. Most parameters of bone microarchitecture, such as BV/TV, Conn.D, and Tb.Th, were higher after 4 weeks of SrRan treatment (Figure 4 and Table 1) compared to the controls. A consistently higher trabecular BV/TV was observed at the early time point of 4 weeks and this difference became significant after 8 and 12 weeks of SrRan treatment (+72% (NS) and +240% [$P < 0.01$] and +168% [$P < 0.01$] at 4, 8, and 12 weeks, respectively, when compared to the time-matched controls). Tb.Th also followed the same trend as BV/TV at 4, 8, or 12 weeks of treatment (+13.6%, +31%, and +28%, resp.). Along with the higher Tb.Th, the SMI, corresponding to 0 and 3 for an ideal plate and rod structure, respectively, was lower by −19%, −35%, and −34% (4, 8, and 12 weeks, resp.) in SrRan-treated rats *versus* time-matched

Table 1: Effect of 4, 8, or 12 weeks of SrRan or vehicle administration on micro-CT analysis of trabecular bone healing a bone defect in adult female rat tibiae.

Trabecular bone	Treatment	Time of treatment		
		4 weeks	8 weeks	12 weeks
Conn. D (1)	vehicle	40.56 ± 11.08	14.70 ± 4.49	22.86 ± 6.74
	SrRan	75.24 ± 15.15	50.73 ± 7.64*	74.87 ± 11.62*
TbN (1/mm)	vehicle	4.38 ± 0.33	3.75 ± 0.14	3.91 ± 0.16
	SrRan	4.60 ± 0.22	4.20 ± 0.10°	4.41 ± 0.17
TbTh (1/mm)	vehicle	0.066 ± 0.005	0.062 ± 0.003	0.064 ± 0.005
	SrRan	0.075 ± 0.005	0.081 ± 0.002#	0.082 ± 0.002*
SMI (1)	vehicle	2.78 ± 0.27	3.30 ± 0.24	2.88 ± 0.30
	SrRan	2.25 ± 0.28	2.14 ± 0.13*	1.91 ± 0.23°

Averages ± SEM; Mann-Whitney; °$P < 0.05$, *$P < 0.01$, #$P < 0.001$ versus time-matched vehicle.

Table 2: Effect of 4, 8, or 12 weeks of SrRan or vehicle administration on micro-CT analysis of a circular band of 0.45 mm wide selected on the peripheral portion of a bone defect in adult female rat tibiae.

Trabecular bone bordering defect	Treatment	Time of treatment		
		4 weeks	8 weeks	12 weeks
BV/TV (%)	vehicle	16.86 ± 4.61	14.16 ± 1.45	14.50 ± 1.86
	SrRan	26.57 ± 4.06°	22.84 ± 1.77°	27.86 ± 2.92*
TbN (1/mm)	vehicle	5.00 ± 0.37	4.40 ± 0.11	4.46 ± 0.28
	SrRan	5.66 ± 0.40	4.99 ± 0.21	5.21 ± 0.18°
TbTh (mm)	vehicle	0.072 ± 0.007	0.082 ± 0.009	0.074 ± 0.003
	SrRan	0.083 ± 0.004	0.084 ± 0.002	0.084 ± 0.003°
TbSp (mm)	vehicle	0.217 ± 0.015	0.231 ± 0.006	0.248 ± 0.014
	SrRan	0.189 ± 0.014	0.216 ± 0.010	0.196 ± 0.008*
SMI (1)	vehicle	2.487 ± 0.454	2.767 ± 0.137	2.505 ± 0.116
	SrRan	1.640 ± 0.368	1.706 ± 0.177°	1.544 ± 0.251°

Averages ± SEM; Mann-Whitney; °$P < 0.05$; *$P < 0.01$ versus time-matched vehicle.

controls. A higher Conn.D was observed also after 4 weeks of SrRan treatment (+86%) and an even larger difference was detected after 8 and 12 weeks (245%, $P < 0.01$; 228%; $P < 0.01$, resp.) when compared to vehicle-treated rats. However, Tb.N was not increased at any time point following SrRan treatment. When analyzing trabecular bone by μCT within a circular band of 0.45 mm at the periphery of the defect and omitting the central part of the cavity, the average BV/TV values measured in SrRan-treated rats were all above 20% (Figure 1 and Table 2). These values are higher than BV/TV measured in the secondary spongiosa of proximal tibiae in intact rats of the same age and strain (BV/TV = 15% [35]). By 12 weeks, higher BV/TV in this region was associated with significantly higher Tb.N. and Tb.Th and lower Tb.Sp and SMI *versus* controls.

3.3. Effect of SrRan on Material Level Properties of Cortical Bone Spreading from the Defect Limit. By 4 weeks of SrRan treatment a higher elastic modulus, hardness, and working energy of cortical bone bridging the defect (+37%, $P < 0.001$; +43%, $P < 0.01$; and +30%, $P < 0.001$, resp.) were observed when compared to vehicle-treated rats (Table 3). Working energy was also higher after 8 weeks of SrRan treatment, whereas values by week 12 were close to those observed in time-matched vehicles. By weeks 8 and 12, elastic modulus and hardness of cortical bone were similarly higher both in SrRan- and vehicle-treated groups. Bone material level properties were higher in cortical bone as compared to trabecular bone. The bone tissue organization and mineralization as well as intensity of mechanical loading [36] could account for this difference between cortical and trabecular bone.

3.4. Effect of SrRan on Material Level Properties of Trabecular Bone Broadening from the Defect Limit. By 4 weeks, SrRan treatment was associated with higher elastic modulus, hardness, and working energy of trabecular bone expanding from the defect rim (+26%, $P < 0.01$; +26%, $P < 0.05$; and +23%, $P < 0.05$, resp.) when compared to the time-matched vehicle-treated rats (Table 4). Elastic modulus, hardness, and working energy were higher by weeks 8 and 12 in both SrRan and vehicle groups; working energy remained significantly higher by week 12 of SrRan treatment when compared to time-matched vehicles.

3.5. Wavelength X-Ray Dispersive Spectroscopy. Elemental mapping of Sr in the bone defect of two representative samples at week 12 is presented in Figure 5. The mean atomic percentage of Sr, Ca, and P resulted from the evaluation of

Table 3: Effect of 4, 8, or 12 weeks of SrRan administration on material level properties of cortical bone healing a bone defect in adult female rat tibiae.

Cortical bone	Treatment	Time of treatment		
		4 weeks	8 weeks	12 weeks
Modulus (gPa)	Vehicle	8.31 ± 0.39	10.55 ± 0.37	14.87 ± 0.43
	SrRan	11.39 ± 0.60$^{\#}$	11.00 ± 0.71	14.40 ± 0.67
Hardness (mPa)	Vehicle	275.1 ± 17.8	291.3 ± 13.9	477.4 ± 23.0
	SrRan	394.5 ± 31.3*	347.5 ± 29.3	482.8 ± 29.9
Working Energy (pJ)	Vehicle	1970.3 ± 96.4	1933.2 ± 68.4	3076.4 ± 102.6
	SrRan	2561.6 ± 113.1$^{\#}$	2269.5 ± 142.3°	3105.5 ± 123.3

Averages ± SEM; 2-way ANOVA; $^{\circ}P < 0.05$; $^{*}P < 0.01$; $^{\#}P < 0.001$ versus vehicle.

Table 4: Effect of 4, 8, or 12 weeks of SrRan administration on material level properties of trabecular bone healing a bone defect in adult female rat tibiae.

Trabecular bone	Treatment	Time of treatment		
		4 weeks	8 weeks	12 weeks
Modulus (gPa)	vehicle	9.17 ± 0.39	11.20 ± 0.53	13.50 ± 0.49
	SrRan	11.51 ± 0.58*	11.66 ± 0.60	13.85 ± 0.43
Hardness (mPa)	vehicle	356.1 ± 24.2	507.31 ± 27.22	588.38 ± 19.48
	SrRan	449.6 ± 28.6°	534.51 ± 29.04	640-67 ± 20.06
Working Energy (pJ)	vehicle	2224.8 ± 135.9	2769.7 ± 139.4	3365.7 ± 104.2
	SrRan	2725.6 ± 145.8°	3006.3 ± 152.8	3758.2 ± 97.4*

Averages ± SEM; 2 ways ANOVA; $^{\circ}P < 0.05$; $^{*}P < 0.01$ versus vehicle.

profiles selected in trabecular bone extending from the periphery of the defect. Sr was detected in trabecular bone healing the defect and all around in cortical bone, mainly in zones characterized by new and less mineralized bone. Sr was only detected in traces in time-matched vehicle rats. The mean percentages of Ca and P, as well as the ratio of Ca/P, were similar in SrRan and vehicle-treated rats.

3.6. Effect of SrRan Treatment on Insulin-Growth Factor (IGF-I) Level in Serum. Overall, the concentration of IGF-I lowered in serum harvested at the time of the euthanasia *versus* values measured before surgery (Table 5). Nevertheless, by weeks 4 and 8 the concentration of IGF-I was higher in SrRan-treated rats compared to time-matched vehicle animals, and by week 12, IGF-I levels were similar in both SrRan- and vehicle-treated groups.

4. Discussion

An accelerated repair of a bone defect represents a challenge to reconstruct bone integrity in individuals in whom bone loss is the consequence of traumatic events, surgery, or tooth extraction. SrRan has demonstrated some uncoupling between bone formation and bone resorption, as shown by a series of studies in vitro and in vivo [29–35, 37]. The aim of this study was to investigate whether the systemic administration of SrRan accelerates the healing of a bone defect drilled in rat secondary spongiosa of proximal tibiae. SrRan was orally administered at a dose of 625 mg/kg (5 days/week), and effects on bone defect repair were evaluated after 4, 8, and 12 weeks and subsequently compared with time-matched vehicle animals.

The μCt analysis showed that the mean cortical thickness was higher after 4 weeks of SrRan administration when compared to vehicle animals; in the latter group, the cortical shell bridging the defect still presented a few holes by 8 and 12 weeks, the cortices were thicker and formed a continuous shell in both SrRan- and vehicle-treated rats, completely sealing the defect. A former study showed that prolonged SrRan treatment increases bone diameter by inducing periosteal apposition and decreasing bone endocortical resorption [26]. The novelty of this study is in the evidence that SrRan accelerates the repair of damaged cortical bone. However, the mechanism by which SrRan influences the expansion of the cortical shell over the defect requires complementary investigations, that is, the histomorphometric quantification of parameters of bone formation/resorption.

The kinetics of trabecular bone healing of the defect seem to be delayed compared to those of cortical bone. Indeed, a significant increase in the parameters of cancellous bone microarchitecture was observed after 8 and 12 weeks of SrRan treatment *versus* time-matched vehicle animals, that is, 4 weeks later compared to the cortical bone. BV/TV and Tb.Th of cancellous bone filling the defect cavity were higher after SrRan treatment compared to vehicles. By contrast, the same region was still almost completely devoid of trabecular bone in rats treated with vehicle during the 12 weeks. This evidence clearly indicates that SrRan administration enhances the healing of a bone defect in rat tibiae. These observations are in agreement with other studies showing that SrRan treatment of rats carrying endosseous titanium cylinders in the proximal tibia increased the trabecular bone BV/TV at the

Table 5: Effect of 4, 8, or 12 weeks of SrRan or vehicle administration on IGF-I concentration in serum of adult female rats before surgery and after euthanasia.

Treatment	Surgery	4 weeks	8 weeks	12 weeks
vehicle	1181.1 ± 87.7	946.8 ± 50.8*		
SrRan	1216.6 ± 77.9	1056.6 ± 49.1°		
vehicle	1034.1 ± 71.6		774.9 ± 82.0**	
SrRan	1146.7 ± 47.9		966.2 ± 45.6$^{\circ\circ}$	
vehicle	1196.7 ± 101.9			882.39 ± 79.37†
SrRan	1064.5 ± 79.2			886.39 ± 67.44

Averages (IGF-I; ng/mL) ± SEM.
4 wks: $P < 0.05$ compared to vehicle (*) or SrRan group at surgery ($^{\circ}$).
8 wks: $P < 0.01$ compared to vehicle (**) or SrRan group at surgery ($^{\circ\circ}$).
12 wks: $P < 0.05$ compared to vehicle group at surgery (†).

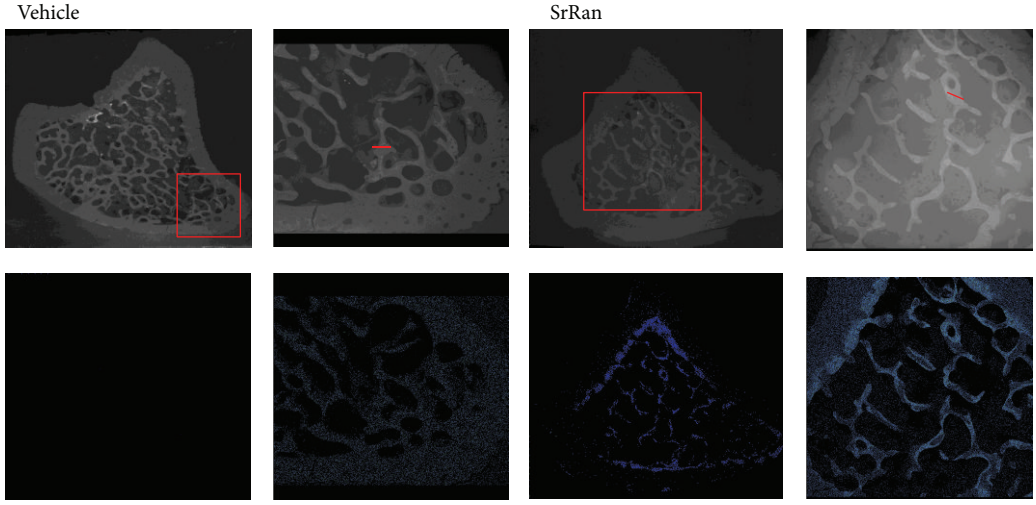

Trab defect	*A*% Ca	*A*% Pi	Ca/Pi	*A*% Sr	*A*% Sr min–max	Sr + Ca/Pi
Vehicle	7.512 ± 0.144	4.417 ± 0.096	1.716 ± 0.044	0.00247 ± 0.0005	0.0000–0.0090	1.717 ± 0.044
SrRan	7.283 ± 0.257	4.159 ± 0.138	1.750 ± 0.007	0.153 ± 0.009	0.1047–0.1863	1.787 ± 0.007

Figure 5: X-Ray spectroscopy of proximal tibia cross-section of two representative specimens following 12 weeks of vehicle or SrRan administration. Squares show strontium distribution in bone tissue in greater detail. Strontium deposits in both newly formed cortical and trabecular bone in SrRan treated rats, including the defect area. In the table, the atomic percent averages of Sr, Ca, and Pi were determined in profiles along trabecular units at the edge of the defect and are depicted by straight lines in the figure.

bone-titanium interface, enhancing implant osseointegration [38].

The 3D reconstructions of μCt scans showed that trabecular bone heals from the periphery toward the centre of the defect. When excluding the central cavity, the analysis of trabecular bone located in a circular subregion of 0.45 mm at the periphery of the defect showed a significant increase in BV/TV in all groups of SrRan-treated rats. The mass and microarchitecture of cancellous bone after 12 weeks of SrRan administration were consistently improved when compared to values measured within the proximal tibia metaphysis of intact rats [35]. This suggests that SrRan administration improves the structure of bone healing the defect *versus* normal, undamaged bone. In addition, SrRan administration for a longer period of time might further improve the microarchitecture of bone extending through the central cavity from the periphery of the defect.

The SrRan-dependent increase in bone strength relies on the sum of positive effects on both microarchitecture and material properties as shown by a finite element analysis [39]. In the present study, the nanoindentation analysis showed a clear effect of SrRan on material level properties of both cortical and trabecular bone repairing the defect when compared to vehicle-treated rats. The increase in elastic modulus, hardness, and working energy was mainly observed after 4 weeks of SrRan administration *versus* time-matched vehicle animals, in both cortical and trabecular bone healing the defect. An effect of SrRan on working energy persisted in trabecular bone after 12-week treatment. In previous reports, it was shown that SrRan administration also improves bone strength by increasing the elastic modulus, hardness, and working energy in rat vertebrae [25, 26, 28]. A similar positive effect of SrRan on tissue quality was also observed in bone growing on implant surfaces [38]. To our knowledge, our

findings provide evidence for the first time that systemic administration of SrRan improves the quality of healing bone in the context of a bone defect.

The incorporation of Sr in cancellous bone filling the defect was confirmed by WDS, while only traces were detectable in vehicle animals. In agreement with former reports, Sr was more concentrated in younger and less mineralized trabecular bone, including the cortical endosteal surface [40]. So far, the mechanism by which SrRan ameliorates tissue properties is unclear. Bone sustainability to mechanical deformation at nanometer scale is regulated by the interaction between collagen, noncollagenous protein, and mineral phase, which allows the load to be efficiently transferred across multiple structural levels through the slipping of matrix-fibrillar interfaces [41].

We hypothesised that the mechanism by which SrRan affects bone material properties may rely on a chemical effect on bone components (matrix and/or mineral phases), in addition to the biological effect on bone cells. This is supported by an ex vivo experiment, which showed the association between Sr content and the improvement of tissue properties in bone sections immerged in $SrCl_2$ solution [42]. The unfolding of sacrificial bonds represents one possibility which allows bone tissue to withstand deformation. These interactions between mineral and organic phases act as a kind of "glue" opposing the separation of mineralized collagen fibrils [43, 44]. The adhesion of Sr to the hydrated layer may account for the improvement in tissue properties, as was proved by indentation performed under dry conditions in which no significant difference was observed between SrRan and vehicle-treated rats [26]. In addition, the hydration level of bone influences the interaction of the organic matrix with the mineral phase and dehydration is associated with a degradation of the plastic properties [45].

Previous findings have shown that Sr is mainly deposited in young bone, within the hydrated layer surrounding the hydroxyapatite crystals [46]. By contrast, the uptake of Sr ions in crystals in place of Ca^{++} ions is quite a rare event to induce an important change in bone material properties. This observation is of major importance as only young bone was formed in the defect in our model. We observed that only a borderline modification of the Ca/P ratio could be observed under SrRan treatment compared to the control group, and this observation is in agreement with the fact that Sr is essentially integrated into the hydrated layer and is rare in the hydroxyapatite crystal.

The mechanisms by which SrRan affects bone formation and trabecular bone remodelling in our model of bone defect were not specifically investigated in the present study. Multiple scenarios may be envisaged by referring to published in vitro and in vivo studies. The effect of SrRan on the production of hormones known to control cortical bone growth, such as IGF-I, might be incriminated. SrRan was demonstrated to increase plasma IGF-I in patients [47] and in rats [26]. In our study, SrRan administration was not associated with a significant change in plasma level of IGF-I and only a trend was observed. However, it cannot be excluded that SrRan might influence the local expression of IGF-I in bone. Interestingly, recent evidence has shown that the overexpression of IGF-I in osteoblasts of transgenic mice protected the bone microstructure from the negative effect of a low protein diet, despite the decrease in circulating levels of IGF-I [48]. The effect of SrRan on the fate of multipotent progenitors migrating through the site of injury at the time of blood vessel invasion during the early phases of bone defect repair must be taken into consideration. Indeed, it was shown that bone marrow stromal cells derived from ovariectomized rats treated with SrRan preferentially differentiate *versus* the osteoblastic lineage [49]. A more recent study showed that SrRan administration in mice lowers bone marrow adiposity and increases trabecular BV/TV in proximal tibia metaphysic [50]. Accordingly, in our model of tibial defect, SrRan may promote osteogenesis by downregulating genes driving the commitment of multipotent mesenchymal stem cells *versus* the adipocyte lineage and inducing genes involved in early phases of osteoblastogenesis. However another possible explanation may be that SrRan could positively influence defect vascularization by modulating the production of vascular endothelial growth factor (VEGF) from osteoblasts. In a recent study, it was shown in vitro that the release of strontium from strontium-doped calcium polyphosphate scaffolds was associated with the increase of VEGF mRNA and protein secretion from cultures of differentiating osteoblasts [51]. However, the association between SrRan administration and vasculogenesis in vivo has not been demonstrated yet.

5. Conclusions

In conclusion, our study demonstrates that the systemic administration of SrRan accelerates the healing of a bone defect created in rat proximal tibiae, with a significant effect on cortical thickness at 4 weeks and on trabecular microarchitecture at 8 and 12 weeks *versus* vehicle animals. Sr is integrated both in cortical and in trabecular bone healing the defect in SrRan-treated rats and improves the bone material level properties of the healing bone mainly after 4 weeks of treatment. These results open up new perspectives for the use of SrRan in clinical studies as a pharmacologic agent with a potential beneficial effect on bone defect repair.

Conflict of Interests

The authors declare that they have no conflict of interests regarding the publication of this paper.

Acknowledgments

The authors would like to thank S. Clement for animal management and technical assistance, I. Badoud for biomechanical testing, and Dr F. Bussy (University Lausanne, Switzerland) for wavelength X-ray dispersive spectroscopy testing.

References

[1] M. Schürch, R. Rizzoli, D. Slosman, L. Vadas, P. Vergnaud, and J. Bonjour, "Protein supplements increase serum insulin-like growth factor-I levels and attenuate proximal femur bone loss in patients with recent hip fracture. A randomized, double-blind, placebo-controlled trial," *Annals of Internal Medicine*, vol. 128, no. 10, pp. 801–809, 1998.

[2] A. E. Oostlander, N. Bravenboer, E. Sohl et al., "Histomorphometric analysis reveals reduced bone mass and bone formation in patients with quiescent crohn's disease," *Gastroenterology*, vol. 140, no. 1, pp. 116–123, 2011.

[3] T. Kasahara, S. Imai, H. Kojima et al., "Malfunction of bone marrow-derived osteoclasts and the delay of bone fracture healing in diabetic mice," *Bone*, vol. 47, no. 3, pp. 617–625, 2010.

[4] L. C. Gerstenfeld, D. M. Cullinane, G. L. Barnes, D. T. Graves, and T. A. Einhorn, "Fracture healing as a post-natal developmental process: molecular, spatial, and temporal aspects of its regulation," *Journal of Cellular Biochemistry*, vol. 88, no. 5, pp. 873–884, 2003.

[5] M. P. Lutolf, F. E. Weber, H. G. Schmoekel et al., "Repair of bone defects using synthetic mimetics of collagenous extracellular matrices," *Nature Biotechnology*, vol. 21, no. 5, pp. 513–518, 2003.

[6] J. H. Holstein, M. Orth, C. Scheuer et al., "Erythropoietin stimulates bone formation, cell proliferation, and angiogenesis in a femoral segmental defect model in mice," *Bone*, vol. 49, no. 5, pp. 1037–1045, 2011.

[7] S. P. Bruder, A. A. Kurth, M. Shea, W. C. Hayes, N. Jaiswal, and S. Kadiyala, "Bone regeneration by implantation of purified, culture-expanded human mesenchymal stem cells," *Journal of Orthopaedic Research*, vol. 16, no. 2, pp. 155–162, 1998.

[8] R. Cancedda, M. Mastrogiacomo, G. Bianchi, A. Derubeis, A. Muraglia, and R. Quarto, "Bone marrow stromal cells and their use in regenerating bone," *Novartis Foundation Symposium*, vol. 249, pp. 133–147, 2003.

[9] Y. Yang, B. Hallgrimsson, and E. E. Putnins, "Craniofacial defect regeneration using engineered bone marrow mesenchymal stromal cells," *Journal of Biomedical Materials Research A*, vol. 99, no. 1, pp. 74–85, 2011.

[10] M. A. Matos, U. Tannuri, and R. Guarniero, "The effect of zoledronate during bone healing," *Journal of Orthopaedics and Traumatology*, vol. 11, no. 1, pp. 7–12, 2010.

[11] J. Li, S. Mori, Y. Kaji, T. Mashiba, J. Kawanishi, and H. Norimatsu, "Effect of bisphosphonate (incadronate) on fracture healing of long bones in rats," *Journal of Bone and Mineral Research*, vol. 14, no. 6, pp. 969–979, 1999.

[12] M. Nagashima, A. Sakai, S. Uchida, S. Tanaka, M. Tanaka, and T. Nakamura, "Bisphosphonate (YM529) delays the repair of cortical bone defect after drill-hole injury by reducing terminal differentiation of osteoblasts in the mouse femur," *Bone*, vol. 36, no. 3, pp. 502–511, 2005.

[13] M. M. McDonald, S. Dulai, C. Godfrey, N. Amanat, T. Sztynda, and D. G. Little, "Bolus or weekly zoledronic acid administration does not delay endochondral fracture repair but weekly dosing enhances delays in hard callus remodeling," *Bone*, vol. 43, no. 4, pp. 653–662, 2008.

[14] M. Saito, A. Shiraishi, M. Ito et al., "Comparison of effects of alfacalcidol and alendronate on mechanical properties and bone collagen cross-links of callus in the fracture repair rat model," *Bone*, vol. 46, no. 4, pp. 1170–1179, 2010.

[15] D. E. Komatsu, K. A. Brune, H. Liu et al., "Longitudinal in vivo analysis of the region-specific efficacy of parathyroid hormone in a rat cortical defect model," *Endocrinology*, vol. 150, no. 4, pp. 1570–1579, 2009.

[16] S. Komatsubara, S. Mori, T. Mashiba et al., "Human parathyroid hormone (1-34) accelerates the fracture healing process of woven to lamellar bone replacement and new cortical shell formation in rat femora," *Bone*, vol. 36, no. 4, pp. 678–687, 2005.

[17] B. Chalidis, C. Tzioupis, E. Tsiridis, and P. V. Giannoudis, "Enhancement of fracture healing with parathyroid hormone: preclinical studies and potential clinical applications," *Expert Opinion on Investigational Drugs*, vol. 16, no. 4, pp. 441–449, 2007.

[18] J. E. Compston, "Skeletal actions of intermittent parathyroid hormone: effects on bone remodelling and structure," *Bone*, vol. 40, no. 6, pp. 1447–1452, 2007.

[19] P. J. Marie, M. T. Garba, M. Hott, and L. Miravet, "Effect of low doses of stable strontium on bone metabolism in rats," *Mineral and Electrolyte Metabolism*, vol. 11, no. 1, pp. 5–13, 1985.

[20] P. J. Marie, M. Hott, D. Modrowski et al., "An uncoupling agent containing strontium prevents bone loss by depressing bone resorption and maintaining bone formation in estrogen-deficient rats," *Journal of Bone and Mineral Research*, vol. 8, no. 5, pp. 607–615, 1993.

[21] E. Canalis, M. Hott, P. Deloffre, Y. Tsouderos, and P. J. Marie, "The divalent strontium salt S12911 enhances bone cell replication and bone formation in vitro," *Bone*, vol. 18, no. 6, pp. 517–523, 1996.

[22] P. J. Marie, "Optimizing bone metabolism in osteoporosis: insight into the pharmacologic profile of strontium ranelate," *Osteoporosis International*, vol. 14, supplement 3, pp. S9–12, 2003.

[23] E. Bonnelye, A. Chabadel, F. Saltel, and P. Jurdic, "Dual effect of strontium ranelate: Stimulation of osteoblast differentiation and inhibition of osteoclast formation and resorption in vitro," *Bone*, vol. 42, no. 1, pp. 129–138, 2008.

[24] P. Delannoy, D. Bazot, and P. J. Marie, "Long-term treatment with strontium ranelate increases vertebral bone mass without deleterious effect in mice," *Metabolism: Clinical and Experimental*, vol. 51, no. 7, pp. 906–911, 2002.

[25] P. Ammann, V. Shen, B. Robin, Y. Mauras, J. Bonjour, and R. Rizzoli, "Strontium ranelate improves bone resistance by increasing bone mass and improving architecture in intact female rats," *Journal of Bone and Mineral Research*, vol. 19, no. 12, pp. 2012–2020, 2004.

[26] P. Ammann, I. Badoud, S. Barraud, R. Dayer, and R. Rizzoli, "Strontium ranelate treatment improves trabecular and cortical intrinsic bone tissue quality, a determinant of bone strength," *Journal of Bone and Mineral Research*, vol. 22, no. 9, pp. 1419–1425, 2007.

[27] J. Buehler, P. Chappuis, J. L. Saffar, Y. Tsouderos, and A. Vignery, "Strontium ranelate inhibits bone resorption while maintaining bone formation in alveolar bone in monkeys (Macaca fascicularis)," *Bone*, vol. 29, no. 2, pp. 176–179, 2001.

[28] S. D. Bain, C. Jerome, V. Shen, I. Dupin-Roger, and P. Ammann, "Strontium ranelate improves bone strength in ovariectomized rat by positively influencing bone resistance determinants," *Osteoporosis International*, vol. 20, no. 8, pp. 1417–1428, 2009.

[29] Y. F. Li, E. Luo, G. Feng, S. S. Zhu, J. H. Li, and J. Hu, "Systemic treatment with strontium ranelate promotes tibial fracture healing in ovariectomized rats," *Osteoporosis International*, vol. 21, no. 11, pp. 1889–1897, 2010.

[30] K. E. Ozturan, B. Demir, I. Yucel, H. Cakici, F. Yilmaz, and A. Haberal, "Effect of strontium ranelate on fracture healing in the

osteoporotic rats," *Journal of Orthopaedic Research*, vol. 29, no. 1, pp. 138–142, 2011.

[31] B. Habermann, K. Kafchitsas, G. Olender, P. Augat, and A. Kurth, "Strontium ranelate enhances callus strength more than PTH 1-34 in an osteoporotic rat model of fracture healing," *Calcified Tissue International*, vol. 86, no. 1, pp. 82–89, 2010.

[32] A. Laib, O. Barou, L. Vico, M. H. Lafage-Proust, C. Alexandre, and P. Rügsegger, "3D micro-computed tomography of trabecular and cortical bone architecture with application to a rat model of immobilisation osteoporosis," *Medical & Biological Engineering & Computing*, vol. 38, no. 3, pp. 326–332, 2000.

[33] R. Müller, M. Hahn, M. Vogel, G. Delling, and P. Rüegsegger, "Morphometric analysis of noninvasively assessed bone biopsies: comparison of high-resolution computed tomography and histologic sections," *Bone*, vol. 18, no. 3, pp. 215–220, 1996.

[34] T. Hildebrand and P. Rüegsegger, "Quantification of bone microarchitecture with the structure model index," *Computer Methods in Biomechanics and Biomedical Engineering*, vol. 1, no. 1, pp. 15–23, 1997.

[35] S. Mekraldi, A. Toromanoff, R. Rizzoli, and P. Ammann, "Pamidronate prevents bone loss and decreased bone strength in adult female and male rats fed an isocaloric low-protein diet," *Journal of Bone and Mineral Research*, vol. 20, no. 8, pp. 1365–1371, 2005.

[36] S. Hengsberger, P. Ammann, B. Legros, R. Rizzoli, and P. Zysset, "Intrinsic bone tissue properties in adult rat vertebrae: modulation by dietary protein," *Bone*, vol. 36, no. 1, pp. 134–141, 2005.

[37] D. N. Alegre, C. Ribeiro, C. Sousa, J. Correia, L. Silva, and L. de Almeida, "Possible benefits of strontium ranelate in complicated long bone fractures," *Rheumatology International*, vol. 32, no. 2, pp. 439–443, 2012.

[38] L. Maïmoun, T. C. Brennan, I. Badoud, V. Dubois-Ferriere, R. Rizzoli, and P. Ammann, "Strontium ranelate improves implant osseointegration," *Bone*, vol. 46, no. 5, pp. 1436–1441, 2010.

[39] S. K. Boyd, E. Szabo, and P. Ammann, "Increased bone strength is associated with improved bone microarchitecture in intact female rats treated with strontium ranelate: a finite element analysis study," *Bone*, vol. 48, no. 5, pp. 1109–1116, 2011.

[40] G. Boivin, P. Deloffre, B. Perrat et al., "Strontium distribution and interactions with bone mineral in monkey iliac bone after strontium salt (S 12911) administration," *Journal of Bone and Mineral Research*, vol. 11, no. 9, pp. 1302–1311, 1996.

[41] H. S. Gupta, J. Seto, W. Wagermaier, P. Zaslansky, P. Boesecke, and P. Fratzl, "Cooperative deformation of mineral and collagen in bone at the nanoscale," *Proceedings of the National Academy of Sciences of the United States of America*, vol. 103, no. 47, pp. 17741–17746, 2006.

[42] M. Cattani-Lorente, R. Rizzoli, and P. Ammann, "In vitro bone exposure to strontium improves bone material level properties," *Acta Biomaterialia*, vol. 9, no. 6, pp. 7005–7013, 2013.

[43] G. E. Fantner, T. Hassenkam, J. H. Kindt et al., "Sacrificial bonds and hidden length dissipate energy as mineralized fibrils separate during bone fracture," *Nature Materials*, vol. 4, no. 8, pp. 612–616, 2005.

[44] G. E. Fantner, E. Oroudjev, G. Schitter et al., "Sacrificial bonds and hidden length: unraveling molecular mesostructures in tough materials," *Biophysical Journal*, vol. 90, no. 4, pp. 1411–1418, 2006.

[45] J. S. Nyman, A. Roy, X. Shen, R. L. Acuna, J. H. Tyler, and X. Wang, "The influence of water removal on the strength and toughness of cortical bone," *Journal of Biomechanics*, vol. 39, no. 5, pp. 931–938, 2006.

[46] D. Farlay, G. Boivin, G. Panczer, A. Lalande, and P. J. Meunier, "Long-term strontium ranelate administration in monkeys preserves characteristics of bone mineral crystals and degree of mineralization of bone," *Journal of Bone and Mineral Research*, vol. 20, no. 9, pp. 1569–1578, 2005.

[47] I. Gulhan, S. Bilgili, R. Gunaydin, S. Gulhan, and C. Posaci, "The effect of strontium ranelate on serum insulin like growth factor-1 and leptin levels in osteoporotic post-menopausal women: a prospective study," *Archives of Gynecology and Obstetrics*, vol. 278, no. 5, pp. 437–441, 2008.

[48] T. C. Brennan-Speranza, R. Rizzoli, B. E. Kream, C. Rosen, and P. Ammann, "Selective osteoblast overexpression of IGF-I in mice prevents low protein-induced deterioration of bone strength and material level properties," *Bone*, vol. 49, no. 5, pp. 1073–1079, 2011.

[49] S. Peng, X. S. Liu, T. Wang et al., "In vivo anabolic effect of strontium on trabecular bone was associated with increased osteoblastogenesis of bone marrow stromal cells," *Journal of Orthopaedic Research*, vol. 28, no. 9, pp. 1208–1214, 2010.

[50] C. Fournier, A. Perrier, M. Thomas et al., "Reduction by strontium of the bone marrow adiposity in mice and repression of the adipogenic commitment of multipotent C3H10T1/2 cells," *Bone*, vol. 50, no. 2, pp. 499–509, 2012.

[51] F. Liu, X. Zhang, X. Yu, Y. Xu, T. Feng, and D. Ren, "In vitro study in stimulating the secretion of angiogenic growth factors of strontium-doped calcium polyphosphate for bone tissue engineering," *Journal of Materials Science: Materials in Medicine*, vol. 22, no. 3, pp. 683–692, 2011.

Hindawi Publishing Corporation
BioMed Research International
Volume 2014, Article ID 347508, 9 pages
http://dx.doi.org/10.1155/2014/347508

Research Article

Tooth Movement out of the Bony Wall Using Augmented Corticotomy with Nonautogenous Graft Materials for Bone Regeneration

Kye-Bok Lee,[1] Dong-Yeol Lee,[2] Hyo-Won Ahn,[1] Seong-Hun Kim,[1] Eun-Cheol Kim,[2] and Igor Roitman[3]

[1] *Department of Orthodontics, School of Dentistry, Kyung Hee University, No.1 Hoegi-dong, Dongdaemun-gu, Seoul 130-701, Republic of Korea*
[2] *Department of Oral and Maxillofacial Pathology and Research Center for Tooth & Periodontal Regeneration (MRC), School of Dentistry, Kyung Hee University, Seoul 130-701, Republic of Korea*
[3] *Division of Periodontology, Department of Orofacial Science, University of California, San Francisco, CA 94122, USA*

Correspondence should be addressed to Seong-Hun Kim; bravortho@khu.ac.kr and Eun-Cheol Kim; eckim@khu.ac.kr

Received 6 April 2014; Accepted 30 July 2014; Published 27 August 2014

Academic Editor: Homayoun H. Zadeh

This prospective randomized split-mouth study was performed to compare the effects of augmented corticotomy with those of different nonautogenous bone graft materials combined with orthodontic tooth movement in dogs. Decortication was performed on the buccal bone surface of 6 male beagle dogs that were randomly assigned to receive grafts of deproteinized bovine bone mineral, irradiated cortical bone, or synthetic bone. Immediate orthodontic force was applied to the second and third premolars for buccal tipping for 6 weeks. The pocket depth and width of keratinized tissue (WKT) were measured. Histologic and histomorphometric analyses were performed. The probing depth, WKT, and ratio of the area of new bone to that of total bone on the buccal side were not significantly different between groups. All groups had considerable new bone formation on the pressure side. New bone formation on the buccal side and buccal plate formation in the coronal direction along the root surfaces were induced by the bone-derived and PDL-derived mesenchymal matrix, respectively. The angular change between groups was significantly different ($P < 0.001$). Augmented corticotomy using nonautogenous graft materials facilitated tooth movement without fenestrations and accelerated new bone formation on the pressure side.

1. Introduction

During orthodontic treatment, tipping movement of teeth commonly occurs. However, buccolingual movement exceeding the alveolar housing may result in bony dehiscence at the crest area and cause gingival recession, especially in the decompensation of class III patients [1], maximum retraction of anterior teeth in bialveolar protrusion patients [2], and transverse expansion of upper molars by rapid palatal expansion [3]. Wainwright et al. [4] reported that once the cortical plate has been penetrated during tipping movement, the buccal root surface becomes devoid of cortical bone. Repair, not regeneration, of the perforation site took place only after the teeth had relapsed. However, no histologic studies have demonstrated the regeneration or reestablishment of the cortical plate [5, 6].

Corticotomy-facilitated tooth movement with alveolar bone augmentation may facilitate the retention of the periodontal ligament, thereby preventing bony dehiscence and gingival recession [7, 8]. Wilcko et al. [9] reported that alveolar augmentation could reinforce the dentoalveolar deficiency when the teeth were tipped labially and suggested that alveolar bone augmentation could provide patients with a more structurally intact periodontium at the completion of the orthodontic treatment. Moreover, corticotomy on alveolar bone resulted in more rapid orthodontic tooth movement than that obtained with conventional methods [10, 11]. The regional acceleratory phenomenon (RAP) can

accelerate both hard tissue healing and soft tissue healing by 2- to 10-fold, thus leading to decreased regional bone density [12, 13]. A recent clinical study [7] showed that the augmented corticotomy provided effective decompensation of the mandibular incisors in skeletal class III patients while maintaining labial bone thickness with no periodontal side effects. However, histological observations related to the periodontal reaction to augmented corticotomy are rare.

In recent years, nonautogenous bone grafts, especially synthetic bone substitutes, have played an increasingly crucial role in surgical dentistry. Wilcko et al. [8, 9] reported satisfactory results with a combination of demineralized freeze-dried bone allografts (DFDBA), xenografts, or bioabsorbable alloplastic grafts for alveolar augmentation. They reported only one human histologic case study in which deproteinized bovine bone mineral was used [14]. However, no studies have focused on the influence of graft materials with different origins, especially synthetic bone, when combined with corticotomy and further orthodontic tooth movement. Because most of what is known about the decortication procedures in orthodontic treatment is based on case reports, more laboratory and clinical studies are necessary to better elucidate the biological mechanisms involved at the tissue level. The purpose of this study was to compare the effects of deproteinized bovine bone mineral (DBBM: Bio-Oss; Geistlich Pharma AG, Wolhuser, Switzerland), irradiated cortical bone (ICB: Rocky Mountain Tissue Bank, Aurora, CO), or synthetic bone (SB: MBCP$^+$; micromacroporous biphasic calcium phosphate; Biomatlante, Vigneux de Bretagne, France) in an augmented corticotomy procedure for periodontal tissue reconstruction in the context of uncontrolled buccal tipping movement of teeth in beagle dogs.

2. Materials and Methods

2.1. Animals. This study was a prospective, split-mouth, randomized controlled experimental design using 6 male beagle dogs; dogs were randomly assigned to Groups A, B, and C. Augmented corticotomy was performed with DBBM in Group A, ICB in Group B, and SB in Group C. Groups A and B were used as positive controls in our study because Wilcko et al. [14] had reported them as such, and one of the goals of this study was to evaluate SB in comparison to other options. Buccal tipping of the second (P2) and third premolars (P3) was planned on the upper and lower arches for 6 weeks. All animals were 1-2 years old and weighed between 10 and 13 kg. They were caged individually, fed soft food and a standard diet, and given water ad libitum. The experimental protocols in this study were approved by the Institutional Animal Care and Use Committee (KHMC-IACUC-11-021, KHMC-IACUC-10-070).

2.2. Clinical Examination. During the examinations and surgical procedures, the dogs were anesthetized with a mixture of tiletamine-zolazepam (5–10 mg/kg; Zoletil 100; Virbac, Carros, France) and xylazine (5 mg/kg,; Rompun; Bayer Korea Ltd., Seoul, Korea) intramuscularly (IM) and intravenously (IV). Intravenous medications were administered using a catheter in the vessel of the ear. The PD and WKT were measured at the mesial, middle, and distal buccal sides of each tooth with a periodontal probe, and the periodontal conditions at baseline and 6 weeks after the procedure were compared. Following these measurements, scaling was performed. An alginate impression was taken to make a study model to fabricate orthodontic appliances (band and wire). The canine (C) and fourth premolar (P4) were used as anchorage, and thick wire (ø 0.9 mm) with traction hooks was welded to the buccal surface of the bands [15]. At the second (P2) and third premolars (P3), the lingual button was welded on the lingual surface of the band. Immediately after augmented corticotomy, an orthodontic force (200 g) for buccal tipping was applied to the lingual buttons of P2 and P3 for 6 weeks. The period of 6 weeks was considered to be sufficient to form new bone and induce tooth movement in augmented corticotomy.

2.3. Surgical Procedure. After 2 weeks, the animals were anesthetized to fix the orthodontic appliances to the teeth, and lidocaine hydrochloride (2% lidocaine with 1 : 100,000 epinephrine; Huons Co., Seoul, Republic of Korea) was infiltrated into the surgical sites for local anesthesia. An intrasulcular incision was made from the canine to the first molar. Then, a full-thickness flap was elevated carefully. The circumscribing corticotomy was performed at the buccal bone surface only with a round bur (ø 1.5 mm) under sterile saline irrigation. The DBBM, ICB, and SB were grafted (1 cc per surgical site) onto the buccal bone surface randomly. Each animal received only one graft depending on the group it was assigned to. The mucoperiosteal flaps were repositioned and sutured with 5–0 nylon. Primary closure was obtained. A closed coil spring with a tensile strength of 200 g was applied in the buccolingual direction immediately, and P2 and P3 were activated for buccal tipping (Figure 1).

After surgery, gentamicin (Dongwha-Pharm. Co., Seoul, Korea) and ketoprofen (Ketopro; Uni Biotech, Chungnam, Korea) were administered IM two times daily for 6 days, and irrigation with 1% chlorhexidine-gluconate solution was performed simultaneously for infection control. Scaling and mechanical plaque control were performed once per week. Six weeks after the procedure, PD and WKT were measured under general anesthesia, and the animals were humanely euthanized with an overdose of thiopental sodium.

2.4. Histological Examination. The mandibles and maxillae of all experimental animals were dissected, and block specimens were obtained. The retrieved block specimens were rinsed in sterile saline and immediately immersed in 10% neutral buffered formalin for 14 days. Decalcification was performed using 5% nitric acid for 6 days [16]. Following decalcification, the specimens were dehydrated through a series of ethanol and embedded in paraffin. Buccolingual sections were sliced with the microtome set at 5 μm and stained with Masson's trichrome [11, 17].

Histologic evaluations were performed using a light microscope (Olympus BX51; Olympus, Tokyo, Japan) equipped with an Olympus DP21 microscope camera. CellSens imaging software (version 1.6; Olympus Corporation, Tokyo, Japan) was used to measure the angle and bone area. After

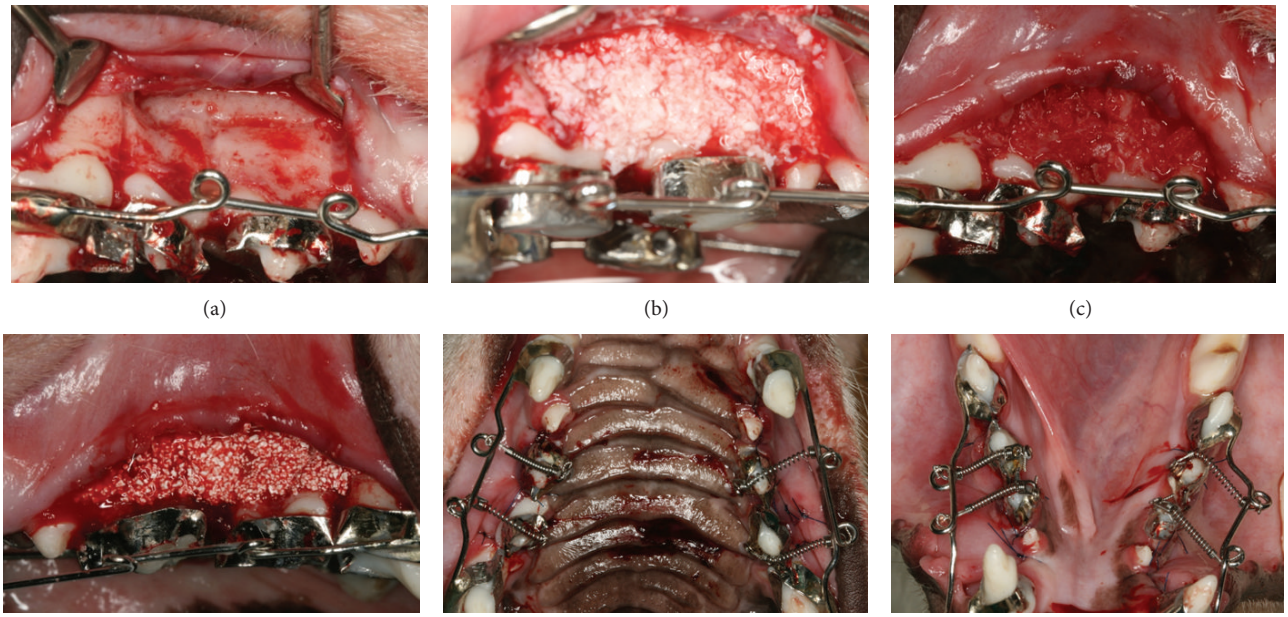

Figure 1: Surgical procedure. Full-thickness flap elevation and corticotomy were performed on the buccal side (a). Deproteinized bovine bone mineral (DBBM) particles (b), irradiated cortical bone (ICB) particles (c), and micromacroporous biphasic calcium phosphate (SB: MBCP$^+$) particles (d) were grafted. Primary closure was obtained, and activation of P2 and P3 for buccal tipping was started with a closed coil spring (200 g) ((e) and (f)).

microscopic examination, a photograph of each slide was taken, and the resulting images were saved. The tipping angle and buccal bone area were measured independently by 3 examiners who were blinded to all group information. The buccal tipping angle was measured from the reversal line of the palatal/lingual bone to the lingual/palatal sides of the root surface. The total buccal bone wall area and old bone area were measured, and the new bone area was calculated by subtracting the old bone area from the total bone area. Grafted particles embedded in and bridged with newly formed bone were included in the new bone area, but floating particles without new bone in soft connective tissue were excluded (Figure 2).

2.5. Statistical Analysis. Descriptive statistics (mean ± SD) for each parameter were evaluated in all groups. Within each group, the measurements from the mandible and maxilla were not different; therefore, they (the maxilla and mandible) were combined for analysis. The first, second, and third measurements were compared within each group using Pearson's correlation coefficient, which was higher than 0.98 at the 95% confidence level; therefore, the mean value of the three datasets was used for further description. For histomorphometric analysis, the buccal tipping angle and ratio of new bone area/total bone area were analyzed by the nonparametric Kruskal-Wallis test because the measured number of teeth in each group was not normally distributed. The paired t-test was used to compare the soft tissue measurements at baseline and 6 weeks after the surgery. Statistical significance was defined at $P < 0.05$. Three examiners measured angles and bone area. Intraclass correlation analysis was used to analyze interexaminer difference. All statistical analyses were performed using SPSS statistical software (version 18.0; SPSS Inc., Chicago, IL).

3. Results

All sites showed uneventful healing, with no to minimal signs of inflammation.

3.1. Soft Tissue. Significant differences were observed between the groups for PD but not WKT. The PD at baseline and at 6 weeks after surgery (1.37 ± 0.59 mm and 1.99 ± 0.91 mm, resp.) was significantly different ($P < 0.001$); however, the difference was only approximately 0.4 mm, and this difference was regarded as not physiologically or clinically significant. The WKT at 6 weeks after surgery (3.94 ± 1.04 mm) did not differ significantly from that at baseline (3.90 ± 1.15 mm) ($P = 0.704$). These results were combined from all of the groups.

3.2. Buccal Tipping Angle. All groups had uncontrolled buccal tipping of P2 and P3. There was a significant difference in the angular change between groups (Group A, 20.81 ± 8.07°; Group B, 16.08 ± 4.14°; and Group C, 27.26 ± 7.27°) (Figure 3(a)). Statistical significance was found between groups, specifically between Groups A and B, $P = 0.137$; Groups B and C, $P = 0.000$; and Groups A and C, $P = 0.019$. The intraclass correlation coefficient (r) was 0.997 and the correlation was statistically significant ($P = 0.000$).

3.3. Ratio of New Bone Area on Pressure Sides. All groups showed significant new bone formation at the buccal sides.

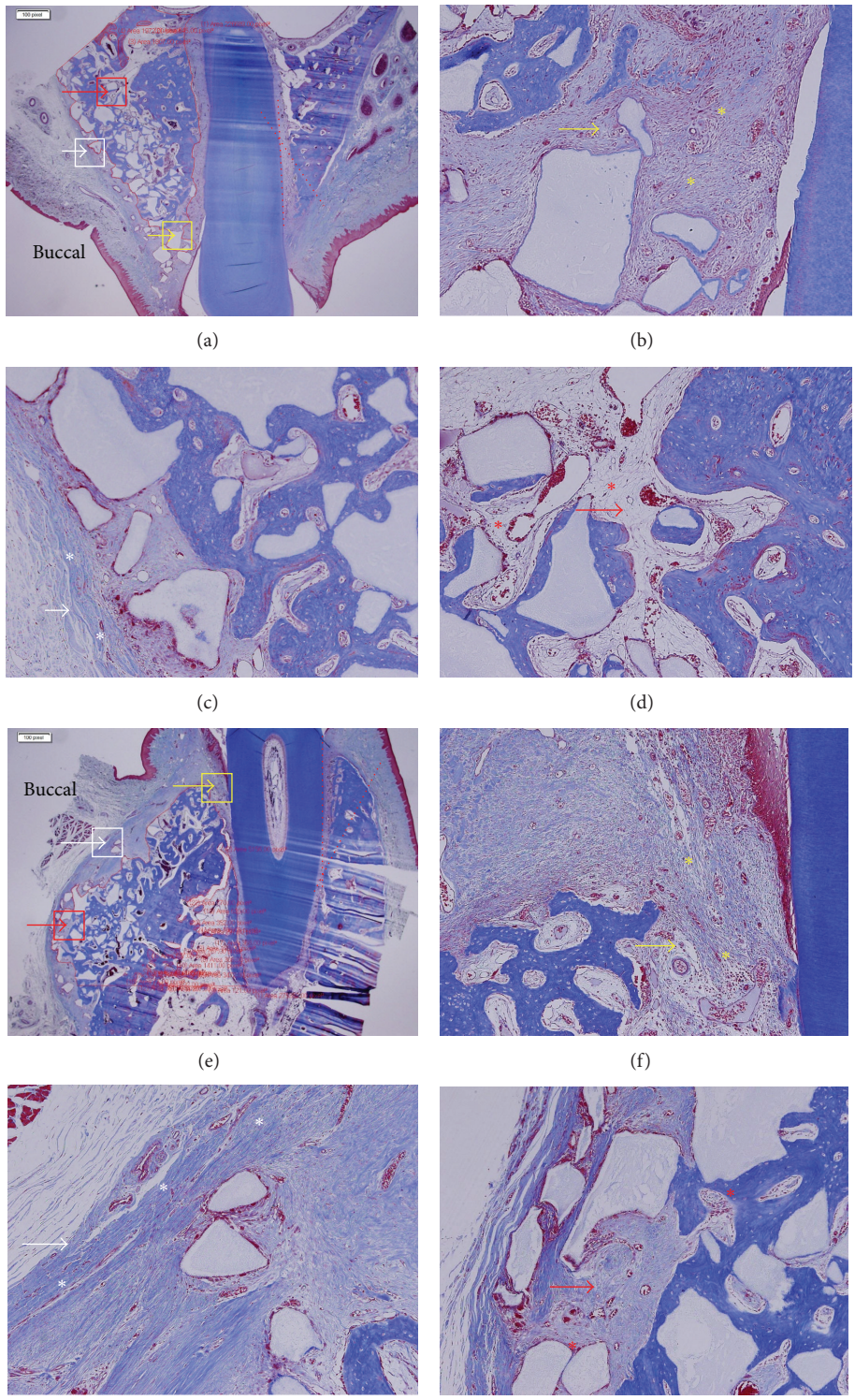

Figure 2: Methods of measurements. (a)–(d) Maxilla, buccal tipping angle (red dotted line) and buccal bone wall area. (e)–(h) Mandible, buccal tipping angle (red dotted line) and buccal bone wall area. Yellow arrow indicates PDL-derived mesenchymal matrix, white arrow indicates buccal mesenchymal matrix, and red arrow indicates bone-derived mesenchymal matrix. (b), (f) Yellow arrow and stars indicate PDL-derived mesenchymal matrix. New bone formation was observed around grafted particles that were embedded in PDL-derived mesenchymal matrix. (c), (g) White arrow and stars indicate the buccal mesenchymal matrix, which plays the role of thick periosteum. (d), (h) Red arrow and stars indicate bone-derived mesenchymal matrix that appears to be loose connective tissue. Masson's trichrome stain. Original magnification for (a) and (e): ×12.5; for (b), (c), (d), (f), (g), (h): ×100.

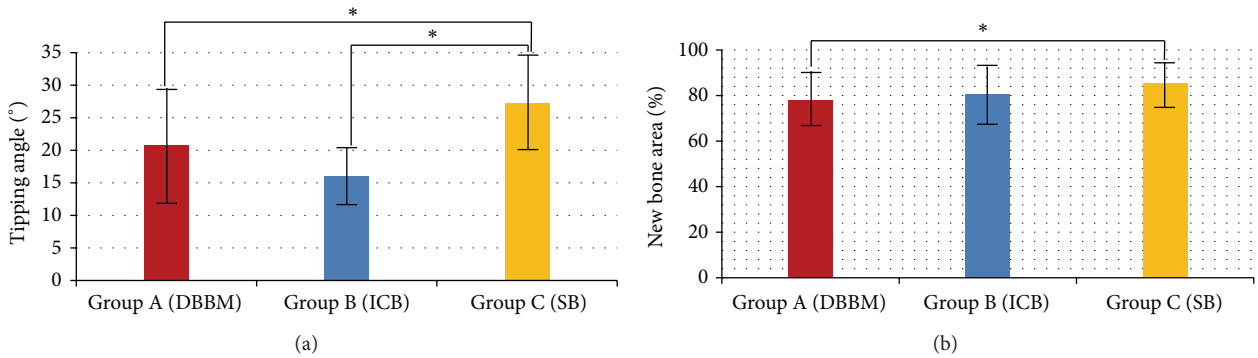

FIGURE 3: (a) Buccal tipping angle (°). (b) New bone area (NB, %). $^{*}P < 0.05$.

The ratio of new bone area to total bone area on the buccal side in the different groups was as follows: Group A, 77.7 ± 11.5%; Group B, 80.6 ± 12.7%; and Group C, 85.4 ± 8.8%. The difference between Groups A and C was statistically significant ($P = 0.046$) (Figure 3(b)). The intraclass correlation coefficient (r) was 0.709, and the correlation was statistically significant ($P = 0.000$).

3.4. Histological Observations. In all groups, considerable new bone formation was observed on the pressure side after 6 weeks (Figures 4 and 5).

For histologic evaluation, in this study, the mesenchymal matrix was designated as PDL-derived, bone-derived, or buccal mesenchymal matrix depending on its origin in the PDL, buccal bone, or the thick, dense connective tissue that covered the buccal bone surface and appeared to play the role of periosteum, respectively. The grafted DBBM, ICB, and MBCP^{+} particles were partially or mostly resorbed, embedded in or bridged with new bone, and/or encapsulated by dense fibrous connective tissue. Most grafted ICB particles were resorbed, whereas more MBCP^{+} and Bio-Oss particles remained in a partially resorbed state. The buccal and lingual/palatal crest level was maintained in all groups. On the pressure sides, the apical root surface resorption was localized in the cementum at the lingual/palatal side because of the force of the uncontrolled buccal tipping. The modeling and remodeling pattern of the alveolar bone on the buccal side had distinguishing features irrespective of the graft material.

In the bone modeling/remodeling at the buccal side, two characteristic appearances were observed: one was a large amount of new bone formation on the buccal side induced by the bone-derived mesenchymal matrix, and the other was new bone formation induced by the PDL-derived mesenchymal matrix producing a buccal bone plate in the coronal direction along the root surfaces. Bone modeling/remodeling was not localized and was observed in all alveolar and basal bone buccolingually. Dense buccal mesenchymal matrix covered the buccal bone surfaces and appeared to protect the bone area.

4. Discussion

The augmented corticotomy procedure has expanded the frontier of conventional orthodontic treatment. Generally, the labial and lingual cortical plates at the level of the incisor apex are considered to be the anatomic limits of tooth movement [18]. Although a basic axiom in orthodontics is that "bone traces tooth movement," the ratio of bone modeling to tooth movement varies according to the direction of orthodontic tooth movement. Buccolingual tipping exceeding alveolar housing may result in bony dehiscence at the crest area and gingival recession, especially in the thin biotype. During presurgical decompensation in class III patients, labial tipping of the lower incisors up to 8–10° is generally expected [19]. In our study, although the amount of labial tipping exceeded twice that of the clinical outcome, the periodontal tissue was surprisingly well maintained at the crest level on the pressure sides. The extent of buccal tipping indicates that the native buccal bone plate had been totally resorbed and was replaced by a newly formed buccal bone plate. Corticotomy-facilitated tooth movement with alveolar bone augmentation is likely to facilitate the retention of the periodontal ligament, thus preventing bony dehiscence and gingival recession [7, 8, 20].

The concept of corticotomy relies on creating bony blocks with embedded teeth that can be moved rapidly with strong forces [21–23]. However, Wilcko et al. [8] suggested that transient localized demineralization/remineralization occurs after corticotomy and that the demineralization of the alveolar bone over the root surfaces leaves the collagenous soft tissue matrix of the bone, which can be carried with the root surface and then remineralized following the completion of the orthodontic treatment. They named this process "bone matrix transportation." However, in our study, these phenomena were observed as bone modeling/remodeling. In this study, we observed the following two characteristic appearances in the bone modeling/remodeling on the buccal side: (1) a considerable amount of new bone was formed by the bone-derived mesenchymal matrix and (2) new bone formation in the coronal direction along the root surface was induced by the PDL-derived mesenchymal matrix. Bone modeling/remodeling was not restricted to the local area; rather, it was observed buccolingually throughout the alveolar and basal bone. This bone metabolism is considered to be a part of the simultaneously coordinated modeling and remodeling induced by the different types of mesenchymal matrix and not representative of the sequential process of bone matrix transportation as put forth by Wilcko et al.

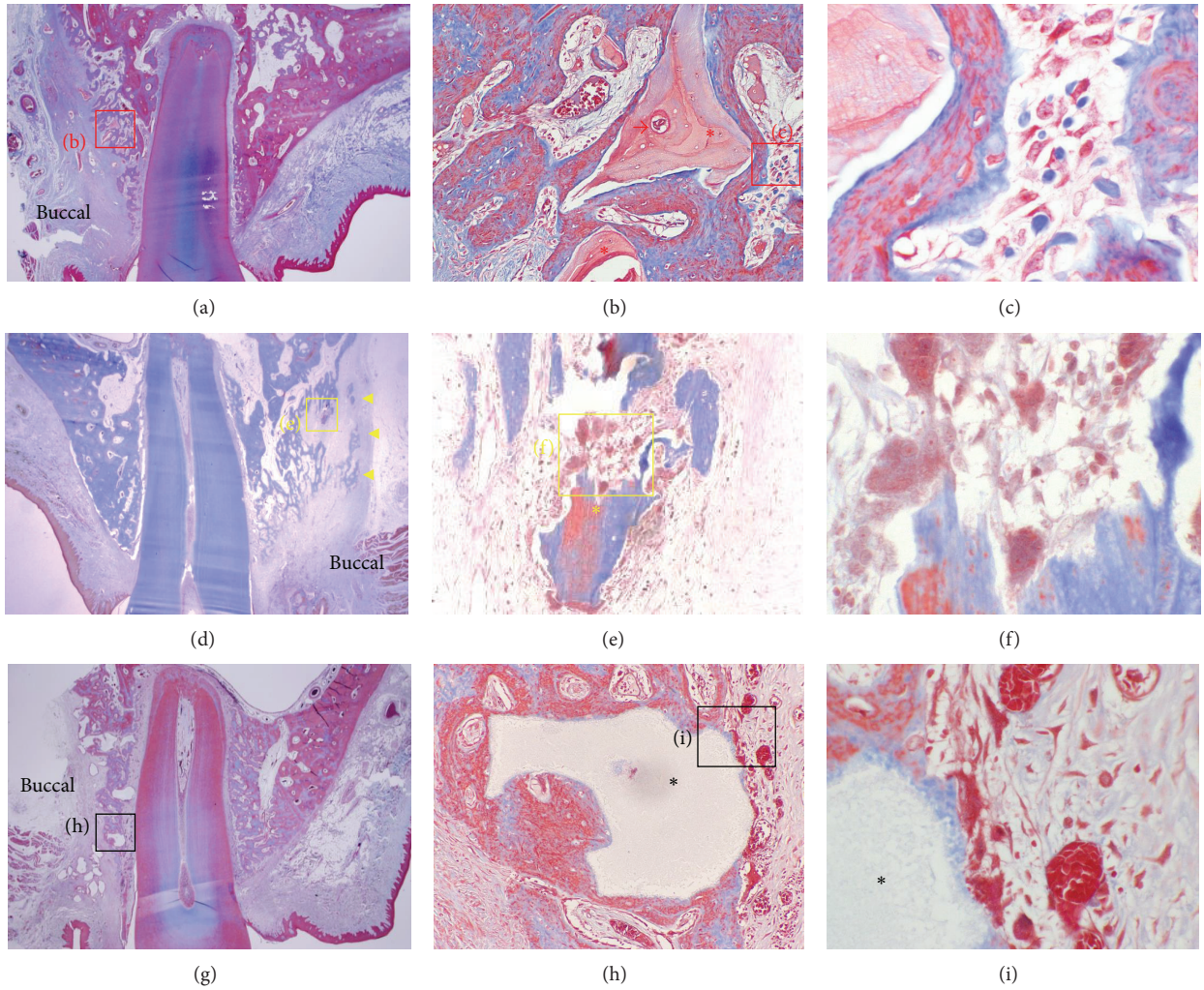

Figure 4: Microphotograph of a buccopalatal section from the maxilla. (a) Deproteinized bovine bone mineral (DBBM) graft. (b) Higher magnification of (a). Red stars indicate DBBM particles that were embedded in and bridged with newly formed bone within the bone-derived mesenchymal matrix. (c) Higher magnification of (b). Active aggregated osteoblasts were observed to form new bone matrix. (d) Irradiated cortical bone (ICB) graft. Most of the grafted ICB particles were resorbed. Grafted ICB particles were embedded in bone-derived mesenchymal matrix, encircled by a newly formed bone wall (yellow arrows). Newly formed bone walls in the mesenchymal matrix appeared to represent buccal bone expansion or bursting. (e) Higher magnification of (d). Grafted particles were bridged with newly formed bone. (f) Higher magnification of (e). Active osteoclasts and osteoblasts are shown. Grafted ICB particles were still resorbed by osteoclasts within the bone-derived mesenchymal matrix. (g) Micromacroporous biphasic calcium phosphate (SB; MBCP$^+$) graft. Some of the grafted SB particles were embedded in the newly formed buccal bone wall and faced the PDL-derived mesenchymal matrix. (h) Higher magnification of (g). Grafted SB particles were resorbed by osteoclasts in the PDL-derived mesenchymal matrix and embedded in newly formed buccal bone. Small capillaries were abundant around the grafted particles (black star). (i) Higher magnification of (h). The surface of grafted SB particles was covered with newly formed bone and resorbed by osteoclasts in the process of remodeling. Masson's trichrome stain. Original magnification for (a), (d), and (g): ×12.5; for (b), (e), and (h): ×100; for (c), (f), and (i): ×400.

Augmented corticotomy with a bone graft is a complex procedure that considers multiple factors, such as the timing of orthodontic force application, design and extent of corticotomy, and biological characteristics of the bone graft material. As the length of the RAP is known to be approximately 4 months [24], orthodontic tooth movement should be initiated as early as possible. A previous study regarding orthodontic tooth movement into grafted sites showed a slight increase in the rate of tooth movement immediately after grafting when compared to nongrafted control sites [25]. In our clinic, augmented corticotomy has been performed immediately before the target tooth movement in the same manner used in the present experimental design. The original corticotomy-facilitated orthodontic treatments involved buccal and lingual osteotomy cuts with orthopedic forces, and the use of alveolar augmentation with a demineralized bone graft was advocated to cover any fenestrations or dehiscences and to increase the bony support for both the teeth and the overlying soft tissues [8, 9]. Some case reports showed that selective corticotomy limited to the buccal and

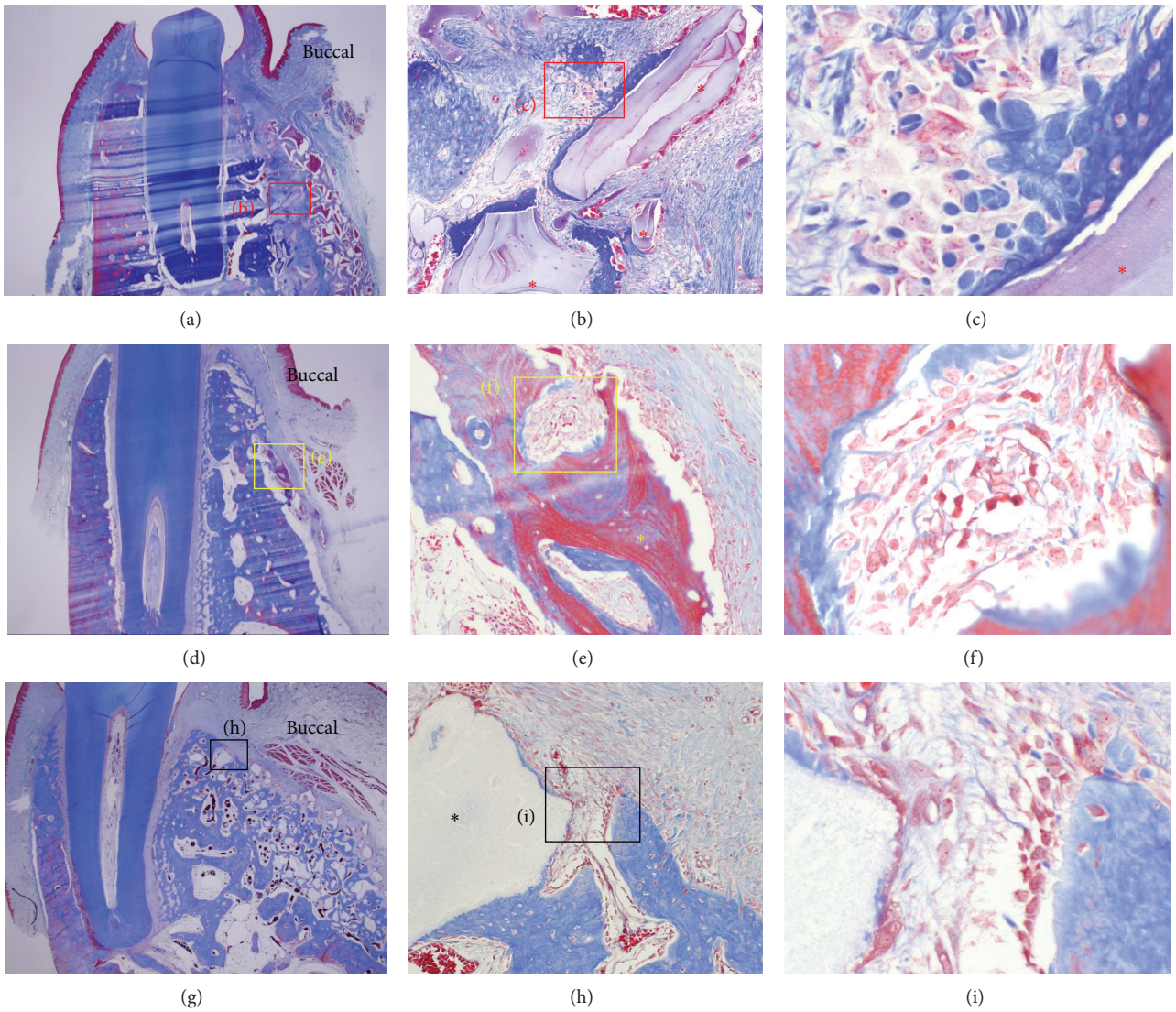

Figure 5: Photomicrograph of a buccolingual section from the mandible. (a) Deproteinized bovine bone mineral (DBBM) graft. (b) Higher magnification of (a). DBBM particles (red star) were embedded in and bridged with newly formed bone within the bone-derived mesenchymal matrix. Resorption by osteoclasts at the buccal side and new bone formation at the inner side by osteoblasts were observed simultaneously. (c) Higher magnification of (b). New bone formation on the surface of the grafted DBBM particles (red star) and active osteoblasts were observed. (d) Irradiated cortical bone (ICB) graft. Most grafted ICB particles were resorbed. Grafted ICB particles were embedded in bone-derived mesenchymal matrix, encircled by a newly formed bone wall. (e) Higher magnification of (d). Grafted ICB particles (yellow star) were still resorbed by osteoclasts within the bone-derived mesenchymal matrix, and newly formed bone was bridged with and formed in the grafted particle. (f) Higher magnification of (e). Active osteoblasts forming new bone were observed inside the grafted ICB particles. (g) Micromacroporous biphasic calcium phosphate (SB; MBCP$^+$) graft. Most of the grafted SB particles were embedded in the newly formed bone-derived mesenchymal matrix that formed buccal bone. The thickness of the newly formed bone wall was outstanding. (h) Higher magnification of (g). Grafted SB particles (black star) were embedded in and bridged with newly formed buccal bone. (i) Higher magnification of (h). Active new bone-forming osteoblasts were observed at the outer surface of the buccal bone wall. Masson's trichrome stain. Original magnification for (a), (d), and (g): ×12.5; for (b), (e), and (h): ×100; for (c), (f), and (i); ×400.

labial surfaces reduced the operation time and postoperative patient discomfort [26, 27]. However, in our study, only buccal corticotomy was designed to cover the target area of the thin buccal plate on the pressure sides.

An ideal bone graft substitute should have osteoconductive, osteoinductive, and osteogenic properties. Autogenous bone grafts are the gold standard among the graft materials because they provide all of these properties and contain viable cells that can proliferate and contribute to the formation of new bone [28]. However, they have several limitations, such as the perioperative pain and morbidity associated with harvesting the graft, uncertain quality and quantity of the graft, and limited graft shapes and sizes. To overcome these limitations, nonautogenous bone grafts are being utilized more commonly, and the current study was conducted to investigate the effect of various nonautogenous bone grafts,

including allografts, xenografts, and alloplasts, on augmented corticotomy. The DBBM used in our study (Bio-Oss) was selected as a positive control because it is one of the most widely used xenograft materials and is hydroxyapatite of bovine origin [29], and it has well-established satisfactory outcomes in periodontal regeneration [30]. The structural properties of Bio-Oss, such as high porosity and the presence of hydroxyapatite crystals, provide sufficient surface area and stability for the migration and adhesion of osteogenic cells. For mineralized bone allografts, irradiated cancellous bone (ICB) obtained from human cadaver sources is often used [31]. Sterilization by irradiation is performed to reduce the incidence of infection [32]. In the present study, cortical ICB was used because it is resorbed more slowly than the cancellous type. For synthetic alloplasts, a hydroxyapatite/tricalcium phosphate (HA/TCP) mixture is the first choice [33]. Hydroxyapatite provides long-term stability, and β-TCP releases ions that form acellular apatite crystals. In the current study, MBCP$^+$ (a 20:80 HA:β-TCP mixture) was used because it was reported to have a bone formation rate 20% higher than that of conventional MBCP (a 60:40 HA:β-TCP mixture).

Surprisingly, all groups had a buccal plate that was newly formed at the buccal side from the crestal area to the apical area of the pressure side. In this study, the SB group had the largest amount of new bone formation, despite the large angular changes during orthodontic tooth movement. These results suggest that the osteoconductive synthetic graft material is not inferior to other grafts when used for augmented corticotomy. Although statistically significant differences were observed, these differences are not considered to be physiologically or clinically significant. All of the graft materials contributed to new buccal bone formation. The synthetic bone substitute is advantageous because it is inexpensive, does not elicit an immune reaction, and is available in sufficient quantities; therefore, it is expected to be the preferred option in augmented corticotomy.

This pilot study had certain limitations regarding the experimental design. Further studies with a larger sample size and negative control (corticotomy only) are necessary. Additionally, the 1-walled defect model, which would be the most challenging model for securing of graft materials, differs between dogs and humans. The buccal alveolar wall is more concave in dogs than in humans; therefore, these results should be applied to clinical situations cautiously.

5. Conclusion

Augmented corticotomy effectively reestablished the periodontal soft and hard tissue after buccal tooth tipping movement on the pressure sides, regardless of the type of graft material used. The synthetic bone graft group, which had the largest angular changes during tipping, had the most new bone formation and maintained the soft tissue intact. This technique may be beneficial for preventing loss of the periodontal support during orthodontic tooth movement beyond the thin alveolar bone plate.

Disclosure

All of the authors of this paper certify that this research is original, not under publication consideration elsewhere, and Drs. Kye-Bok Lee and Dong-Yol Lee are joint first authors.

Conflict of Interests

The authors declare that there is no conflict of interests regarding the publication of this paper.

Authors' Contribution

Seong-Hun Kim and Eun-Cheol Kim equally contributed to this work.

Acknowledgment

This work was supported by the National Research Foundation of Korea (NRF) funded by the Korea government (MEST) (no. 2012R1A5A2051388).

References

[1] K. F. G. Yared, E. G. Zenobio, and W. Pacheco, "Periodontal status of mandibular central incisors after orthodontic proclination in adults," *American Journal of Orthodontics and Dentofacial Orthopedics*, vol. 130, no. 1, pp. 6.e1–6.e8, 2006.

[2] H. Ahn, S. Moon, and S. Baek, "Morphometric evaluation of changes in the alveolar bone and roots of the maxillary anterior teeth before and after en masse retraction using cone-beam computed tomography," *The Angle Orthodontist*, vol. 83, no. 2, pp. 212–221, 2013.

[3] A. Vardimon, A. Spiegler, and S. Pitaru, "Rapid palatal expansion. Part 2: dentoskeletal changes in cats with patent versus synostosed midpalatal suture," *American Journal of Orthodontics and Dentofacial Orthopedics*, vol. 113, no. 5, pp. 488–497, 1998.

[4] W. M. Wainwright, "Faciolingual tooth movement: its influence on the root and cortical plate," *The American Journal of Orthodontics*, vol. 64, no. 3, pp. 278–302, 1973.

[5] C. E. Wingard and G. M. Bowers, "The effects of facial bone from facial tipping of incisors in monkeys," *Journal of Periodontology*, vol. 47, no. 8, pp. 450–454, 1976.

[6] T. Karring, S. Nyman, B. Thilander, and I. Magnusson, "Bone regeneration in orthodontically produced alveolar bone dehiscences," *Journal of Periodontal Research*, vol. 17, no. 3, pp. 309–315, 1982.

[7] H. Ahn, D. Lee, Y. Park, S. Kim, K. Chung, and G. Nelson, "Accelerated decompensation of mandibular incisors in surgical skeletal Class III patients by using augmented corticotomy: a preliminary study," *The American Journal of Orthodontics and Dentofacial Orthopedics*, vol. 142, no. 2, pp. 199–206, 2012.

[8] M. T. Wilcko, W. M. Wilcko, and N. F. Bissada, "An evidence-based analysis of periodontally accelerated orthodontic and osteogenic techniques: a synthesis of scientific perspectives," *Seminars in Orthodontics*, vol. 14, no. 4, pp. 305–316, 2008.

[9] W. M. Wilcko, D. J. Ferguson, J. E. Bouquot, and M. T. Wilcko, "Rapid orthodontic decrowding with alveolar augmentation: case report," *World Journal of Orthodontics*, vol. 4, pp. 197–205, 2003.

[10] H. Köle, "Surgical operations on the alveolar ridge to correct occlusal abnormalities," *Oral Surgery, Oral Medicine, Oral Pathology*, vol. 12, no. 5, pp. 515–529, 1959.

[11] S. Iino, S. Sakoda, G. Ito, T. Nishimori, T. Ikeda, and S. Miyawaki, "Acceleration of orthodontic tooth movement by alveolar corticotomy in the dog," *The American Journal of Orthodontics and Dentofacial Orthopedics*, vol. 131, no. 4, pp. 448–e1, 2007.

[12] H. M. Frost, "The regional acceleratory phenomenon: a review," *Henry Ford Hospital Medical Journal*, vol. 31, no. 1, pp. 3–9, 1983.

[13] H. M. Frost, "The biology of fracture healing. An overview for clinicians. Part I," *Clinical Orthopaedics and Related Research*, no. 248, pp. 283–293, 1989.

[14] M. T. Wilcko, W. M. Wilcko, J. J. Pulver, N. F. Bissada, and J. E. Bouquot, "Accelerated osteogenic orthodontics technique: A 1-stage surgically facilitated rapid orthodontic technique with alveolar augmentation," *Journal of Oral and Maxillofacial Surgery*, vol. 67, no. 10, pp. 2149–2159, 2009.

[15] D. Y. Lee, H. W. Ahn, Y. Herr, S. H. Kim, E. C. Kim, and Y. H. Kwon, "Periodontal responses to augmented corticotomy with collagen membrane application during orthodontic buccal tipping in dogs," *Biomed Research International*, vol. 2014, Article ID 347508, 9 pages, 2014.

[16] J. B. Matthews and G. I. Mason, "Influence of decalcifying agents on immunoreactivity of formalin-fixed, paraffin-embedded tissue," *Histochemical Journal*, vol. 16, no. 7, pp. 771–787, 1984.

[17] N. Oh, E. Kim, Y. Kook, D. Jeong, I. Cho, and G. Nelson, "Evaluation of stability of surface-treated mini-implants in diabetic rabbits," *International Journal of Dentistry*, vol. 2014, Article ID 838356, 7 pages, 2014.

[18] C. S. Handelman, "The anterior alveolus: its importance in limiting orthodontic treatment and its influence on the occurrence of iatrogenic sequelae," *Angle Orthodontist*, vol. 66, no. 2, pp. 95–110, 1996.

[19] H. Ahn and S. Baek, "Skeletal anteroposterior discrepancy and vertical type effects on lower incisor preoperative decompensation and postoperative compensation in skeletal Class III patients," *The Angle Orthodontist*, vol. 81, no. 1, pp. 64–74, 2011.

[20] F. Al-Naoum, M. Hajeer, and A. Al-Jundi, "Does alveolar corticotomy accelerate orthodontic tooth movement when retracting upper canines? A split-mouth design randomized controlled trial," *Journal of Oral and Maxillofacial Surgery*, vol. 72, no. 10, pp. 1880–1889, 2014.

[21] K. R. Chung, M. Y. Oh, and S. J. Ko, "Corticotomy-assisted orthodontics," *Journal of Clinical Orthodontics*, vol. 35, no. 5, pp. 331–339, 2001.

[22] H. Suya, "Corticotomy in orthodontics," in *Mechanical and Biological Basics in Orthodontic Therapy*, E. Hösl and A. Baldauf, Eds., pp. 207–226, Hüthig Buch, Heidelberg, Germany, 1991.

[23] J. M. Anholm, D. A. Crites, R. Hoff, and W. E. Rathbun, "Corticotomy-facilitated orthodontics," *Journal California Dental Association*, vol. 14, no. 12, pp. 7–11, 1986.

[24] D. P. Mathews and V. G. Kokich, "Accelerating tooth movement: the case against corticotomy-induced orthodontics," *The American Journal of Orthodontics and Dentofacial Orthopedics*, vol. 144, no. 1, pp. 5–13, 2013.

[25] M. Seifi and S. A. Ghoraishian, "Determination of orthodontic tooth movement and tissue reaction following demineralized freeze-dried bone allograft grafting intervention," *Dental Research Journal*, vol. 9, pp. 203–208, 2012.

[26] D. Germeç, B. Giray, I. Kocadereli, and A. Enacar, "Lower incisor retraction with a modified corticotomy," *Angle Orthodontist*, vol. 76, no. 5, pp. 882–890, 2006.

[27] H. Nowzari, F. K. Yorita, and H. Chang, "Periodontally accelerated osteogenic orthodontics combined with autogenous bone grafting," *Compendium of Continuing Education in Dentistry*, vol. 29, no. 4, pp. 200–206, 2008.

[28] C. G. Finkemeier, "Bone-grafting and bone-graft substitutes," *Journal of Bone and Joint Surgery A*, vol. 84, no. 3, pp. 454–464, 2002.

[29] C. Reichert, W. Götz, R. Smeets, M. Wenghöfer, and A. Jäger, "The impact of nonautogenous bone graft on orthodontic treatment," *Quintessence International*, vol. 41, no. 8, pp. 665–672, 2010.

[30] J. T. Mellonig, "Human histologic evaluation of a bovine-derived bone xenograft in the treatment of periodontal osseous defects," *The International Journal of Periodontics and Restorative Dentistry*, vol. 20, no. 1, pp. 19–29, 2000.

[31] D. W. Lee, S. H. Pi, S. K. Lee, and E. C. Kim, "Comparative histomorphometric analysis of extraction sockets healing implanted with bovine xenografts, irradiated cancellous allografts, and solvent-dehydrated allografts in humans," *The International Journal Of Oral & Maxillofacial Implants*, vol. 24, no. 4, pp. 609–615, 2009.

[32] B. Loty, J. P. Courpied, B. Tomeno, M. Postel, M. Forest, and R. Abelanet, "Bone allografts sterilised by irradiation: biological properties, procurement and results of 150 massive allografts," *International Orthopaedics*, vol. 14, no. 3, pp. 237–242, 1990.

[33] E. B. Nery, R. Z. LeGeros, K. L. Lynch, and K. Lee, "Tissue response to biphasic calcium phosphate ceramic with different ratios of HA/beta TCP in periodontal osseous defects," *Journal of Periodontology*, vol. 63, no. 9, pp. 729–735, 1992.

Hindawi Publishing Corporation
BioMed Research International
Volume 2014, Article ID 940860, 10 pages
http://dx.doi.org/10.1155/2014/940860

Research Article

Immobilization of Murine Anti-BMP-2 Monoclonal Antibody on Various Biomaterials for Bone Tissue Engineering

Sahar Ansari,[1] Marcelo O. Freire,[2,3] Eun-Kyoung Pang,[4] Alaa I. Abdelhamid,[5] Mohammad Almohaimeed,[5] and Homayoun H. Zadeh[1,6]

[1] *Laboratory of Immune Regulation and Tissue Engineering, Herman Ostrow School of Dentistry, University of Southern California, Los Angeles, CA, USA*
[2] *Department of Applied Oral Sciences, The Forsyth Institute, Cambridge, USA*
[3] *Department of Oral Medicine, Infection and Immunity, Harvard School of Dental Medicine, Boston, MA, USA*
[4] *Department of Periodontology, Graduate School of Medicine, Ewha Womans University, Seoul, Republic of Korea*
[5] *Dental Research Center (DRC) and Tissue Engineering Unit (TERU), Qassim College of Dentistry, Qassim University, Saudi Arabia*
[6] *Laboratory of Immune Regulation and Tissue Engineering (LITE), Division of Periodontology, Diagnostic Sciences & Dental Hygiene, Ostrow School of Dentistry, University of Southern California, 925 34th Street, Room 4278, Los Angeles, CA 90089-0641, USA*

Correspondence should be addressed to Homayoun H. Zadeh; zadeh@usc.edu

Received 6 May 2014; Accepted 2 July 2014; Published 23 July 2014

Academic Editor: Seong-Hun Kim

Biomaterials are widely used as scaffolds for tissue engineering. We have developed a strategy for bone tissue engineering that entails application of immobilized anti-BMP-2 monoclonal antibodies (mAbs) to capture endogenous BMPs in vivo and promote antibody-mediated osseous regeneration (AMOR). The purpose of the current study was to compare the efficacy of immobilization of a specific murine anti-BMP-2 mAb on three different types of biomaterials and to evaluate their suitability as scaffolds for AMOR. Anti-BMP-2 mAb or isotype control mAb was immobilized on titanium (Ti) microbeads, alginate hydrogel, and ACS. The treated biomaterials were surgically implanted in rat critical-sized calvarial defects. After 8 weeks, *de novo* bone formation was assessed using micro-CT and histomorphometric analyses. Results showed *de novo* bone regeneration with all three scaffolds with immobilized anti-BMP-2 mAb, but not isotype control mAb. Ti microbeads showed the highest volume of bone regeneration, followed by ACS. Alginate showed the lowest volume of bone. Localization of BMP-2, -4, and -7 antigens was detected on all 3 scaffolds with immobilized anti-BMP-2 mAb implanted in calvarial defects. Altogether, these data suggested a potential mechanism for bone regeneration through entrapment of endogenous BMP-2, -4, and -7 proteins leading to bone formation using different types of scaffolds *via* AMOR.

1. Introduction

The goal of bone tissue engineering is the regeneration of a construct that matches the physical and biological properties of the natural bone tissue and reestablishes function [1]. Bone tissue reconstruction is usually necessary due to congenital anomalies, infection, trauma, and skeletal diseases. Autologous and allogenic bone grafts are currently the main treatment options and comprise about 90% of grafts performed each year [1, 2]. However, there are several disadvantages associated with these modalities of treatment. These include significant potential morbidity of the donor site, operative and recovery time, and high expense of autologous grafts harvesting. Moreover, osteoconductive graft materials such as allografts, xenografts, and alloplastic material have limited ability to repair large defects, due to their inherent inability to initiate bone formation. For these reasons, alternative bone regeneration treatment modalities are desirable. Bone tissue engineering strategies have offered promising alternatives, developing biological bone substitutes that restore, maintain, or improve bone tissue function [3]. Bone tissue engineering aims to combine biomaterial scaffolds, cells, and molecular signals that can mediate tissue regeneration, matching the physical and biological properties of the natural tissue [3–5].

Currently, there are multiple bone tissue engineering strategies available, including gene therapy, stem cell therapy, exogenous growth factors, or a combination of these strategies. Growth factors such as bone morphogenetic proteins (BMPs), platelet-derived growth factors (PDGFs), and insulin-like growth factors (IGFs) have been utilized for bone tissue engineering with promising results [6–8]. Several *in vitro* studies have confirmed that BMP-2, BMP-4, and BMP-7 have the ability to stimulate the differentiation of osteoprogenitor cells into mature osteoblasts. Preclinical and clinical studies have demonstrated the osteoinductive potential of some BMPs, leading to the FDA approval of recombinant human BMP-2 (rhBMP-2) and rhBMP-7 for clinical applications [9–12]. However, there are a number of limitations to the application of exogenous rhBMPs, including reduced potency compared to their endogenous counterparts, requiring the administration of superphysiologic concentrations which in turn leads to significant side effects and high cost [13, 14].

An alternative treatment option to the administration of exogenous rhBMP-2 is the application of anti-BMP-2 monoclonal antibodies (mAbs) immobilized on a solid scaffold, in an effort to capture endogenous BMP-2. This approach, termed antibody-mediated osseous regeneration (AMOR), was first reported by Freire et al. [15]. In previous studies, immobilized murine anti-BMP-2 mAbs were immobilized on absorbable collagen sponge (ACS) and implanted within rat calvarial defects, demonstrating repair of the bone defects [15]. The *in vivo* osteogenic action of AMOR was later characterized by increased endogenous BMP-2, BMP-4, and BMP-7 in the microenvironment of the defect [16]. Consistent with our hypothesis that the osteogenic mechanism of AMOR is due to the capture and biologic action of endogenous BMPs, the initial regulatory mechanism has been shown to be mediated by the Smad intracellular signaling pathway [17]. While these mechanisms have begun to elucidate the osteogenic actions of AMOR, it is unknown whether the use of more versatile biomaterials, such as titanium or alginate, influences bone regeneration mediated by anti-BMP-2 mAbs.

In view of the important role of biomaterials in bone regenerative therapies, it will be desirable to examine their role in AMOR [18, 19]. ACS has been a convenient scaffold in our previous studies [15–17] and has been approved by FDA as a carrier for rhBMP-2 [20]. Moreover, because of its radiolucent properties, it is simple to demonstrate *de novo* bone formation. While ACS has excellent biocompatibility and did not interfere with AMOR in previous studies, its mechanical properties and rapid resorption are considerable deficiencies. Hence, the goal of this study was to evaluate the relative merits of alternative scaffolds with varying chemical, physical, and mechanical properties, including titanium and alginate. The efficacy of three different biomaterials has been compared in the immobilization of anti-BMP-2 mAbs for AMOR.

2. Materials and Methods

2.1. Materials. 3G7 mAb (Abnova, Taipei, Taiwan), a murine monoclonal anti-BMP-2 antibody, was used in this study. Isotype-matched mAb (Iso, anti-rabbit IgG mAb, Biovision, Mountain View, CA) with no specific affinity to BMP-2 was used as the negative control. Anti-BMP-2 and isotype control mAbs were diluted with plain phosphate-buffered saline (PBS) at 25 μg/mL and immobilized on each of the scaffolds according to the protocol previously reported by Freire et al., 2011. Three different scaffold materials were used in this study, including grade IV titanium microbeads with 250 μm diameter (Sybron Dental Implants, Orange, CA), alginate hydrogel (NovaMatrix FMC Biopolymer, Norway), and ACS (Helicote, Miltex, Plainsboro, NJ). The effect of alginate volume of the dilution of the mAb was considered.

2.2. In Vitro mAb Binding and Release Kinetics Study. In order to evaluate the kinetics of murine anti-BMP-2 mAb release from each scaffold, 25 μg/mL of mAb was immobilized on each scaffold (titanium microbeads, alginate hydrogel, and ACS) according to methods already described in the literature [17]. The mAb-loaded scaffolds were suspended in 5 mL of PBS (pH = 7.4). At various time points (1, 3, 7, and 14 days), the amount of released mAb was determined by UV absorption spectroscopy (Beckman, Brea, CA). In addition, the retained mAb was detected with FITC-conjugated goat anti-mouse IgG antibody (Santa Cruz Biotechnology Inc., CA) and measured using confocal laser scanning microscopy (CLSM). The fluorescence intensity was quantified by Spot analysis software (SPOT Imaging Solutions, Sterling Heights, MI).

2.3. Rat Critical Size Calvarial Defect. Thirty 2-month-old virgin female Sprague-Dawley rats (Harlan Laboratories, Livermore, CA) were housed at 22°C under a 12 h light and 12 h dark cycle and fed *ad libitum* (Purina Inc., Baldwin Park, CA). All animals were treated according to the guidelines and regulations for the use and care of animals at the University of Southern California. Full-thickness skin flaps were raised, exposing the parietal bones. 7 mm diameter defects in the parietal bones were generated using a trephine under copious saline irrigation. Each of the scaffold materials containing 25 μg/mL of mAbs was placed inside each of the calvarial defects. At the end of the treatment period, 8 weeks after implantation, animals were sacrificed in a CO_2 chamber and the skulls were harvested and stored in buffered formalin until further analysis.

2.4. Micro-CT Analysis. Retrieved specimens from the animals were scanned using a high-resolution micro-CT system (MicroCAT II, Siemens Medical Solutions Molecular Imaging, Knoxville, TN) for evaluation of ectopic mineralization. The specimens were scanned at widths of every 10 μm at 60 kV and 110 μA at a resolution of 20 μm. Bone volume fraction (BV/TV) for each construct was calculated.

2.5. Histochemical Analysis. For histochemical analysis, the retrieved specimens were fixed with 4% (v/v) paraformaldehyde for 30 min at room temperature and then placed in PBS for 15 minutes prior to dehydration. Serial dehydration was achieved by placing the specimens in a sequential series of

increasing ethanol concentrations to remove all the water. The ethanol was then completely replaced with increasing concentrations of xylene solution followed by a 100% xylene step prior to incubation with paraffin-saturated xylene at room temperature overnight. The specimens were then serially sectioned (6 μm) and adhered to glass slides. The paraffin was completely removed by immersion in xylene, followed by decreasing ethanol concentrations, and then by washing with tap water. The sections were stained with hematoxylin and eosin (H&E). Images were captured using an Olympus DP50 digital camera (Olympus Optical Co., Japan) and analyzed using Analysis imaging software (Soft Image System GmbH, Germany).

2.6. Scanning Electron Microscopy (SEM). In order to characterize the morphology of the scaffold materials used in this study and the early interaction of the implanted scaffolds and cells, scanning electron microscopy (SEM) (JEOL 5300, Peabody, MA) was used. The specimens were harvested from the animals 24 hrs after implantation. They were then rinsed with 2 mL of PBS and fixed with 1% glutaraldehyde overnight. Samples were dehydrated using graded alcohol solutions and sputter-coated with gold.

2.7. Confocal Laser Scanning Microscopy (CLSM). In order to show the capacity of the murine anti-BMP-2 mAb immobilized on different scaffolds to attract and hold BMP-2, -4, and -7 ligands, CLSM was utilized. Briefly, specimens were retrieved eight weeks after implantation, fixed in 10% formalin solution, dehydrated in an ascending series of ethanol solutions, and embedded in paraffin. Six-micrometer sections were cut using a microtome and mounted on glass slides. For immunofluorescence staining, deparaffinized samples were treated with 3% H_2O_2, followed by a blocking buffer (1% BSA and 0.25% Triton X-100 in PBS), stained with rabbit polyclonal anti-BMP-2, BMP-4, and BMP-7 antibodies (Abcam, Cambridge, MA) at 4°C overnight, and detected using Alexa Fluor-conjugated secondary antibody (1 : 200 dilution; Invitrogen) using CLSM (Fluoview FV10i, Olympus Corp., Tokyo, Japan). The fluorescence intensity was analyzed and quantified by Spot analysis software (SPOT Imaging Solutions, Sterling Heights, MI) with the same fluorescence threshold.

2.8. Statistical Analysis of Data. Quantitative data were expressed as mean ± standard deviation (SD). One-way and two-way analyses of variance (ANOVA), followed by Tukey's test at a significance level of $\alpha = 0.05$, were used for the comparison of multiple sample means.

3. Results

3.1. In Vitro Binding and Release Characteristics of Anti-BMP-2 mAb. A study of *in vitro* binding and release kinetics was performed to examine potential differences in the binding and release profile of the murine mAb on the three different scaffolds. Results demonstrated that immediately after immobilization of anti-BMP-2 mAb, the levels of the antibody detected on all 3 scaffolds were equivalent (Figures 1(a) and 1(b)). Approximately 20% of mAb remained on the scaffolds after 2 weeks of *in vitro* incubation. The release profile of the murine mAb from each of the scaffolds showed sustained release for up to 14 days (Figure 1(c)). While alginate hydrogel showed a significantly lower ($P < 0.05$) initial release profile, no significant difference ($P > 0.05$) was observed in the amounts of release after day 3. Since ACS and alginate are bioresorbable scaffolds, we hypothesized that the kinetics of mAb retention and release were likely to be different *in vivo.*

3.2. In Vivo Bone Regeneration. Micro-CT analysis (Figure 2(a)) showed a significant volume of *de novo* bone formation within the calvarial defects implanted with each of the three scaffolds immobilized with anti-BMP-2 mAb. In contrast, substitution of the mAb with isotype-matched control mAb did not mediate a significant degree of calvarial bone repair after 8 weeks of implantation. Quantified micro-CT results confirmed that sites with anti-BMP-2 mAb on Ti microbeads exhibited the largest volume of bone formation. However, it should be noted that Ti microbeads contributed to this large volume, as they are radiopaque and are not biodegradable. No significant difference was observed between the ACS and alginate groups ($P > 0.05$) (Figure 2(b)).

The histological analysis of rat calvarial defects implanted with anti-BMP-2 mAb immobilized on 3 different scaffolds is presented in Figure 3(a). The histomicrograms illustrated the presence of vital bone, indicated by the presence of osteocytes in lacunae within each of the scaffolds with immobilized anti-BMP-2 mAb. The degree of bone repair was significantly higher in sites with immobilized anti-BMP-2 mAb than in sites with isotype-matched control mAb. Due to their biodegradability, collagen scaffolds exhibited the most volumetric shrinkage, followed by alginate. Anti-BMP-2 mAb immobilized on titanium exhibited the largest volume of bone within the calvarial defects ($P < 0.05$). The histomorphometric analysis (Figure 3(b)) showed no significant difference between the proportions of *de novo* bone formation between alginate and ACS. Ti microbeads showed the largest amount of bone regeneration, followed by ACS. Alginate hydrogels samples showed the least amount of regenerated bone. The isotype mAb groups demonstrated significantly lower amounts of bone regeneration ($P < 0.05$). It is notable that the morphology of regenerated bone in the sites implanted anti-BMP-2 mAb and each of the three scaffolds was normal with no evidence of inflammation or any adverse effects.

3.3. SEM Analysis of Different Scaffolds. The morphology of the scaffold materials and the initial interaction of host tissues and cells with implanted scaffolds were characterized using SEM. The representative SEM photomicrographs of pristine scaffolds, as well as scaffolds with immobilized anti-BMP-2 following retrieval 24 hours after implantation into rat calvarial defects, are shown in Figure 4. The SEM images confirmed that both alginate and ACS scaffolds had porous structures, while the spheroidal Ti microbeads appeared to have

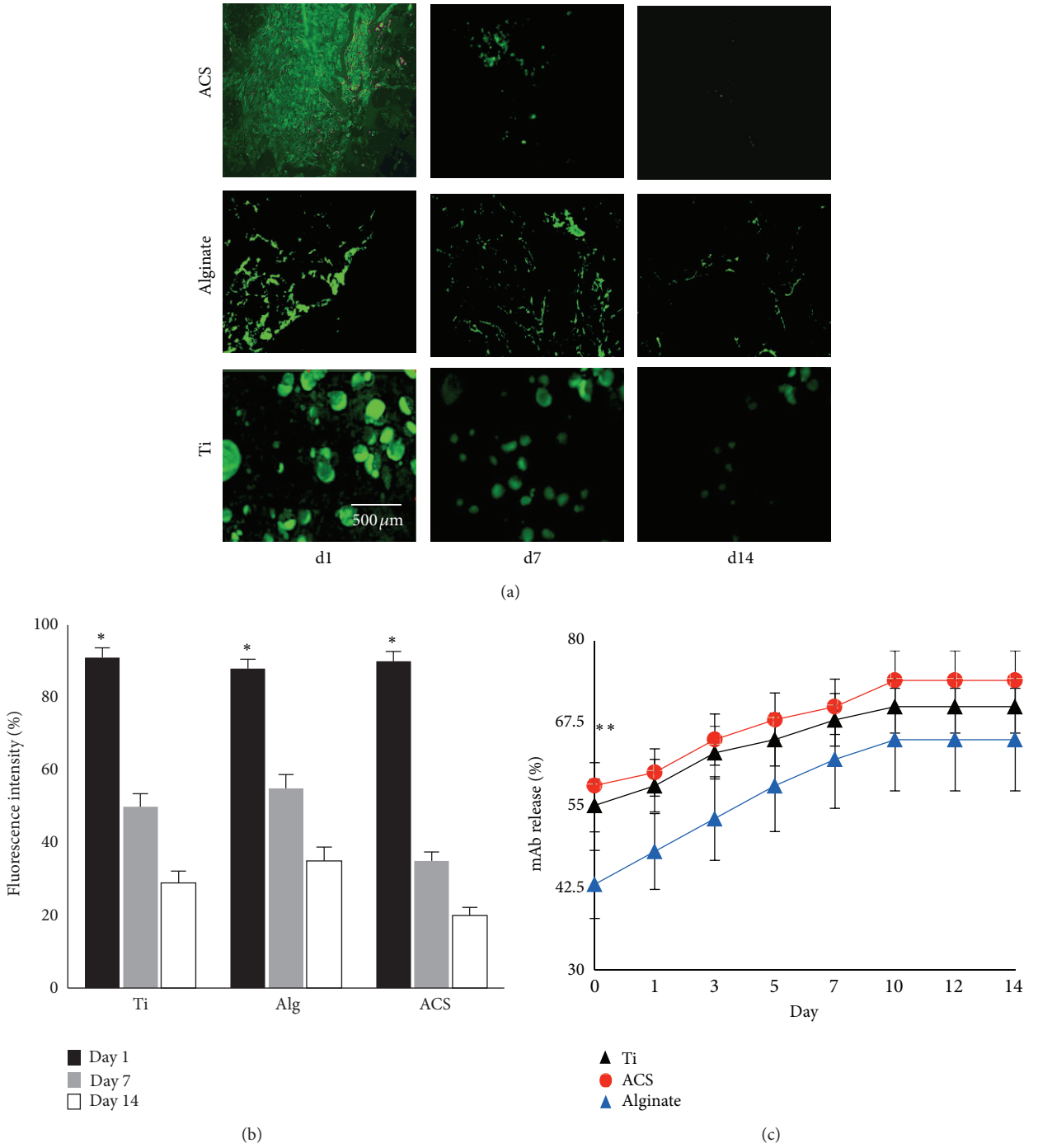

Figure 1: Characterizationof the *in vitro* binding and release profile of murine anti-BMP-2 mAb-loaded scaffolds. (a) CLSM analysis showing binding of anti-BMP-2 mAb on each scaffold detected by FITC-conjugated goat anti-mouse secondary antibody. Day 1 represents detection of binding of anti-BMP-2 mAb immediately after immobilization of the mAb on the scaffolds, confirming that murine mAb is retained on all tested scaffolds for up to two weeks *in vitro*. (b) Quantitative analysis of fluorescence intensity showing initial binding (day 1) of anti-BMP-2 mAb to the scaffolds and the *in vitro* persistence of anti-BMP-2 at 7 and 14 days later ($n = 4$). (c) The *in vitro* release of anti-BMP-2 mAb was calculated by measuring mAb concentrations in solution at various time points. $^{*}P < 0.05$.

relatively smooth surface. Significant cellular infiltration was observed on all the scaffolds immobilized with anti-BMP-2 mAb. Comparatively, scaffolds immobilized with isotype control mAb exhibited significantly less cellular infiltration (data not shown). The cells infiltrating anti-BMP-2 mAb-immobilized scaffolds appeared adherent with spreading on these scaffolds. Greater cell infiltration and adhesion were observed onto ACS and alginate hydrogel scaffolds.

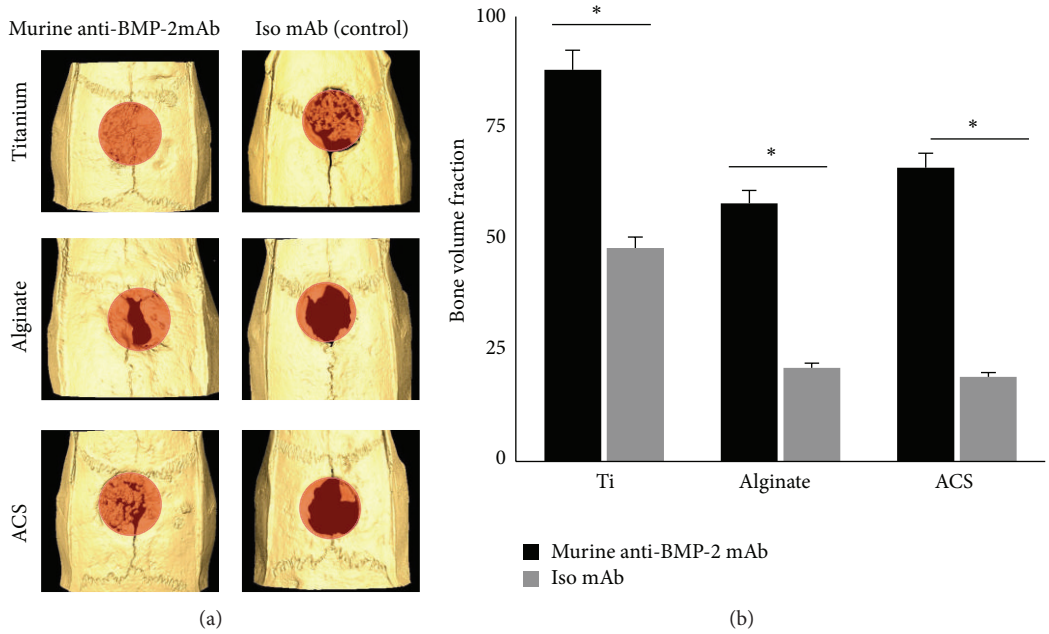

FIGURE 2: (a) Micro-CT images of rat calvarial defects 8 weeks after implantation of different biomaterials preloaded either with anti-BMP-2 mAb or isotype mAb as the negative control. (b) Quantitative analysis via micro-CT images showing the bone volume fraction (BV/TV) for each group ($N = 4$). $^*P < 0.05$.

3.4. CLSM Analysis. In order to evaluate the capacity of the murine anti-BMP-2 mAb immobilized on different scaffolds to bind BMP-2, -4, and -7 *in vivo*, the 3 scaffolds with immobilized anti-BMP-2 mAb were implanted in calvarial defects. The animals were sacrificed 8 weeks after implantation. CLSM analysis confirmed that murine anti-BMP-2 mAb immobilized on different scaffolds exhibited significant binding of BMP-2, BMP-4, and BMP-7 ligands following implantation (Figure 5(a)). As expected, the defects implanted with isotype-matched control mAb failed to bind BMP-2, -4, and -7 ligands. Results revealed the capacity of the murine mAb to localize increase concentrations of BMP-2, -4, and -7 ligands in all tested scaffolds. Titanium specimens showed higher fluorescence intensity ($P < 0.05$), while no significant difference was observed between the fluorescence intensity levels of alginate and ACS ($P > 0.05$) (Figure 5(b)).

4. Discussion

Implanted autogenous, allogeneic, xenogenic, and synthetic biomaterials are the common treatment modalities currently used for bone regeneration in craniofacial reconstructive surgeries and for other areas of regenerative medicine. While autologous grafts are considered the gold standard, they have many limitations; allografts, xenografts, and alloplastic biomaterials have therefore been used as alternatives. These biomaterials have found clinical applications in the reconstruction of large osseous defects. However, due to their lack of osteoinduction and unpredictable resorption rates, variable clinical outcomes have been observed. Recombinant BMPs have shown promise clinically as an alternative bone regeneration therapy [21–25]. BMP-2 is a member of the TGF-β family that assembles into a biologically active homodimer and binds to heterodimeric type I and type II receptors for BMP-2 [26, 27]. Other osteogenic BMPs include BMP-4 and BMP-7. Currently, the FDA has approved rhBMP-2 and rhBMP-7 for repair and regeneration of skeletal defects. However, there are several drawbacks to the application of recombinant growth factors, including their supraphysiologic dose requirement and some potentially serious side effects, as well as high cost. Our laboratory has therefore introduced AMOR as an alternative strategy to the current approaches of administering exogenous growth factors [15, 16].

It has been proposed that appropriate signaling molecules acting on progenitor cells within a suitable scaffold can lead to tissue regeneration. Our previous studies have established that when anti-BMP-2 mAbs are implanted *in vivo*, they can capture endogenous BMP-2, BMP-4, BMP-7 that provide the osteogenic signals to progenitor cells to regenerate bone [15, 16, 23]. Therefore, the current study sought to compare the efficacy of various scaffolds in the pursuit of optimizing this novel strategy. To that end, we examined the suitability of three different biomaterials with different physical and chemical properties as scaffolds when immobilized with anti-BMP-2 Abs for AMOR.

The results of the present study demonstrated that all of the tested biomaterials (Ti, alginate, and ACS) can be utilized as drug delivery vehicles for immobilized anti-BMP-2 mAb. Moreover, all three scaffolds have favorable binding and release profile characteristics. Alginate hydrogel showed a significantly lower initial release profile, with release characteristics becoming comparable to the other tested

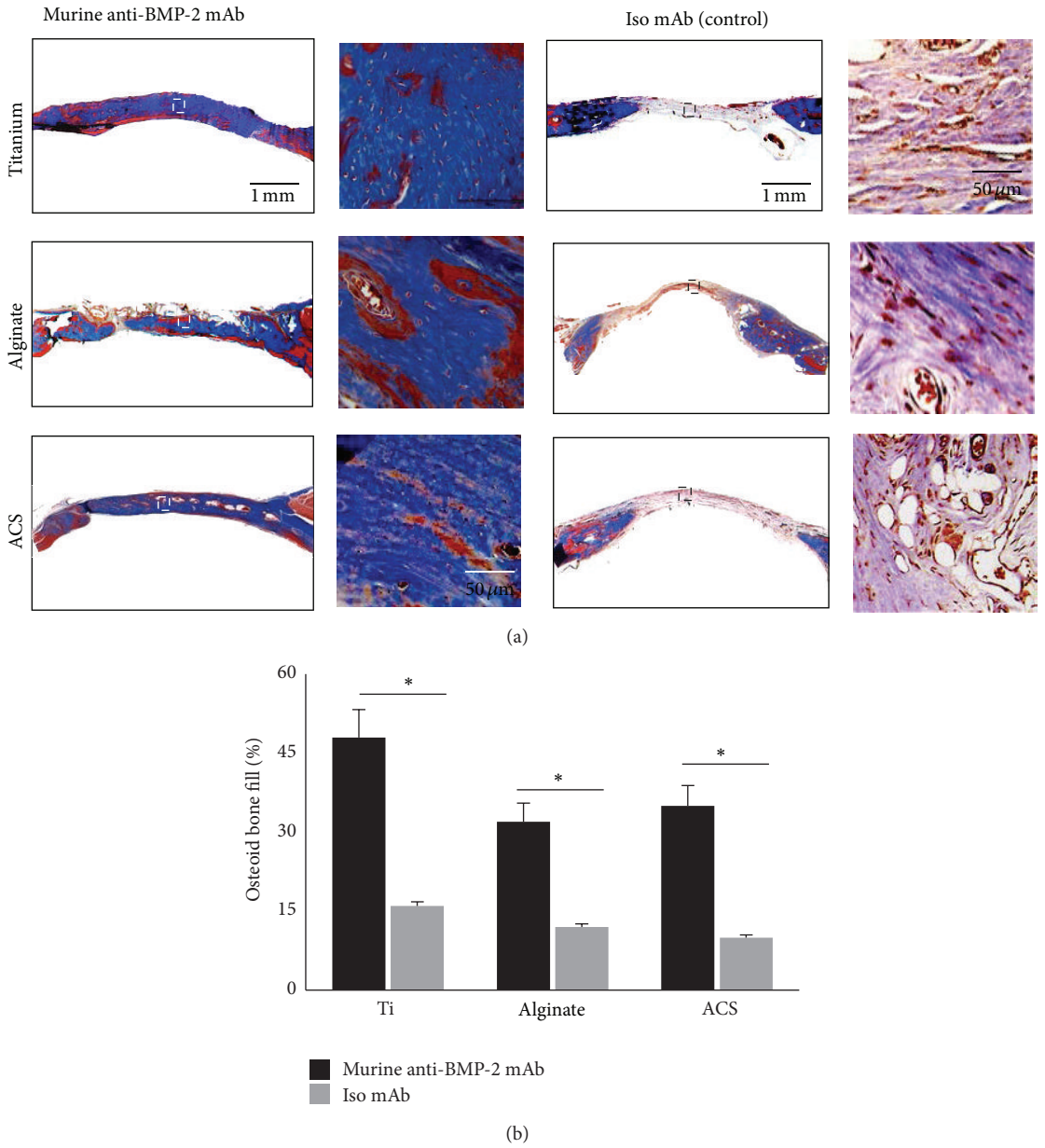

FIGURE 3: (a) Histological analysis of rat calvarial bone defects implanted with anti-BMP-2 mAb immobilized on scaffolds showing presence of vital bone in implantation sites. No evidence of bone formation was observed in sites implanted with isotype-matched control Ab. Collagen exhibited the most compression, followed by alginate, while titanium had the best tissue volume maintenance. (b) Histomorphometric analysis of rat calvarial bone defects implanted with anti-BMP-2 mAb immobilized on 3 different scaffolds. Histomorphometric analysis was performed on Trichrome-stained sections and percentage of new bone formation was quantified. No significant difference was observed between the proportions of new bone formation for each biomaterial ($N = 4$). $^{*}P < 0.05$.

biomaterials after day 3. This phenomenon might be due to surface adsorption of the murine mAb on Ti and ACS, while the mAb was encapsulated within the alginate hydrogel. Due to the biodegradability of ACS and alginate, it is likely that the kinetics of mAb anti-BMP-2 retention and release will be different *in vivo*.

We also confirmed that all three scaffolds, when functionalized with the murine anti-BMP-2 mAb, mediated bone regeneration within calvarial defects. Several differences in the outcomes were noted, which could affect their potential clinical applications. Both ACS and alginate are biodegradable materials and, as such, their volumes decreased after implantation. In contrast, titanium is a biologically stable material and maintained its volume. Titanium is used extensively in orthopedic and dental implant therapies, and anti-BMP-2 mAb could potentially be utilized as a surface

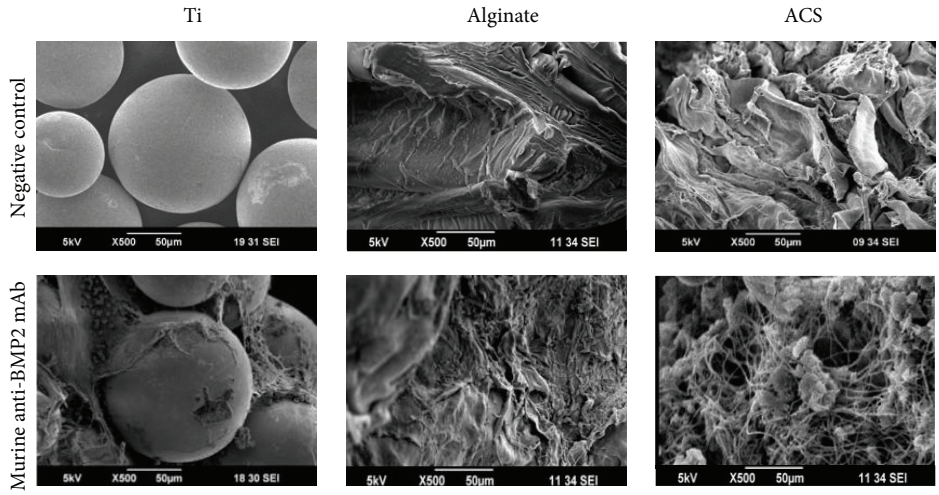

Figure 4: Representative SEM photomicrographs of scaffolds prior to implantation (-) or with immobilized murine anti-BMP-2 retrieved 24 hours after implantation into rat critical-sized calvarial defects. Significant cellular infiltration and adhesion were observed on scaffolds immobilized with murine anti-BMP-2 mAb. Both alginate and ACS scaffolds had porous structure while the spheroidal Ti microbeads had an average diameter of 250 μm.

modification strategy in such applications. It may be possible to exploit the modulatory effects of anti-BMP-2 mAb on wound healing, to enhance osseointegration of implants. The titanium beads utilized in the present study were relatively smooth. It has been demonstrated that titanium surface microtexture can significantly affect the binding and behavior of osteogenic progenitor cells [28–30]. Though rough surface of implants is initially conducive to greater degree and more accelerated osseointegration, these surfaces have the drawback of promoting biofilm attachment and possibly peri-implantitis. Immobilized anti-BMP-2 may be used as an alternative surface modification strategy to enhance osseointegration. Titanium granules can be considered as potential graft material for the repair of skeletal defects [31]. However, in some applications, it may be desirable to have a biodegradable scaffold, so that the regenerated tissue does not contain remnants of the scaffold material. Alginate hydrogel, a natural heteropolysaccharide, can be formulated as an injectable and biodegradable scaffold [32, 33] and has been used extensively in bone tissue engineering [17, 23]. Immobilization of anti-BMP-2 mAb on alginate scaffold will improve its bone regenerative properties. In such situations, alginate and collagen may be more appropriate options. There are many strategies available to modulate the rate of degradation of collagen by cross-linking [34] and alginate by oxidation [33]. Currently, we are investigating the physical properties of sites regenerated with each of these scaffolds using AMOR to characterize the physical strength of the regenerated tissues (manuscript in preparation). This information will further aid in the selection of appropriate scaffold for each tissue engineering application.

Taking into account the high degree of homology between BMP-2 and other osteogenic BMPs, such as BMP-4 and BMP-7, the binding capacity of murine anti-BMP-2 mAb with BMP-4 and BMP-7 has been examined *in vitro* and *in vivo* [16]. The cross-reactivity of murine anti-BMP-2 observed in our previous studies with BMP-4 and BMP-7 using ACS suggests that anti-BMP-2 immobilized on Ti and alginate might be able to capture multiple endogenous osteogenic BMPs, leading to *de novo* bone formation. This implies that the efficacy of AMOR may be in part attributable to the capacity of anti-BMP-2 mAb to capture multiple osteogenic mediators. In view of the significant degree of homology (92.2%) between the human and rat for BMP-2 proteins [16], the results of our calvarial defect model are likely to extend to clinical and translational applications of anti-BMP-2 mAb for mediating *de novo* bone regeneration. The feasibility of immobilizing this mAb on different types of scaffolds with unique physical properties makes this novel treatment modality even more versatile.

5. Conclusions

We report here on the application of immobilized murine anti-BMP-2 mAb to three different types of biomaterial to investigate their ability to mediate AMOR. The results demonstrated significant *de novo* bone formation with all three scaffolds immobilized with murine anti-BMP-2 mAb. Osseous defects regenerated with anti-BMP-2 mAb immobilized on collagen sponge and alginate exhibited more volumetric shrinkage than titanium. During early healing, significant cellular infiltration and adhesion were observed on scaffolds immobilized with murine anti-BMP-2 mAb. The present study demonstrated the possibility of utilizing different scaffolds with varying physical properties as scaffolds immobilized with anti-BMP-2 to participate in AMOR. These data have potential implications for the mechanism of action of AMOR, suggesting that anti-BMP-2 may capture endogenous osteogenic BMPs, which may in turn mediate *de novo* bone formation.

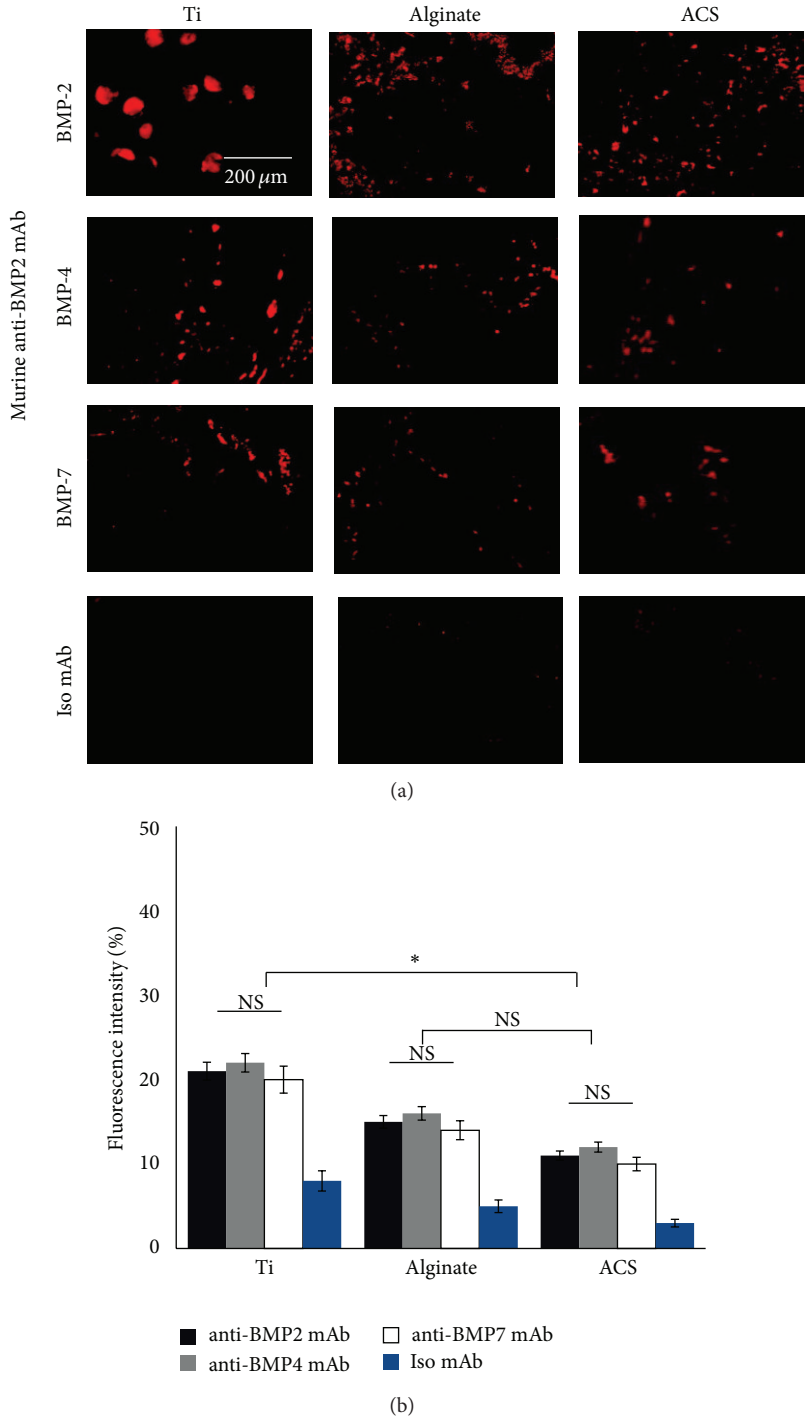

Figure 5: Localization of BMP-2, BMP-4, and BMP-7 antigens within defect sites with immobilized anti-BMP-2 mAb following *in vivo* implantation and retrieval after 8 weeks. (a) Representative CLSM images of titanium, alginate, and ACS groups with immobilized anti-BMP-2 mAb harvested from calvarial defects after 8 weeks. The immunofluorescence results revealed the capacity of the murine mAb to attract and hold BMP-2, -4, and -7 ligands. Scaffolds immobilized with nonspecific isotype mAb failed to show any positive staining. (b) Quantitative analysis of red fluorescence intensity of the images shown in (a). $N = 4$ for each group. $^{*}P < 0.05$; NS: not significant.

Conflict of Interests

The authors declare no potential conflict of interests with respect to the authorship and/or publication of this paper.

Acknowledgments

The first author (Sahar Ansari) was supported by a NIDCR training Grant (T90DE021982). This work was partially

supported by The Long Term Comprehensive National Plan for Science, Technology and Innovation Grant from Saudi Arabia (10BIO1228-09) to the fourth author (Alaa I. Abdelhamid).

References

[1] C. Chen, F. Loe, A. Blocki, Y. Peng, and M. Raghunath, "Applying macromolecular crowding to enhance extracellular matrix deposition and its remodeling in vitro for tissue engineering and cell-based therapies," *Advanced Drug Delivery Reviews*, vol. 63, no. 4, pp. 277–290, 2011.

[2] E. Sachlos, J. T. Czernuszka, S. Gogolewski, and M. Dalby, "Making tissue engineering scaffolds work. Review on the application ofsolid freeform fabrication technology to the production of tissue engineering scaffolds," *European Cells and Materials*, vol. 5, pp. 29–40, 2003.

[3] E. D. Arrington, W. J. Smith, H. G. Chambers, A. L. Bucknell, and N. A. Davino, "Complications of iliac crest bone graft harvesting," *Clinical Orthopaedics and Related Research*, no. 329, pp. 300–309, 1996.

[4] J. R. Porter, T. T. Ruckh, and K. C. Popat, "Bone tissue engineering: a review in bone biomimetics and drug delivery strategies," *Biotechnology Progress*, vol. 25, no. 6, pp. 1539–1560, 2009.

[5] E. Monaco, M. Bionaz, S. J. Hollister, and M. B. Wheeler, "Strategies for regeneration of the bone using porcine adult adipose-derived mesenchymal stem cells," *Theriogenology*, vol. 75, no. 8, pp. 1381–1399, 2011.

[6] M. Chin, T. Ng, W. K. Tom, and M. Carstens, "Repair of alveolar clefts with recombinant human bone morphogenetic protein (rhBMP-2) in patients with clefts," *Journal of Craniofacial Surgery*, vol. 16, no. 5, pp. 778–789, 2005.

[7] P. Tayalia and D. J. Mooney, "Controlled growth factor delivery for tissue engineering," *Advanced Materials*, vol. 21, no. 32-33, pp. 3269–3285, 2009.

[8] D. Chen, M. Zhao, and G. R. Mundy, "Bone morphogenetic proteins," *Growth Factors*, vol. 22, no. 4, pp. 233–241, 2004.

[9] U. M. E. Wikesjö, G. Polimeni, and M. Qahash, "Tissue engineering with recombinant human bone morphogenetic protein-2 for alveolar augmentation and oral implant osseointegration: experimental observations and clinical perspectives.," *Clinical Implant Dentistry and Related Research*, vol. 7, no. 2, pp. 112–119, 2005.

[10] W. Zhu, B. A. Rawlins, O. Boachie-Adjei et al., "Combined bone morphogenetic protein-2 and -7 gene transfer enhances osteoblastic differentiation and spine fusion in a rodent model," *Journal of Bone and Mineral Research*, vol. 19, no. 12, pp. 2021–2032, 2004.

[11] A. R. Vaccaro, T. Patel, J. Fischgrund et al., "A pilot safety and efficacy study of OP-1 putty (rhBMP-7) as an adjunct to iliac crest autograft in posterolateral lumbar fusions," *European Spine Journal*, vol. 12, no. 5, pp. 495–500, 2003.

[12] S. N. Khan and J. M. Lane, "The use of recombinant human bone morphogenetic protein-2 (rhBMP-2) in orthopaedic applications," *Expert Opinion on Biological Therapy*, vol. 4, no. 5, pp. 741–748, 2004.

[13] J. B. Oldham, L. Lu, X. Zhu et al., "Biological activity of rhBMP-2 released from PLGA microspheres," *Journal of Biomechanical Engineering*, vol. 122, no. 3, pp. 289–297, 2000.

[14] H. Ishikawa, H. Kitoh, F. Sugiura, and N. Ishiguro, "The effect of recombinant human bone morphogenetic protein-2 on the osteogenic potential of rat mesenchymal stem cells after several passages," *Acta Orthopaedica*, vol. 78, no. 2, pp. 285–292, 2007.

[15] M. O. Freire, H.-K. You, J.-K. Kook, J.-H. Choi, and H. H. Zadeh, "Antibody-mediated osseous regeneration: a novel strategy for bioengineering bone by immobilized anti-bone morphogenetic protein-2 antibodies," *Tissue Engineering A*, vol. 17, no. 23-24, pp. 2911–2918, 2011.

[16] M. O. Freire, H. K. Kim, J. Kook, A. Nguyen, and H. H. Zadeh, "Antibody-mediated osseous regeneration: the early events in the healing response," *Tissue Engineering A*, vol. 19, no. 9-10, pp. 1165–1174, 2013.

[17] S. Ansari, A. Moshaverinia, A. Han, S. H. Pi, A. I. Abdelhamid, and H. H. Zadeh, "Functionalization of scaffolds with chimeric anti-BMP-2 monoclonal antibodies for osseous regeneration," *Biomaterials*, vol. 34, no. 38, pp. 10191–10198, 2013.

[18] B. P. T. Kruithof, S. N. Duim, A. T. Moerkamp, and M. J. Goumans, "TGFβ and BMP signaling in cardiac cushion formation: lessons from mice and chicken," *Differentiation*, vol. 84, no. 1, pp. 89–102, 2012.

[19] A. Moshaverinia, C. Chen, K. Akiyama et al., "Alginate hydrogel as a promising scaffold for dental-derived stem cells: an *in vitro* study," *Journal of Materials Science: Materials in Medicine*, vol. 23, no. 12, pp. 3041–3051, 2012.

[20] A. Valentin-Opran, J. Wozney, C. Csimma, L. Lilly, and G. E. Riedel, "Clinical evaluation of recombinant human bone morphogenetic protein-2," *Clinical Orthopaedics and Related Research*, no. 395, pp. 110–120, 2002.

[21] C. Parada and Y. Chai, "Roles of BMP signaling pathway in lip and palate development," *Frontiers of Oral Biology*, vol. 16, pp. 60–70, 2012.

[22] Z. Li and Y. G. Chen, "Functions of BMP signaling in embryonic stem cell fate determination," *Experimental Cell Research*, vol. 319, no. 2, pp. 113–119, 2013.

[23] A. Moshaverinia, S. Ansari, C. Chen et al., "Co-encapsulation of anti-BMP2 monoclonal antibody and mesenchymal stem cells in alginate microspheres for bone tissue engineering," *Biomaterials*, vol. 34, no. 28, pp. 6572–6579, 2013.

[24] J. Guo and G. Wu, "The signaling and functions of heterodimeric bone morphogenetic proteins," *Cytokine and Growth Factor Reviews*, vol. 23, no. 1-2, pp. 61–67, 2012.

[25] X. Guo and X. Wang, "Signaling cross-talk between TGF-β/BMP and other pathways," *Cell Research*, vol. 19, no. 1, pp. 71–88, 2009.

[26] G. Semb, "Alveolar bone grafting," *Frontiers of Oral Biology*, vol. 16, pp. 124–136, 2012.

[27] D. Liu, J. Zhang, Q. Zhang, S. Wang, and M. Yang, "TGF-β/BMP signaling pathway is involved in cerium-promoted osteogenic differentiation of mesenchymal stem cells," *Journal of Cellular Biochemistry*, vol. 114, no. 5, pp. 1105–1114, 2013.

[28] M. M. Shalabi, A. Gortemaker, M. A. Van't Hof, J. A. Jansen, and N. H. J. Creugers, "Implant surface roughness and bone healing: a systematic review," *Journal of Dental Research*, vol. 85, no. 6, pp. 496–500, 2006.

[29] K. Lee, E. A. Silva, and D. J. Mooney, "Growth factor delivery-based tissue engineering: general approaches and a review of recent developments," *Journal of the Royal Society Interface*, vol. 8, no. 55, pp. 153–170, 2011.

[30] V. Rosen and R. S. Thies, "The BMP proteins in bone formation and repair," *Trends in Genetics*, vol. 8, no. 3, pp. 97–102, 1992.

[31] D. M. Brunette, P. Tengvall, and M. Textor, *Titanium in Medicine. Properties and Biological Significance of Natural Oxide Films on Titanium and Its Alloys*, Springer, 2001.

[32] R. M. Meffert, B. Langer, and M. E. Fritz, "Dental implants: a review," *Journal of Periodontology*, vol. 63, no. 11, pp. 859–870, 1992.

[33] E. Alsberg, K. W. Anderson, A. Albeiruti, R. T. Franceschi, and D. J. Mooney, "Cell-interactive alginate hydrogels for bone tissue engineering," *Journal of Dental Research*, vol. 80, no. 11, pp. 2025–2029, 2001.

[34] L. H. H. Olde Damink, P. J. Dijkstra, M. J. A. van Luyn, P. B. van Wachem, P. Nieuwenhuis, and J. Feijen, "*In vitro* degradation of dermal sheep collagen cross-linked using a water-soluble carbodiimide," *Biomaterials*, vol. 17, no. 7, pp. 679–684, 1996.

Hindawi Publishing Corporation
BioMed Research International
Volume 2014, Article ID 801358, 6 pages
http://dx.doi.org/10.1155/2014/801358

Research Article

Modified Titanium Implant as a Gateway to the Human Body: The Implant Mediated Drug Delivery System

Young-Seok Park,[1,2] Joo-Youn Cho,[3] Shin-Jae Lee,[4] and Chee Il Hwang[4,5]

[1] *Department of Oral Anatomy, Seoul National University School of Dentistry and Dental Research Institute, Seoul 110-749, Republic of Korea*
[2] *Department of Oral and Maxillofacial Diagnostic Sciences, University of Florida College of Dentistry, Gainesville, FL 32610, USA*
[3] *Department of Pharmacology and Clinical Pharmacology, Seoul National University College of Medicine, Seoul 110-744, Republic of Korea*
[4] *Department of Orthodontics, Seoul National University School of Dentistry and Dental Research Institute, Seoul 110-768, Republic of Korea*
[5] *Hwang Chee Il Dental Office, Incheon 402-201, Republic of Korea*

Correspondence should be addressed to Shin-Jae Lee; nonext@snu.ac.kr

Received 29 June 2014; Accepted 10 July 2014; Published 22 July 2014

Academic Editor: Seong-Hun Kim

The aim of this study was to investigate the efficacy of a proposed new implant mediated drug delivery system (IMDDS) in rabbits. The drug delivery system is applied through a modified titanium implant that is configured to be implanted into bone. The implant is hollow and has multiple microholes that can continuously deliver therapeutic agents into the systematic body. To examine the efficacy and feasibility of the IMDDS, we investigated the pharmacokinetic behavior of dexamethasone in plasma after a single dose was delivered via the modified implant placed in the rabbit tibia. After measuring the plasma concentration, the areas under the curve showed that the IMDDS provided a sustained release for a relatively long period. The result suggests that the IMDDS can deliver a sustained release of certain drug components with a high bioavailability. Accordingly, the IMDDS may provide the basis for a novel approach to treating patients with chronic diseases.

1. Introduction

In general, drug delivery systems are designed to effectively deliver the required drug amounts while maximizing the efficacy and effectiveness of drugs and minimizing their side effects. The new drug delivery systems and technologies that are currently being developed promise to make the administration of medicines more efficient and less painful [1]. The efficacy and effectiveness of drug delivery systems are of particular importance to chronic illness sufferers, who often require drugs to be continuously administered for long periods.

The most common type of drug administration is oral administration. However, patients often fail to take orally administered drugs regularly when they are prescribed for long periods. For some pharmacological agents, more direct therapeutic approaches are required to bypass the gastrointestinal barrier and deliver the drugs directly into the blood stream. A common alternative is to administer periodic injections through devices such as the insulin pump used by diabetics who require daily injections of insulin. However, the insulin pump employs an injection needle and the frequent injections are poorly tolerated by patients. There patients often experience pain, fear, and unnecessary limitations to daily life, which can be considerable inconvenience. These drawbacks have led to the development of alternative delivery systems to needle injections [1, 2].

An effective alternative drug delivery system needs to address the natural question of how to avoid painful yet frequent needle injections and maintain the drug efficacy while

requiring minimal long-term compliance from patients. To reduce the aforementioned inconveniences while maximizing drug efficacy, new drug delivery systems need to be developed that can control the release of drugs and reduce the number of drug administrations. In the field of ophthalmology, the implantation of sustained drug release devices in the eye has been proposed as an alternative option [1, 3, 4]. However, the frequent surgical placement and removal of drug-containing implants is not practical for the routine management of chronic diseases. The new drug delivery system proposed in this study is a specially designed nonabsorbable implant that is capable of acting as a gate into the body. This permanent gateway can provide patients with sustainable drug release when required over long periods without requiring multiple needle injections or frequent drug uptake.

The use of titanium implants has become increasingly widespread and is gaining popularity, especially in contemporary dentistry [5–7]. Recent studies have demonstrated that titanium implants have a reliable success rate due to their well-documented biocompatibility [8–11]. Various types of such implants are widely used today to substitute for missing teeth and to act as supporting retentive structures or anchorage devices [7, 12–16].

The aim of this study was to examine the efficacy and feasibility of the proposed new implant mediated drug delivery system (IMDDS), which does not require frequent oral administration or painful needle injections. A pharmacokinetic study using dexamethasone was conducted on rabbits to investigate how the IMDDS works in an animal model.

2. Materials and Methods

2.1. Animal Subject. Fourteen New Zealand white male rabbits weighing 2.5–3 kg were prepared as the experimental animal. The rabbits were kept in separate cages and fed a standard rabbit diet. The selection, care, surgical protocol, and preparation of the animals were all conducted according to the guidelines of the Institutional Animal Care and Use Committee of the Seoul National University School of Dentistry. The internal review board approved the protocol for the rabbit experiments in this study (IRB no. SNU-140103-3).

2.2. The Modified Implant Design. Threaded implants were custom made by machining a block of pure titanium (grade 4). The implants used in the IMDDS comprised several components: an implant configured to be implanted in the bone, an accommodating part formed therein to allow a drug cartridge or a drug cassette to be seated within the implant, multiple diffusion holes formed in the circumferential wall of the implant from which the content of the drug cartridge can penetrate and disperse into the body system, and a cover unit coupled to the implant that closes the gate of the IMDDS (Figure 1).

2.3. Surgical Procedure. During the implant placement, general anesthesia was induced by the intramuscular injection of 10 mg/kg of Zoletil (Virbac) and 0.15 mL/kg of Rompun (Bayer Korea, Seoul, Korea). Prior to surgery, the skin in the mesial proximal tibia was shaved and then washed

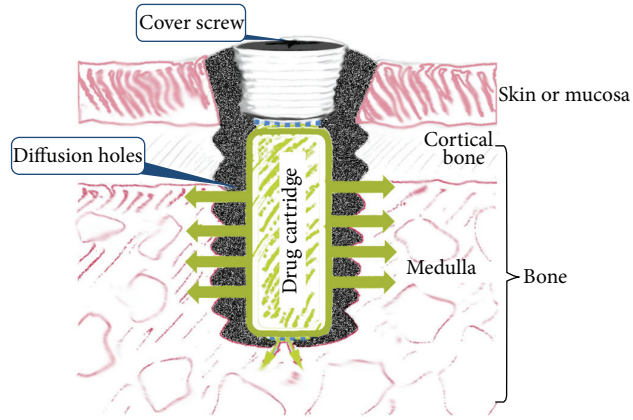

Figure 1: The implant used in the IMDDS comprised several components: a hollow titanium implant configured to be implanted in bone, an accommodating part formed therein to allow a drug cartridge to be seated, multiple diffusion holes formed in the circumferential wall of the implant, and a cover screw on top of the implant to close the gate of the IMDDS.

with an iodine solution. A preoperative antibiotic (0.15 g kanamycin intramuscularly) was also administered prophylactically. One milliliter of a 2% lidocaine solution with 1 : 100,000 epinephrine was injected into the region of the planned surgery. A periosteal incision was made to expose the tibia. After dissecting the muscles and periosteum, the flat surface on the lateral aspect of the proximal tibia was selected for implant placement. A low-speed rotary engine was used to drill the hole for the implant under profuse irrigation with sterile saline. Each rabbit received one implant in the tibia. The entire surgery procedure was performed under sterile conditions to prevent infection. After surgery, each rabbit received an intramuscular injection of antibiotics (Figure 2). A more detailed description of the procedure is available in the previous publication by Lee et al. (2009) [17].

2.4. Pharmacokinetic Investigation. Pharmacokinetic studies are crucial for understanding drug delivery systems. Such studies involve measuring the concentration of a drug in plasma or blood at several time points after drug administration [18].

In this study, a pharmacokinetic investigation was performed using an administration of dexamethasone, which has well-established pharmacokinetic properties [19, 20]. Dexamethasone is an efficient anti-inflammatory drug used in the treatment of several chronic diseases.

The dexamethasone powder (D1756-1G, Sigma-Aldrich, St Louis, MO) was prepared in 23 mg cartridges. A single cartridge of dexamethasone was inserted within the implant and sealed with a cover screw (Figure 2).

2.5. Experimental Design and the Measurement of the Dexamethasone Concentration. Three-milliliter blood samples were taken from the marginal vein of the ear at predetermined time intervals from immediately after the dexamethasone administration up to the longest follow-up time of 15 weeks

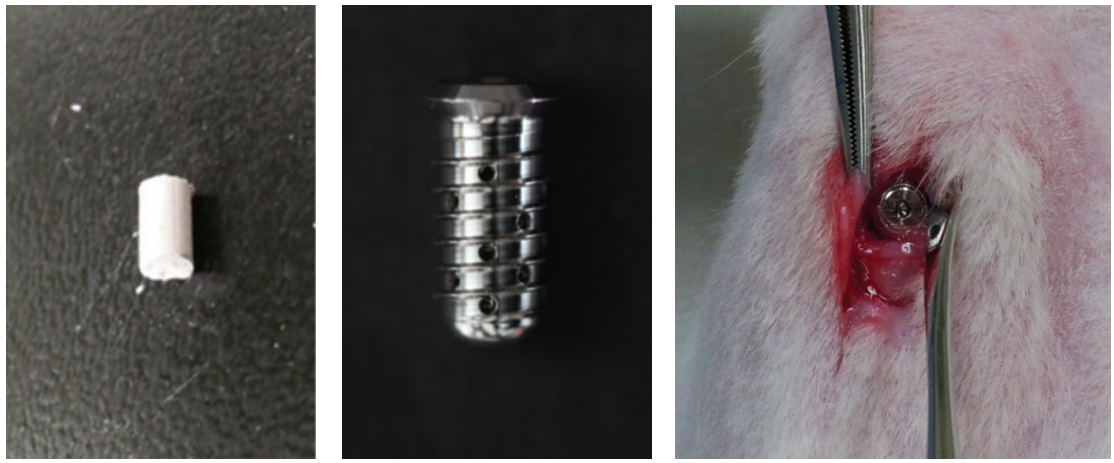

(a) (b) (c)

Figure 2: The dexamethasone cartridge (a), the cartridge inserted into the implant (b), and the implant placed in the rabbit tibia (c).

(3 months and 2 weeks). The blood samples were collected in heparin tubes and divided into two 1.5 mL tubes for centrifugation. The plasma was taken for analysis after separation via centrifugation (3,000 rpm, 10 minutes in 4°C). The plasma concentration of the dexamethasone was determined using liquid chromatography tandem mass spectroscopy (LC-MS/MS System, AB SCIEX, Framingham, MA) at each time point.

Considering the ethics of animal experimentations and the restricted rabbit blood volume, a batch experimental design was used for the sampling schedule instead of the classic complete data design. Unlike the complete data design, which samples each subject at all predefined time points, the batch design takes samples more than once from each subject, but not at all time points [18].

To distinguish the sustained release of the dexamethasone from the implant from the carry-over effect of dexamethasone metabolism, the implants were removed from two of the rabbits. The blood sampling was then repeated 2 weeks after the removal of the implants.

2.6. Statistical Data Analysis. The R programming language [21] and the R package PK [22] were used to perform the data analysis. The area under the concentration versus time curve (AUC) for the dexamethasone concentration was calculated.

3. Results

There were no abnormalities, mobility, or inflammation on the implant sites up to 8 months after the placement of the implants.

The cumulative release profiles of dexamethasone were obtained for 12 of 14 rabbits, with the 2 other rabbits being used for pilot experiments. Considerable variation was observed in the dexamethasone concentrations in each experimental rabbit. However, two common features were observable. First, the release profile demonstrated no lag time immediately after the dexamethasone administration. Second, a sustained release pattern was observed up to 7 weeks after administration. After 10 weeks, the dexamethasone was not detectable.

To concisely describe the results, the release profiles of two selected rabbits were depicted in Figure 3. During the first day after the drug cartridge insertion, a considerable amount of the drug was released and the maximum concentration was detected at between 4 hours and 12 hours after administration (Figure 3). From the second day, a sustained release of dexamethasone was maintained and relatively constant levels were provided for more than 7 weeks.

The biological half-life of dexamethasone is relatively long, at 36–54 hours in rabbits [19, 20]. The prolonged detection may have been the result of the IMDDS's sustained release pattern or a carry-over effect of the drug in rabbits. To distinguish the cause of the sustained release, we removed the implants from 2 rabbits at 1 week after drug administration. Again, the dexamethasone concentration was evaluated for up to 1 week (Figure 4). After the removal, as the drug depleted, the dexamethasone release rate declined sharply. No later than 4 days after the implant removal, dexamethasone was not detectable. This finding suggests that the sustained detection was unlikely to have been influenced by the long half-life of dexamethasone in the rabbit body.

The AUC is a reliable index for estimating the bioavailability of drugs [3]. Calculation of the areas under the curve revealed that the total AUC was 12.0 mg/mL. The AUCs for each experimental unit demonstrated that the longer the follow-up time, the greater the AUC (Table 1). To restate, the drug release pattern of the IMDDS showed a sustained release for a relatively long period. Based on the AUC, the bioavailability of dexamethasone in the rabbits treated with the IMDDS appeared evident.

4. Discussion

All of the inserted implants remained intact without any complication in their original position during and after the experiment. This result is not surprising, because the stability

Table 1: Area under the curve (AUC) of the plasma concentration of dexamethasone.

Experimental units	Number of rabbits per unit batch, n	Maximum follow-up time	AUC (mg/mL)
Batch number 1	4	3 months and 2 weeks	16.69 (7.33)
Batch number 2	2	7 weeks	2.83 (0.39)
Batch number 3	2	7 days	1.48 (0.74)
Batch number 4	4	1 day	1.20 (0.23)
Pooled data	$N = 12$		12.00 (1.58)

The values in parentheses are the standard errors.

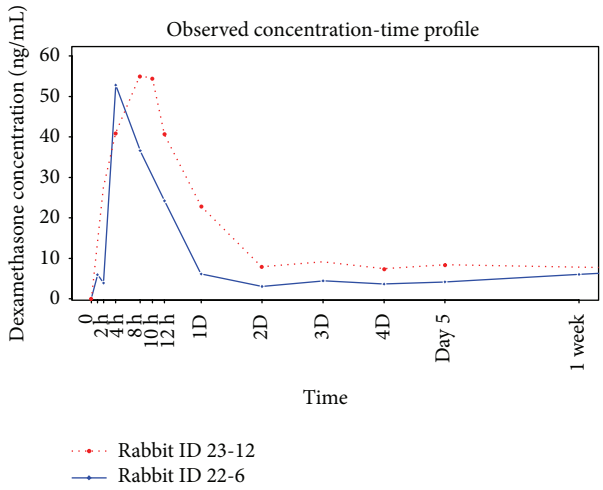

Figure 3: Dexamethasone release profiles of the 2 representative rabbits (rabbits ID 22-6 and ID 23-12). There was no lag period immediately after dexamethasone administration. During the first day after the drug cartridge insertion, a considerable amount of the drug was released and the maximum concentration was detected at between 4 hours and 12 hours after administration. From the second day, a sustained release was maintained and the concentration provided relatively constant levels of dexamethasone for more than 7 weeks.

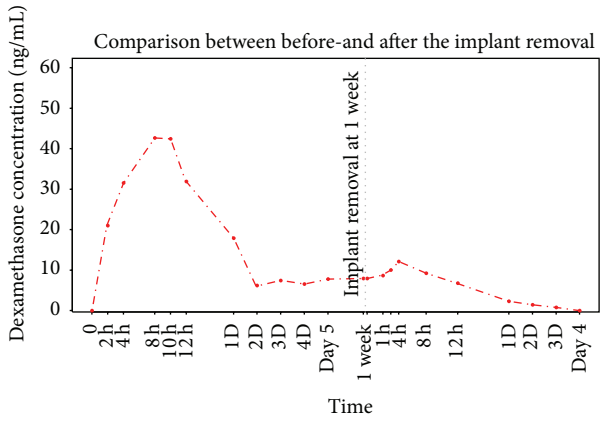

Figure 4: Comparison of the dexamethasone release profile before and after the implant removal. After the removal, as the drug depleted, the dexamethasone release rate declined sharply. Four days after the implant removal, dexamethasone was not detectable.

and biocompatibility of titanium implants have been reported to be almost perfect [5, 11, 13]. In fact, the high survival rate of titanium implants is not greatly influenced by clinical factors. For example, characteristics such as whether the site of implantation was located in the mandible or in the maxilla [6, 7], anywhere in the oral cavity, or in extremities such as the rabbit tibia; whether the implant length was short or long; or whether the diameter was large or small did not affect the high survival rate [9, 10, 13]. Accordingly, it is unlikely to be biocompatibility issues with the titanium implants used in the IMDDS. Because the implants for the IMDDS come into direct contact with the body, the implants must be made from materials that are biocompatible and pharmacologically inert.

To the best of our knowledge, this study is the first to report a drug delivery system using a titanium implant. The proposed idea for the study was simple, to examine whether a modified dental implant is capable of providing a gate for delivering drugs continuously for a long period. The dexamethasone delivery using the IMDDS demonstrated promising results in the rabbit experiment. The findings also suggest that drug delivery by the IMDDS is relatively steady over a relatively long time. From the sustained drug release profile, it can be clearly inferred that the IMDDS allowed a constant release of the drug without any apparent lag phase or conspicuous initial burst. Sustained release systems are very useful for the long-term administration of drugs because a single administration can achieve the same effect as multiple doses.

Several chronic diseases are often treated with repeated needle injections to maintain drug concentrations. Furthermore, if the drugs have a short half-life, multiple repeated injections are required. However, repeated injections over an extended period to ensure therapeutic levels often lead to reduced patient compliance or an increased likelihood of complications [3, 23]. The search for a slow or sustained release drug delivery system situated in the ocular area led to the development of a biodegradable intraocular implant [4], which has been introduced in the field of ophthalmology. The intraocular implant, which was designed to release dexamethasone for an extended period at a steady rate, was developed to treat inflammation after cataract surgery to decrease the risk of systemic toxicity and ocular side effects [3, 4, 24].

If the direct administration of drugs to a specific localized lesion is required [25], placing the implant as close as possible to the lesion could be more efficient. This could provide a more direct way of achieving the required therapeutic concentration through the local anatomy. In this regard,

the IMDDS may provide a more satisfactory means of access than the systemic administration of drugs through the blood vessels or oral uptake. Moreover, placing the implant at the site closest to the target lesion may enable more direct administration, which may also prevent the adverse effects associated with systemic administration. The IMDDS would be beneficial in this case because it is capable of providing a fast, more direct, and sustained release of the therapeutic agent to local bone areas. The intraosseous application of drugs can also bypass the systemic circulation, allowing for the accumulation of higher intrabony drug concentrations than can be achieved by systemic or surface administration.

The anatomic and physiological differences between rabbits and humans should be considered before applying the findings of this study to humans. The past findings for rabbits should also be differentiated from what may happen in humans. For example, rabbits have a smaller body mass; it has been shown that a dose of 25 mg dexamethasone in rabbits is equivalent to 500 mg in a 70 kg man [2]. Accordingly, the drug concentrations measured in rabbits tend to be significantly higher than those recorded in humans. For potential human applications, a thorough understanding of the pharmacokinetics of the IMDDS is necessary.

Implementing the IMDDS for clinical use may also be challenging. As with any new technique, clinicians would require training and education on the use of the new drug delivery system. Because the IMDDS is not 100% safe, skilled clinicians would be needed to administer the system. We do not anticipate that the IMDDS would be used by home use patients who self-manipulate, as the drug delivery system is designed for professional use only. To maintain or reassemble the drug cartridge or cassette, patients would need to visit a trained clinician such as a dentist.

Although we were not able to directly determine the efficiency of the IMDDS in this study, we found that the implant had satisfactory stability without inflammation and obtained promising pharmacokinetic characteristics using an animal experiment. However, further research is necessary to achieve a more controlled drug release via the IMDDS. A lag period or initial burst immediately after drug administration is common in oral and injection administrations. Although the IMDDS did not show a lag time, a delayed type of initial burst was observed. This could be controlled by the physicochemical properties of the cartridge to guarantee sustained release. Whether the drug preparation is a gel type or a powder type may influence the duration of the release and the peak concentration. It may also be possible to develop an electronic smart module that can control the release pattern of the IMDDS and monitor the drug release. The drug concentration may vary with factors such as the type and material of the drug cartridge, the implantation site, and the viscosity and solubility of the drug components. Through several alterations of these factors, the IMDDS would be a versatile drug delivery system that can provide the controlled sustained release of drugs.

The IMDDS is currently in the early stages of development. The major advantages of the IMDDS are the elimination of broken needles and a more constant delivery of drugs with minimal patient compliance. The implants for the IMDDS are customizable to each anatomical location of the body and can be modified to optimize the efficiency and efficacy of the system. The implantation site is a crucial element in ensuring that a proper dosage is released in recipients. There may be as yet unknown variables that prevent proper dosing with the IMDDS. Proper administration is highly dependent on numerous possible factors. Therefore, it may be pragmatic to develop a more convenient drug cartridge, such as a disposable type of drug cassette. This would have the added advantage of enabling a variety of different doses or different drugs to be loaded in the implant for use in the treatment of various diseases.

We envision that the IMDDS will be capable of providing a relatively safe method of administrating prolonged therapeutic levels of drugs. We hope that the IMDDS will provide an alternative to the existing needle-based drug delivery systems for chronic sufferers.

5. Conclusions

We conducted the first investigation of a drug delivery system using a modified titanium implant based on a study of the pharmacokinetics of dexamethasone in rabbits. To examine the efficacy and feasibility of the proposed IMDDS, we investigated the pharmacokinetic behavior of dexamethasone in plasma after delivering a single dose via the modified implant placed in the rabbit tibia. Our results indicate that drug delivery using the modified dental implant has a number of promising features. In particular, the IMDDS allows sustained drug delivery with a prolonged duration of drug action and a high bioavailability, therefore providing the basis for a novel approach to treating patients with chronic diseases. The chief advantage of the system is that no repeated needle injections or timely oral uptakes are necessary to maintain the critical drug concentrations. Although further experiments are necessary, the IMDDS shows great promise for the treatment of chronic diseases that require repeated drug administration or when timely periodic drug uptake is of the utmost importance.

Conflict of Interests

The authors declare that they have no conflict of interests. The authors certify that no financial support was received from commercial sponsors to conduct this study or in the preparation of this paper. Dr. Chee Il Hwang and the Seoul National University R&DB Foundation currently hold the IMDDS patent (PCT/KR2012/004795 date of issue, June 18, 2012; Patent no. 10-1336780 date of issue, November 28, 2013). Drs. Young-Seok Park, Shin-Jae Lee, and Chee Il Hwang are listed as inventors of the IMDDS patent. Dr. Joo-Youn Cho has nothing to disclose that is relevant to this paper.

Acknowledgments

The authors are grateful for the technical assistance of Hong-Kyun Kim and Min Chang Kim of Seoul National University, Seoul, Korea. This research was supported by a grant from the Korea Health Technology R&D Project through the Korea

Health Industry Development Institute (KHIDI), funded by the Ministry of Health and Welfare, Republic of Korea (Grant no. H I13C1474). Shin-Jae Lee was partly supported by the National Research Foundation of Korea (Grant no. 2012-047622).

References

[1] R. B. Kumar, "Needle free injection systems," *The Pharma Innovation*, vol. 1, no. 9, pp. 57–72, 2012.

[2] C. N. J. McGhee, "Pharmacokinetics of ophthalmic corticosteroids," *British Journal of Ophthalmology*, vol. 76, no. 11, pp. 681–684, 1992.

[3] L. Zhang, Y. Li, C. Zhang, Y. Wang, and C. Song, "Pharmacokinetics and tolerance study of intravitreal injection of dexamethasone-loaded nanoparticles in rabbits," *International Journal of Nanomedicine*, vol. 4, pp. 175–183, 2009.

[4] J. Chang-Lin, J. A. Burke, Q. Peng et al., "Pharmacokinetics of a sustained-release dexamethasone intravitreal implant in vitrectomized and nonvitrectomized eyes," *Investigative Ophthalmology and Visual Science*, vol. 52, no. 7, pp. 4605–4609, 2011.

[5] Y. C. Cho, J. Y. Cha, C. J. Hwang, Y. Park, H. Jung, and H. Yu, "Biologic stability of plasma ion-implanted miniscrews," *Korean Journal of Orthodontics*, vol. 43, no. 3, pp. 120–126, 2013.

[6] J. H. Choi, H. S. Yu, K. J. Lee et al., "Three-dimensional evaluation of maxillary anterior alveolar bone for optimal placement of miniscrew implants," *Korean Journal of Orthodontics*, vol. 44, no. 2, pp. 54–61, 2014.

[7] J. Kim and Y. Park, "Evaluation of mandibular cortical bone thickness for placement of temporary anchorage devices (TADs)," *Korean Journal of Orthodontics*, vol. 42, no. 3, pp. 110–117, 2012.

[8] K. J. Park, J. Y. Kwon, S. K. Kim et al., "The relationship between implant stability quotient values and implant insertion variables: a clinical study," *Journal of Oral Rehabilitation*, vol. 39, no. 2, pp. 151–159, 2012.

[9] S. Kim, I. Yeo, S. Lee, D. Kim, B. M. Jang, and J. Han, "Clinical use of alumina-toughened zirconia abutments for implant-supported restoration: prospective cohort study of survival analysis," *Clinical Oral Implants Research*, vol. 24, no. 5, pp. 517–522, 2013.

[10] S. J. Lee, L. Lin, S. H. Kim et al., "Survival analysis of a miniplate and tube device designed to provide skeletal anchorage," *American Journal of Orthodontics and Dentofacial Orthopedics*, vol. 144, no. 3, pp. 349–356, 2013.

[11] S. Karmarker, W. Yu, and H. Kyung, "Effect of surface anodization on stability of orthodontic microimplant," *Korean Journal of Orthodontics*, vol. 42, no. 1, pp. 4–10, 2012.

[12] S. H. Chung, S. J. Heo, J. Y. Koak et al., "Effects of implant geometry and surface treatment on osseointegration after functional loading: a dog study," *Journal of Oral Rehabilitation*, vol. 35, no. 3, pp. 229–236, 2008.

[13] S. J. Lee, S. J. Ahn, J. W. Lee, S. Kim, and T. Kim, "Survival analysis of orthodontic mini-implants," *American Journal of Orthodontics and Dentofacial Orthopedics*, vol. 137, no. 2, pp. 194–199, 2010.

[14] S. Lee, S. Jang, Y. Chun, and W. H. Lim, "Three-dimensional analysis of tooth movement after intrusion of a supraerupted molar using a mini-implant with partial-fixed orthodontic appliances," *Angle Orthodontist*, vol. 83, no. 2, pp. 274–279, 2013.

[15] J. S. Kim, S. H. Choi, S. K. Cha et al., "Comparison of success rates of orthodontic mini-screws by the insertion method," *Korean Journal of Orthodontics*, vol. 42, no. 5, pp. 242–248, 2012.

[16] H. M. Park, B. H. Kim, I. H. Yang, and S. Baek, "Preliminary three-dimensional analysis of tooth movement and arch dimension change of the maxillary dentition in class II division 1 malocclusion treated with first premolar extraction: conventional anchorage vs. mini-implant anchorage," *Korean Journal of Orthodontics*, vol. 42, no. 6, pp. 280–290, 2012.

[17] J. E. Lee, S. J. Heo, and J. Y. Koak, "Healing response of cortical and cancellous bone around titanium implants," *International Journal of Oral & Maxillofacial Implants*, vol. 24, no. 4, pp. 655–662, 2009.

[18] T. Jaki and M. J. Wolfsegger, "Non-compartmental estimation of pharmacokinetic parameters for flexible sampling designs," *Statistics in Medicine*, vol. 31, no. 11-12, pp. 1059–1073, 2012.

[19] D. Provan, R. Stasi, A. C. Newland et al., "International consensus report on the investigation and management of primary immune thrombocytopenia," *Blood*, vol. 115, no. 2, pp. 168–186, 2010.

[20] R. Schmelzeisen and J. C. Frolich, "Prevention of postoperative swelling and pain by dexamethasone after operative removal of impacted third molar teeth," *European Journal of Clinical Pharmacology*, vol. 44, no. 3, pp. 275–277, 1993.

[21] R Development Core Team, *R: A Language and Environment for Statistical Computing*, R Foundation for Statistical Computing, Vienna, Austria, 2014.

[22] T. Jaki and M. J. Wolfsegger, "Estimation of pharmacokinetic parameters with the R package PK," *Pharmaceutical Statistics*, vol. 10, no. 3, pp. 284–288, 2011.

[23] C. Gómez-Gaete, E. Fattal, L. Silva, M. Besnard, and N. Tsapis, "Dexamethasone acetate encapsulation into Trojan particles," *Journal of Controlled Release*, vol. 128, no. 1, pp. 41–49, 2008.

[24] J. Hsu, "Drug delivery methods for posterior segment disease," *Current Opinion in Ophthalmology*, vol. 18, no. 3, pp. 235–239, 2007.

[25] M. Caglaroglu and A. Erdem, "Histopathologic investigation of the effects of prostaglandin E2 administered by different methods on tooth movement and bone metabolism," *Korean Journal of Orthodontics*, vol. 42, no. 3, pp. 118–128, 2012.

Hindawi Publishing Corporation
BioMed Research International
Volume 2014, Article ID 452175, 12 pages
http://dx.doi.org/10.1155/2014/452175

Research Article

Differential Expression of Osteo-Modulatory Molecules in Periodontal Ligament Stem Cells in Response to Modified Titanium Surfaces

So Yeon Kim,[1] Ji-Yeon Yoo,[2] Joo-Young Ohe,[2] Jung-Woo Lee,[2] Ji-Hoi Moon,[1] Yong-Dae Kwon,[2] and Jung Sun Heo[1]

[1] *Department of Maxillofacial Biomedical Engineering and Institute of Oral Biology, School of Dentistry, Kyung Hee University, 26 Kyunghee-daero, Dongdaemun-gu, Seoul 130-701, Republic of Korea*
[2] *Department of Oral & Maxillofacial Surgery, School of Dentistry, Kyung Hee University, 26 Kyunghee-daero, Dongdaemun-gu, Seoul 130-701, Republic of Korea*

Correspondence should be addressed to Yong-Dae Kwon; kwony@khu.ac.kr and Jung Sun Heo; heojs@khu.ac.kr

Received 5 March 2014; Accepted 11 April 2014; Published 25 June 2014

Academic Editor: Seong-Hun Kim (Sunny)

This study assessed differential gene expression of signaling molecules involved in osteogenic differentiation of periodontal ligament stem cells (PDLSCs) subjected to different titanium (Ti) surface types. PDLSCs were cultured on tissue culture polystyrene (TCPS), and four types of Ti discs (PT, SLA, hydrophilic PT (pmodPT), and hydrophilic SLA (modSLA)) with no osteoinductive factor and then osteogenic activity, including alkaline phosphatase (ALP) activity, mRNA expression of runt-related gene 2, osterix, FOSB, FRA1, and protein levels of osteopontin and collagen type IA, were examined. The highest osteogenic activity appeared in PDLSCs cultured on SLA, compared with the TCPS and other Ti surfaces. The role of surface properties in affecting signaling molecules to modulate PDLSC behavior was determined by examining the regulation of Wnt pathways. mRNA expression of the canonical Wnt signaling molecules, Wnt3a and β-catenin, was higher on SLA and modSLA than on smooth surfaces, but gene expression of the calcium-dependent Wnt signaling molecules Wnt5a, calmodulin, and NFATc1 was increased significantly on PT and pmodPT. Moreover, integrin $\alpha 2/\beta 1$, sonic hedgehog, and Notch signaling molecules were affected differently by each surface modification. In conclusion, surface roughness and hydrophilicity can affect differential Wnt pathways and signaling molecules, targeting the osteogenic differentiation of PDLSCs.

1. Introduction

Titanium (Ti) substrates are commonly used as biomaterials in dental implantology because they provide excellent biocompatibility for peri-implant bone formation. Many clinical and experimental studies have demonstrated that surface properties, such as topography, roughness, surface energy, and hydrophilicity, are pivotal factors in enhancing osseointegration [1, 2]. Although surface roughness and hydrophilicity remain the major variables determining cell response, different types of cell derived from various tissues also react differently to surface properties [3, 4].

Preliminary assessments of potential biomaterials are often made using osteoblasts, osteoblast-like cells, or bone marrow-derived mesenchymal stem cells [5, 6]. Periodontal ligament stem cells (PDLSCs) are attractive for assessing osseointegration between titanium implants and bone tissue because they are known to self-renew, differentiate into multiple lineages, and function in periodontal tissue regeneration [7]. Moreover, PDLSCs can be obtained more readily than other adult stem/progenitor cells (e.g., bone marrow-derived mesenchymal stem cells or osteoblasts, which are commonly used in implantology).

Studies using various cell culture models have shown different biological behaviors of cells reflecting differences in surface properties [8, 9]. In a recent study, the cell spreading, survival, and *in vitro* osteogenic differentiation of an immortalized human PDL cell line cultivated on two

Ti scaffolds with different topographies were analyzed; the responses of these cells differed from those of osteoblasts, suggesting the cell-type specificity of responses to different surface structures [10]. However, the mechanism of the physiological transition between the nonphysiological Ti surface and surrounding cells has not been determined. Moreover, considering the biological role of PDLSCs in osteogenic differentiation, the characterization of their responses to Ti surfaces with different topographies and hydrophilicities is important.

Thus, in the present study, we first tested Ti substrates using PDLSCs to demonstrate the usefulness of this model for novel strategies in PDL engineering and secondly classified the influence of different topographies and hydrophilicities of Ti surfaces on the expression of various functional factors in PDLSCs involved in osteogenesis in the absence of osteogenic supplements, and finally we evaluated biomarkers of cellular activity, including the expression of transcription factors and signaling molecules of PDLSCs on the Ti surfaces.

2. Materials and Methods

2.1. Materials. Fetal bovine serum (FBS) was purchased from Gibco-BRL (Gaithersburg, MD, USA). Collagen type I (COLIA), osteopontin (OPN), β-actin, goat anti-mouse, and goat anti-rabbit antibodies were supplied by Santa Cruz Biotechnology (Santa Cruz, CA, USA). Unless otherwise specified, chemicals and laboratory wares were from Sigma Chemical Company (St. Louis, MO, USA) and Falcon Labware (Becton-Dickinson, Franklin Lakes, NJ, USA), respectively.

2.2. Surface Characterization of Titanium. Ti discs with 15 mm diameters and 1 mm thicknesses to fit a 24-well tissue culture plate were prepared and supplied by Institut Straumann AG (Basel, Switzerland). The water contact angle was determined tensiometrically with a telescopic goniometer (Phoenix 300; SEO, South Korea). The morphologies of the PDLSCs growing on Ti discs were examined by scanning electron microscopy (SEM; S-2300; Hitachi, Japan). The discs were washed with phosphate-buffered saline (PBS) and fixed with 2.5% glutaraldehyde in 0.1 M phosphate buffer (pH 7.3) for 30 min and 1% osmium tetroxide in 0.1 M cacodylate buffer (pH 7.4) for 1 h. The discs were then washed with PBS three times, dehydrated through a graded ethanol series, placed in a 100% ethanol bath, and rinsed three times. They were dried and sputter coated with gold (Eiko IB, Japan) and then observed by SEM. Photographs were taken at 15 kV using various magnifications and angles. The surfaces of the Ti were also analyzed using an atomic force microscope (AFM) (XE-100; PSIA Inc., Suwon, Korea) in noncontact mode. The AFM observation was measured at an ambient temperature under a 0.5 Hz scan rate. Digital NC-AFM images were acquired by using XEI 4.1.1 program. Seven measurements were performed at PT and SLA implant; they included height-descriptive parameters, Sq: root mean square roughness, Ssk: skewness, Sku: kurtosis, Sp: maximum peak height, and hybrid-descriptive parameters, Sdq: root mean square surface slope, Sdr: developed interfacial area ratio.

2.3. Periodontal Ligament Stem Cell Culture. Periodontal ligaments were obtained from extracted human molars donated by the Department of Oral and Maxillofacial Surgery, Kyung Hee University. All subjects involved in this study were informed about its purpose and procedures, and the study was approved by the Review Board of Kyung Hee University. Written informed consent was obtained from all donors and guardians on behalf of minor participants.

Periodontal ligaments were collected from the middle thirds of roots and cultured in α minimal essential medium (α-MEM; Invitrogen, Carlsbad, CA, USA) containing 10% FBS, penicillin (100 U/mL), and streptomycin (100 μg/mL; Sigma Chemical Company) according to a previously described method [11, 12]. After two passages, the cells were subjected to magnetic isolation with antibodies to detect the STRO-1 antigen (mesenchymal stem cell marker; Millipore, Billerica, MA, USA) and magnetic beads (Miltenyi Biotec, Germany). The resulting STRO-1(+) cell population was cultured in α-MEM plus 10% FBS at 37°C with a humidified gas mixture of 5% CO_2/95% air. All experiments were carried out with passage 4–7 cells.

2.4. Alkaline Phosphatase Activity. ALP activity was performed as previously described [12]. Briefly, Cells were washed twice with PBS and lysed in 50 mM Tris-HCl buffer (pH 7.0) containing 1% (v/v) Triton X-100 and 1 mM phenylmethylsulfonyl fluoride. Total protein was then quantified using the Bradford procedure [13]. The entire cell lysate was assayed by adding 200 μL *p*-nitrophenylphosphate (Sigma Chemical Company) as a substrate for 30 min at 37°C. The reaction was stopped by adding 3 M NaOH and the absorbance was read spectrophotometrically at 405 nm. The enzyme activity was expressed as mM/100 μg protein.

2.5. RNA Isolation and Real-Time Reverse-Transcriptase Polymerase Chain Reaction. This process was performed as described in our previous study [12]. Total RNA was extracted from the cells using TRIzol reagent (Invitrogen), following the manufacturer's protocol. Real-time quantification of RNA targets was then performed with a Rotor-Gene 2000 real-time thermal cycling system (Corbett Research, Australia) using a QuantiTect SYBR Green reverse-transcriptase polymerase chain reaction (RT-PCR) kit (Qiagen, CA, USA). The reaction mix (20 μL) contained 200 ng total RNA, 0.5 μM of each primer, and appropriate amounts of enzymes and fluorescent dyes, as recommended by the supplier. The Rotor-Gene 2000 cycler was programmed as follows: 30 min at 50°C for reverse transcription, 15 min at 95°C for DNA polymerase activation, 15 s at 95°C for denaturing, and 45 cycles of 15 s at 94°C, 30 s at 55°C, and 30 s at 72°C. Data were collected during the extension step (30 s at 72°C). The PCR reaction was followed by melting curve analysis to verify the specificity and identity of the RT-PCR products; this analysis can distinguish specific PCR products from nonspecific PCR products resulting from primer dimer formation. The temperature of the PCR products was increased from 65°C to 99°C at a rate of 1°C/5 s, and the resulting data were analyzed using the software provided by the manufacturer. The primer sequences are listed in Table 1.

Table 1: Primer sequences used for real-time RT-PCR analysis of gene expression.

Gene	Forward primer (5′-3′)	Reverse primer (5′-3′)
RUNX2	GTCTCACTGCCTCTCACTTG	CACACATCTCCTCCCTTCTG
OSX	TGAGGAGGAAGTTCACTATGG	TTCTTTGTGCCTGCTTTGC
FOSB	TCCAGGCGGAGACAGATCAGTTG	TCTTCGTAG GGGATCTTGCAGCC
FRA1	CCCTGCCGCCCTGTACCTTGTATC	AGACATTGGCTAGGGTGGCATCTGCA
Wnt3a	GTCCCGTCCCTCCCTTTC	ACCTCTCTTCCTACCTTTCCC
Wnt5a	TCTCAGCCCAAGCAACAAGG	GCCAGCATCACATCACAACAC
β-catenin	GGCAGCAACAGTCTTACC	TCCACATCCTCTTCCTCA
Integrin α2	ACTGTTCAAGGAGGAGAC	GGTCAAAGGCTTGTTTAGG
Integrin β1	ATTACTCAGATCCAACCAC	TCCTCCTCATTTCATTCATC
Calmodulin	CAGATATTGATGGAGACGGA	GAGCACACGAAGTACAAGAG
NFATc1	CCTTCGGAAGGGTGCCTTTT	AGGCGTGGGGCCTCAGCAGG
Shh	CGCCAGCGGAAGGTATGAAG	CAACTTGTCCTTACACCTCTGAGTC
Gli1	AATGCTGCCATGGATGCTAGA	GAGTATCAGTAGGTGGGAAGTCCATAT
Notch	GCCGCCTTTGTGCTTCTGTTC	CCGGTGGTCTGTCTGGTCGTC
Hes-1	AGGCGGACATTCTGGAAATG	CGGTACTTCCCCAGCACACTT
GAPDH	GCTCTCCAGAACATCATCC	TGCTTCACCACCTTCTTG

2.6. Western Blot Analysis. Western blot analysis was conducted as previously reported [12]. Protein extract samples (20 μg) were separated by 8–10% sodium dodecyl sulfate polyacrylamide gel electrophoresis and blotted onto polyvinylidene difluoride membranes. The blots were washed with TBST [10 mM Tris-HCl (pH 7.6), 150 mM NaCl, 0.05% Tween-20], blocked with 5% skim milk for 1 h, and incubated with the appropriate primary antibodies (anti-COLIA, anti-OPN, or anti-β-actin; Santa Cruz Biotechnology) at the dilutions recommended by the supplier. The membranes were then washed and the primary antibodies were detected with goat anti-rabbit immunoglobulin G (IgG) or goat anti-mouse IgG conjugated to horseradish peroxidase. The blots were developed with enhanced chemiluminescence (Santa Cruz Biotechnology) and exposed to X-ray film (Eastman-Kodak, Rochester, NY, USA).

2.7. Immunofluorescence Staining. Cells were fixed and treated with mouse anti-COLIA or anti-OPN antibody (1 : 100; Santa Cruz Biotechnology) for 1 h at room temperature. Fluorescein isothiocyanate-conjugated anti-mouse IgG (1 : 100) was then added for 1 h at room temperature. as previously reported [12]. Images were obtained using a fluorescence microscope (Fluoview 300; Olympus).

2.8. siRNA Transfection. Cells were transfected for 24 h with a Stealth small interfering RNA (siRNA) specific to β-catenin (5′-CCC UCA GAU GGU GUC UGC CAU UGU A-3′, 200 pmol/L; Invitrogen) or an unrelated control siRNA targeting the green fluorescent protein (5′-CCA CTA CCT GAG CAC CCA GTT-3′), using the Lipofectamine 2000 according to the manufacturer's instructions. as previously described [12].

2.9. Statistical Analysis. All data are expressed as means ± standard deviations. One-way analysis of variance was used for multiple comparisons (Duncan's multiple range test). Analyses were performed with the SPSS software (ver. 10.0; SPSS Inc., Chicago, IL, USA). A P value < 0.05 was considered to indicate statistical significance.

Table 2: Titanium surface roughness data.

	PT	SLA
Height parameters		
Sq (μm)	0.1097	0.4151
Ssk	0.2341	−0.0547
Sku (μm)	2.5841	2.4423
Sp (μm)	0.3489	0.9488
Sa (μm)	0.0889	0.3376
Hybrid parameters		
Sdq (rad)	0.28	1.8217
Sdr (%)	3.7307	85.24

3. Results

3.1. Surface Characteristics. The PT and SLA surfaces showed water contact angles of 82.23° and 79.22°, respectively, whereas the contact angles of pmodPT and modSLA surfaces were close to 0°, indicating that the PT and SLA surfaces were hydrophobic, while the pmodPT and modSLA substrates were hydrophilic (Figure 1(a)). SEM images showed morphological differences between the PT and SLA surfaces; the PT surfaces were smooth and planar in comparison with the SLA substrates, consistent with previous reports (Figure 1(b)). The surface roughness of PT and SLA was evaluated by AFM (Figures 1(c) and 1(d)). As shown in Table 2, profile topography measurements revealed significant differences of roughness between PT and SLA implants.

3.2. Effect of Surface-Modified Ti Implants on Osteogenic Differentiation of PDLSCs. To confirm the effects of surface

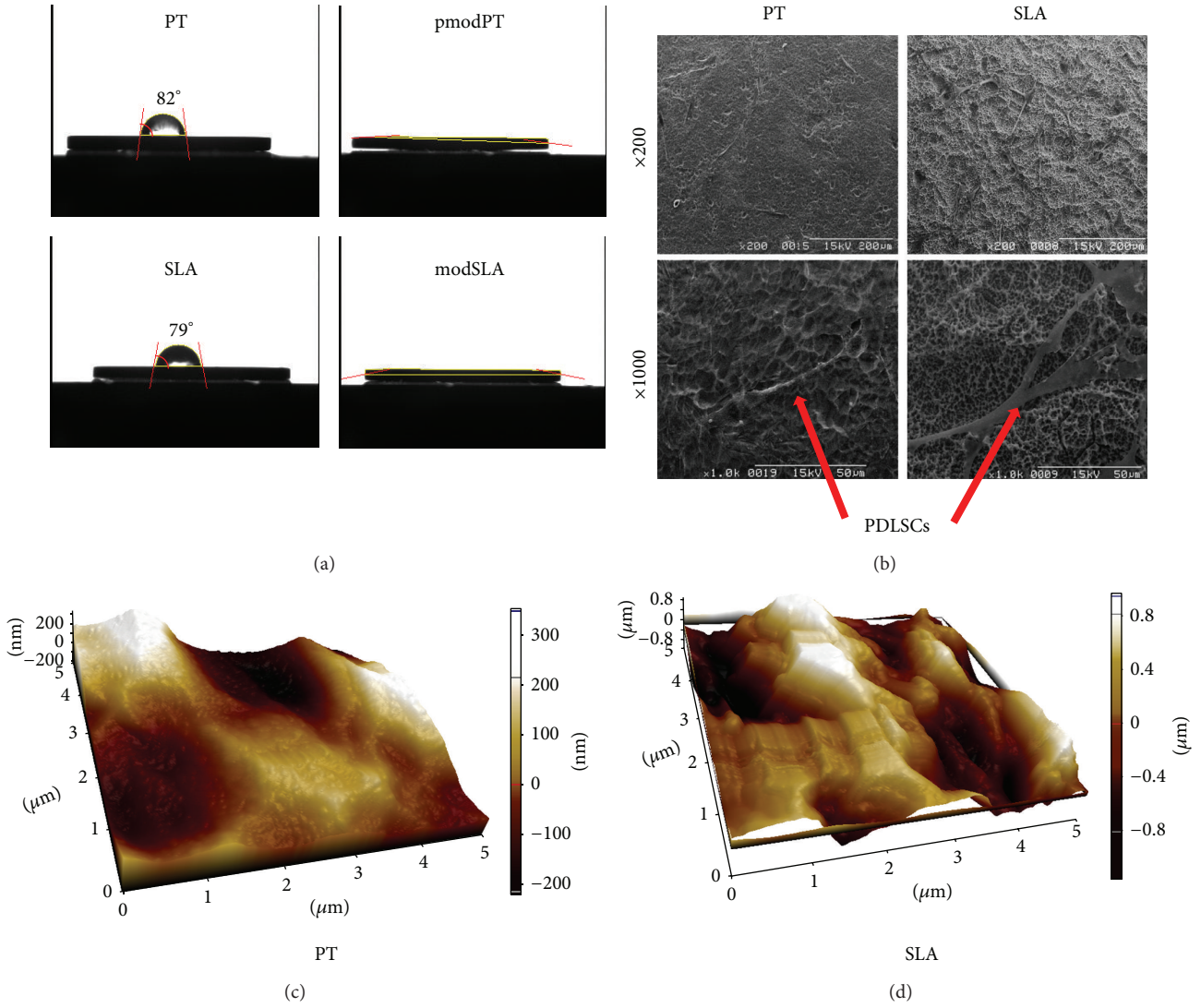

Figure 1: Characterization of titanium substrates. (a) The water contact angles of pretreatment (PT), hydrophilic PT (pmodPT), sand-blasted, large-grit acid-etched (SLA), and hydrophilic SLA (modSLA) substrates were assessed. (b) Topographical features of PT and SLA substrates were examined by scanning electron microscopy at ×200 (upper panels; scale bar = 200 μm) or ×1000 (lower panels; scale bar = 50 μm) magnification. The AFM images of (c) PT and (d) SLA.

topography on the biological responses of PDLSCs, the cells were cultured on tissue culture polystyrene (TCPS), PT, pmodPT, SLA, and modSLA surfaces, and alkaline phosphatase (ALP) activity was then assessed 4 and 7 days after induction to identify surface-specific osteogenic differentiation of PDLSCs. ALP activity was significantly higher in cells cultured on all Ti surfaces compared with the control TCPS (Figures 2(a) and 2(b)). In particular, the highest ALP activity appeared in cells on the SLA surface. Interestingly, more ALP activity was observed on hydrophilic pmodPT than on hydrophobic PT surfaces, whereas more activity was observed on hydrophobic SLA than on hydrophilic modSLA surfaces.

To further support the effect of surface properties on PDLSC behavior, we determined the mRNA expression of known osteogenic target genes (runt-related gene 2, osterix, FOSB, and FRA1) using real-time RT-PCR. According to ALP activity, mRNA expression of each osteogenic factor was increased on all Ti surfaces compared with the control TCPS. The expression of all genes was highest on SLA surfaces (Figures 2(c)–2(f)). We also analyzed the Ti surface effect on the osteogenic differentiation of PDLSCs by following the protein level data of osteogenic markers (OPN and COLIA) on day 4 of osteogenic induction. Western blot analysis showed that the level of each protein was increased in cells cultured on all Ti surfaces compared with TCPS. The pattern of protein expression levels in response to each surface was consistent with data from real-time RT-PCR (Figure 2(g)). Moreover, immunofluorescence staining for OPN and COLIA confirmed that PDLSCs on Ti surfaces

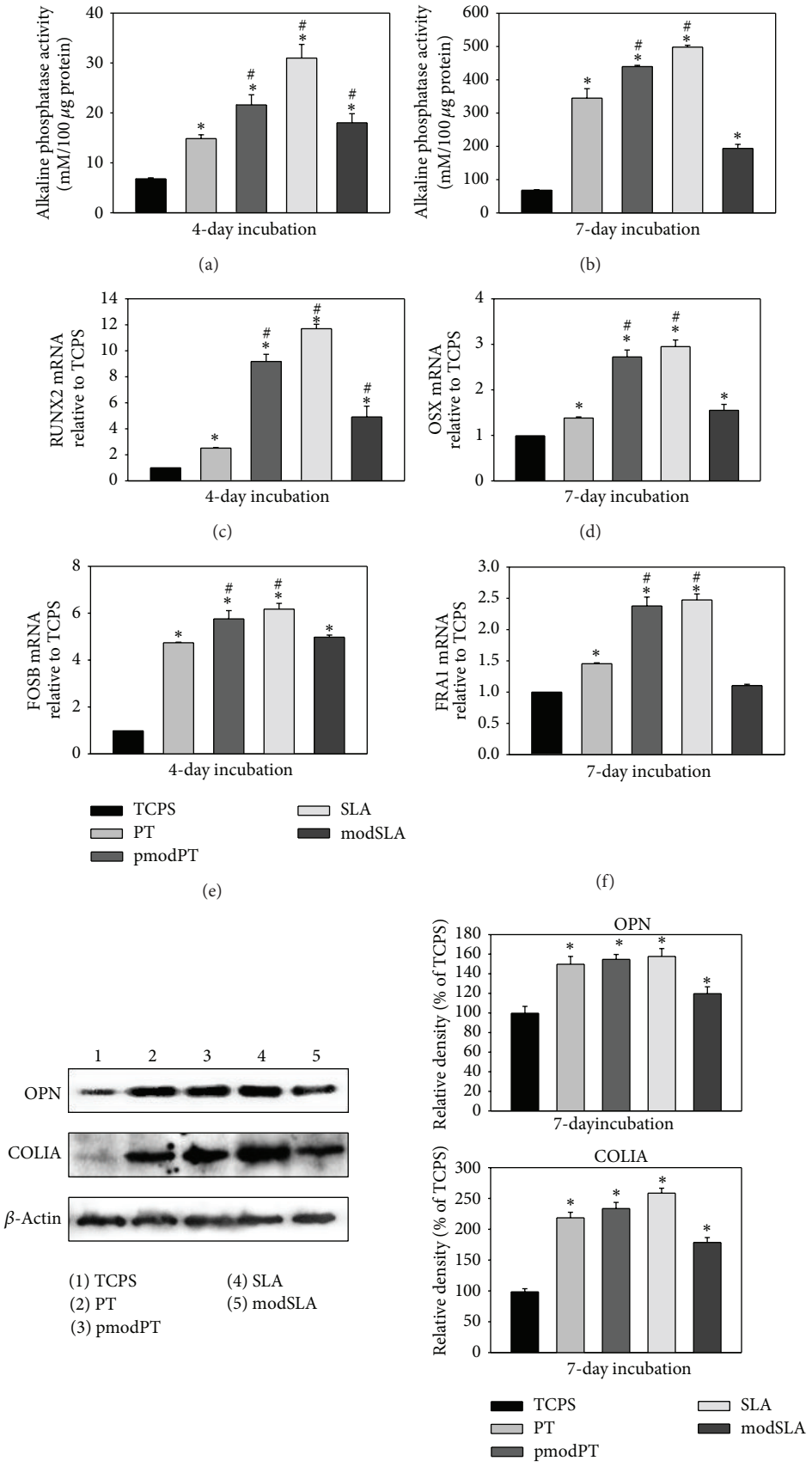

Figure 2: Continued.

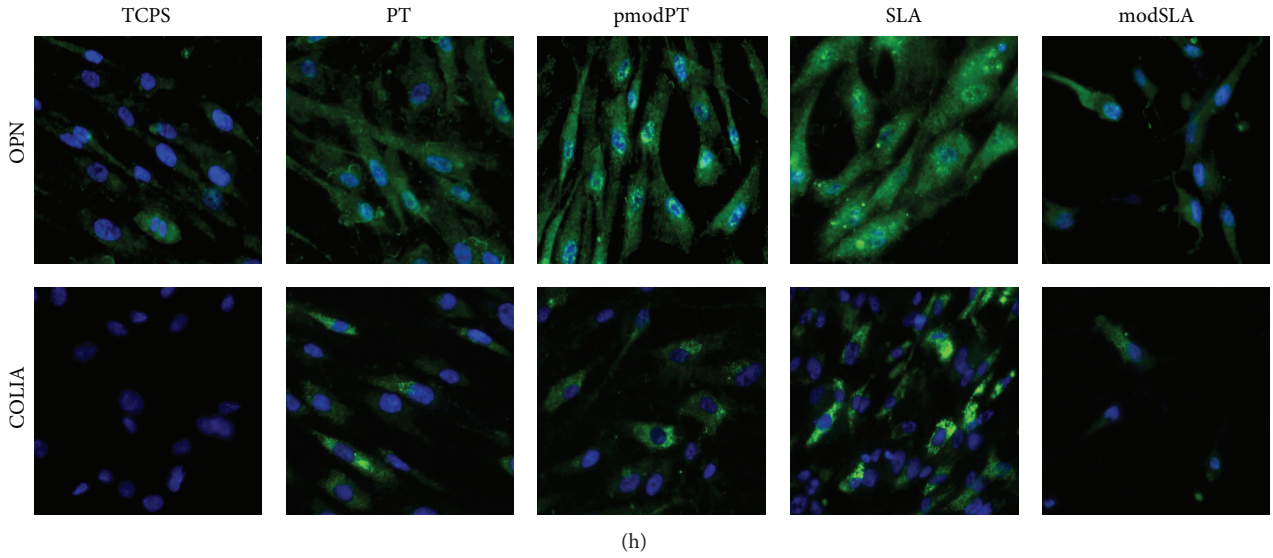

Figure 2: Osteogenic activity of periodontal ligament stem cells in response to titanium surfaces. Cells were cultured on pretreatment (PT), hydrophilic PT (pmodPT), sand-blasted, large-grit acid-etched (SLA), or hydrophilic SLA (modSLA) substrates for 4 or 7 days, and ALP activity ((a), (b)), real time RT-PCR ((c)–(f)), Western blot (g), and immunofluorescence staining (h) of osteogenic markers were then assessed as described in Section 2. Reported values are the means ± standard deviations of five independent experiments. Panels (bars) denote the means ± standard deviations of five experiments for each condition, determined from densitometry relative to β-actin. $^{*}P < 0.05$ versus control (tissue culture polystyrene); $^{\#}P < 0.05$ versus PT substrate. Nuclei were stained with DAPI (blue). A representative result from three independent experiments is shown.

showed enhanced differentiation into the osteogenic lineage (Figure 2(h)).

3.3. Effect of Ti Roughness and Hydrophilicity on Gene Expression of Signaling Molecules. In comparative experiments to determine the role of surface property in the variation in possible signaling molecules during osteogenic differentiation of PDLSCs, we first found that mRNA expression levels of the canonical Wnt signaling molecules, Wnt3a and β-catenin, were higher on SLA and modSLA surfaces than on TCPS and smooth surfaces. In contrast, gene expression of the calcium-dependent Wnt signaling molecules Wnt5a, calmodulin, and NFATc1 was increased significantly on PT and pmodPT surfaces compared with TCPS, but it was downregulated on SLA and modSLA surfaces in comparison with TCPS and PT surfaces (Figures 3(a)–3(e)). The mRNA expression of the adhesion molecules integrin α2 and β1 increased with surface roughness in PDLSCs (Figures 3(f) and 3(g)). Moreover, sonic hedgehog (Shh) expression was slightly increased on SLA and modSLA surfaces but much more increased on PT and pmodPT surfaces (11-fold and 25-fold versus TCPS; $P < 0.05$). Gene expression of the transcription factor for Shh, Gli1, was also increased significantly on smooth substrates (8-fold for PT and 13-fold for pmodPT versus TCPS; $P < 0.05$), but it was decreased on SLA and modSLA surfaces in comparison with PT (Figures 3(h) and 3(i)). However, mRNA expression of Notch and its target gene Hes-1 was increased markedly in PDLSCs cultured on hydrophobic PT and SLA surfaces (7.7-fold and 10-fold versus TCPS for Notch; 2.3-fold and 3.3-fold versus TCPS for Hes-1; $P < 0.05$), but it was unchanged on hydrophilic PT and SLA surfaces compared with TCPS (Figures 3(j) and 3(k)).

3.4. Relationships among Wnt Signaling, Integrin, Shh, and Notch during PDLSC Osteogenesis. To determine whether the changes in integrins, Shh, and Notch expression were dependent on canonical Wnt signaling, cells were transfected with β-catenin siRNA. Knockdown of β-catenin by siRNA transfection blocked the increases in integrin α2, integrin β1, Shh, Gli1, Notch, and Hes-1 gene expression of cells on SLA and modSLA surfaces but did not affect those genes on PT or pmodPT surfaces (Figures 4(a)–4(f)). On the other hand, treatment of NFAT inhibitor diminished Shh, Gli1, Notch, and Hes-1 gene expression of cells on PT and pmodPT surfaces, but there were no changes of each gene on SLA and modSLA (Figures 4(g)–4(l)).

Subsequently, we assessed whether surface-specific activated canonical or noncanonical Wnt pathways influenced the osteogenic differentiation of PDLSCs. Nuclear factor of activated T cells (NFAT) inhibitor treatment decreased ALP activity of cells on PT and pmodPT surfaces but had no effect on SLA and modSLA surfaces, indicating that calcium-dependent Wnt signaling played a prominent role in regulating PDLSC osteogenesis on smooth surfaces (Figure 5(a)). However, when cells were transfected with β-catenin siRNA, ALP values were reduced significantly only on SLA and modSLA surfaces, suggesting the osteoinductive function of the canonical Wnt/β-catenin pathway on rough substrates (Figure 5(b)).

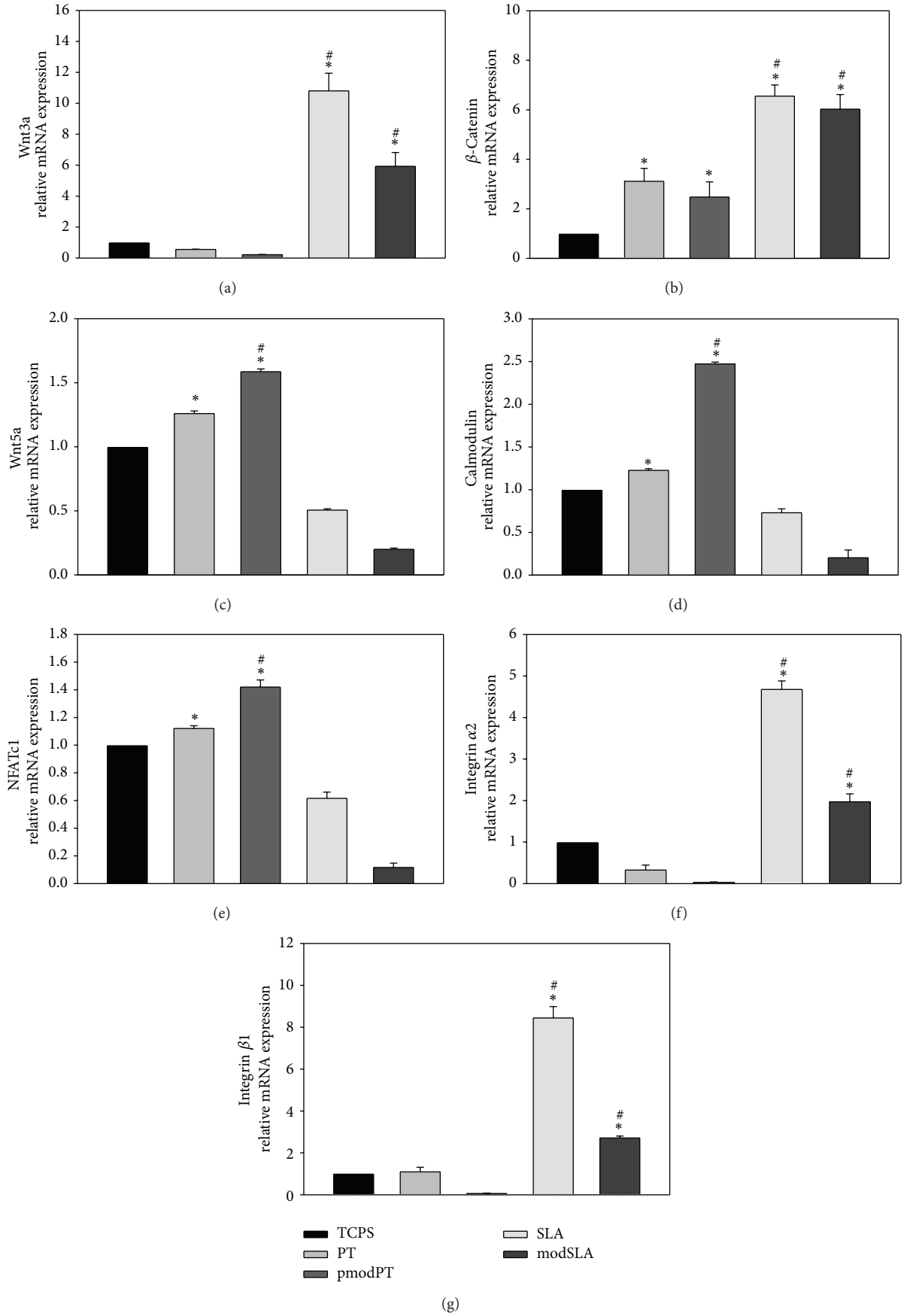

Figure 3: Continued.

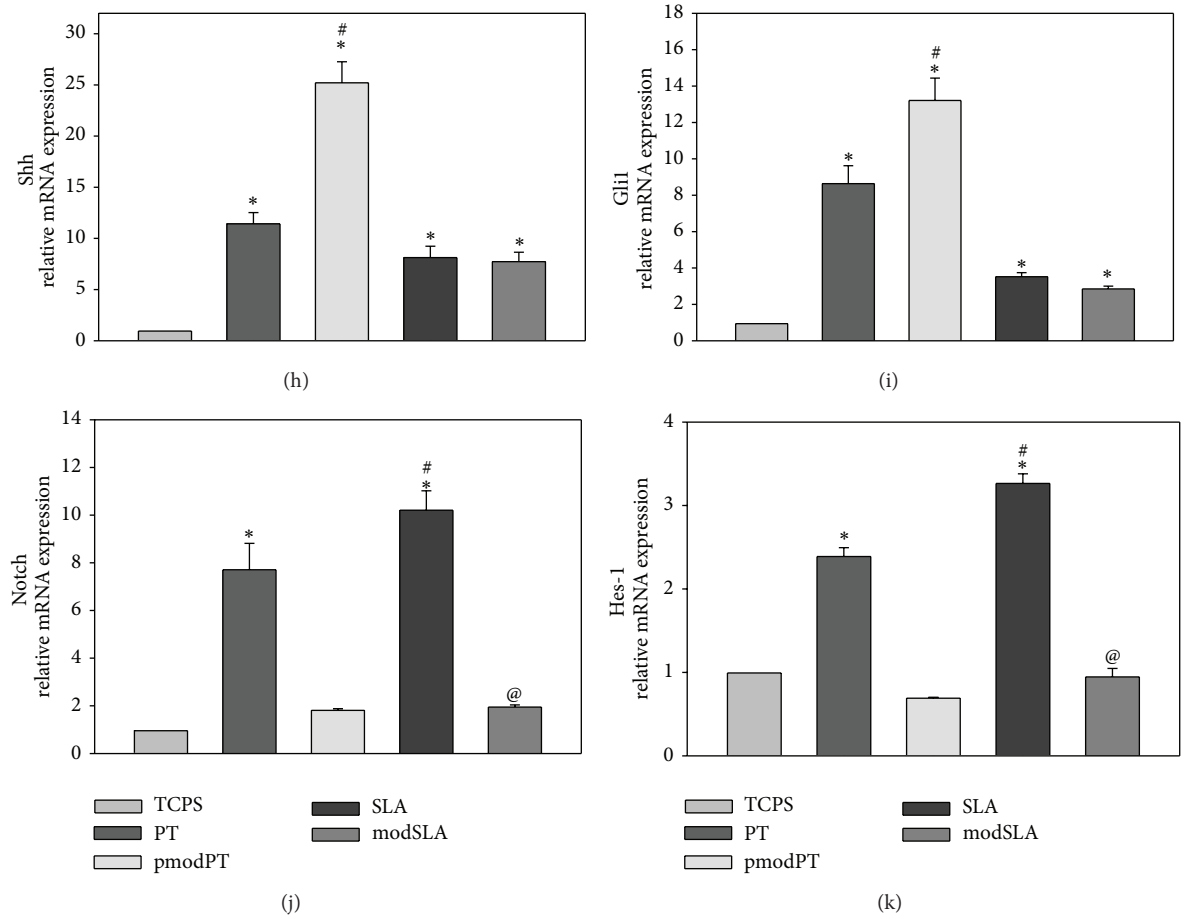

Figure 3: Effect of titanium surface structure on Wnt, integrins, Shh, and Notch signaling molecules. Cells were cultured on each substrate and the mRNA levels of (s) Wnt3a, (b) β-catenin, (c) Wnt5a, (d) calmodulin, (e) NFATc1, (f) integrin α2, (g) integrin β1, (h) Shh, (i) Gli1, (j) Notch, and (k) Hes-1 were analyzed using real-time RT-PCR after 4 days of culture. The values reported are the means ± standard deviations of five independent experiments. $^{*}P < 0.05$ versus control (tissue culture polystyrene); $^{\#}P < 0.05$ versus pretreatment substrate; $^{@}P < 0.05$ versus sand-blasted, large-grit acid-etched substrate.

4. Discussion

In the present study, we provide experimental evidence that implant roughness and hydrophilicity can affect differential signaling molecules targeting the early stages of osteogenic differentiation of PDLSCs. Moreover, the PDLSC osteogenic response was regulated in a roughness-dependent manner, in which osteogenesis-related factors were increased on SLA surfaces compared with PT surfaces. However, increased hydrophilicity contributed to cell response in a different way; the osteogenic properties of PDLSCs were hydrophilicity dependent on PT, but not on SLA, surfaces. This unexpected response is not consistent with previous reports of increased osteogenic activity of cells on hydrophilic compared with conventional SLA surfaces *in vitro* and *in vivo* [9, 13]. The reason that the modSLA surface did not elicit the strongest PDLSC response remains unclear. Several recent studies have shown that not only roughness but also wettability can control osteoblast responses to a biomaterial [14, 15]. However, the precise roles of surface property are unclear and optimal implant characteristics are still debated. Moreover, many studies have used osteoblast and bone marrow-derived mesenchymal stem cell models with more differentiated osteogenic phenotypes than PDLSCs, indicating the cell-type specificity of responses on Ti substrates. This finding is also consistent with previous reports that matrix mineralization and proliferation were reduced significantly on textured surfaces compared with smooth surfaces in a murine femoral stromal cell system [16]. Moreover, immortalized PDL-hTERT cells show increased spreading, survival, and differentiation on smooth *versus* rough surfaces [10]. In a study conducted to develop a surface wettability gradient, the most water-wettable surfaces showed decreased osteoblast differentiation compared with less water-wettable surfaces [17]. Thus, these findings suggest very cell-type specific responses to different surface textures and hydrophilicity. We suggest that (1) our findings may be a consequence of reduced cell spreading, growth, and survival on the modSLA surface, indicating that hydrophilicity was not the only factor regulating biological cell responses; (2) PDLSCs recognize SLA surface conditions as an ideal environment for differentiation; and (3) the seemingly significant differences

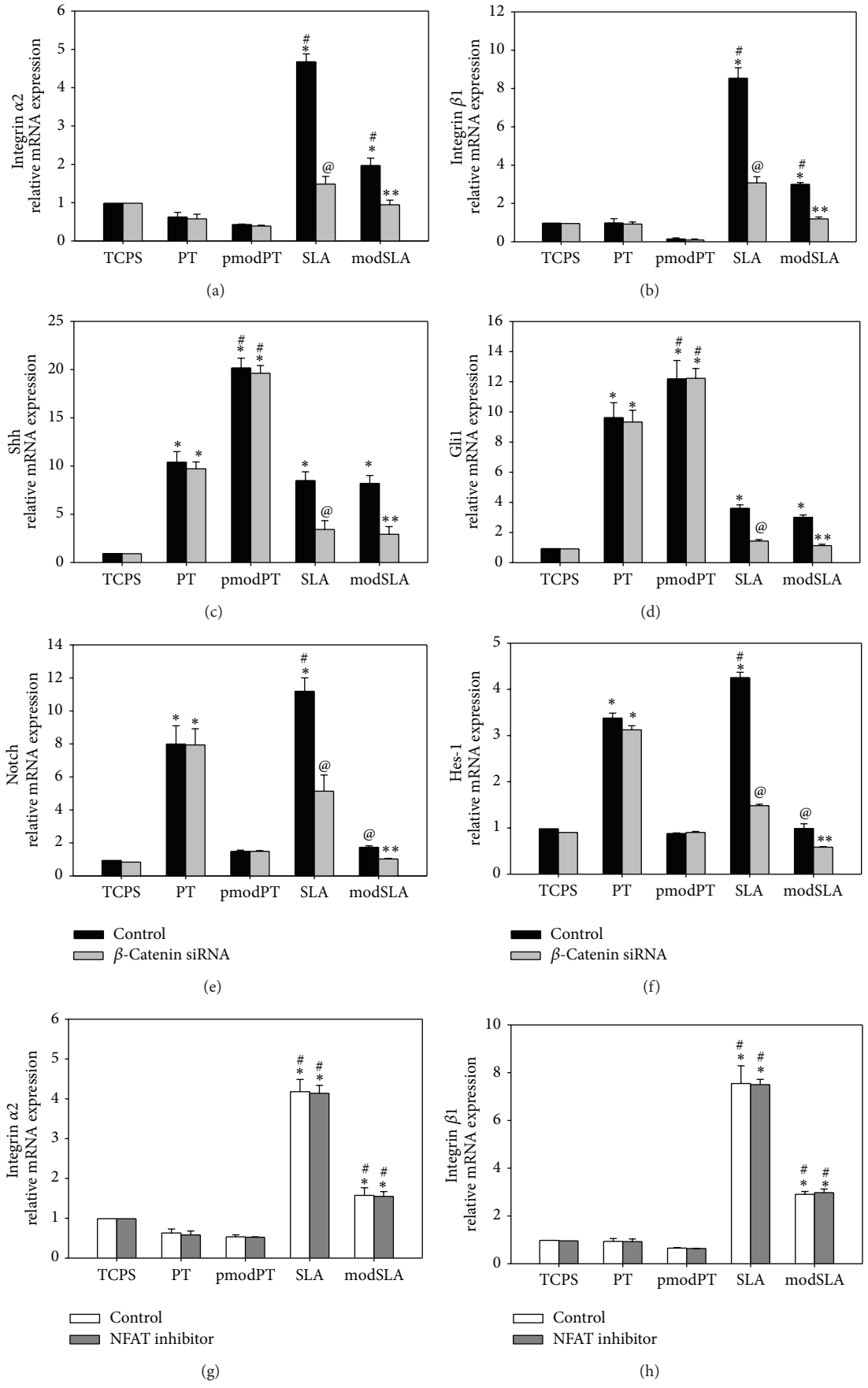

Figure 4: Continued.

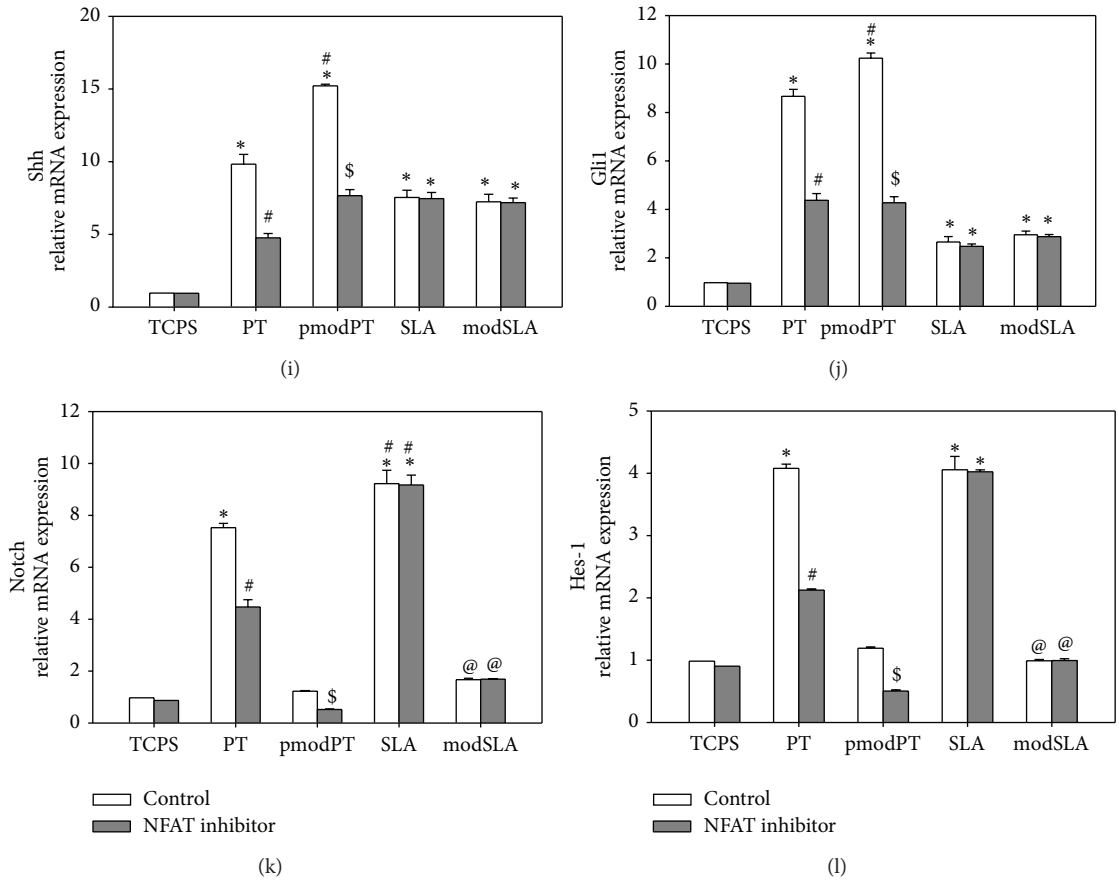

Figure 4: Effect of β-catenin knockdown or NFAT inhibitor on integrins, Shh/Gli, and Notch/Hes-1 gene expression. mRNA expression levels of integrin $\alpha 2$, integrin $\beta 1$, Shh, Gli1, Notch, and Hes-1 were analyzed after cells were transfected with β-catenin-specific siRNA for 48 h or treated with NFAT inhibitor VIVIT (500 nM). A representative result from four independent experiments is shown. $^{*}P < 0.05$ versus control (tissue culture polystyrene); $^{\#}P < 0.05$ versus pretreatment substrate; $^{\$}P < 0.05$ versus modified PT substrate; $^{@}P < 0.05$ versus sand-blasted, large-grit acid-etched (SLA) substrate; $^{**}P < 0.05$ versus modified SLA substrate.

in responses to each surface between the *in vivo* and *in vitro* environments need further confirmation.

Cell fate depends on mutual extracellular signaling and the activation or repression of specific transcription factors that affect common intracellular signaling cascades. The gene expression analysis conducted in this study indicated that differential, substrate-dependent signaling activation may be responsible for the increased osteogenic activity of PDLSCs. We first identified the dependence of Wnt factor regulation on implant surfaces. The role of Wnt signaling in bone formation has been examined recently, and it is considered to be a fundamental signaling cascade for osteoblast differentiation [18]. Moreover, surface topography and chemistry have been shown to regulate Wnt signaling, a pivotal pathway for the commitment of mesenchymal stem cells to the osteoblast lineage [6]. Wnt signaling has several molecular pathways: the canonical Wnt pathway, which requires β-catenin, and the noncanonical Wnt pathways, which activates downstream signaling independent of β-catenin [19, 20]. Interestingly, our findings demonstrated that cell expression profiles of Wnt factors differed among Ti surfaces. Specifically, cells on rough SLA surfaces exhibited increased mRNA expression of the canonical Wnt signaling molecules Wnt3a and β-catenin, whereas smooth PT surfaces affected one noncanonical Wnt pathway, the calcium-dependent molecules Wnt5a, calmodulin, and NFATc1. Consistently, previous studies reported that different Wnt pathways were activated in response to individual implant properties [21–23]. Thus, implant topographical characteristics can modulate canonical and noncanonical pathways in various cell types, including PDLSCs.

In addition to Wnt signaling pathways, the present study classified several other molecules supporting the osteogenic response of PDLSCs to Ti surfaces. Among them, integrin $\alpha 2$ and $\beta 1$ signaling is known to regulate the osteogenic factor osteoprotegerin and the integrin $\alpha 2/\beta 1$ pair is required for osteoblast differentiation on microstructured Ti [24, 25]. Similarly, we found increased mRNA expression of integrin $\alpha 2/\beta 1$ on SLA and modSLA substrates, consistent with the pattern of canonical Wnt signaling molecules, and decreased integrin expression with β-catenin siRNA, suggesting that the canonical pathways are involved in the regulation of integrins.

We have also demonstrated the different involvement of Shh/Gli and Notch signal transduction pathways with the

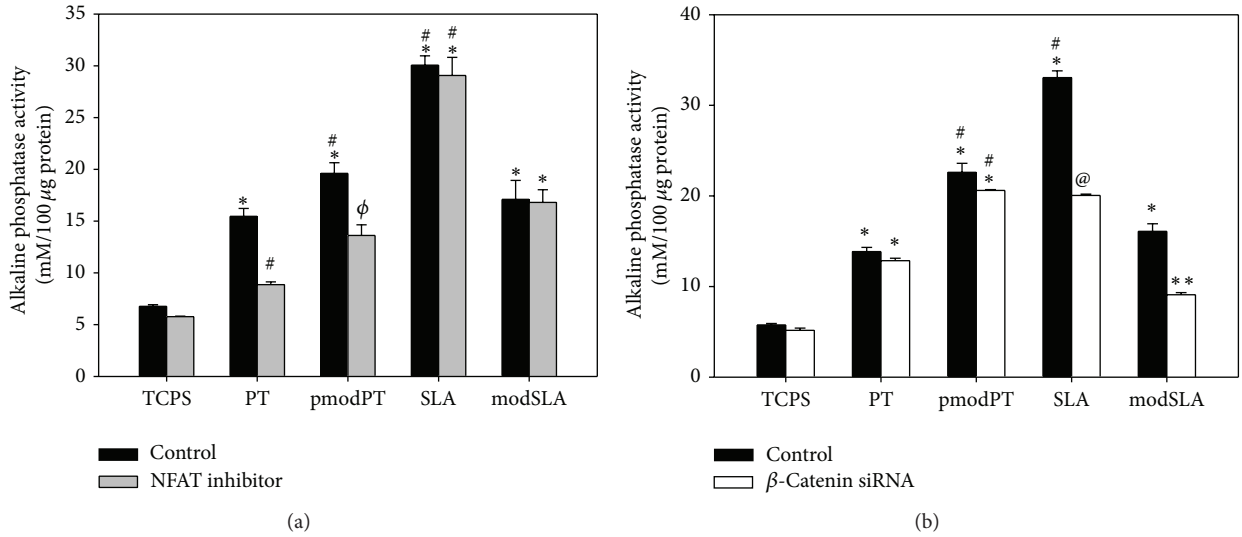

Figure 5: Effect of NFAT inhibitor or β-catenin knockdown on surface-dependent alkaline phosphatase (ALP) activity. (a) Cells were treated with the NFAT inhibitor VIVIT (500 nM) or (b) transfected with β-catenin-specific siRNA, and ALP activity was assessed after 4 days of periodontal ligament stem cell culture. A representative result from three independent experiments is shown. $^{*}P < 0.05$ versus control (tissue culture polystyrene); $^{\#}P < 0.05$ versus pretreatment (PT) substrate; $^{@}P < 0.05$ versus sand-blasted, large-grit acid-etched substrate; $^{\phi}P < 0.05$, versus modified PT substrate.

different substrates. Each pathway has been suggested to play an important role in various cell types by regulating cell fate determination and differentiation [26–28]. Several studies have suggested that Shh/Gli and Notch signaling are important mechanisms involved in osteoblast differentiation and bone regeneration [27, 29, 30]. In dentistry-related research, cementogenesis by PDL cells on certain bioactive scaffolds was stimulated by activation of Wnt and Shh signaling pathways [31]. Moreover, a previous study evaluated surfaces with the immobilized Notch ligand Jagged-1; the osteogenic differentiation of human PDLSCs was increased significantly compared with untreated groups [32]. We also observed that blocking of canonical Wnt with β-catenin siRNA and noncanonical Wnt pathway with NFAT inhibitor decreased mRNA expression of Shh and Notch signaling molecules. Thus, our findings demonstrated that these signaling molecules involved in osteogenesis were differentially expressed according to implant properties and that Wnt signaling may act as an upstream regulator of the Shh and Notch pathways. Finally, ALP activity on smooth and rough substrates was inhibited by an NFAT inhibitor (blocking calcium-dependent Wnt5a) and a β-catenin knockdown using siRNA (blocking canonical Wnt/β-catenin), respectively. These results suggest that differentially activated Wnt pathways, depending on Ra and hydrophilicity, play important roles in the osteoinductive activity of PDLSCs.

These findings show that implant properties exert complex modulation of PDLSC differentiation through these various pathways. In future studies, the interactions of these pathways will be explored in detail. In conclusion, the present study showed that Ti implant surfaces can increase the osteogenic capacity of PDLSCs with no added osteoinductive factor and suggest what kinds of surface topography and chemistry may be optimal for PDLSCs. Moreover, we suggest that the many signaling molecules may play roles in surface-induced osteogenic differentiation of PDLSCs, and they may represent useful therapeutic targets for improving clinical performance and future cell-based implant engineering.

Conflict of Interests

All the authors claimed no conflict of interests.

Acknowledgments

This work was supported by a Grant from the Kyung Hee University in 2012 (KHU20120799) and the authors thank Straumann AG (Basel, Switzerland) for providing the titanium disks used in this research.

References

[1] D. L. Cochran, R. K. Schenk, A. Lussi, F. L. Higginbottom, and D. Buser, "Bone response to unloaded and loaded titanium implants with a sandblasted and acid-etched surface: a histometric study in the canine mandible," *Journal of Biomedical Materials Research*, vol. 40, no. 1, pp. 1–11, 1998.

[2] T. W. Oates, P. Valderrama, M. Bischof et al., "Enhanced implant stability with a chemically modified SLA surface: a randomized pilot study," *The International Journal of Oral & Maxillofacial Implants*, vol. 22, no. 5, pp. 755–760, 2007.

[3] M. Kononen, M. Hormia, J. Kivilahti, J. Hautaniemi, and I. Thesleff, "Effect of surface processing on the attachment, orientation, and proliferation of human gingival fibroblasts on titanium," *Journal of Biomedical Materials Research*, vol. 26, no. 10, pp. 1325–1341, 1992.

[4] C. Oakley and D. M. Brunette, "Response of single, pairs, and clusters of epithelial cells to substratum topography," *Biochemistry and Cell Biology*, vol. 73, no. 7-8, pp. 473–489, 1995.

[5] X. Rausch-fan, Z. Qu, M. Wieland, M. Matejka, and A. Schedle, "Differentiation and cytokine synthesis of human alveolar osteoblasts compared to osteoblast-like cells (MG63) in response to titanium surfaces," *Dental Materials*, vol. 24, no. 1, pp. 102–110, 2008.

[6] R. Olivares-Navarrete, S. L. Hyzy, J. H. Park et al., "Mediation of osteogenic differentiation of human mesenchymal stem cells on titanium surfaces by a Wnt-integrin feedback loop," *Biomaterials*, vol. 32, no. 27, pp. 6399–6411, 2011.

[7] S. Ge, N. Zhao, L. Wang et al., "Bone repair by periodontal ligament stem cell seeded nanohydroxyapatite-chitosan scaffold," *International Journal of Nanomedicine*, vol. 7, pp. 5405–5414, 2012.

[8] N. An, A. Schedle, M. Wieland, O. Andrukhov, M. Matejka, and X. Rausch-Fan, "Proliferation, behavior, and cytokine gene expression of human umbilical vascular endothelial cells in response to different titanium surfaces," *Journal of Biomedical Materials Research A*, vol. 93, no. 1, pp. 364–372, 2010.

[9] Z. Qu, X. Rausch-Fan, M. Wieland, M. Matejka, and A. Schedle, "The initial attachment and subsequent behavior regulation of osteoblasts by dental implant surface modification," *Journal of Biomedical Materials Research A*, vol. 82, no. 3, pp. 658–668, 2007.

[10] D. Docheva, D. Padula, C. Popov et al., "Establishment of immortalized periodontal ligament progenitor cell line and its behavioural analysis on smooth and rough titanium surface," *European Cells & Materials*, vol. 19, pp. 228–241, 2010.

[11] B.-M. Seo, M. Miura, S. Gronthos et al., "Investigation of multipotent postnatal stem cells from human periodontal ligament," *The Lancet*, vol. 364, no. 9429, pp. 149–155, 2004.

[12] S. Y. Kim, J.-Y. Lee, Y.-D. Park, K. L. Kang, J.-C. Lee, and J. S. Heo, "Hesperetin alleviates the inhibitory effects of high glucose on the osteoblastic differentiation of periodontal ligament stem cells," *PLoS ONE*, vol. 8, no. 6, Article ID e67504, 2013.

[13] M. M. Bradford, "A rapid and sensitive method for the quantitation of microgram quantities of protein utilizing the principle of protein-dye binding," *Analytical Biochemistry*, vol. 72, no. 1-2, pp. 248–254, 1976.

[14] G. Zhao, Z. Schwartz, M. Wieland et al., "High surface energy enhances cell response to titanium substrate microstructure," *Journal of Biomedical Materials Research A*, vol. 74, no. 1, pp. 49–58, 2005.

[15] Z. Schwartz, R. Olivares-Navarrete, M. Wieland, D. L. Cochran, and B. D. Boyan, "Mechanisms regulating increased production of osteoprotegerin by osteoblasts cultured on microstructured titanium surfaces," *Biomaterials*, vol. 30, no. 20, pp. 3390–3396, 2009.

[16] G. Altankov, F. Grinnell, and T. Groth, "Studies on the biocompatibility of materials: fibroblast reorganization of substratum-bound fibronectin on surfaces varying in wettability," *Journal of Biomedical Materials Research*, vol. 30, no. 3, pp. 385–391, 1996.

[17] S. A. Hacking, E. Harvey, P. Roughley, M. Tanzer, and J. Bobyn, "The response of mineralizing culture systems to microtextured and polished titanium surfaces," *Journal of Orthopaedic Research*, vol. 26, no. 10, pp. 1347–1354, 2008.

[18] J. H. Park, C. E. Wasilewski, N. Almodovar et al., "The responses to surface wettability gradients induced by chitosan nanofilms on microtextured titanium mediated by specific integrin receptors," *Biomaterials*, vol. 33, no. 30, pp. 7386–7393, 2012.

[19] B. O. Williams and K. L. Insogna, "Where Wnts went: the exploding field of Lrp5 and Lrp6 signaling in bone," *Journal of Bone and Mineral Research*, vol. 24, no. 2, pp. 171–178, 2009.

[20] A. J. Mikels and R. Nusse, "Purified Wnt5a protein activates or inhibits β-catenin-TCF signaling depending on receptor context," *PLoS Biology*, vol. 4, no. 4, article e115, 2006.

[21] M. Kühl, L. C. Sheldahl, C. C. Malbon, and R. T. Moon, "Ca^{2+}/calmodulin-dependent protein kinase II is stimulated by Wnt and Frizzled homologs and promotes ventral cell fates in *Xenopus*," *The Journal of Biological Chemistry*, vol. 275, no. 17, pp. 12701–12711, 2000.

[22] C. Galli, G. Passeri, F. Ravanetti, E. Elezi, M. Pedrazzoni, and G. M. MacAluso, "Rough surface topography enhances the activation of Wnt/β-catenin signaling in mesenchymal cells," *Journal of Biomedical Materials Research A*, vol. 95, no. 3, pp. 682–690, 2010.

[23] I. Wall, N. Donos, K. Carlqvist, F. Jones, and P. Brett, "Modified titanium surfaces promote accelerated osteogenic differentiation of mesenchymal stromal cells *in vitro*," *Bone*, vol. 45, no. 1, pp. 17–26, 2009.

[24] E. J. Arnsdorf, P. Tummala, and C. R. Jacobs, "Non-canonical Wnt signalling and N-cadherin related β-catenin signalling play a role in mechanically induced osteogenic cell fate," *PLoS ONE*, vol. 4, no. 4, Article ID e5388, 2009.

[25] F. Schwarz, M. Wieland, Z. Schwartz et al., "Potential of chemically modified hydrophilic surface characteristics to support tissue integration of titanium dental implants," *Journal of Biomedical Materials Research B: Applied Biomaterials*, vol. 88, no. 2, pp. 544–557, 2009.

[26] B. G. Keselowsky, L. Wang, Z. Schwartz, A. J. Garcia, and B. D. Boyan, "Integrin α_5 controls osteoblastic proliferation and differentiation responses to titanium substrates presenting different roughness characteristics in a roughness independent manner," *Journal of Biomedical Materials Research A*, vol. 80, no. 3, pp. 700–710, 2007.

[27] P. N. de Aza, Z. B. Luklinska, A. Martinez et al., "Morphological and structural study of pseudowollastonite implants in bone," *Journal of Microscopy*, vol. 197, no. 1, pp. 60–67, 2000.

[28] M. I. Dishowitz, S. P. Terkhorn, S. A. Bostic, and K. D. Hankenson, "Notch signaling components are upregulated during both endochondral and intramembranous bone regeneration," *Journal of Orthopaedic Research*, vol. 30, no. 2, pp. 296–303, 2012.

[29] T. A. Mitsiadis, A. Feki, G. Papaccio, and J. Catón, "Dental pulp stem cells, niches, and notch signaling in tooth injury," *Advances in Dental Research*, vol. 23, no. 3, pp. 275–279, 2011.

[30] W.-K. Kim, V. Meliton, N. Bourquard, T. J. Hahn, and F. Parhami, "Hedgehog signaling and osteogenic differentiation in multipotent bone marrow stromal cells are inhibited by oxidative stress," *Journal of Cellular Biochemistry*, vol. 111, no. 5, pp. 1199–1209, 2010.

[31] G. L. Lin and K. D. Hankenson, "Integration of BMP, Wnt, and notch signaling pathways in osteoblast differentiation," *Journal of Cellular Biochemistry*, vol. 112, no. 12, pp. 3491–3501, 2011.

[32] P. Han, C. Wu, J. Chang, and Y. Xiao, "The cementogenic differentiation of periodontal ligament cells via the activation of Wnt/β-catenin signalling pathway by Li^+ ions released from bioactive scaffolds," *Biomaterials*, vol. 33, no. 27, pp. 6370–6379, 2012.